Nonoxido and Oxido Vanadium Complexes Featuring O- and N- donor Ligands in Relation to Biological and Catalytic Activities

Thesis submitted in partial fulfillment of the requirements for the degree of

Doctor of Philosophy

by

Subhashree Priyadarsini Dash

Under the guidance of

Dr. Rupam Dinda

Department of Chemistry
National Institute of Technology, Rourkela
Rourkela-769008, Odisha, India

CERTIFICATE

This is to certify that the thesis entitled **"Nonoxido and Oxido Vanadium Complexes Featuring O- and N- donor Ligands in Relation to Biological and Catalytic Activities"** submitted by **Subhashree Priyadarsini Dash** of the Department of Chemistry, National Institute of Technology, Rourkela, India, for the degree of **Doctor of Philosophy** is a record of bona fide research work carried out by her under my guidance and supervision. I am satisfied that the thesis has reached the standard fulfilling the requirements of the regulations relating to the nature of the degree. To the best of my knowledge, the matter embodied in the thesis has not been submitted to any other University/Institute for the award of any degree or diploma.

Supervisor

Dr. Rupam Dinda,
Department of Chemistry
National Institute of Technology,
Rourkela-769008, Odisha, India

Place: Rourkela
Date:

Acknowledgements

This thesis is the account of five years of devoted work in the field of synthetic & bio-inorganic chemistry in relation to biological and catalytic application at Department of Chemistry, National Institute of Technology, Rourkela, India, which would not have been possible without the help of many.

I would like to give my deep sense of gratitude and respectful regards to my supervisor Dr. Rupam Dinda for associating me in his research group. I would like to thank him with immense pleasure for his stimulating guidance and constant encouragements. Without his expertise and guidance, this thesis would not be written.

I am thankful to the Director, National Institute of Technology, Rourkela for providing me the use of all infrastructural facilities. I would also like to thank Dr. N. Panda, HOD of our Department for providing me the various laboratory and instrumental facilities during my Ph.D. work.

I sincerely thank Dr. A. Sahoo, Dr. B. G. Mishra and Dr. Usharani Subuddhi for evaluating my progress reports and seminars, their helpful comments and valuable discussion during the Ph. D. program. I am sincerely thankful to all the faculty members and staff of our Department for their constant help. Helps received from Dr. S. Chatterjee and Dr. D. Sarkar deserves special mention. I am thankful to the members of our research group Sagarika Pasayat, Saswati, Satabdi Roy and Sudarshana Majumder for their active cooperation during my research work.

Thanks are also to Sumanta K. Patel, Paresh K. Majhi, Vijaylakshmi Tirkey, Ayan Dasgupta, Sasmita Mishra, Avishek Ghosh, Smriti Dewangan, Rajkumar Boddhula, Yogesh P. Patil, Manasi R. Hardikar, Sarita Dhaka, Alok K. Panda, Hirak R. Das and Subhadip Mukhopadhyay for their cooperation.

I am thankful to Prof. M. R. Maurya, Department of Chemistry, IIT Roorkee for the study of catalysis and his valuable suggestions during manuscript preparation. I am thankful to Prof. S. K.

Chattopadhyay, Department of Chemistry, IIEST, Shibpur, for his generous help in electrochemical studies. I would also thankful to Dr. Ashis Biswas, School of Basic Sciences, IIT, Bhubaneswar, Dr. Surajit Das and Dr. S. K. Bhutia, Department of Life Science, NIT, Rourkela for the help in pharmacological studies. Also thanks to Dr. Bimba N. Joshi, for biological studies, Dr. T. K. Maji for the magneto chemistry, Dr. T. K. Paine, Dr. P. Sen, and Dr. B. Mondal for EPR analysis.

I am grateful to Prof. Edward R. T. Tiekink, Department of Chemistry, University of Malaya, Prof. Dr. Hans Reuter, Institute of Chemistry of New Materials, University of Osnabrueck, Prof. Krzysztof Brzezinski, Institute of Chemistry, University of Bialystok, Prof. Ekkehard Sinn, Department of Chemistry, Western Michigan University, Kalamazoo, Dr. Werner Kaminsky, Department of Chemistry, University of Washington and Prof. M. Nethaji, Department of IPC, IISc. Bangalore for their kind cooperation in determining the X-ray structures of synthesized complexes.

Financial assistance received from the Department of Science and Technology, New Delhi [Grant SR/WOS-A/CS-145/2011 and grant SR/FT/CS-016/2008], the Council of Scientific and Industrial Research, New Delhi [Grant No. 01(2735)/13/EMR-II] is gratefully acknowledged. I am thankful to the Department of Science and Technology, New Delhi [Grant SR/WOS-A/CS-145/2011] for providing me fellowship.

Last but not the least, I would like to record deep respect to my elder sisters and parents for selflessly extending their ceaseless blessings, love, encouragement and moral support at all times without which this work wouldn't be possible.

Date: Subhashree Priyadarsini Dash

ABSTRACT

Nonoxido and Oxido Vanadium Complexes Featuring O- and N- donor Ligands in Relation to Biological and Catalytic Activities

Subhashree Priyadarsini Dash

Department of chemistry, National Institute of Technology, Rourkela-769008, Odisha, India

---

Chapter 1: In this chapter the scope of the present investigation is delineated briefly along with the aim of the work.

Chapter 2: Synthesis, X-ray structure and characterization of three highly stable, hexacoordinated nonoxido vanadium(IV), $V^{IV}(L)_2$, complexes with tridentate aroylhydrazonates containing ONO- donor atoms have been reported. All the complexes are stable in open air in the solid state as well as in solution, a phenomenon rarely observed in nonoxido vanadium(IV) complexes. The complexes have good solubility in organic solvents, permitting electrochemical and various spectroscopic investigations. The existence of nonoxido vanadium(IV) complexes was confirmed by elemental analysis, ESI mass spectroscopy, cyclic voltammetry, EPR and magnetic susceptibility measurements. X-ray crystallography showed the N_2O_4 donor set to define a trigonal prismatic geometry in each case. All the complexes show *in vitro* insulin mimetic activity against insulin responsive L6 myoblast cells. In addition, the *in vitro* antiproliferative activity of all the complexes against HeLa cell line was assayed, where the complexes found to show good cytotoxic activity.

Chapter 3: Some new oxido vanadium(V) complexes $[VOL^{1\text{-}3}(OEt)(EtOH)]$ (**1**-**3**) have been reported which were obtained from the reaction of the Schiff bases ($H_2L^{1\text{-}3}$) (Where H_2L^1= salicylhydrazone of diacetyl monoxime; H_2L^2= 4-methoxy salicylhydrazone of diacetyl monoxime and H_2L^3 = 4-hydroxy salicylhydrazone of diacetyl monoxime) with $VO(acac)_2$ in 1:1 molar ratio. Three 4-R- aroylhydrazoneoximes have been used as ligands in the present study, differing in the inductive effect of the substituent R (R = H, OCH_3 and OH), in order to observe their influence, if any, on the redox potentials and biological activity of the complexes. All the synthesized ligands and the metal complexes were successfully characterized by elemental

analysis, IR, UV-Vis and NMR spectroscopy. X-ray diffraction study of [VOL^1(OEt)(EtOH)], **1** reveals that the metal centre is in distorted octahedral O_5N coordination spheres where the ONO-donor ligand and the ethoxido group constitute a satisfactory O_3N basal plane. Cyclic voltammetry of the complexes show a quasi-reversible cyclic voltammetric response in the potential range of 0.29−0.36 V involving single electron V(V)−V(IV) reduction. The complexes have also been screened for their antibacterial activity against *Escherichia coli, Bacillus, Proteus and Klebsiella*. Minimum inhibitory concentration of these complexes and antibacterial activity indicates the compound **1** as the potential lead molecule for drug designing.

Chapter 4: Four oxidoalkoxido vanadium(V) [$V^VO(L^{1-4})$OEt] (**1**–**4**) and one dinuclear oxidoethoxido mixed-ligand vanadium(V) [{$VO(L^2)OEt\}_2$(Q)]{Q = 4,4'-bipyridine}(**5**), complexes, taking potentially tridentate binegative aroylhydrazone ligands are reported [where H_2L^1 = anthranylhydrazone of 2-hydroxy-1-napthaldehyde, H_2L^2 = salicylhydrazone of 2-hydroxy-1-napthaldehyde, H_2L^3 = benzoylhydrazone of 2-hydroxy-1-acetonaphthone, H_2L^4 = anthranylhydrazone of 2-hydroxy-1-acetonaphthone]. All the complexes were characterized by various physicochemical techniques. Single crystal X-ray crystallography of **1**–**4** reveals that the metal centre is in distorted square pyramidal geometry with O_4N coordination spheres, whereas **5** exhibits a distorted octahedral geometry around the metal center. The solution behavior of the oxidoethoxido vanadium(V) species was studied, which indicates the existence of two species (1:1 ratio) in solution. Catalytic potential of these complexes was tested for the oxidative bromination of styrene, salicylaldehyde and oxidation of methyl phenyl sulphide. All the complexes (**1**–**5**) showed good DNA binding and photo-nuclease propensity. Among these, **3** and **4** show high binding affinity towards CT-DNA than others.

Chapter 5: Eight alkali metal ion-mediated dioxido vanadium(V), [{$V^VO_2L^{1-6}$}$A(H_2O)_n]_\infty$(**1-8**), complexes for A = Li^+, Na^+, K^+ and Cs^+, containing tridentate ONO- donor aroylhydrazonate ligands are described. All the synthesised ligands and the metal complexes were successfully characterised by elemental analysis, IR, UV-Vis and NMR spectroscopy. X-ray crystallographic investigation of **3**, **5**−**7** shows the presence of distorted NO_4 coordination geometry. The dioxido vanadium(V) complexes were found to exhibit DNA binding activity due to their interaction with CT-DNA by the groove binding mode, with binding constants ranging from 10^3-10^4 M^{-1}.

Complexes **1**−**8** were also tested for DNA nuclease activity against pUC19 plasmid DNA which showed that **6** and **7** had the best DNA binding and photonuclease activity; these results support their good protein binding and cleavage activity with binding constants ranging from 10^4 −10^5 M^{-1}. Finally, the *in vitro* antiproliferative activity of all complexes was assayed against the HeLa cell line. Some of the complexes **(2**, **5**, **6** and **7**) show considerable activity compared to commonly use chemotherapeutic drugs.

Chapter 6: In this chapter, four neutral oxido vanadium(V) complexes $[VO_2L^1]$(**1**), $[VO_2L^2]$(**2**), $[VOL^3(OEt)]$(**3**), $[VOL^4(OEt)EtOH]$(**4**) [where HL^1 = 2-thiophenoylhydrazone of 2-acetylpyridine, HL^2 = 2-amino benzoylhydrazone of 2-benzoyl pyridine, H_2L^3 = isonicotinoylhydrazone of 2-hydroxy acetophenone, H_2L^4 = 2-furoylhydrazone of 2-hydroxy-1-napthaldehyde] with a bioactive hydrazone scaffold containing furan, thiophene and pyridine-residues have been synthesized. All complexes were thoroughly characterized by various spectroscopic (IR, UV-Vis, NMR and ESI-MS) and single crystal X-ray diffraction techniques. Biological studies reveal that, **1**–**4** show good DNA binding propensity and interact with CT-DNA by a minor groove binding mode, with binding constants ranging from 10^3–10^5 M^{-1}. All complexes show good photo-induced cleavage of pUC19 supercoiled plasmid DNA with **3** showing the highest photo-induced DNA cleavage activity of ~ 65%. Additionally, **1**–**4** show satisfactory cytotoxic activity against the human cervical cancer cell line (HeLa) following the order **4** > **2** > **3** > **1** with IC_{50} values ranging from 10 to 20 μM.

Chapter 7: A series of nonoxido vanadium(IV) $[V^{IV}(L^{1-4})_2]$ (**1**–**4**), oxidoethoxido vanadium(V) $[V^{V}O(L^{1-4})OEt]$ (**5**–**8**), and μ-oxido divanadium(V) $[V^{V}{}_2O_3(L^1)_2]$ (**9**) complexes, taking potentially tridentate dibasic aroylhydrazone ligands are reported [where H_2L^1 = 2-furoyl hydrazone of 2-hydroxy-1-acetonaphthone, H_2L^2 =2-thiophenoylhydrazone hydrazone of 2-hydroxy-1-acetonaphthone, H_2L^3 =1-napthoyl hydrazone of 2-hydroxy-1-acetonaphthone, H_2L^4 =3-hydroxy-2-napthoyl hydrazone of 2-hydroxy-1-acetonaphthone]. All the complexes were characterized by elemental analysis as well as various spectroscopic techniques. Most of the complexes (**2**, **3**, **5**, **6** and **8**) were also characterized by single crystal X-ray crystallography. The nonoxido vanadium(IV) complexes are quite stable in open air as well as in solution. The solution chemistry of the oxidoethoxido vanadium(V) complexes were reported. This indicates

the existence of two different species in solution. The new species, a μ-oxido divanadium(V) complex, $[V_2O_3(L^1)_2]$ (**9**), is successfully isolated in solid state and fully characterized by several physicochemical techniques & single crystal X-ray crystallography.

Keywords: Aroylhydrazones / Nonoxido vanadium(IV) and oxido vanadium(V) Complexes / Solution chemistry / X-ray crystal structure / Pharmacological (Cytotoxic, Antibacterial, Insulin mimetic, DNA and BSA binding and cleaving) activity / Catalytic oxidation & oxidative bromination.

Table of Contents

		Page No
Preface		1
Chapter 1:	**Scope of the present investigation**	5
1.1	**Review on nonoxido vanadium(IV) and oxido vanadium(V) complexes with O- and N- donor ligands**	6
1.2.	**Aim of the present work**	23
1.3.	**The main objectives of the present study**	26
1.4.	**References**	27
Chapter 2:	**Highly stable hexacoordinated nonoxido vanadium(IV) complexes of sterically constrained ligands: Syntheses, structure and study of antiproliferative and insulin mimetic activity**	31
	Abstract	32
2.1.	**Introduction**	33
2.2.	**Experimental section**	35
2.2.1.	General methods and materials	35
2.2.2.	Synthesis of ligands (H_2L^{1-3})	35
2.2.3.	Synthesis of complexes $[V^{IV}(L^{1-3})_2]$ (**1**–**3**)	36
2.2.4.	X-ray crystallography	38
2.2.5.	In vitro Insulin mimetic activity	40
2.2.6.	Cytotoxic assay	40
2.2.7.	Nuclear staining assay	40
2.3.	**Results and discussion**	41
2.3.1.	Synthesis	41
2.3.2.	Structure description	45
2.3.3.	Spectral characteristics	53
2.3.4.	Electrochemical properties	57
2.3.5.	Magnetic properties	59
2.3.6.	EPR spectroscopy	60

2.3.7.	In vitro Insulin mimetic activity	62
2.3.8.	Inhibition of cancer cell viability	64
2.3.9.	Nuclear staining assay	64
2.4.	**Conclusions**	67
2.5.	**References**	68
Chapter 3:	**Oxido vanadium(V) complexes incorporating tridentate aroylhydrazoneoximes: Synthesis, characterizations and antibacterial activity**	75
	Abstract	76
3.1.	**Introduction**	77
3.2.	**Experimental section**	79
3.2.1.	General methods and materials	79
3.2.2.	Synthesis of ligands ($H_2L^{1–3}$)	79
3.2.3.	Synthesis of complexes (**1**–**3**)	79
3.2.4.	X-ray crystallography	80
3.2.5.	Antimicrobial activity	82
3.3.	**Results and discussion**	83
3.3.1.	Synthesis	83
3.3.2.	Spectral characteristics	83
3.3.3.	Electrochemical properties	87
3.3.4.	Description of crystal structure of (**1**)	90
3.3.5.	Antimicrobial activity	94
3.4.	**Conclusions**	96
3.5.	**References**	97
Chapter 4:	**Study of bio- and catalytic potential of oxidoethoxido vanadium(V) complexes with aroylhydrazones of naphthol-derivative: Special focus on their solution behavior**	101
	Abstract	102
4.1.	**Introduction**	103

4.2.	**Experimental section**	104
4.2.1.	General methods and materials	104
4.2.2.	Synthesis of ligands ($H_2L^{1–4}$).	105
4.2.3.	Synthesis of complexes [VO($L^{1–4}$)OEt] (**1**–**4**)	106
4.2.4.	Synthesis of mixed-ligand complex (**5**)	107
4.2.5.	Solution state characterization of [VO($L^{1–4}$)OEt] (**1**–**4**)	107
4.2.6.	X-ray crystallography	109
4.2.7.	Catalytic reactions	111
4.2.7.1.	Oxidative bromination of styrene	111
4.2.7.2.	Oxidative bromination of salicylaldehyde	111
4.2.7.3.	Oxidation of methyl phenyl sulfide	111
4.2.8.	DNA binding experiments	112
4.2.8.1.	Absorption spectral studies	112
4.2.8.2.	Thermal denaturation studies	112
4.2.8.3.	Circular dichroism studies	112
4.2.9.	DNA cleavage experiments	113
4.2.9.1.	Chemical-induced DNA cleavage	113
4.2.9.2.	Photo-induced DNA cleavage	113
4.3.	**Results and discussion**	115
4.3.1.	Synthesis and structure	115
4.3.2.	Description of the X-ray structure of complexes (**1**−**5**)	116
4.3.3.	IR spectroscopy.	122
4.3.4.	Electronic spectra	122
4.3.5.	Study of solution behavior of complexes (**1**−**4**)	123
4.3.6.	Catalytic activity studies	131
4.3.6.1.	Oxidative bromination of styrene	131
4.3.6.2.	Oxidative bromination of salicylaldehyde	137
4.3.6.3.	Oxidation of methyl phenyl sulfide	139
4.3.7.	DNA binding studies	143
4.3.7.1.	Absorption spectroscopic studies	143

4.3.7.2.	Thermal denaturation studies	146
4.3.7.3.	Circular dichroism studies	147
4.3.8.	DNA cleavage studies	148
4.3.8.1.	Chemical-induced DNA cleavage	148
4.3.8.2.	Photo-induced DNA cleavage	148
4.4.	**Conclusions**	151
4.5.	**References**	152
Chapter 5:	**Syntheses and structural investigation of some alkali metal ion-mediated $LV^{V}O_2^-$ (L^{2-} = Tridentate ONO ligands) species: DNA binding, photo-induced DNA cleavage and cytotoxic activities**	155
	Abstract	156
5.1.	**Introduction**	157
5.2.	**Experimental section**	160
5.2.1.	General methods and materials	160
5.2.2.	Synthesis of ligands (H_2L^{1-6})	160
5.2.3.	Synthesis of complexes $[\{VO_2L^{1-6}\}A(H_2O)_n]_\infty$ (**1**–**8**)	162
5.2.4.	X-ray crystallography	164
5.2.5.	DNA binding experiments	168
5.2.5.1.	Absorption spectral studies	168
5.2.5.2.	Thermal denaturation studies	168
5.2.5.3.	Circular dichroism studies	168
5.2.6.	DNA cleavage experiments	169
5.2.6.1.	Chemical-induced DNA cleavage	169
5.2.6.2.	Photo-induced DNA cleavage	169
5.2.7.	Protein binding and cleavage experiments	170
5.2.7.1.	Bovine serum albumin (BSA) interaction studies	170
5.2.7.2.	BSA photo-induced cleavage studies	170
5.2.8.	Cytotoxicity Studies	171
5.2.8.1.	MTT assay	171
5.2.8.2.	Nuclear staining assay	171

5.3.	**Results and discussion**	172
5.3.1.	Synthesis	172
5.3.2.	Spectral characteristics	173
5.3.3.	Description of the X-ray structure of complexes.	177
5.3.4.	DNA binding studies	188
5.3.4.1.	Absorption spectroscopic studies	188
5.3.4.2.	Thermal denaturation studies	191
5.3.4.3.	Circular dichroism studies	191
5.3.5.	DNA cleavage studies	194
5.3.5.1.	Chemical-induced DNA cleavage	194
5.3.5.2.	Photo-induced DNA cleavage	194
5.3.6.	Protein binding and cleavage experiments	198
5.3.6.1.	Bovine serum albumin (BSA) binding studies	198
5.3.6.2.	BSA cleavage activity	198
5.3.7.	Cytotoxicity studies	202
5.3.7.1.	MTT assay	202
5.3.7.2.	Nuclear staining assay	202
5.4.	**Conclusions**	206
5.5	**References**	208
Chapter 6:	**Oxido vanadium(V) complexes of aroylhydrazones containing bioactive heterocycles: Synthesis, characterisation and study of DNA binding, photo-induced DNA cleavage and cytotoxic activities**	213
	Abstract	214
6.1.	**Introduction**	215
6.2.	**Experimental section**	217
6.2.1.	General methods and materials	217
6.2.2.	Synthesis of ligands (HL^{1-2}, H_2L^{3-4})	218
6.2.3.	Synthesis of complexes (**1**–**4**)	219
6.2.4.	X-ray crystallography	221

6.2.5.	DNA binding experiments	223
6.2.5.1.	Absorption spectral studies	223
6.2.5.2.	Thermal denaturation studies	223
6.2.6.	DNA cleavage experiments	223
6.2.6.1.	Chemical-induced DNA cleavage	223
6.2.6.2.	Photo-induced DNA cleavage	223
6.2.7.	Cytotoxicity Studies	224
6.2.7.1.	MTT assay	224
6.2.7.2.	Nuclear Staining	224
6.3.	**Results and discussion**	225
6.3.1.	Synthesis	225
6.3.2.	Spectral characteristics	225
6.3.3.	Description of the X-ray structure of complexes (**1**–**4**)	226
6.3.4.	DNA binding studies	241
6.3.4.1.	Absorption spectroscopic studies	241
6.3.4.2.	Thermal denaturation studies	244
6.3.5.	DNA cleavage studies	245
6.3.5.1.	Chemical-induced DNA cleavage	245
6.3.5.2.	Photo-induced DNA cleavage	245
6.3.6.	Cytotoxicity studies	249
6.3.6.1.	MTT assay	249
6.3.6.2.	Nuclear staining assay	249
6.4.	**Conclusions**	253
6.5.	**References**	254

Chapter 7:	**Chemistry of mononuclear nonoxido V^{IV}, oxido V^{V}, and binuclear oxido $V^{V}V^{V}$ complexes with a tridentate (ONO) ligand: Exploration of solution behavior of oxido vanadium(V) complexes**	260
	Abstract	261
7.1.	**Introduction**	262
7.2.	**Experimental section**	263
7.2.1.	General methods and materials	263
7.2.2.	Synthesis of ligands ($H_2L^{1–4}$)	263
7.2.3.	Synthesis of nonoxido vanadium(IV) complexes (**1**–**4**)	264
7.2.4.	Synthesis of oxidoethoxido vanadium(V) complexes (**5**–**8**)	265
7.2.4.1.	Solid state characterization of (**5**–**8**)	266
7.2.4.2.	Solution state characterization of (**5**–**8**)	266
7.2.5.	Synthesis of μ-oxido divanadium(V) complexes (**9**)	268
7.2.6.	X-ray crystallography	269
7.3.	**Results and discussion**	271
7.3.1.	Mononuclear nonoxido vanadium(IV) $[V^{IV}(L^{1-4})_2]$ (**1**–**4**) and oxidoalkoxido vanadium(V) $[V^{V}O(L^{1-4})OEt]$ (**5**–**8**) complexes	271
7.3.2.	μ-oxido dioxido divanadium(V) complex, $[V^{V}_2O_3(L^{1})_2]$ (**9**)	291
7.4.	**Conclusions**	298
7.5.	**References**	299
	A brief resume of the work embodied in this dissertation and concluding remark	303
	Publications	308
	Bio-data	309

Preface

The present dissertation describes the design, synthesis, full characterization and the exploration of solution chemistry, chemical, electrochemical properties and the study of catalytic and pharmacological activity of a series of mono- and binuclear variable- valence nonoxido and oxido vanadium complexes of some selected multidentate ONO- and ONN- donor ligands. Structures of nineteen important nonoxido and oxido vanadium complexes are determined by single crystal X-ray analysis. Structure-reactivity relations are discussed and implications of structure determination on the design of new complexes using the structurally characterized compounds as precursors are elaborated. All the complexes described in this dissertation are characterized by various physicochemical techniques such as elemental analysis, measurement of magnetic susceptibility at room temperature in solid state, measurement of conductivity in solution and by various spectroscopic techniques (UV-Vis, IR, NMR, EPR and ESI-MS). Electrochemical characteristics of the complexes were studied by cyclic voltammetry and, as pointed out before, single crystal X-ray crystallography were used to find out crystal and molecular structure of all the compounds of mononuclear nonoxido vanadium(IV) and mono- and binuclear oxido vanadium(V) complexes. Biological activities particularly antimicrobial, antiproliferative, insulin mimetic, DNA and BSA binding and cleavage activity and catalytic activities of some of the above complexes particularly oxidation of sulphides and oxidative bromination of aromatic aldehydes were also studied. The subject matter of this dissertation is divided into seven chapters containing the chemistry of nonoxido vanadium(IV) and oxido vanadium(V) ligated to selected O- and N- donor ligands and a *brief resume* of the work embodied in this dissertation and *concluding remarks*.

Chapter 1 is a general introduction to the entire work described in the present dissertation and spells out the objectives of the thesis. The objectives of the works are placed at the end of the general introduction**.** The entire subject matter of this dissertation is organized as follows:

Chapter 2 deals with the synthesis, X-ray structure and characterization of three highly stable, hexacoordinated nonoxido vanadium(IV), $V^{IV}(L)_2$, complexes with tridentate aroylhydrazonates containing ONO- donor ligands. All the complexes are stable in open air in the solid state as well as in solution, a phenomenon rarely observed in nonoxido vanadium(IV) complexes. The complexes have good solubility in organic solvents, permitting electrochemical and various

spectroscopic investigations. The existence of nonoxido vanadium(IV) complexes was confirmed by elemental analysis, ESI mass spectroscopy, cyclic voltammetry, EPR and magnetic susceptibility measurements. X-ray crystallography showed the N_2O_4 donor set to define a trigonal prismatic geometry in each case. All the complexes show *in vitro* insulin mimetic activity against insulin responsive L6 myoblast cells. In addition, the *in vitro* antiproliferative activity of all the complexes against HeLa cell line was assayed, where the complexes found to show good cytotoxic activity.

In ***Chapter 3*** the chemistry of some new oxido vanadium(V) complexes $[VOL^{1\text{-}3}(OEt)(EtOH)]$ (**1**-**3**) have been reported which were obtained from the reaction of the Schiff bases ($H_2L^{1\text{-}3}$) (Where H_2L^1= salicylhydrazone of diacetyl monoxime; H_2L^2= 4-methoxy salicylhydrazone of diacetyl monoxime and H_2L^3 = 4-hydroxy salicylhydrazone of diacetyl monoxime) with $VO(acac)_2$ in 1:1 molar ratio. Three 4-R- aroylhydrazoneoximes have been used as ligands in the present study, differing in the inductive effect of the substituent R (R = H, OCH_3 and OH), in order to observe their influence, if any, on the redox potentials and biological activity of the complexes. All the synthesized ligands and the metal complexes were successfully characterized by elemental analysis, IR, UV-Vis and NMR spectroscopy. X-ray diffraction study of $[VOL^1(OEt)(EtOH)]$, **1** reveals that the metal centre is in distorted octahedral O_5N coordination spheres where the ONO- donor ligand and the ethoxo group constitute a satisfactory O_3N basal plane. Cyclic voltammetry of the complexes show a quasi-reversible cyclic voltammetric response in the potential range of 0.29−0.36 V involving single electron V(V)−V(IV) reduction. The complexes have also been screened for their antibacterial activity against *Escherichia coli, Bacillus, Proteus and Klebsiella*. Minimum inhibitory concentration of these complexes and antibacterial activity indicates the compound **1** as the potential lead molecule for drug designing.

Chapter 4 describes the report of four oxidoethoxido vanadium(V) $[V^VO(L^{1\text{-}4})OEt]$ (**1**–**4**) and one dinuclear oxidoalkoxido mixed-ligand vanadium(V) $[\{VO(L^2)OEt\}_2(Q)]$\{Q = 4,4'-bipyridine\}(**5**), complexes, taking potentially tridentate binegative aroylhydrazone ligands [where H_2L^1 = anthranylhydrazone of 2-hydroxy-1-napthaldehyde, H_2L^2 = salicylhydrazone of 2-hydroxy-1-napthaldehyde, H_2L^3 = benzoylhydrazone of 2-hydroxy-1-acetonaphthone, H_2L^4 = anthranylhydrazone of 2-hydroxy-1-acetonaphthone]. All the complexes were characterized by various physicochemical techniques. Single crystal X-ray crystallography of **1**–**4** reveals that the metal centre is in distorted square pyramidal geometry with O_4N coordination spheres, where as

5 exhibits a distorted octahedral geometry around the metal center. The solution behavior of the oxidoethoxido vanadium(V) species was studied, which indicates the existence of two species (1:1 ratio) in solution. Catalytic potential of these complexes was tested for the oxidative bromination of styrene, salicylaldehyde and oxidation of methyl phenyl sulphide. All the complexes (**1**–**5)** showed good DNA binding and photo-nuclease propensity. Among these, **3** and **4** show high binding affinity towards CT-DNA than others.

In ***chapter 5*** eight alkali metal ion-mediated dioxido vanadium(V), $[\{V^{V}O_2L^{1\text{-}6}\}A(H_2O)_n]_\infty$ (**1**–**8**), complexes for A = Li^+, Na^+, K^+ and Cs^+, containing tridentate ONO- donor aroylhydrazonate ligands are described. All the synthesised ligands and the metal complexes were successfully characterised by elemental analysis, IR, UV-Vis and NMR spectroscopy. X-ray crystallographic investigation of **3**, **5**−**7** shows the presence of distorted NO_4 coordination geometry. The dioxido vanadium(V) complexes were found to exhibit DNA binding activity due to their interaction with CT-DNA by the groove binding mode, with binding constants ranging from 10^3-10^4 M^{-1}. Complexes **1**−**8** were also tested for DNA nuclease activity against pUC19 plasmid DNA which showed that **6** and **7** had the best DNA binding and photonuclease activity; these results support their good protein binding and cleavage activity with binding constants ranging from 10^4-10^5 M^{-1}. Finally, the *in vitro* antiproliferative activity of all complexes was assayed against the HeLa cell line. Some of the complexes **(2**, **5**, **6** and **7**) show considerable activity compared to commonly use chemotherapeutic drugs.

In this ***chapter*** (***6***), four neutral oxido vanadium(V) complexes $[VO_2L^1]$(**1**), $[VO_2L^2]$(**2**), $[VOL^3(OEt)]$(**3**), $[VOL^4(OEt)EtOH]$(**4**) [where HL^1 = 2-thiophenoylhydrazone of 2-acetylpyridine, HL^2 = 2-amino benzoylhydrazone of 2-benzoyl pyridine, H_2L^3 = isonicotinoylhydrazone of 2-hydroxy acetophenone, H_2L^4 = 2-furoylhydrazone of 2-hydroxy-1-napthaldehyde] with a bioactive hydrazone scaffold containing furan, thiophene and pyridine-residues have been synthesized. All complexes were thoroughly characterized by various spectroscopic (IR, UV-Vis, NMR and ESI-MS) and single crystal X-ray diffraction techniques. Biological studies reveal that, **1**–**4** show good DNA binding propensity and interact with CT-DNA by a minor groove binding mode, with binding constants ranging from 10^3-10^5 M^{-1}. All complexes show good photo-induced cleavage of pUC19 supercoiled plasmid DNA with **3** showing the highest photo-induced DNA cleavage activity of ~ 65%. Additionally, **1**–**4** show

satisfactory cytotoxic activity against the human cervical cancer cell line (HeLa) following the order **4** > **2** > **3** > **1** with IC_{50} values ranging from 10 to 20 μM.

The essence of the work presented in ***chapter 7*** is the detailed account of a series of nonoxido vanadium(IV) $[V^{IV}(L^{1\text{-}4})_2]$ (**1**–**4**), oxidoethoxido vanadium(V) $[V^{V}O(L^{1\text{-}4})OEt]$ (**5**–**8**), and μ-oxido divanadium(V) $[V^{V}{}_2O_3(L^1)_2]$ (**9**) complexes, taking potentially tridentate dibasic aroylhydrazone ligands [where H_2L^1 = 2-furoyl hydrazone of 2-hydroxy-1-acetonaphthone, H_2L^2 =2-thiophenoylhydrazone hydrazone of 2-hydroxy-1-acetonaphthone, H_2L^3 =1-napthoyl hydrazone of 2-hydroxy-1-acetonaphthone, H_2L^4 =3-hydroxy-2-napthoyl hydrazone of 2-hydroxy-1-acetonaphthone]. All the complexes were characterized by elemental analysis as well as various spectroscopic techniques. Most of the complexes (**2**, **3**, **5**, **6** and **8**) were also characterized by single crystal X-ray crystallography. The nonoxido vanadium(IV) complexes are quite stable in open air as well as in solution. The solution chemistry of the oxidoethoxido vanadium(V) complexes were reported. This indicates the existence of two different species in solution. The new species, a μ-oxido divanadium(V) complex, $[V_2O_3(L^1)_2]$ (**9**), is successfully isolated in solid state and fully characterized by several physicochemical techniques & single crystal X-ray crystallography.

Chapter 1

Scope of the Present Investigation

Chapter 1

Scope of the present investigation

Abstract: In this chapter the scope of the present investigation is delineated briefly along with the aim of the work.

1.1. REVIEW ON NONOXIDO VANADIUM(IV) AND OXIDO VANADIUM(V) COMPLEXES WITH O- AND N- DONOR LIGANDS

The studies described in the present dissertation involve coordination complexes of variable-valence vanadium featuring O- and N- donor ligands in relation to their biological and catalytic activities. The coordination chemistry of metal complexes with aroylhydrazone ligands has attracted continuing attention for the synthetic chemist due to their ease of synthesis and stability under a variety of oxidative and reductive conditions. Hydrazone moieties are the most important pharmacophoric cores of several anticancer, antiinflammatory, antinociceptive, and antiplatelet drugs.[1] Vanadium plays number of roles in the biological systems and has been found in many naturally occurring compounds.[2] In humans, V compounds exhibit a wide variety of pharmacological properties, and many complexes have been tested as antiparasitic, spermicidal, antiviral, anti-HIV, antituberculosis, and antitumor agents.[3] Particularly, vanadium has been proved to be one of the most efficient metal ions with potential antidiabetic activity.[4] Vanadium complexes show varied stereochemistry. It can form compounds with inorganic and organic ligands, with particular preference for oxygen, nitrogen and sulphur donor atoms.

Again, coordination chemistry of variable valence vanadium assumed special importance due to the following reasons:

1. Vanadium in higher oxidation states (+5 and +4) is oxidophilic. It forms various types of oxido species depending on the charge and denticity of the coordinating ligand attached to the metal centers.[5] Among these compounds, those containing the VO^{n+} (n = 2-3) and $[V_2O_3]^{n+}$ (n = 2−4) cores belong to the largest family.

2. Although the chemistry of oxido vanadium(IV) and (V) complexes is well developed, the number of nonoxido vanadium(IV) complexes in the electronic Cambridge Structural Database remains scarce. Formation of nonoxido or ‘bare’ hexacoordinated vanadium(IV)

complexes is rather difficult because the strong V=O bond must be broken and the oxido ligand must leave the complex as a good leaving group.

3. Many oxidation states of vanadium are relevant for biological systems like +III, +IV, and +V.[6,7] However, V^{III} is very susceptible to oxidation and appears to be of less importance than V^{IV} and V^{V}.

4. Vanadium is a ubiquitous trace element[6] and is present in two families of enzymes, i.e., vanadium-dependent haloperoxidases[8] and nitrogenases.[9] It is accumulated in several marine organisms such as ascidians[10] and polychaete fan worms,[11] and it is also found in very high concentrations in amavadin, the complex isolated from Amanita muscaria.[12]

5. Moreover, a number of vanadium(IV) and (V) complexes, were found to show their profound catalytic activity to carry out a variety of oxidation reactions, including alkene epoxidation and hydroxylation, aromatic alkane and alcohol oxidation, sulfide and halide oxidation, and also in oxidative bromination reaction.[13]

In this context, role of the coordination environment around the central metal (vanadium) ion is most important. Variation in the coordination environment can only bring about corresponding variation in the properties of the complexes. Chemistry of non oxidovanadium(IV) and mono- and binuclear oxido vanadium(V) with ligands of various types has been of significant importance in this regard. Review on some of the recent reports of the nonoxido vanadium(IV) and mono- and binuclear oxido vanadium(V) complexes with O- and N- donor environments, which are drawing much current attention, are highlighted below.

1.1.1. Nonoxido vanadium(IV) complexes. Vanadium is an oxidophilic metal and has the tendency to form oxido-species in its +5 and +4 oxidation states. But there are certain vanadium complexes which contain no oxido group, and are known to be nonoxido or 'bare' complex. In recent time such species attract special attention to inorganic chemist due to the structural similarities with amavadin. Amavadin is the first octacoordinated vanadium(IV) complex isolated from Amanita mushrooms.[14,15] It is a nonoxido vanadium(IV) complex but this character was established after a long time.[16,17] Three types of nonoxido vanadium(IV) compounds, viz. hexa-, hepta- and octacoordinate, are reported. A characteristic feature of all nonoxido vanadium(IV) complexes is the absence of the (V=O) band in the 935–1035 cm^{-1} region in the IR spectra, which, in contrast, is a signature for all oxido vanadium(IV) and (V) compounds.

P. Chaudhuri[18] and group has contributed a lot in the field of nonoxido vanadium chemistry. In 2011 they have reported the structural and magnetochemical characterization of two nonoxido vanadium(IV) complexes [$LV^{IV}(OCH_3)$] (**1**) (**Figure 1.1**) and [LV^{IV}(acac)] (**2**) using tris(2-hydroxy-3,5-di-*tert* butylbenzyl) amine as ligand (H_3L). The transformation of 5-coordinated TBP nonoxido vanadium complex **1** to the 6-coordinated octahedral complex **2** was observed in presence of a bidentate chelate acetylacetone ligand.

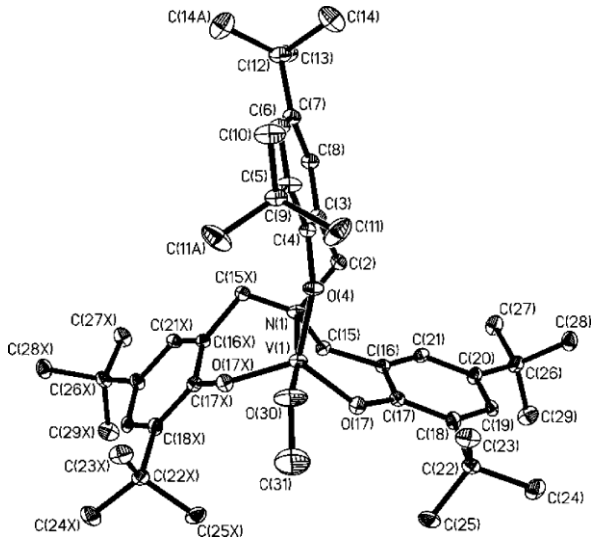

Figure 1.1.

In 2004, the same group has reported, another series of nonoxido vanadium(IV) complexes taking potentially tridentate bisphenol ligands (H_2L) (**Figure 1.2**) containing [O, X, O] donor atoms (X = S (**3)**, Se (**4)**, P (**5)**, or P=O (**6)**).[19] The ligands with different hetero donor atoms yielded different nonoxido vanadium(IV) complexes, $V^{IV}L_2$, having six-coordinated V^{IV}, VO_4X_2, core which was confirmed by X-ray diffraction methods. The paramagnetic and nonoxido nature of **3**–**6** were supported by variable-temperature (2–295 K) magnetic susceptibility measurements, X-band electron paramagnetic resonanace (EPR) (2–60 K) spectroscopy, electrochemical methods, and magnetic circular dichroism (MCD) (5 K) measurements.

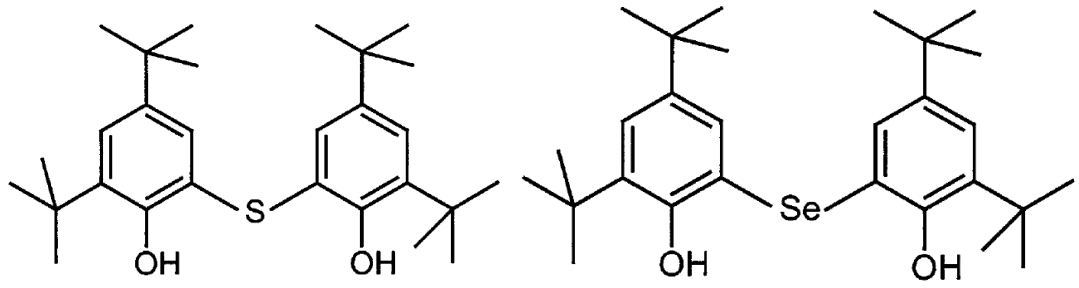

H_2L^S **H_2L^{Se}**

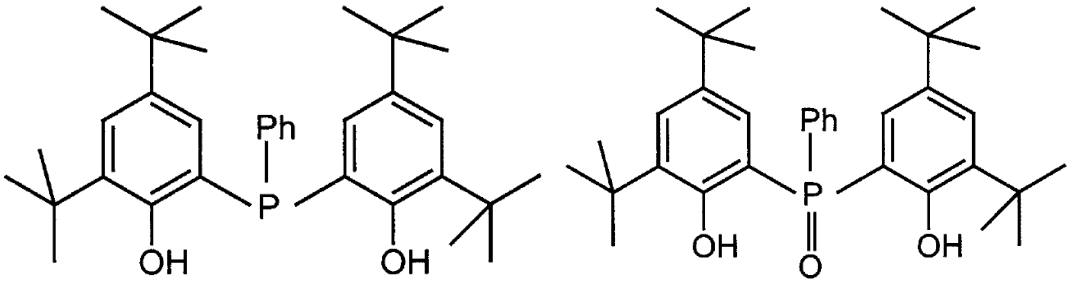

H_2L^P **H_2L^{PO}**

$V^{IV}L^S_2$ (3), $V^{IV}L^{Se}_2$ (4), $V^{IV}L^P_2$ (5), $V^{IV}L^{PO}_2$ (6)

Figure. 1.2

In 2003, Chaudhuri et al.[20] have also reported two mononuclear nonoxido vanadium(IV) complexes, $[V^{IV}LMe_2]$ (**7**) (**Figure 1.3**) and $[V^{IV}Lt Bu_2]$ (**8**), with a tridentate bis(phenol) ligand (H_2L) bearing the O_2N donor atoms and with either dimethyl or di*tert*-butyl substituents. Both the complexes **7** and **8** were structurally characterized and were found to show distorted octahedral geometry. For complex **7**, isomerization of the meridional form to the facial form was observed in solution.

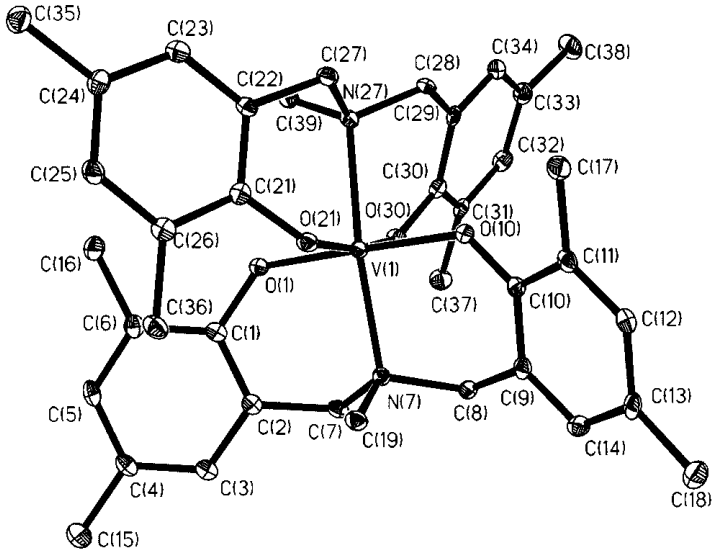

Figure 1.3

Ghosh et al.[21] have reported a very general route for the synthesis of a series of stable octacoordinated nonoxido vanadium(IV) complexes of the general formula VL_2 (where H_2L is a ONNO donor tetradentate hydrazone ligand). These compounds were found to be highly stable in open air, in the solid state as well as in solution and don't require any inert condition for synthesis, which is an unusual phenomenon for such type of complexes. One of these compounds $VL^1{}_2$ (**9**) has been structurally characterized (**Figure 1.4**) {where H_2L^1 = benzildihydrazone of 2-aminobenzoylhydrazine} and was found to exhibit a dodecahedral structure existing in a tetragonal space group $P\bar{4}n2$.

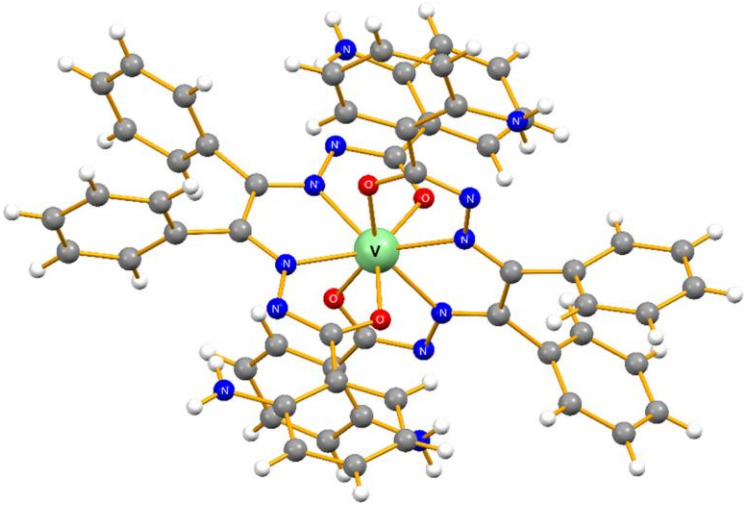

Figure 1.4

Garribba et al.[22] have reported the synthesis and characterization of two nonoxido vanadium(IV) complexes, $[V(H_{-3}ino)_2][K_2(ino)_2].4H_2O$ (**10**) and $[Na_6V(H_{-3}ino)_2](SO_4)_2.6H_2O$ (**11**) {where, ino = cis-inositol}. Structures of both the complexes were determined by single-crystal X-ray analysis. Crystal structure of the **10** (**Figure 1.5**) represents an unusual 1:1 packing of $[V(H_{-3}ino)_2]^{2-}$ dianions and $[K_2(ino)_2]^{2+}$ dications, in which both K^+ ions have a coordination number of nine and are bonded simultaneously to a 1,3,5-triaxial and an 1,2,3-axial-equatorial-axial site of ino.

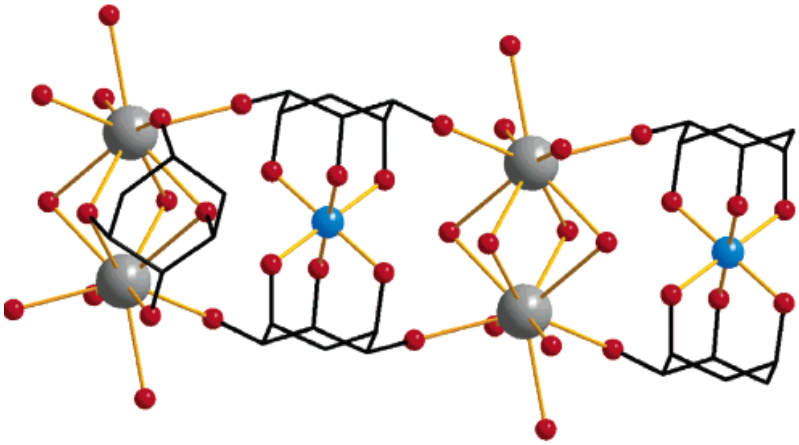

Figure 1.5

1.1.2. Oxidoalkoxido vanadium(V) complexes. Monooxidoalkoxido vanadium(V) complexes, [$V^{V}O(OR)$] have been known for a long time[23] and their chemistry has got increased importance in recent years[24-31]. Such species constitute useful oxidants[32] and are bioinorganically relevant in the context of haloperoxidation[33], phosphorylation[34] and insulin mimicking[35].

Recently, M. R. Maurya and coworkers[36] have reported synthesis, characterisation and study of catalytic three alkoxido vanadium(V) complexes [$V^{V}O(OMe)(MeOH)\{Hdfmp(inh)_2\}$] (**12**), [$V^{V}O(OMe)(MeOH)\{Hdfmp(nah)_2\}$] (**13**) and [$V^{V}O(OMe)(MeOH)\{Hdfmp(bhz)_2\}$] (**14**) (**Figure 1.6**) [where, $H_3dfmp(L)_2$ are obtained by the condensation of 2,6-diformyl-4-methylphenol and hydrazones (L), L = isonicotinoylhydrazide (inh), nicotinoylhydrazide (nah) and benzoylhydrazide (bhz)]. The results of catalytic study suggest that these complexes have the potential to be considered as a functional models of VHPOs.

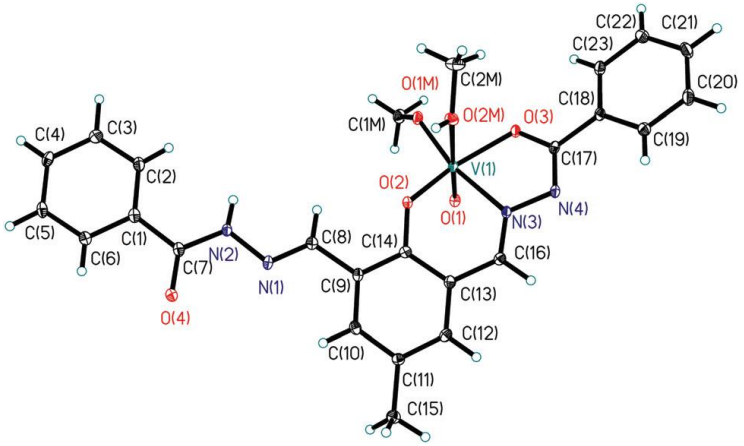

Figure 1.6

S. K. Kar and group[37] has highlighted the structural behavior of two mononuclear oxidoalkoxido vanadium(V) complexes [$\{VO(L_1)(OCH_3)(CH_3OH)\}\{VO(L_1)(OCH_3)\}$] (**15**) and [$VO(L_2)$ $(OCH_3)(CH_3OH)$] (**16**) {HL_1 = [N′-(2-hydroxybenzylidene)-5-methyl-1-(pyridin-2-yl)-1H-pyrazole-3-carbohydrazide] and HL_2 = [1- (4, 6-dimethylpyrimidin-2-yl)-N′-(2-hydroxybenzylidene)-5-methyl-1H-pyrazole-3-carbohydrazide]} where two different coordination geometry around two V(V) centres in the asymmetric unit of complex **15** with ligand HL_1 is observed (**Figure 1.7**). In other compound **16**, the vanadium(V) atom sits in the

distorted octahedral coordination pocket formed by one tridentate ONO binegative ligand molecule (HL_2), one oxido group, one methoxido group and one methanol moiety.

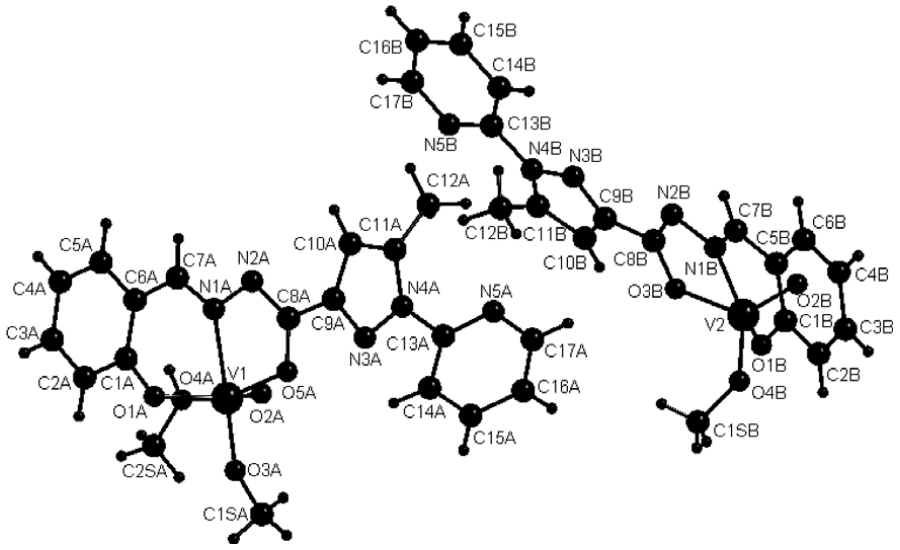

Figure 1.7

Monfared et al.[38] have reported the catalytic potential of three monooxido alkoxido vanadium(V) complexes, [VO(OMe)L^1] (**20**), [VO(OMe)L^2] (**21**) and [VO(OMe)L^3] (**22**), {(H_2L^1 = (E)-3-hydroxy-N′-(2-hydroxy-3-methoxybenzylidene)-2-naphthohydrazide, H_2L^2 = (E)-3-hydroxy-N′-(2-hydroxybenzylidene)-2-naphthohydrazide and H_2L^3 = (E)-N′-(5-bromo-2-hydroxybenzylidene)-3-hydroxy-2-naphthohydrazide} for the oxidation of cyclooctene using H_2O_2 as terminal oxidant. The complex, **21** (**Figure 1.8**) showed the most potent catalytic activity in oxidation of various terminal, cyclic and phenyl substituted olefins.

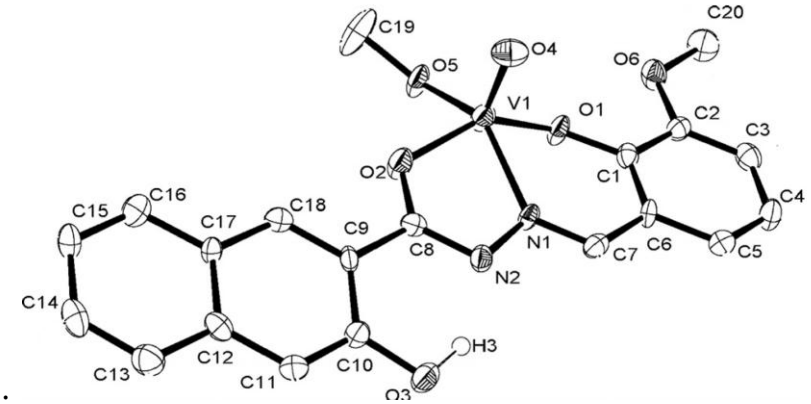

Figure 1.8

There is a report by M. Sutradhar and coworkers,[39] where a mononuclear oxido alkoxido vanadium(V) complex, [VO(OEt)L] (**23**) (**Figure 1.9**) was isolated from the corresponding binuclear precursor ($V_2O_3L_2$) { H_2L = 2-hydroxyacetophenone-2-aminobenzoylhydrazone} with the reaction of excess triphenylphosphine in refluxing ethanol. The reaction proceeds through the oxido bridge splitting of the binuclear species.

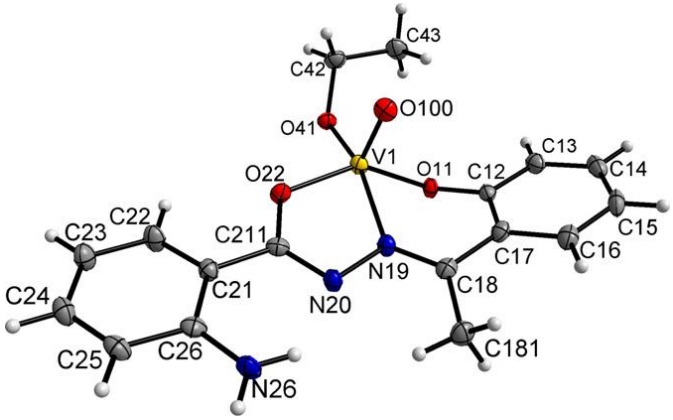

Figure 1.9

Kurup et al.[40] have reported the synthesis, spectral and structural study of some oxidoalkoxido vanadium(IV/V) complexes by taking 2-hydroxyacetophenone-3-hydroxy-2-naphthoylhydrazone (H_2L). Among these complexes, [VOL(OCH_3)] (**24**) was found to exist in two polymorphic forms denoted by **24a** (**Figure 1.10**) and **24b** (**Figure 1.11**), with space groups $Pn2_1a$ and $P\bar{1}$, respectively.

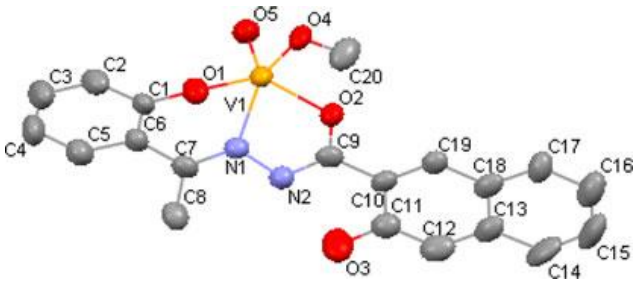

Figure 1.10

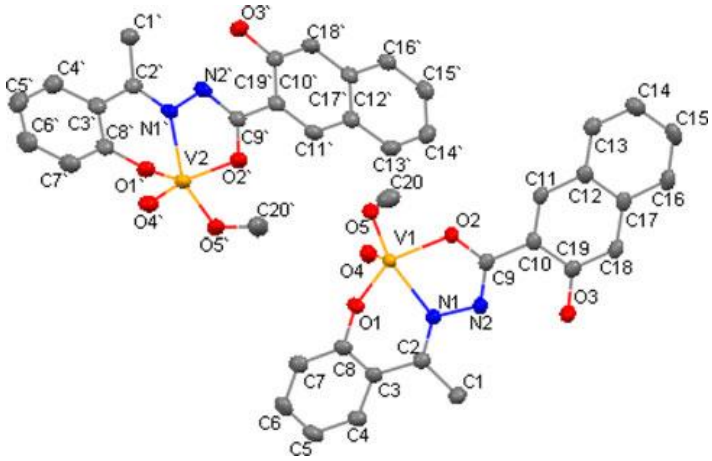

Figure 1.11

Chen et al.[41] and Zhou et al.[42] have structurally characterized alkoxido vanadium(V) complexes, [V($C_{15}H_{12}N_2O_4$)(CH_3O)O] (**25**) and [VO($C_{13}H_{10}N_2O_4$)(OCH_3)] (**26**) where the V^V ion exhibits a distorted square-pyramidal coordination geometry. Similarly, L. Liu[43] and F.-M. Wang[44] have reported the crystal structure of [V($C_{15}H_{10}I_2N_2O_2$)(CH_3O)O(CH_3OH)] (**27**) and [V($C_{14}H_8BrClN_2O_2$)-(CH_3O)O(CH_3OH)] (**28**) respectively, where a distorted octahedral geometry was observed around the central metal atom.

M. S. Lah and group[45] has reported the solution behavior along with the synthesis and structural characterization of a five-coordinated square pyramidal vanadium(V) complex, [VO(Hacshz)(OEt)] (**29**) (**Figure 1.12**), ($Hacshz^{2-}$ = acetylacetosalicylhydrazone). Here the reported complex was found to exist in two forms. Among these two forms, the major one is a monomeric species, as isolated in the solid-state, and the minor species was found to get converted to the monomeric form in the presence of a small amount of ethanol.

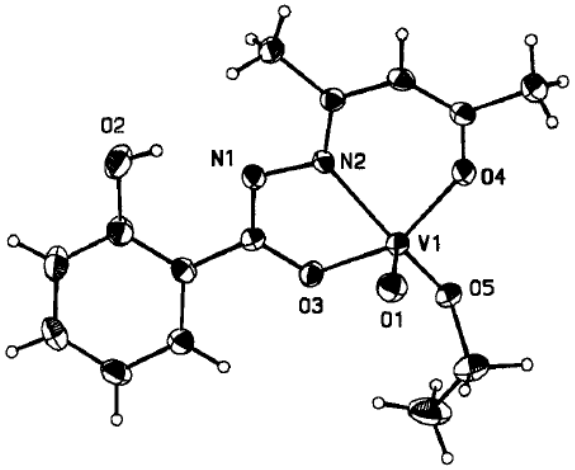

Figure 1.12

In the context of solution behavior, an interesting observation was reported by Dinda et al.[46] where monooxido alkoxido vanadium(V) complex [VO(OEt)L], (**30**) {H_2L= 2-hydroxybenzaldehydehydrazone of 2-hydroxybenzoylhydrazine} gets transformed to corresponding monooxidobridged divanadium(V,V) complex [$(VOL)_2O$] in solution. It was observed that, by controlled potential electrolysis it leads to the generation of a mixed valence vanadium(IV,V) species. This mixed valence species is identified and studied by EPR technique (at room temperature (**Figure 1.13a**) as well as in liquid nitrogen temperature (**Figure 1.13b**) and also by UV-Vis spectroscopy (**Figure 1.14**).

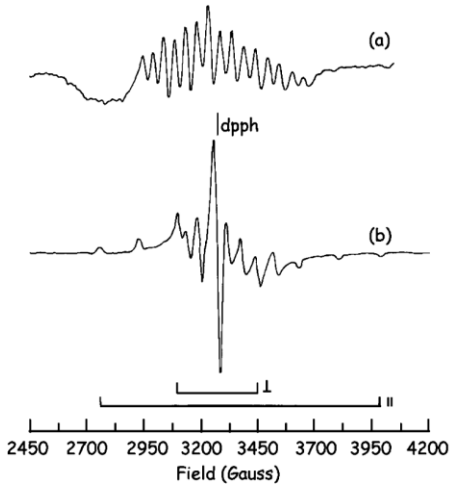

Figure 1.13

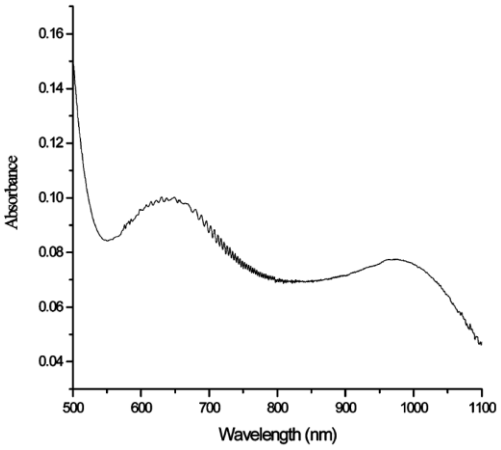

Figure 1.14

1.1.3. Dioxido vanadium(V) complexes. The dioxido vanadium(V) complexes constitute a large class of vanadium(V) complex like that of monooxido vanadium(V) complexes. The formation of the dioxido vanadium(V) complexes largely depends on the basic character of the ligands and sometimes addition of base to the reaction medium promotes their formation from the corresponding oxido vanadium(V) complexes.

Plass and coworkers[47] have reported the first supramolecular inclusion compound, a *cis*-dioxido vanadium(V) complex K[VO_2(salhybiph)@ β-CD] (**31**) (**Figure 1.15**) by the reaction of potassium vanadate and the hydrazone ligand derived from Schiff base condensation of salicylaldehyde and biphenyl-4-carboxylic acid hydrazide (H_2salhybiph) in the presence of β-cyclodextrin (β-CD) in water. It is expected that, through modification of the CD-host, it may be possible to utilize this concept for the generation of novel systems in oxidation catalysis, including the potential influence of the sugar backbone on chiral induction of vanadium-catalyzed oxidation reactions.

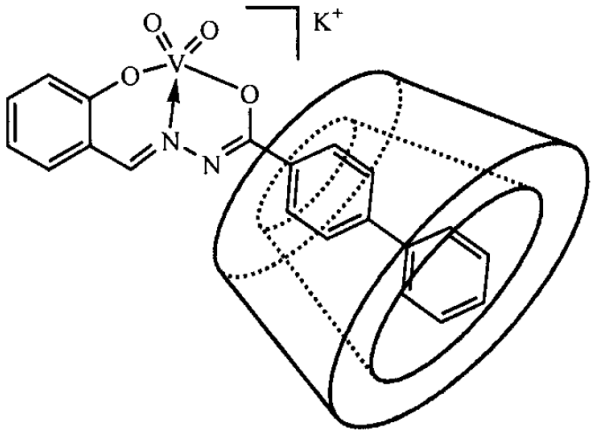

Figure 1.15

This group has also reported[48] the synthesis, characterization and crystal structure of a dioxido vanadium(V) complex $NH_4[VO_2(salhyph)]$ (**32**) with the tridentate Schiff base ligand derived from salicylaldehyde and benzoic acid hydrazide (H_2salhyph), where the vanadium atom of the dioxido vanadium(V) moiety has a distorted square-pyramidal geometry. Extensive hydrogen bonding was observed between the ammonium cation and the oxygen atoms coordinated to the vanadium atom yielding a two-dimensional network (**Figure 1.16**), where the complex anions were arranged in a bilayer manner. Additional crystal packing within the bilayer appears to be controlled mostly by π stacking between the aromatic rings of the ligand.

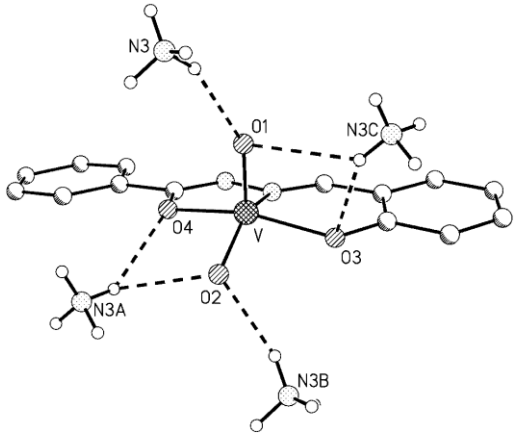

Figure 1.16

M. R. Maurya and group[49] has reported the synthesisis and characterization of $[V^VO_2(acac\text{-}ambmz)]$ (**33**), $[V^VO_2(sal\text{-}ambmz)]$ (**34**) and $[V^VO_2(sal\text{-}aebmz)]$ (**35**) (**Figure 1.17**) {Hacac-ambmz = Schiff base derived from acetylacetone and

2-aminomethylbenzimidazole, Hsal-ambmz = Schiff base obtained by the condensation of salicylaldehyde and 2-aminomethylbenzimidazole, Hsal-aebmz = derived from salicylaldehyde and 2-aminoethylbenzimidazole}, among which, **33** and **35** can be considered to be structural models of VHPO due to their structural similaries. Moreover, all the complexes, **33**–**35** are found to catalyze the oxidation of methyl phenyl sulfide to methyl phenyl sulfoxide and methyl phenyl sulfone .

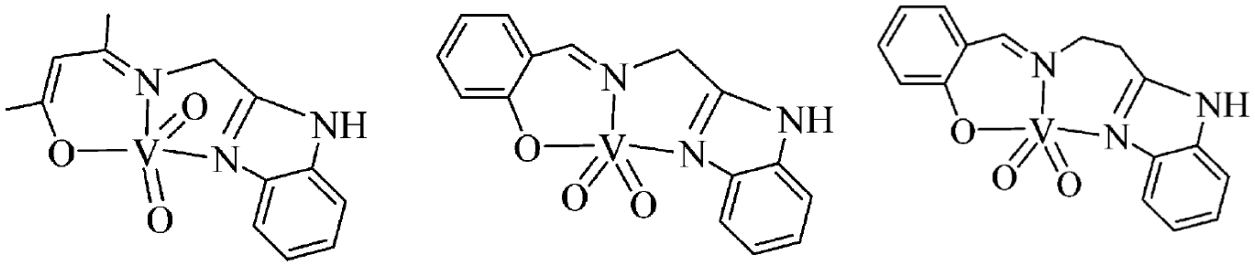

33 **34** **35**

Figure 1.17

In 2004, Gambino et al.[50] have reported three new dioxido(semicarbazone) vanadium(V) complexes *cis*-$VO_2L^{1–3}$(**36**–**38**) {where L^1 = salicylaldehyde semicarbazone, L^2 = salicylaldehyde 4-*n*-butylsemicarbazone, L^3 = salicylaldehyde 4-(2-naphthyl) semicarbazone} which were tested for their insulin-mimetic activity. The observation suggested that all dioxido vanadium(V) complexes exhibited essentially no *in vitro* insulin-mimetic activity, except VO_2L^2 (**37**), that developed activity in the presence of ascorbic acid, similar to that of vanadyl sulfate.

The same group in 2005, has reported[51] the synthesis of five dioxido vanadium(V) semicarbazone complexes with the formula cis-VO_2L, where L = 5-bromosalicylaldehyde semicarbazone and 2-hydroxynaphtalen-1-carboxaldehyde semicarbazone. All the complexes were tested in three different human tumor cell lines where they showed selective cytotoxicity on TK-10 cell line. Results suggested that structural modifications on the semicarbazone moiety could have a significant effect on the anti-tumor activity of the vanadium complexes. The molecular structure of the novel [V^VO_2(5-bromosalicylaldehyde semicarbazone)] (**39**) (**Figure 1.18**) complex was solved by X-ray diffraction methods, where vanadium atom was surrounded by distorted square pyramidal coordination sphere.

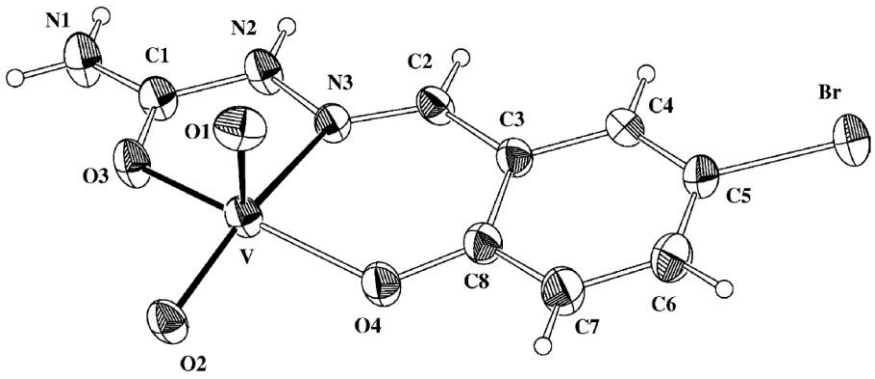

Figure 1.18

Dinda et al.[52] have reported the syntheses and characterization of two alkali metal complexes $[\{VO_2L\}M(H_2O\}_n]$ [M = Na^+ (**40**), K^+ (**41**)] of anionic cis-dioxido vanadium(V) species (LVO_2^-) {L = 2-hydroxybenzoylhydrazone of 2-hydroxybenzaldehyde}. These compounds represent a class of metal-mediated supramolecular assembly $[\{VO_2L\}M(H_2O\}_n]$ with an infinite polymeric structure containing an alternating array of cis-dioxido vanadium(V), $[VO_2L]^-$, units and aquated metal ion centres which was confirmed by X-ray crystallographic investigation of both the complexes. Staircase like arrangement of complex **41** along the a axis is shown in **Figure 1.19**.

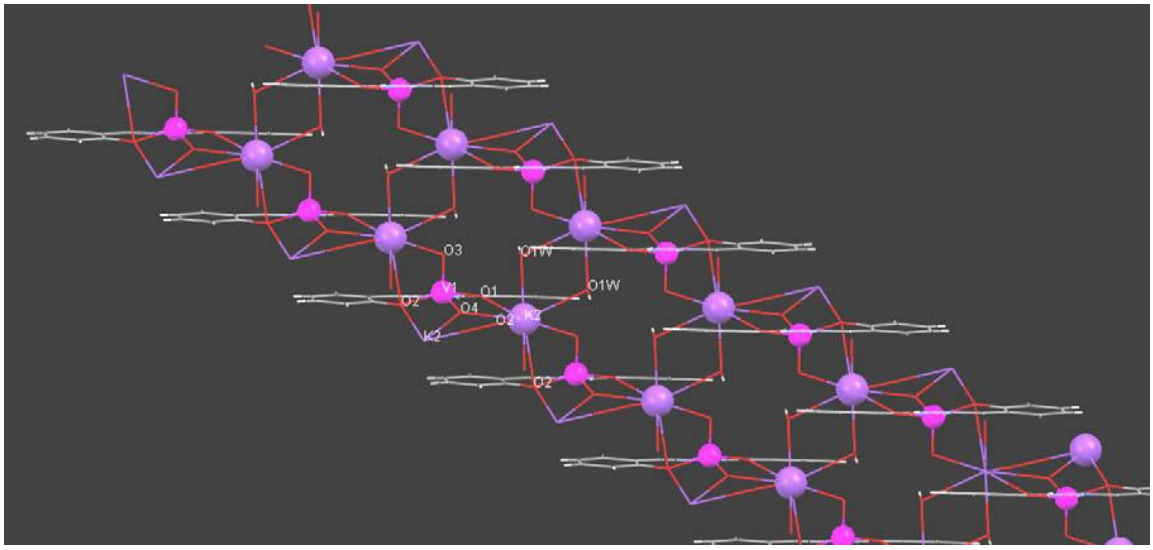

Figure 1.19

S. K. Kar and group[53] has reported the anionic cis-dioxido vanadium(V) complexes, LVO_2^- and $L_1VO_2^-$ of two tridentate ONO ligands that bind alkali metal ions in a bis-monodentate fashion like a bridging carboxylate group. Where the complementary units are held together by hydrogen bonding and coulombic interactions. Among these complexes $[L_1VO_2Li(H_2O)_2]_\infty$ (**42**), $[LVO_2Na(H_2O)_2]_\infty$ (**43**) and $[LVO_2K(H_2O)_2]_\infty$ (**44**) were crystallographically characterized. {H_2L = (N′-[(E)-(2-hydroxyphenyl) methylidene]-3-methyl-1H-pyrazole-5-carbohydrazide) and H_2L_1 = (N′-[(1E)-1-(2-hydroxyphenyl) ethylidene]-3-methyl-1H-pyrazole-5-carbohydrazide)}. A 3D polymeric cluster of **44** is shown in **Figure 1.20**.

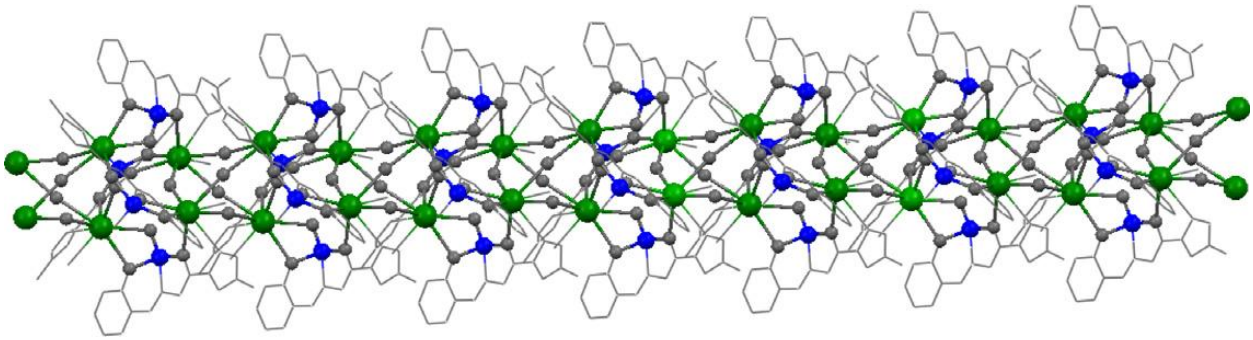

Figure 1.20

1.1.4. Binuclear dioxido vanadium(V) complexes. Binuclear complexes of oxido vanadium(V) usually display a bridging ligand, connecting the two oxido vanadium(V) centers, of the types, μ-oxido, di-μ-oxido or di-μ-alkoxido. Binuclear metal complexes connected by a sole μ-oxido bridge continue to attract increasing attention in contemporary coordination chemistry. Such species, often supported by ancillary bridging ligand(s) (viz. carboxylates, etc.) are known to play pivotal roles in biology during dioxygen activation by a host of metalloenzymes, namely, methane monooxygenase, Δ^9-desaturase, ribonucleotide reductase, cytochrome *c* oxidase, and so forth.[54-56]

Kurup and group[57] has reported the crystal structure of $[VO(BPB)(\mu_2\text{-}O)]_2$ (**45**) (**Figure1.21**) and $[VO(DKN)(\mu_2\text{-}O)]_2 .½H_2O$ (**46**) {HBPB = 2-benzoylpyridine benzoyl hydrazone, HDKN = di-2-pyridyl ketone nicotinoyl hydrazone}. Each of the complexes exhibits a binuclear structure where two vanadium(V) centres are bridged by two oxygen atoms to form distorted octahedral structures within cis-N_2O_4 donor sets.

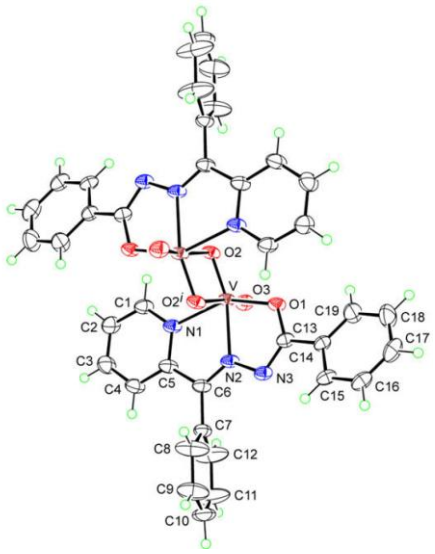

Figure 1.21

H. H. Monfared and group[58] has reported the structure and characterization of the methoxidobridged divanadium(V) complex $[V^{V}O(\mu_2\text{-}OCH_3)(L^1)]_2$ (**47**) (**Figure 1.22**) (H_2L^1 = benzoylhydrazone of acetylacetone). The complex was found to show a distorted octahedral geometry around the vanadium(V) centre. The catalytic activity of **47** was examined for the oxidation of various hydrocarbons (alkanes, alkenes and aromatic hydrocarbons) with H_2O_2 in acetonitrile under mild condition.

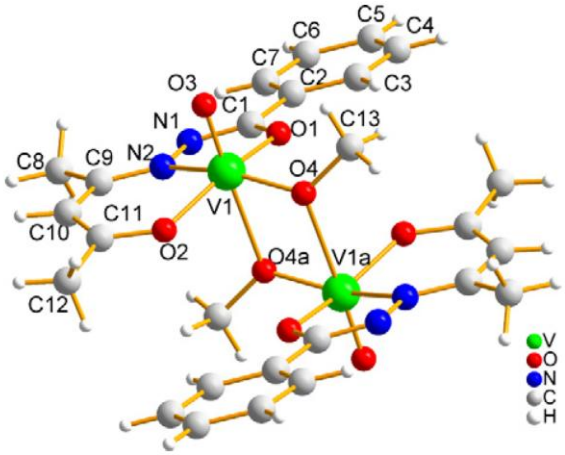

Figure 1.22

M. Chaudhury and group[59] has reported for the first time a general protocol for the synthesis of mixed ligand oxido bridged binuclear oxido vanadium(V) complexes, [LOV(μ-O)VO(Salen)] (**48**-**50**). L_2^- is tridentate biprotic ONO donor Schiff-base ligands (**Figure 1.23**) and H_2Salen = *N*,

N′-bis(salicylidene)-1,2-diaminoethane. Molecular structure and atom-numbering scheme for **49** is shown in **Figure 1.24**. Where one of the vanadium centers in these compounds has an octahedral environment, completed by tetradentate Salen ligand, whereas the remaining center has a square pyramidal geometry, made up of tridentate biprotic type donor combinations. The existence of two different vanadium(V) centers was confirmed by ^{51}V NMR spectroscopy.

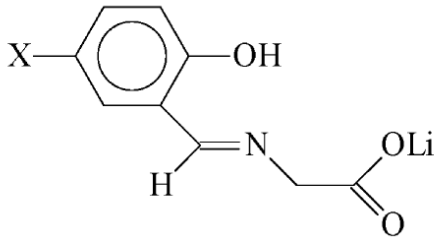

X = H, $LiHL^1$ (**48**)

= Br, $LiHL^2$ (**49**)

= NO_2, $LiHL^3$ (**50**)

Figure 1.23

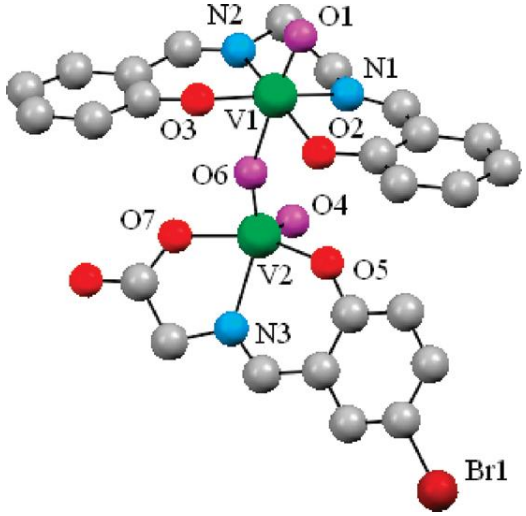

Figure 1.24

M. Chaudhury[60] and group has also reported a new class of divanadium(V) compounds connected by an unsupported hydroxido bridge. Dinuclear oxido vanadium(V) compounds of general formula [$LV^VO(\mu$-OH)OV^VL](PF_6) [H_2L = *N*,*N*′-tert-ethylene bis(salicylideneimine) (H_2Salen) and its derivatives] (**51**–**53**) were obtained by aerial oxidation of $V^{IV}OL$ precursors in THF in the presence of NH_4PF_6. The observation was explained with the possibility that, probably, the oxidized vanadium(V) extracts an OH- ligand from the residual moisture in the solvent and retained as an unsupported hydroxido-bridge between the metal centers of these compounds as confirmed by single-crystal X-ray diffraction analyses. The molecules of **51**–**53** have centrosymmetric structures with each vanadium center having a distorted octahedral geometry. One of the hydroxido bridged compounds (**51**) is shown in **Figure 1.25**.

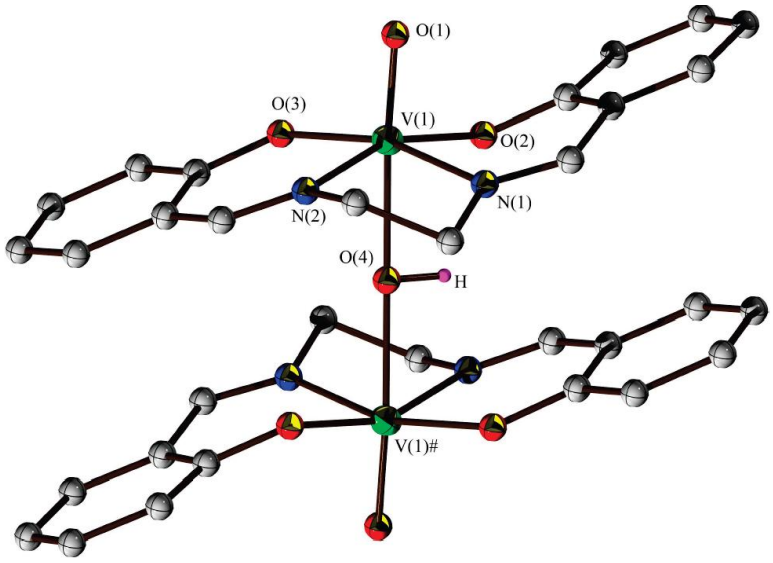

Figure 1.25

1.2. AIM OF THE PRESENT WORK

The primary aim of the present work has been to study the chemistry of vanadium(IV/V) complexes with -ONO / -ONN donor ligand systems. The different ligands that has been used for this purpose are shown below, along with their observed coordination modes.

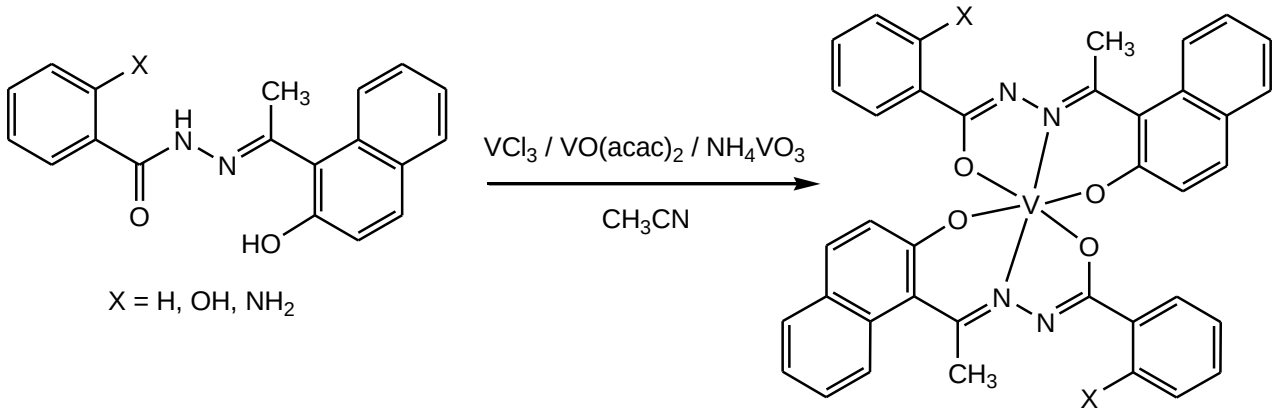

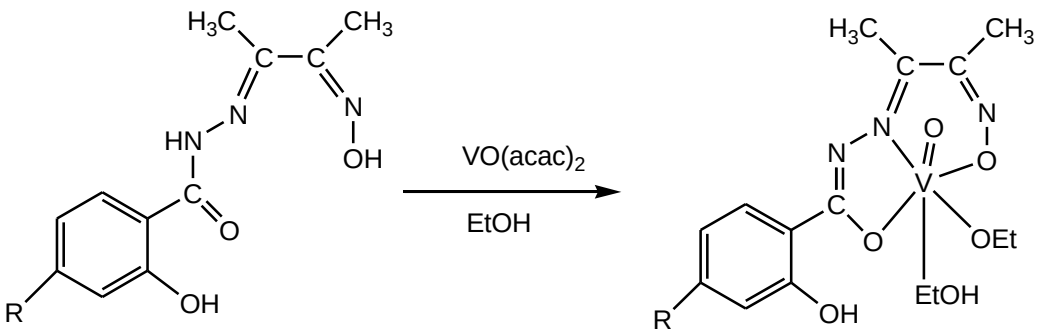

R = H, OCH_3, OH

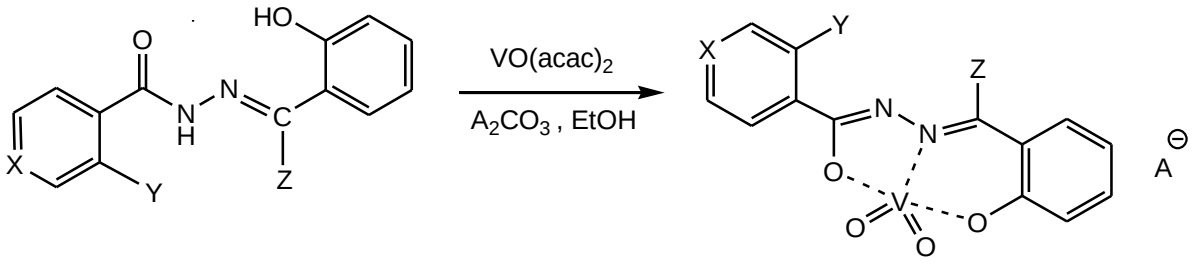

X = C, N

Y = H, OH, NH_2

Z = H, CH_3

$[VO_2L]$ A

A = Li, Na, K, Cs

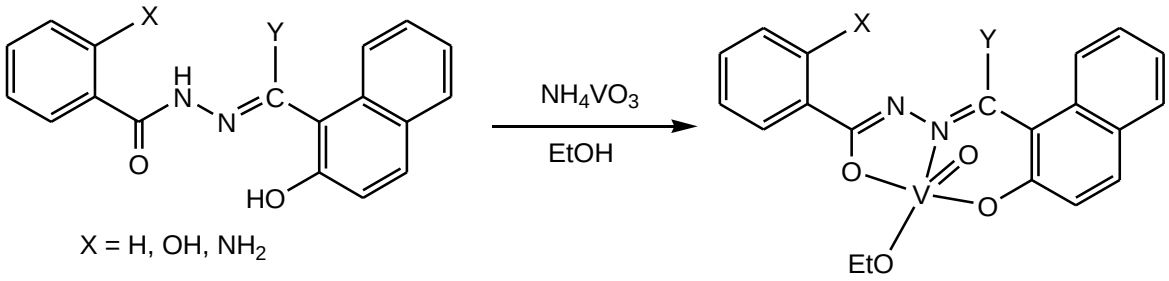

X = H, OH, NH_2

Y = H, CH_3

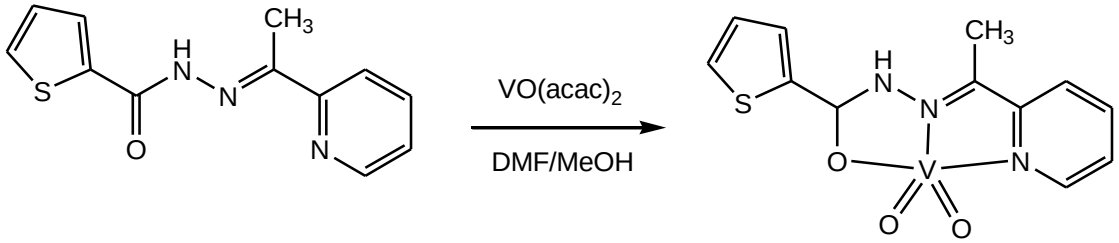

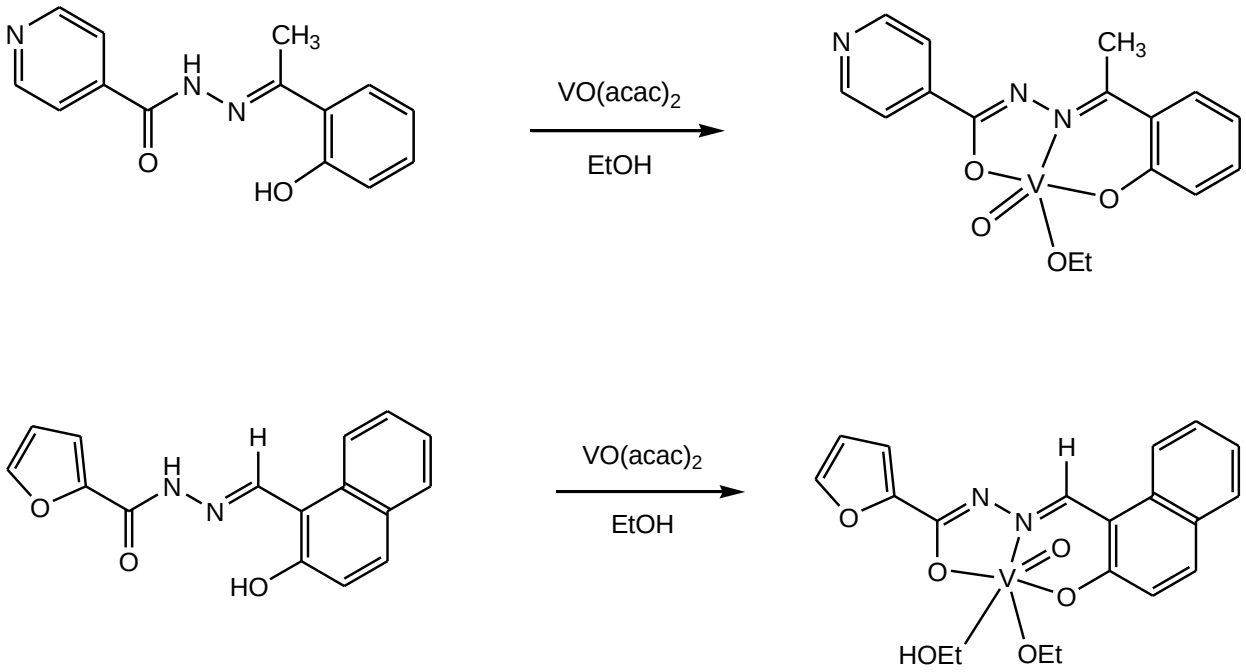
VO(acac)2
EtOH
VO(acac)2
EtOH
CH2Cl2+CH3CN

1.3. THE MAIN OBJECTIVES OF THE PRESENT STUDY

1. To develop some O- and N- donor mono- and binucleating ligand systems, (especially aroylhydrazones and oximes) inspired by the paradigm of biologically and catalytically important vanadium complexes.
2. To develop versatile, new-generation nonoxido vanadium(IV) and mono- and binuclear oxido vanadium(V) systems, for use as reagents in some bio- and catalytic reactions and as model complex of few metalloenzymes. This work uses synthetic and analytical approaches to generate and study vanadium-(IV), and -(V) complexes complexes, relying upon current mechanistic understanding of their mode of action.
3. Study the properties of these metal complexes, such as spectral, magnetic and redox behavior. Solve the X-ray structure of these complexes and develop the structure-reactivity correlation.
4. Exploration of pharmacological studies such as antimicrobial, DNA & protein binding, cleavage, insulin mimetic and antiproliferative activity. Study of catalytic activities particularly oxidation of methyl phenyl sulphide and oxidative bromination of styrene and salicylaldehyde using synthesised metal complexes.

1.4. REFERNCES

(1) (a) Cunha, A. C.; Figueiredo, J. M.; Tributino, J. L. M.; Miranda, A. L. P.; Castro H. C.; Zingali, R. B.; Fraga, C. A. M.; Souza, M. C. B. V.; Ferreira, V. F.; Barreiro, E. *J. Bioorg. Med. Chem.* **2003**, *11*, 2051. (b) Easmon, J.; Puerstinger, G.; Thies, K.-S.; Heinisch, G.; Hofmann, J. *J. Med. Chem.* **2006**, *49*, 6343. (c) Chaston, T. B.; Watts, R. N.; Yuan, J.; Richardson, D. R. *Clin Cancer Res* **2004**, *10*, 7365. (d) Fan, C. D.; Su, H.; Zhao, J.; Zhao, B. X.; Zhang, S. L.; Miao, J. Y. *Eur. J. Med. Chem.* **2010**, *45*, 1438. (e) Dandawate, P.; Khan, E.; Padhye, S.; Gaba, H.; Sinha, S.; Deshpande, J.; Venkateswara S., K.; Khetmalas, M.; Ahmad, A.; Sarkar, F. H. *Bioorg. Med. Chem. Lett.* **2012**, *22*, 3104.

(2) (a) Crans, D. C.; Smee, J. J.; Gaidamauskas, E.; Yang, L. *Chem. Rev.* **2004**, *104*, 849. (b) Rehder, D. *Bioinorganic Vanadium Chemistry;* John Wiley & Sons Ltd.: Chichester, **2008**.

(3) (a) Rehder, D. *Future Med. Chem.* **2012**, *4*, 1823. (b) Pessoa, J. C.; Tomaz, I. *Curr. Med. Chem.* **2010**, *17*, 3701.

(4) (a) Thompson, K. H.; Orvig, C. *Coord. Chem. Rev.* **2001**, *219−221*, 1033. (b) Shechter, Y.; Goldwaser, I.; Mironchik, M.;Fridkin, M.; Gefel, D. *Coord. Chem. Rev.* **2003**, *237*, 3. (c) Sakurai,H.; Yoshikawa, Y.; Yasui, H. *Chem. Soc. Rev.* **2008**, *37*, 2383.

(5) The Seventh International Symposium on the Chemistry and Biological Chemistry of Vanadium. In *Coordination Chemistry Reviews*; Michibata, H., Kanamori, K., Hirao, T., Eds.; Elsevier BV: Amsterdam, The Netherlands, **2011**, *255*, 2149.

(6) Rehder, D. *Bioinorganic Vanadium Chemistry.* John Wiley & Sons, Ltd: Chichester, U. K. **2008**, 1.

(7) Crans, D. C.; Smee, J. J.; Gaidamauskas, E.; Yang, L. *Chem. Rev.* **2004**, *104*, 849.

(8) (a) Vilter, H.; Sigel, H., Sigel, A., Eds.; In *Met. Ions Biol. Syst*. Marcel Dekker: New York, **1995**, *31*, 325. (b) Pecoraro, V. L.; Slebodnick, C.; Hamstra, B. In *Vanadium Compounds: Chemistry, Biochemistry and Therapeutic Applications;* American Chemical Society: Washington, DC, **1998**, *711*, 157.

(9) (a) Robson, R. L.; Eady, R. R.; Richardson, T. H.; Miller, R. W.; Hawkins, M.; Postgate, J. R. *Nature* **1986**, *322*, 388. (b) Eady, R. R. *Coord. Chem. Rev.* **2003**, *237*, 23.

(10) (a) Michibata, H.; Uyama, T.; Kanamori, K. In *Vanadium Compounds: Chemistry, Biochemistry and Therapeutic Applications*; American Chemical Society: Washington, DC, **1998**, *711*, 248. (b) Ueki, T.; Michibata, H. *Coord. Chem. Rev.* **2011**, *255*, 2249.

(11) (a) Ishii, T.; Nakai, I.; Okoshi, K. In *Met. Ions Biol. Syst*.; Sigel, H., Sigel, A., Eds.; Marcel Dekker: New York, **1995**, *31*, 491. (b) Fattorini, D.; Regoli, F. In Vanadium. Biochemical and Molecular Biological Approaches; Michibata, H., Ed.; Springer: Netherlands, **2012**, 3.

(12) Silva, J. A. L.; Silva, J. J. R. F.; Pombeiro, A. J. L. In *Vanadium. Biochemical and Molecular Biological Approaches*; Michibata, H., Ed.; Springer: Netherlands, **2012**, 35.

(13) (a) Butler, A.; Clague, M. J.; Meister, G. E. *Chem. Rev.* **1994**, *94*, 625. (b) Conte, V.; Di Furia, F.; Moro, S. *Tetrahedron Lett.* **1994**, *35*, 7429. (c) de la Rosa, R. I.; Clague, M. J.; Butler, A. *J. Am. Chem. Soc.* **1992**, *114*, 760.

(14) Bayer, E.; Kneifel, H. Z. *Naturforsch* **1972**, *27B*, 207.

(15) Kneifel, H.; Bayer, E. *Angew. Chem. Int. Ed. Engl.* **1973**, *12*, 508.

(16) de, M. A. A. F.; Carrondo, C. T.; Duarte, M. T. L. S.; Pessoa, J. C.; Silva, J. A. L.; Frausto da Silva, J. J. R.; Vaz, M. C. T. A.; Vilas-Boas, L. F. J. *Chem. Commun.* **1988**, 1158.

(17) Armstrong, E. M.; Beddoes, R. L.; Calviou, L. J.; Charnock, J. M.; Collison, D.; Ertok, N.; Naismith, J. H.; Garner, C. D. *J. Am. Chem. Soc.* **1993**, *115*, 807.

(18) Kajiwara, T.; Wagner, R.; Bill, E.; Weyhermüller, T.; Chaudhuri, P. *Dalton Trans*. **2011**, *40*, 12719.

(19) Paine, T. K.; Weyhermüller, T.; Slep, L. D.; Neese, F.; Bill, E.; Bothe, E.; Wieghardt, K.; Chaudhuri, P. *Inorg. Chem.* **2004**, *43*, 7324.

(20) Paine, T. K.; Weyhermueller, T.; Bill, E.; Bothe, E.; Chaudhuri, P. *Eur. J. Inorg. Chem.* **2003**, 4299.

(21) Sutradhar, M.; Mukherjee, G.; Drew, M. G. B.; Ghosh, S. *Inorg. Chem.* **2007**, *46*, 5069.

(22) Morgenstern, B.; Kutzky, B.; Neis, C.; Stucky, S.; Hegetschweiler, K.; Garribba, E.; Micera, G. *Inorg. Chem.* **2007**, *46*, 3903.

(23) (a) Prandtl W.; Hess, L. Z *Anorg. Chem.* **1913**, *82*, 103. (b) Caughlan, C. N.; Smith, H. M; Watenpaugh. K. *Inorg, Chem.* **1966,** *5*, 2131. (c) Scheidt. W. R. *Inorg. Chem.* **1973**, *12*, 1758.

(24) *Rehder,* D, *Angew. Chem. int. Ed. Engl.* **1991**, *30*, 148.

(25) (a) Bradley, D.C. *Chem. Rev.* ***1989****, 89,* 1317. (b) Caulton, K. G.; Hubert-Pfalzgraf, L. G. *Chem. Rev.* **1990**, *90*, 969. (c) Bradley. D. C. *Polyhedron* **1994**, *13*, 111.

(26) Diarnantis, A. A.; Frederiksen,J. M.; Salam, M. A.; Snow, M. R.; Tiekink, E. R. T. *Aust. J. Chem.* **1986**, *39*, 1081.

(27) Nakajima, K.; Kojima. M.; Toriumi, K.; Sano, K.; Fujita, J. *Bull.Chem. Soc. Jpn.* **1989**, *62* 760.

(28) Priebsch, W.; Rehder, D. *Inorg, Chem.* **1990**, *29*, 3013.

(29) Crans, D. C.; Chen, H.; Felty, R. A. *J. Am. Chem. Soc.* **1992**, *114*, 4543.

(30) Dutta,S.;. Mondal, S; Chakravorty, A. *Polyhedron* **1995**, *14*, 1163,

(31) (a) Chen, Q.; Zubieta, J. *Coord Chem. Rev.*, **1992**, *114*, 107. (b) Khan, I. M.; Chen, Q.; Goshorn,D. P.; Hope, H.; Parkin, S.; Zubieta. J. *J. Am. Chem. Soc.* ***1992***, *114*, 3341.

(32) (a) Hirao, T.; Mori, M.; Ohshiro, Y.; *J. Org. Chem.* **1990**, *55*, 358. (b) Hirao, T.; Fujii, T.; Tanaka, T.; Ohshiro, Y. *J. Chem. Soc. Perkin Trans.* **1994**, 3.

(33) (a) Arber, J. M.; de Boer, E.; Garner, C. D.; Hasnain, S. S.; Wever, R. *Biochemistry* **1989**, *28*, 7968. (b) Clague, M. J.; Keder, N. L.; Butler, A. *Inorg. Chem.* **1993**, *32*, 4754. (c) Carrano, C. J.; Mohan, M.; Holmes, S. M.; de la Rosa, R.; Butler, A.; Charnock, J. M.; Garner, C. D. *lnorg. Chem.* **1994**, *33*, 646.

(34) (a) Gresser, M. J.; Tracey, A. S.; in N.D. Chasteen (ed.), *Vanadium in Biological Systems*, Kluwer, Boston, MA, **1990**, 63. (b) Crans Felty, D. C.; Miller, R. A. M. M. *J Am. Chem. Soc.* **1991**, *113*, 265. (c) Hillerns, F.; Olbrich, F.; Behrens, U.; Rehder, D. *Angew. Chem. Int. Ed. Engl.* **1992**, *31*, 447.

(35) (a) Lindquist, R. N.; Lynn, J. L. Jr.; Lienhard, J. E. *J. Am. Chem.Soc.* **1973**, *95*, 8762. (b) Crans, D. C.; Simone, C. M.; Blanchard, J. S. *J. Am. Chem. Soc.* **1992**, *114*, 4926.

(36) Maurya,M. R.; Haldar, C.; Kumar, A.; Kuznetsov, M. L.; Avecillac, F.; Pessoa, J. C. *Dalton Trans.* **2013**, *42*, 11941.

(37) Mandal, T. N.; Roy, S. ; Barik, A. K. ; Gupta, S. ; Butcher, R. J.; Kar, S. K. *Polyhedron* **2008**, *27*, 3267.

(38) Monfared, H. H.; Bikas, R.; Mayer, P. *Inorg. Chim. Acta* **2010**, *363*, 2574.

(39) Sutradhar, M.; Roy Barman, T.; Ghosh, S.; Drew, M. G. B. *J. Mol. Struct.* **2012**, *1020*, 148.

(40) Kurup, M. R. P.; Seena, E. B.; Kuriakose, M. *Struct. Chem.* **2010**, *21*, 599.

(41) Huang,S.-M.; Jiang, F.-F.; Chen, X.-H.; Wu, Q.-J. *Acta Crystallogr., Sect. E*: *Struct. Rep. Online* **2010**, *66*, m456.

(42) Zhou, Y.; Xing, J.; Xiao, L.; Liu, J.; *Z. Kristallogr., New Cryst. Struct.* **2009**, *224*, 177.

(43) Liu, L.; *Acta Crystallogr., Sect. E: Struct. Rep. Online* **2011,** *67*, m482.

(44) Wang, F.-M.; *Acta Crystallogr., Sect. E: Struct. Rep. Online* **2011**, *67*, m433.

(45) Moon, M.; Pyo, M.; Myoung, Y. C.; Ahn, C. II; Lah, M. S. *Inorg. Chem.* **2001**, *40*, 554.
(46) Dinda, R.; Sengupta, P.; Sutradhar, M.; Mak, T. C. W.; Ghosh, S. *Inorg. Chem.* **2008**, *47*, 5634.
(47) Lippold, I.; Görls, H.; Plass, W. *Eur. J. Inorg. Chem.* **2007**, 1487.
(48) Plass, W.; Yozgatli, H. -P. *Z. Anorg. Allg. Chem.* **2003**, *629*, 65.
(49) Maurya, M. R.; Kumar, A.; Ebel, M.; Rehder, D. *Inorg. Chem.* **2006**, *45*, 5924.
(50) Noblı´a, P.; Baran, E. J.; Otero, L.; Draper, P.; Cerecetto, H.; Gonza´lez, M.; Piro, O. E.; Castellano, E. E.; Inohara, T. ; Adachi, Y.; Sakurai, H.; Gambino, D. *Eur. J. Inorg. Chem.* **2004**, 322.
(51) Noblı´a, P.; Vieites, M.; Parajo´n-Costa, B. S.; Baran, E. J.; Cerecetto, H.; Draper, P.; Gonza´lez, M.; Piro, O. E.; Castellano, E. E.; Azqueta, A.; Lo´pez de Cera´in, A.; Monge-Vega, A.; Gambino, D. *J. Inorg. Biochem.* **2005**, *99*, 443.
(52) Dinda, R.; Majhi, P. K.; Sengupta, P.; Pasayat, S.; Ghosh, S.; Favello, L. R.; Mak, T. C. W.; *Polyhedron* **2010**, *29*, 248.
(53) Hazra, A.; Gupta, S.; Roy, S.; Mandal, T. N.; Das, K.; Konar, S.; Jana, A.; Ray, S. ; Butcher, R. J.; Kar, S. K. *Polyhedron* **2011**, *30*, 187.
(54) (a) Wallar, B. J.; Lipscomb, J. D. *Chem. Re*v. **1996**, *96*, 2625. (b) Solomon, E. I.; Brunold, T. C.; Davis, M. I.; Kemsley, J. N.; Lee, S. K.; Lehnert, N.; Neese, F.; Skulan, A. J.; Yang, Y.-S.; Zhou, J. *Chem. Re*v. **2000**, *100*, 235. (c) Tshuva, E. Y.; Lippard, S. J. *Chem. Re*v. **2004**, *104*, 987. (d) Que, L., Jr.; True, A. E. *Prog. Inorg. Chem.* **1990**, *38*, 97. and references therein.
(55) Ferguson-Miller, S.; Babcock, G. T. *Chem. Re*v. **1996**, *96*, 2889.
(56) Kim, E.; Chufán, E. E.; Kamaraj, K.; Karlin, K. D. *Chem. Re*v. **2004**, *104*, 1077.
(57) Mangalam, N. A.; Sivakumar, S.; Sheeja, S. R.; Kurup, M. R. P.; Tiekink, E. R. T. *Inorg. Chim. Acta* **2009**, *362*, 4191.
(58) Monfared, H. H.; Kheirabadi, S.; Lalami, N. A.; Mayer, P. *Polyhedron* **2011**, *30*, 1375.
(59) Chatterjee, P. B.; Bhattacharya, S.; Audhya, A.; Choi, K.-Y.; Endo, A.; Chaudhury, M. *Inorg. Chem.* **2008**, *47*, 4891.
(60) Chatterjee, P. B.; Mandal, D.; Audhya, A.; Choi, K.-Y.; Endo, A.; Chaudhury, M. *Inorg. Chem.* **2008**, *47*, 3709.

Chapter 2

Highly stable hexacoordinated nonoxido vanadium(IV) complexes of sterically constrained ligands: Syntheses, structure and study of antiproliferative and insulin mimetic activity

Chapter 2

Highly stable hexacoordinated nonoxido vanadium(IV) complexes of sterically constrained ligands: Syntheses, structure and study of antiproliferative and insulin mimetic activity

ABSTRACT

Three highly stable, hexacoordinated nonoxido vanadium(IV), $V^{IV}(L)_2$, complexes (**1**−**3**) have been isolated and structurally characterized with tridentate aroylhydrazonates containing ONO donor atoms. All the complexes are stable in the open air in the solid state as well as in solution, a phenomenon rarely observed in nonoxido vanadium(IV) complexes. The complexes have good solubility in organic solvents, permitting electrochemical and various spectroscopic investigations. The existence of nonoxido vanadium(IV) complexes was confirmed by elemental analysis, ESI mass spectroscopy, cyclic voltammetry, EPR and magnetic susceptibility measurements. X-ray crystallography showed the N_2O_4 donor set to define a trigonal prismatic geometry in each case. All the complexes show *in vitro* insulin mimetic activity against insulin responsive L6 myoblast cells, with complex **3** being the most potent which is comparable to insulin at the complex concentration of 4 μM, while the others have moderate insulin mimetic activity. In addition, the *in vitro* antiproliferative activity of complexes **1**–**3** against HeLa cell line was assayed. The cytotoxicity of the complexes is affected by the various functional groups attached to the bezoylhydrazone derivative and **2** showed considerable antiproliferative activity compared to most commonly use chemotherapeutic drugs.

2.1. INTRODUCTION

Vanadium attracts increasing interest in biochemistry.[1,2] Of the numerous reported effects of vanadium on organisms, its stimulatory effect on the growth of algae and plants,[3] the inhibitory action of vanadate(V) on Na, K-ATPase,[4] the presence of vanadium at the active site of certain enzymes, including haloperoxidases in sea algae and lichens[5] and some nitrogenases in nitrogen-fixing *Azotobacter*[6] are especially worth mentioning. Moreover, inorganic vanadyl and vanadate, as well as some vanadium(IV) and (V) complexes, are potent insulin mimics and as such may find use as alternatives to insulin in the treatment of diabetes.[7] The discovery of the *in vivo* insulin mimesis *per os* of oxido vanadates(V)[8], the oxido vanadium(IV) precursor, vanadyl sulfate,[9] and the much more potent bis(maltolato)-oxido vanadium(IV) (BMOV)[10] stimulates the search for vanadium complexes which may have application in the treatment of type II diabetes.[11,12] Different approaches have been attempted to develop more potent and orally active vanadium-containing insulin enhancing agents.[13] Although the said complexes have shown pharmacological advantages compared to the uncomplexed $VOSO_4$, further improvement in ligand design is needed, focusing on identifying new vanadium complexes with increased potency and decreased toxicity.[14]

In the past few years new metal complexes have been identified as a very promising class of anticancer active compounds.[15–22] Some vanadium complexes, particularly, peroxido vanadates(V) and bis(cyclopentadienyl)vanadium(IV) complexes[23] have been found to possess antitumor activity. Recently, some new type of oxido vanadium(IV) complexes, mono(phenanthroline)oxido vanadium(IV) $[VO(phen)(H_2O)_2]^{2+}$ [24] and bis(1,10-phenanthroline)sulfatooxido vanadium(IV) $[VO(SO_4)(phen)_2]$[25] were reported to exhibit potent antitumor activity against the human nasopharyngeal carcinoma-KB cells line and clonogenic NALM-6 cells line, respectively. Dong et al. have reported the cytotoxic activity of some bis(phenanthroline)oxido vanadium(IV) complexes against the human leukemic NALM-6 cell line.[25] Noleto and co-workers described the cytotoxic activity of some GALMAN-A:$VO^{2+/}VO^{3+}$ and GALMAN-B:$VO^{2+/}VO^{3+}$ complexes against HeLa cells.[26] Very recently, Sasmal et al. have reported the photocytotoxicity of the oxido vanadium(IV) complex $[VO(L)(B)]Cl_2$, where L is bis(2-benzimidazolylmethyl)amine and B is dipyrido[3,2-a:2',3'-c]phenazine against the adenocarcinoma A549 cell line.[27]

However, in contrast to the well known vanadium(IV)/(V) complexes containing VO^{2+} or VO^{3+} units,[28] only very few octahedral nonoxido V^{IV} and V^{V} complexes, the so-called 'bare' complexes, have been isolated and structurally characterized.[29] Amavadin,[30] a compound isolated from the mushroom *Amanita muscaria,* has been shown to contain an octacoordinated V^{4+} ion[31] without oxido ligands but such nonoxido vanadium species are still scarce.[29]

On the other hand, hydrazones, –NH–N=CRR' (R and R′ = H, alkyl, aryl), are versatile ligands due to their applications in the field of analytical[32] and medicinal chemistry.[33] Hydrazone moieties are the most important pharmacophoric cores of several anticancer, antiinflammatory, antinociceptive, and antiplatelet drugs.[34] In the context of the present study it is relevant to mention that although the chemistry of oxido vanadium(IV)-aroylhydrazone complexes is well developed,[35] far less information is available for model nonoxido complexes,[29a,p] particularly concerning their biological properties.

We have been studying the chemistry of oxido-metal complexes including those of vanadium in O–N containing donor environments[36] along with electro generation of mixed-valence divanadium(IV,V) complexes,[36a,b] in this chapter we report the syntheses and X–ray crystal structures of three nonoxido vanadium(IV) complexes containing aroylhydrazones along with special reference to their insulin mimetic and antiproliferative activities. These nonoxido V^{IV} complexes were fully characterized by various physicochemical techniques like IR, EPR, ESI mass, electronic spectroscopy, magnetic susceptibility studies and electrochemical investigations.

2.2. EXPERIMENTAL SECTION

2.2.1. General Methods and Materials. All chemicals were purchased from commercial sources and used without further purification. $[VO(acac)_2]$ was prepared as described in the literature.[37] Reagent grade solvents were dried and distilled prior to use. L6 myoblast cells derived from a rat were procured from NCCS, Pune, India. Penicillin, streptomycin, DMEM, fetal bovine serum and insulin were purchased from Invitrogen (San Diago, CA, USA), and the glucose estimation kit from Randox. MTT (3-[4,5-Dimethylthiazol-2-yl]-2,5-diphenyltetrazolium) and DAPI (4′,6-diamidino-2-phenylindole dihydrochloride) were purchased from Sigma Aldrich (USA). Minimal essential medium (MEM) was purchased from Gibco, India. Elemental analyses were performed on a Vario ELcube CHNS Elemental analyzer. IR spectra were recorded on a Perkin-Elmer Spectrum RXI spectrophotometer. ^{1}H and ^{13}C NMR spectra were recorded on a Bruker Ultrashield 400 MHz spectrometer using $SiMe_4$ as an internal standard. Electronic spectra were recorded on a Lamda25, PerkinElmer spectrophotometer. Mass spectra were obtained on a SQ-300 MS instrument operating in ESI mode. DC magnetic susceptibility measurements were carried out on a Vibrating Sample magnetometer, PPMS (Physical Property Measurement System, Quantum Design, USA) in the temperature range 2−300 K with an applied field of 1 T. Electrochemical data were collected using a PAR electrochemical analyzer and a PC-controlled Potentiostat/Galvanostat (PAR 273A) at 298 K in a dry nitrogen atmosphere. Cyclic voltammetry experiments were carried out with Pt working and auxiliary electrodes, Ag/AgCl as the reference electrode and TEAP as the supporting electrolyte. X-band EPR measurements were performed on a JEOL JES-FA 200 and Bruker EMX EPR Spectrometer.

2.2.2. Synthesis of Ligands (H_2L^{1-3}). Schiff base ligands, anthranylhydrazone of 2-hydroxy-1-acetonaphthone (H_2L^1), salicylhydrazone of 2-hydroxy-1-acetonaphthone (H_2L^2) and benzoylhydrazone of 2-hydroxy-1-acetonaphthone (H_2L^3), were prepared by the condensation of 2-hydroxy-1-acetonapthone and the respective acidhydrazide in equimolar ratio in ethanol by a standard procedure.[38] The resulting white compounds were filtered, washed with ethanol and dried over fused $CaCl_2$. Elemental analysis results, NMR (^{1}H and ^{13}C) and IR data for all of these verified their preparation.

H_2L^1. Yield: 64%. Anal. Calcd. for $C_{19}H_{17}N_3O_2$: C, 71.46; H, 5.36; N, 13.16. Found: C, 71.48; H, 5.37; N, 13.14. IR (KBr pellet, cm^{-1}): 3473 ν(O–H); 3410 $\nu(NH_2)_s$; 3329 $\nu(NH_2)_{as}$; 3221 ν(NH); 1663 ν(C=O); 1553 ν(C=N). ^{1}H NMR (400 MHz, DMSO-d_6): δ 10.35 (s, 1H, naphthyl–OH), 9.17 (s, 1H, NH), 7.91–6.23 (m, 10H, Aromatic), 6.05 (s, 2H, NH_2), 2.35 (s, 3H, CH_3). ^{13}C NMR (100 MHz, DMSO-d_6): δ 153.98 (CO–N), 152.47 (N=C(Me)), 152.36–113.59 (16C, aromatic), 24.15 (–CH_3).

H_2L^2. Yield: 60%. Anal. Calcd. for $C_{19}H_{16}N_2O_3$: C, 71.24; H, 5.03; N, 8.74. Found: C, 71.28; H, 5.01; N, 8.71. IR (KBr pellet, cm^{-1}): 3542 ν(O–H); 3113 ν(N–H); 1661 ν(C=O); 1555 ν(C=N). ^{1}H NMR (400 MHz, DMSO-d_6): δ 10.84 (s, 1H, phenyl–OH), 10.37 (s, 1H, NH), 10.21 (s, 1H, naphthyl–OH), 7.94–6.69 (m, 10H, Aromatic), 2.32 (s, 3H, CH_3). ^{13}C NMR (100 MHz, DMSO-d_6): δ 161.19 (CO–N), 155.89 (N=C(Me)), 152.50–114.52 (16C, aromatic), 24.09 (–CH_3).

H_2L^3. Yield: 58%. Anal. Calcd. for $C_{19}H_{16}N_2O_2$: C, 74.98; H, 5.29; N, 9.20. Found: C, 74.96; H, 5.32; N, 9.21. IR (KBr pellet, cm^{-1}): 3337 ν(O–H); 3071 ν(N–H); 1659 ν(C=O); 1573 ν(C=N). ^{1}H NMR (400 MHz, DMSO-d_6): δ 10.31 (s, 1H, naphthyl–OH), 9.55 (s, 1H, NH), 7.91–7.27 (m, 11H, Aromatic), 2.34 (s, 3H, CH_3).^{13}C NMR (100 MHz, DMSO-d_6): δ 153.71 (CO–N), 152.63 (N=C(Me)), 152.12–113.74 (16C, aromatic), 24.30 (–CH_3).

2.2.3. Synthesis of Complexes $[V^{IV}(L^{1–3})_2]$ (1–3). A general synthetic procedure taking $[VO(acac)_2]$ as representative metal precursor is described below:

$[VO(acac)_2]$ (0.5 mmol) was added to a hot solution of appropriate ligand $H_2L^{1\text{-}3}$ (1.0 mmol) in EtOH (20 mL), the color changed instantly to greenish black. After 3 h of stirring, black crystals were obtained from reaction mixture, which were filtered off, washed thoroughly with ethanol and dried. Some crystals are of diffraction quality and were used directly for X-ray structure determination using single crystal X-ray diffractometer.

$[V^{IV}(L^1)_2]$ (1). Yield: 66%. Anal. Calcd. for $C_{38}H_{30}N_6O_4V$: C, 66.57; H, 4.41; N, 12.26. Found: C, 66.55; H, 4.37; N, 12.29. IR (KBr pellet, cm^{-1}): 3298 $\nu(NH_2)_s$; 3043 $\nu(NH_2)_{as}$; 1589 ν(C=N); 1256 $\nu(C–O)_{enolic}$; 1048 ν(N–N). ESI-MS (CH_2Cl_2): *m/z* 708.49 (53%, $[M + Na]^+$); ESI-MS ($CH_3CN + CH_2Cl_2$) (19:1): *m/z* 708.12 (100%, $[M + Na]^+$); ESI-MS (MeOH + DMF) (19:1): *m/z* 708.21 (100%, $[M + Na]^+$).

$[V^{IV}(L^2)_2]$ (2). Yield: 65%. Anal. Calcd. for $C_{38}H_{28}N_4O_6V$: C, 66.37; H, 4.10; N, 8.15. Found: C, 66.40; H, 4.07; N, 8.17. IR (KBr pellet, cm^{-1}): 3427 ν(O–H); 1591 ν(C=N); 1250 $\nu(C–O)_{enolic}$; 1047 ν(N–N). ESI-MS (CH_2Cl_2): *m/z* 710.10 (50%, $[M + Na]^+$); ESI-MS ($CH_3CN + CH_2Cl_2$) (19:1): *m/z* 710.10 (100%, $[M + Na]^+$); ESI-MS (MeOH + DMF) (19:1): *m/z* 710.20 (100%, $[M + Na]^+$).

$[V^{IV}(L^3)_2]$ (3). Yield: 68%. Anal. Calcd. for $C_{38}H_{28}N_4O_4V$: C, 69.62; H, 4.30; N, 8.54. Found: C, 69.58; H, 4.31; N, 8.57. IR (KBr pellet, cm^{-1}): 1598 ν(C=N); 1243 $\nu(C–O)_{enolic}$; 1046 ν(N–N). ESI-MS (CH_2Cl_2): *m/z* 655.25 (90.27%, $[M]^+$); ESI-MS ($CH_3CN + CH_2Cl_2$) (19:1): *m/z* 678.27 (100%, $[M + Na]^+$); ESI-MS (MeOH + DMF) (19:1): *m/z* 678.25 (100%, $[M + Na]^+$).

Alternatively, these complexes can also be synthesized from the starting materials like VCl_3, $VOSO_4$ and NH_4VO_3 as shown in **Scheme 2.1**. The spectral data matched well with the one reported above.

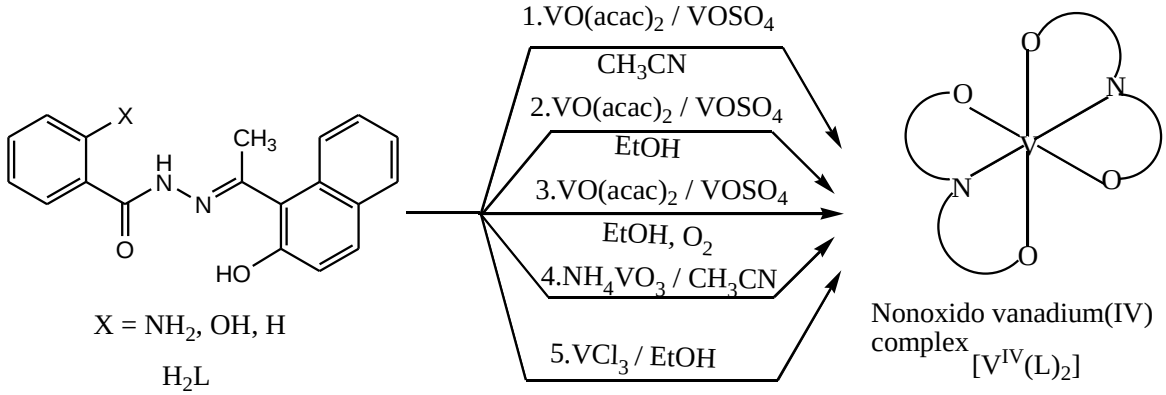

X	Ligand	Nonoxido vanadium(IV) complex
NH_2	H_2L^1	$[V^{IV}(L^1)_2]$ (**1**)
OH	H_2L^2	$[V^{IV}(L^2)_2]$ (**2**)
H	H_2L^3	$[V^{IV}(L^3)_2]$ (**3**)

Scheme 2.1. Schematic diagram of various pathways through which the hexacoordinated $V^{IV}(L)_2$ nonoxido vanadium(IV) (**1**-**3**) complex were synthesized.

2.2.4. X-ray Crystallography. For all three complexes (**1**–**3**) the black crystals were obtained from reaction mixture. Single crystal X-ray diffraction measurements were performed on a Bruker SMART CCD diffractometer employing graphite-monochromated Mo Kα radiation (λ = 0.71073) so that θ_{max} = 27.5°. Data collection and reduction were by standard methods,[39] and absorption corrections were applied based on multiple scans.[40] The structures were solved by direct methods[41] and refined by full-matrix least-squares on F^2.[41] All non-hydrogen atoms were refined anisotropically, C-bound hydrogen atoms were included in the riding model approximation, and O–H and N–H H atoms were refined with the distance constraint 0.82±0.01 and 0.86±0.01 Å, respectively. In the final cycles of each refinement, a weighting scheme of the form $w = 1/[\sigma^2(F_o^2) + aP^2]$, where $P = (F_o^2 + 2F_c^2)/3$, was introduced. The final difference maps were featureless. Molecular structure diagrams of **1**–**3** were drawn with ORTEP-3 for Windows[42a] at the 50% probability level, the overlay diagram of **1**–**3** was drawn with QMol[42b] while remaining crystallographic diagrams were drawn with DIAMOND.[42c] A summary of crystal data and refinement details for **1**–**3** is provided in **Table 2.1.**

Crystallographic data in CIF format for the structures have been deposited in the Cambridge Crystallographic Data Centre; CCDC 928538 for **1**, CCDC 928539 for **2** and CCDC 928540 for **3**.

Table 2.1 Crystal data and refinement details for $[V^{IV}(L^{1-3})_2]$ (1–3)

Parameter	**1**	**2**	**3**
Formula	$C_{38}H_{30}N_6O_4V$	$C_{38}H_{28}N_4O_6V$	$C_{38}H_{28}N_4O_4V$
Formula weight	685.62	687.58	655.58
Crystal habit, color	rectangle, red	block, red	hexagon, dark green
Crystal size, mm	0.06 x 0.07 x 0.17	0.07 x 0.11 x 0.13	0.05 x 0.16 x 0.26
Crystal system	monoclinic	monoclinic	monoclinic
Space group	$P2_1/n$	$P2_1/n$	$P2_1/c$
a, Å	14.608(6)	14.711(4)	13.807(7)
b, Å	14.846(6)	14.697(4)	23.851(12)
c, Å	14.976(6)	15.068(4)	10.249(5)
β, º	97.704(8)	96.590(4)	106.571(10)
V, Å^3	3219(2)	3236.3(15)	3235(3)
Z	4	4	4
Density, g/cm^3 (calculated)	1.415	1.411	1.346
μ, cm^{-1}	0.361	0.362	0.354
Reflections collected	36356	35724	26859
Independent reflections	7362	7419	7320
Reflecitons with $I \geq 2\sigma(I)$	3686	3887	2745
R (observed data)	0.062	0.071	0.074
a in wghting scheme	0.058	0.065	0.064
R_w (all data)	0.158	0.174	0.196
Largest diff. peak and hole e Å^{-3}	0.33 and -0.28	0.34 and -0.28	0.30 and -0.38
CCDC deposition number	928538	928539	928540

2.2.5. In Vitro Insulin Mimetic Activity. L6 myoblast were cultured in DMEM containing 10% FBS, penicillin (100 U/ml) and streptomycin (100 µg/ml) in a humidified 5% CO_2 incubator at 37°C. To differentiate myotubes, the myoblast cells ($5x10^4$) were seeded in 24 well plates in DMEM containing 2% FBS. The myoblast cells ($5x10^4$) were grown for 11 days in 0.4 ml of 2% FBS/DMEM to allow the formation of myotubes. The medium was changed every 2 days. On the 11th day, the cells were washed and incubated in Kreb's bicarbonate buffer (KRBB) for 2 h. Myotubes were then further cultured in KRBB containing 25 mM glucose along with 1, 2 and 4 µM of vanadium complexes (**1**–**3**) and $VO(acac)_2$ for 4 h. The insulin (2 µM) was taken as positive control.[43] The residual glucose in the buffer aliquots remaining in each well after 4 h was estimated using the hexokiase method by Randox autoanalyser.

2.2.6. Cytotoxic Assay. Human cervical cells HeLa were obtained from National Centre of Cell Science (NCCS), Pune, India and were maintained in minimal essential medium supplemented with 10% fetal bovine serum, penicillin-streptomycin solution and incubated at 37°C in 5% CO_2 and 95% humidified incubator. HeLa cells were harvested from maintenance cultures in logarithmic phase, after counting in a hemocytometer using trypan blue solution. The cell concentration was adjusted to $5x10^4$ cells/ml and the cells were plated in a 96 well flat bottom culture plate and incubated for 72 h with various concentrations of the test complexes which were dissolved in a 90% (v/v) DMF solution. The effect of the drugs on the cancer cell viability was studied using MTT dye reduction assay by measuring the optical density at 595 nm using micro-plate reader spectrophotometer (Perkin-Elmer 2030).[44] DMF solutions that was used to dissolve the drugs was used in control group treatment.

2.2.7. Nuclear Staining. Nuclear staining using DAPI stain was performed according to the method previously described.[45] Briefly, HeLa cells either treated or untreated with test compounds were smeared on a clean glass slide, cells were fixed with 3.7% formaldehyde for 15 minutes, permeabilized with 0.1% Triton X-100 and stained with 1 µg/ml DAPI for 5 min at 37 °C. The cells were then washed with PBS and examined by fluorescence microscopy (Olympus IX 71) to ascertain any condensation or fragmentation of the nuclei indicating cells undergoing apoptosis.

2.3. RESULT AND DISSCUSSION

2.3.1. Synthesis. The various pathways through which the nonoxido vanadium(IV) hexacoordinated $[V^{IV}(L)_2]$ complexes were obtained is shown in **Scheme 2.1**. Reactions of aroylhydrazones ($H_2L^{1\text{-}3}$) with $[VO(acac)_2]$ or $VOSO_4$ in acetonitrile or ethanol lead to the formation of monomeric bis(tridentate)-vanadium(IV) complexes $[V^{IV}(L^{1\text{-}3})_2]$ (**1**–**3**). The reactions are clean, affording large quantities of pure crystalline products in good yield (~ 70%). These compounds are highly soluble in CH_2Cl_2, DMF and DMSO and sparingly soluble in MeOH, EtOH and CH_3CN.

Alternatively, these nonoxido V^{IV} complexes can also be isolated directly by the reaction of aroylhydrazones with various oxido vanadium(V), and vanadium(III) compounds as starting materials. The formation of $[V^{IV}(L)_2]$ complexes from oxido vanadium(V), NH_4VO_3, and vanadium(III), VCl_3, species probably involves a one step reduction from vanadium(V) to vanadium(IV), and a one step oxidation from vanadium(III) to vanadium(IV) in open air, respectively, followed by oxido abstraction from the oxido vanadium(IV) species generated *in situ*. It is noteworthy that the entire above synthetic route can be carried out in laboratory grade ethanol or acetonitrile under ambient conditions. The reactions do not require dry solvent, the presence of base, or an inert atmosphere, which is unusual compared to previous reports.[29c,e,o,x, 46]

Complexes **1**–**3** are highly stable both in the solid state and in solution. For example, a solution of **1** in different coordinating or noncoordinating solvents does not give any oxidized product (no color change, no oxido-V^{IV}, no oxido-V^{V}, as confirmed by ESI mass, time dependent UV-Vis and EPR spectroscopy) after exposure to aerial oxygen for 3–4 days or even purging oxygen gas into its solution, a rather uncommon observation for nonoxido vanadium(IV) complexes. Again, to check the stability of these nonoxido vanadium(IV) species, all three complexes (**1**-**3**) were dissolved and recovered back from solvent mixture (MeOH + DMF) (9:1) after keeping three days in solution. The isolated solid products were characterized by different spectroscopic techniques (**Figures 2.1-2.3**). The results matched well regardless of having been recorded using original compound or isolated compound from solvent. The absence of vanadium oxido (V=O) peak in IR spectrum, no disappearance of low energy transition peaks in UV-Vis spectrum and time dependent EPR clearly discard the formation of corresponding V(V) in solution. The

stability of the complexes may be due to the simultaneous removal of the oxido group, complete charge neutralization as well as the formation of six strong covalent bonds at the V^{4+} center from the hard donor atoms N and O, which possibly precludes the approach of a reagent species within the reaction sphere of the well-protected V^{4+} center. Also, the rigidity and steric bulk of the ligands do not permit the formation of the square pyramidal pentacoordinated [V^{V}OL(OR)] complex so familiar in vanadium chemistry, in which the terminal oxygen is in an axial position and the tridentate ligand occupies the equatorial plane.

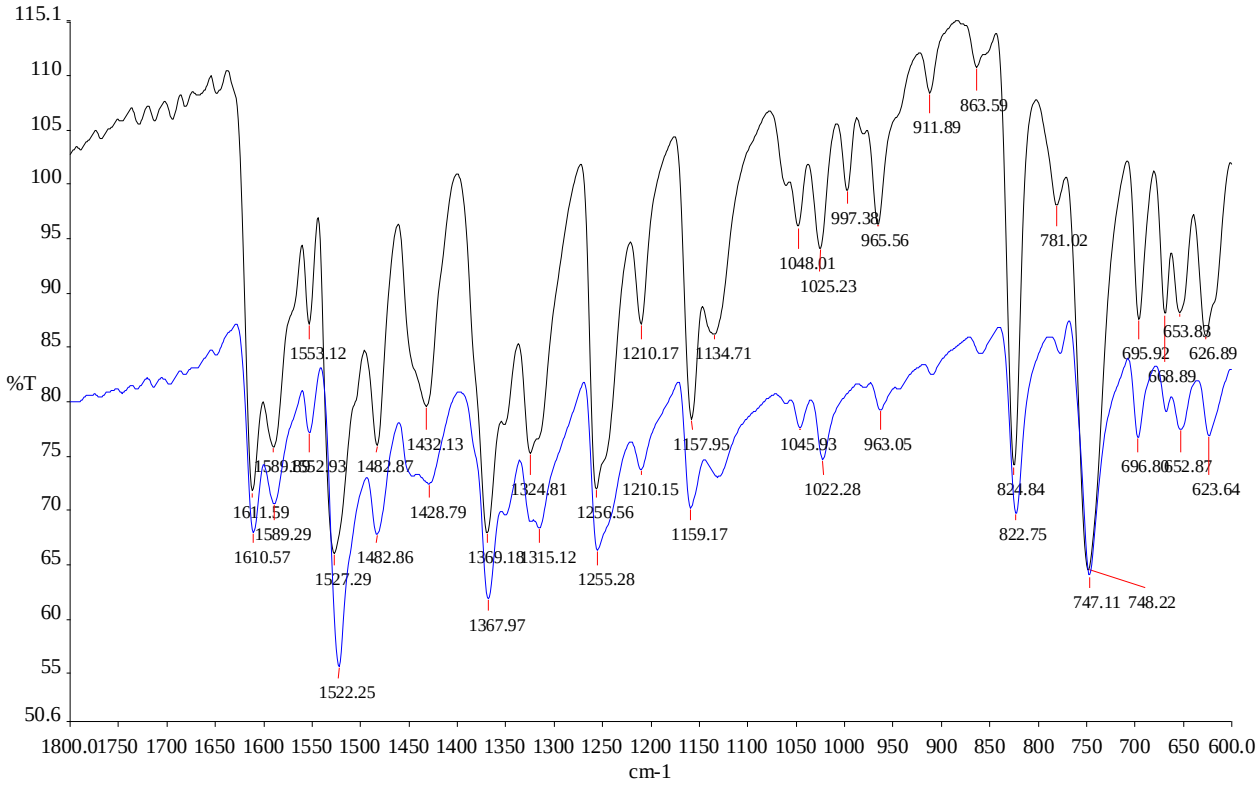

Black- IR spectra of Complex **1** (original crystal)

Blue- IR spectra of Compound **1'** isolated from DMF + MeOH

Figure 2.1. IR spectra of complex **1** and isolated compound **1'** in the range 1800–600 cm^{-1} {compound **1'** is isolated by dissolving complex **1** in solvent mixture (MeOH + DMF) (9:1) after keeping for three days}.

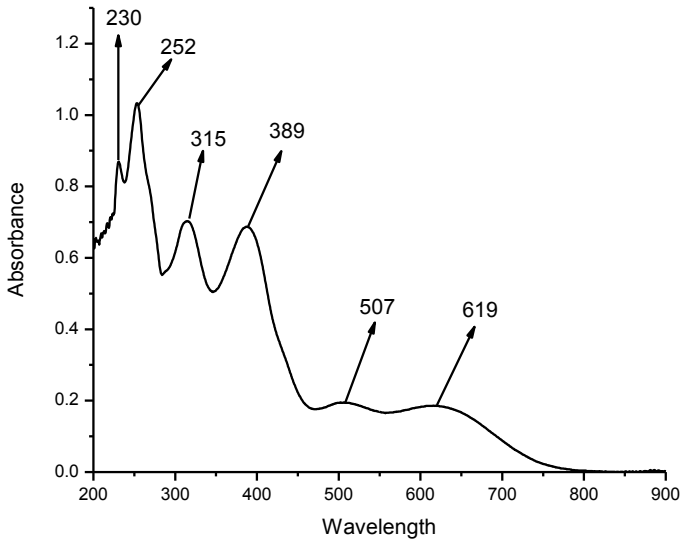

Figure 2.2. UV-Vis spectra of compound **2'** (1.75 X 10^{-5}M) in CH_2Cl_2 as solvent){compound **2'** is isolated by dissolving complex **2** in solvent mixture (MeOH + DMF) (9:1) after keeping for three days}.

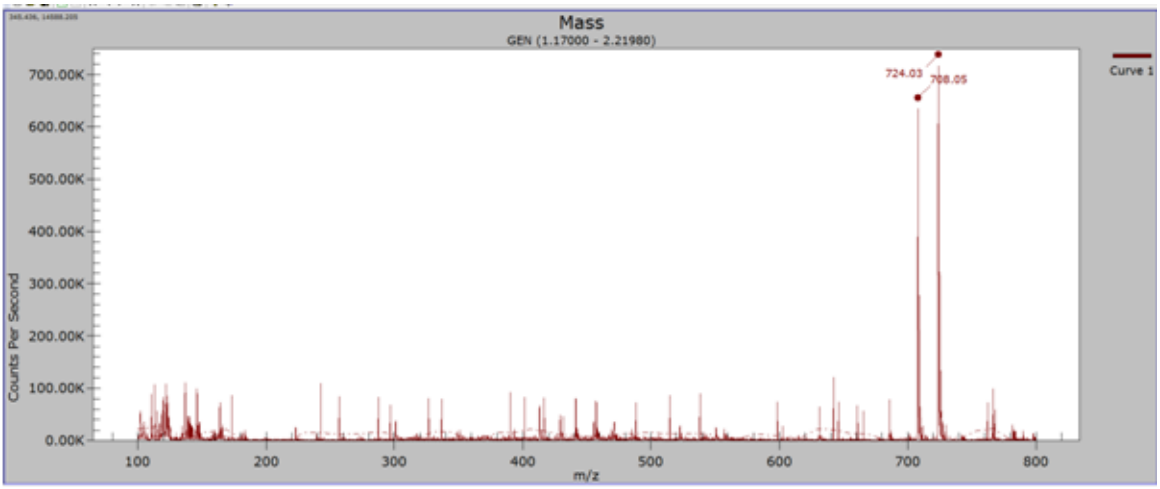

Figure 2.3. ESI mass spectra of isolated compound **1'** in (CH_3CN + CH_2Cl_2 (19:1) {compound **1'** is isolated by dissolving complex **1** in (MeOH + DMF) (9:1) after keeping for three days}.

2.3.2. Structure Description. Crystals were obtained for each of **1**–**3** and their crystal structures determined. Molecular structures are illustrated in **Figure 2.4** and selected geometric parameters are collected in **Table 2.2**. In **1**, the central V atom is coordinated by two dinegative, NO_2 coordinating hydrazone ligands forming five membered CN_2OV and six membered C_3NOV chelate rings. The five membered rings have envelope conformations with the V atom lying 0.215(5) and 0.301(5) Å above the plane of the remaining atoms of the O1 and O3 chelate rings (r.m.s. deviation = 0.0061 Å for each). Each five membered ring is virtually coplanar to the attached benzene ring (dihedral angles between least squares planes = 4.17(16) and 7.04(15)º, respectively) which allows for the formation of intramolecular N–H…N hydrogen bonds between an amino-H and noncoordinating azo N atoms, **Table 2.2**. The six membered chelate rings exhibit significantly greater deviations from planarity and may to a first approximation be described as having an envelope conformation with the V atom lying well out of the plane, i.e., 0.963(3) Å, defined by the remaining five atoms (r.m.s. deviation = 0.0949 Å); the equivalent parameters for the O4 chelate ring are 0.904(3) and 0.1200 Å, respectively. This distortion enables the V atom to exist within a N_2O_4 donor set that approximates a trigonal prism. In this description, the two triangular faces are defined by the (O1, O4, N4) and (O2, O3, N2) atoms. The dihedral angle between the trigonal faces is 2.67(9)º and the twist of one face relative to the other is 13.5º, *cf*., 0º for an ideal trigonal prism and 60º for an ideal octahedron. The structure of **2** is isostructural with **1** and presents very similar coordination geometry.

For the two five membered rings in **2**, the V atom lies 0.196(5) and 0.270(5) Å above the plane defined by the remaining four atoms (r.m.s. deviation = 0.0033 and 0.0061 Å for the O1 and O3 rings, respectively). The adjacent benzene ring is approximately coplanar to the respective five membered ring forming dihedral angles of 1.81(17) and 4.88(17)º; this arrangement enables intramolecular O–H…N hydrogen bonding, **Table 2.2**. Significant distortions are again evident for the six membered chelate rings with the V atom lying 0.960(4) Å out of the plane through the remaining five atoms of the O2 chelate ring (r.m.s. deviation = 0.0943 Å); the equivalent values for the O4 chelate are 0.926(4) and 0.1181 Å, respectively. In terms of coordination geometry, the dihedral angle between the trigonal faces is 2.00(10)º and the twist angle is 10.1º. While not isostructural with **1** and **2**, the structure of **3** presents all the hallmarks just described with the exception of the intramolecular hydrogen bonding.

For the five membered rings rings in **3**, the V atom lies 0.215(6) and 0.252(7) Å out of the planes of the O1 (r.m.s. deviation = 0.0087 Å) and O3 chelate (0.0139 Å) rings, confirming the flattened envelope conformations. Despite the lack of an intramolecular hydrogen bond, as for **1** and **2**, the adjacent five and six membered chelate and benzene rings are coplanar forming dihedral angles of 4.9(3) and 10.4(3)º. For the six membered chelate rings, the V atom lies 0.975(4) Å out of the plane of the remaining atoms (r.m.s. deviation = 0.1064 Å) for the O2 chelate ring; 0.981(5) and 0.1064 Å for the O4 chelate ring. Finally, the dihedral angle between the trigonal face is 2.85(12)º and the twist angle is 10.0º.

The overlap diagram **Figure 2.4d**, where the V,O1,O2 atoms have been superimposed highlights the similarity in the molecular structures of **1**–**3**, there being only minor differences in the orientations of the peripheral substituents. This homogeneity is reflected in the geometric parameters collated in **Table 2.2**, with no significant differences apparent in the bond lengths about the three V atoms. In the same way, no trends are discerned from the bond angles indicating that the amino (**1**) and hydroxyl (**2**) groups do not exert an influence on the molecular structure even though they form intramolecular hydrogen bonds with the noncoordinating azo N atoms.

In the crystal structure of **1**, no specific intermolecular contacts were identified as being significant employing the distance criteria established in PLATON,[47] implying the second amino-H atom does not form a significant intermolecular contact. As shown in **Figure 2.5**, molecules are arranged in rows along the *b*-axis and are surrounded by molecules forming hydrophobic contacts. In isostructural **2**, a similar packing is observed but in this case a C–H…π, edge to face, interaction is formed between methyl-H and the C1-benzene ring of centro symmetrically related molecules to form dimeric aggregates, for details see **Figure 2.6**. As for **1**, no specific intermolecular interactions are noted in the crystal structure of **3**, **Figure 2.7**. A macroscopic difference in the global crystal packing is apparent as molecules in **3** can be described as aggregating in the *bc*-plane with the flat layers stacking along the *a*-axis. By contrast, molecules in each of **1** and **2** aggregate in a zigzag pattern parallel to the *ab*-plane and stack along the *c*-axis.

Table 2.2 Selected geometric parameters (Å, º) for $[V^{IV}(L^{1-3})_2]$ (1–3)

Parameter	**1**	**2**	**3**
Coordination geometry			
V-O1	1.903(2)	1.919(2)	1.903(3)
V-O2	1.895(2)	1.902(2)	1.906(3)
V-O3	1.891(2)	1.908(2)	1.894(3)
V-O4	1.878(2)	1.888(2)	1.900(3)
V-N2	2.053(3)	2.058(3)	2.073(4)
V-N4	2.066(3)	2.081(3)	2.065(4)
O1-V-O2	126.48(10)	127.59(11)	126.66(13)
O1-V-O3	137.78(10)	136.73(11)	136.77(14)
O1-V-O4	87.33(10)	87.26(10)	87.06(14)
O1-V-N2	74.41(10)	74.75(11)	74.22(15)
O1-V-N4	86.84(10)	87.05(11)	86.86(15)
O2-V-O3	86.27(10)	86.23(10)	87.22(14)
O2-V-O4	84.47(9)	83.75(10)	83.87(13)
O2-V-N2	81.43(10)	81.27(11)	82.11(14)
O2-V-N4	143.32(10)	141.64(11)	142.77(14)
O3-V-O4	125.70(10)	126.99(11)	126.80(14)
O3-V-N2	87.21(10)	86.94(11)	86.92(14)
O3-V-N4	74.47(10)	74.65(11)	74.24(15)
O4-V-N2	143.13(10)	141.72(11)	142.62(14)
O4-V-N4	82.14(10)	81.96(11)	82.14(15)
N2-V-N4	127.22(10)	129.20(11)	127.47(15)
Hydrogen bonds			
H…N1	2.03(4)	1.91(4)	
Y…N1	2.710(5) (Y = N5)	2.626(4) (Y = O5)	
H…N3	2.10(4)	1.86(4)	
Y…N3	2.716(4) (Y = N6)	2.628(4) (Y = O6)	
Y-H…N1	135(3) (Y = N5)	147(4) (Y = O5)	
Y-H…N3	128(3) (Y = N6)	153(4) (Y = O6)	

(a)

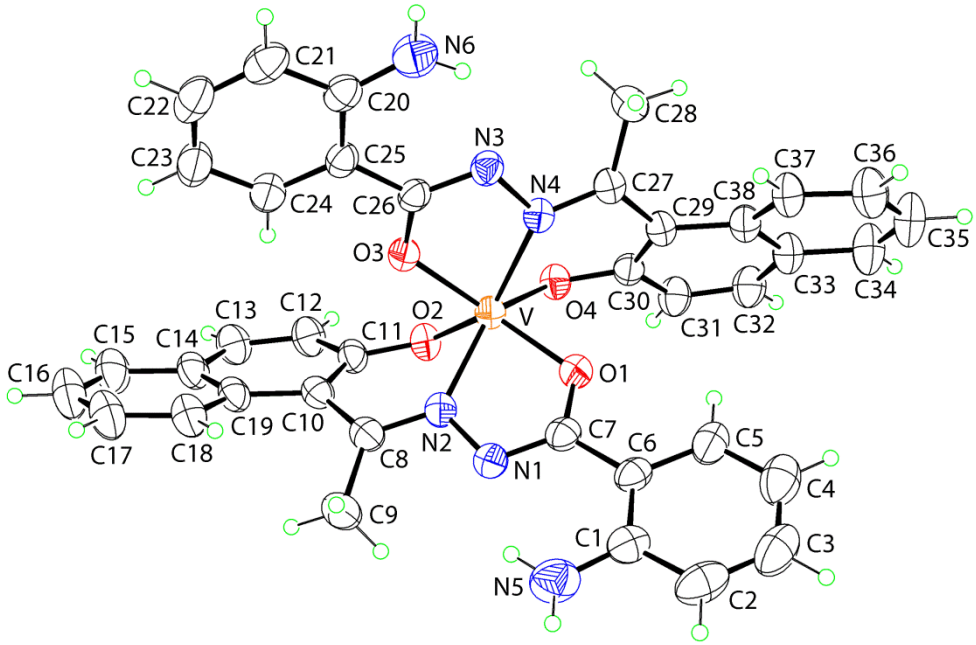
N6
C21
C22
C20
C28
N3
C23
C25
C27
C37
C36
C24
C26
N4
C29
C38
C35
O3
C33
C34
O4
C30
C13
C12
O2
V
C31
C32
C15
C14
C11
O1
C16
C10
N2
C7
C6
C5
C19
C8
N1
C4
C17
C18
C9
C1
C3
N5
C2

(b)

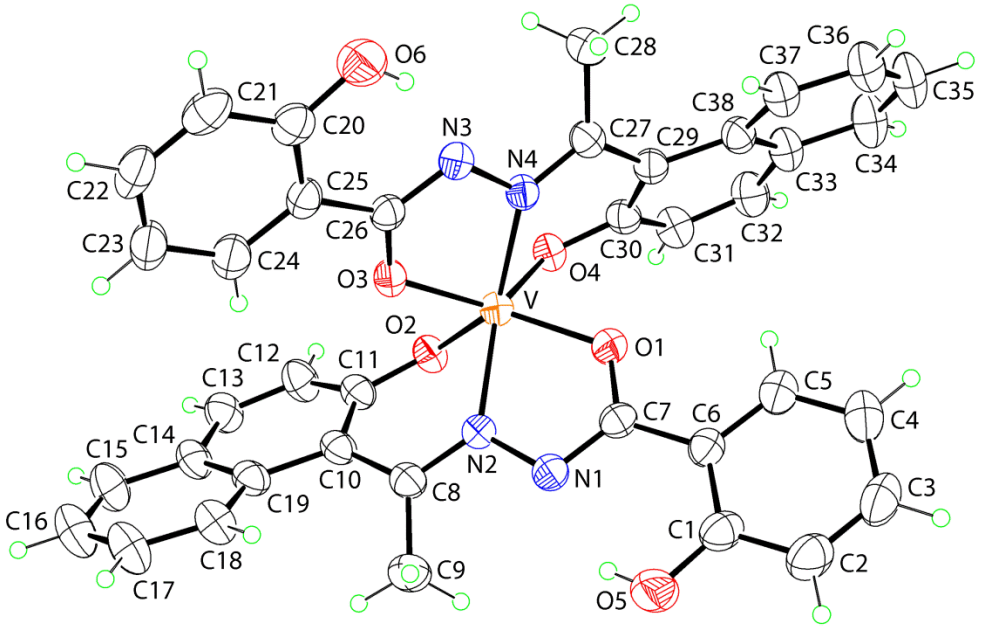
O6
C28
C37
C36
C21
C35
C38
C20
N3
C27
C29
N4
C34
C22
C25
C33
C26
C32
C23
C24
C30
C31
O3
O4
V
O2
O1
C12
C11
C5
C13
C7
C6
C4
C14
C15
N2
N1
C10
C8
C3
C19
C16
C1
C18
C9
C2
C17
O5

(c)

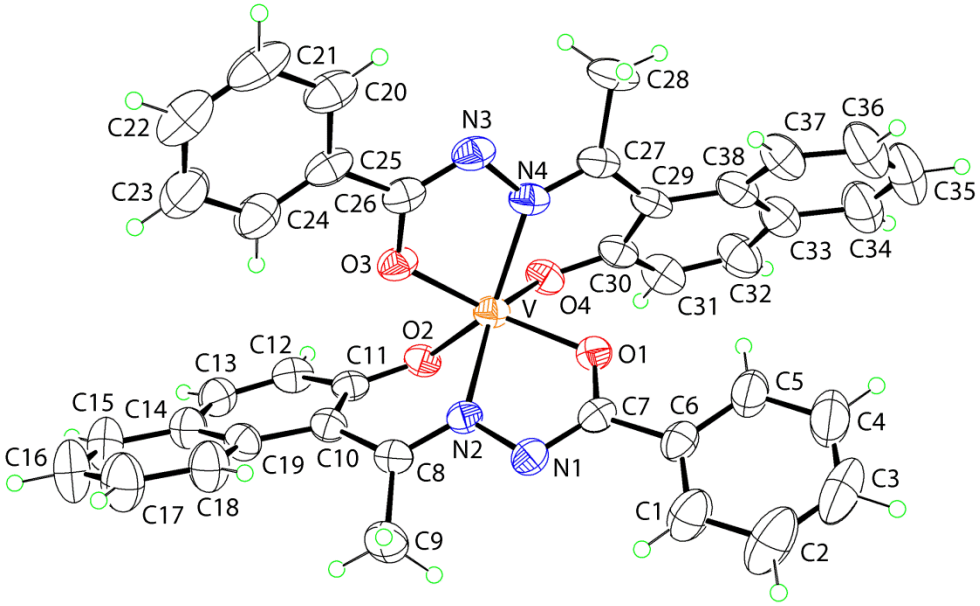

(d)

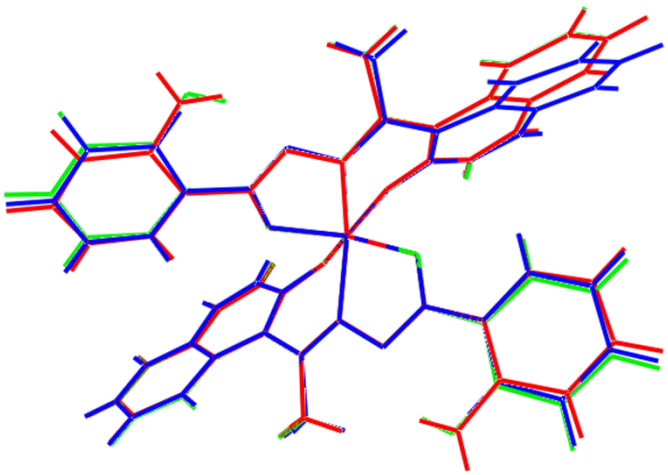

Figure 2.4. Molecular structures of $[V^{IV}(L^1)_2]$ (**1**) (a), $[V^{IV}(L^2)_2]$ (**2**) (b), $[V^{IV}(L^3)_2]$ (**3**) (c), and overlay diagram of of $[V^{IV}(L^1)_2]$ (**1**) (red image), of $[V^{IV}(L^2)_2]$ (**2**) (green) and of $[V^{IV}(L^3)_2]$ (**3**) (blue) drawn so that the V, O1 and O2 atoms are coincident (d).

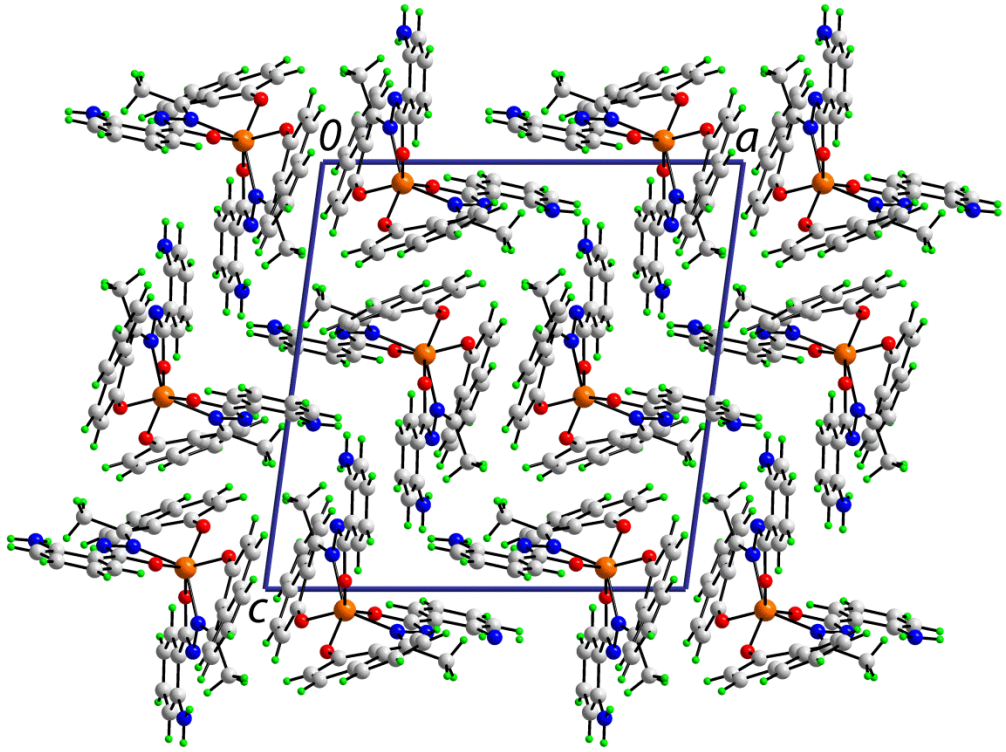

Figure 2.5. View in projection down the *b*-axis of the unit cell contents of $[V^{IV}(L^1)_2]$ (**1**). No significant intermolecular contacts are apparent.

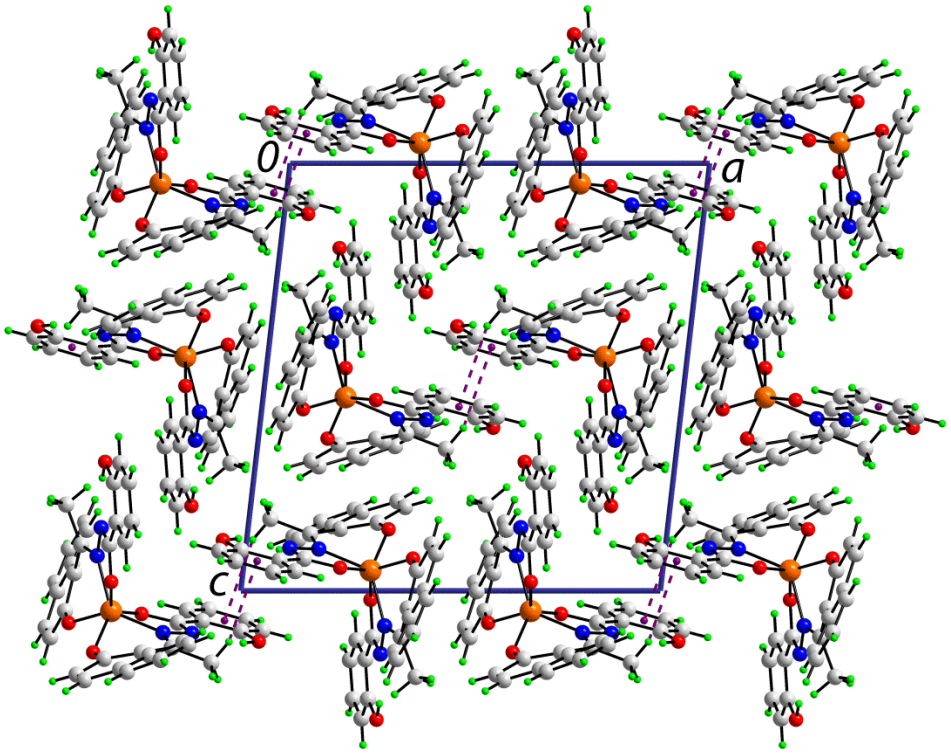

Figure 2.6. View in projection down the *b*-axis of the unit cell contents of of $[V^{IV}(L^2)_2]$ (**2**). The purple dashed lines represent C9–H9c... π (C1-C6), edge to face, interactions: H9c...ring centroid(C1-C6)^{i} = 3.00 Å, C9...ring centroid(C1-C6)^{i} = 3.907(5) Å, angle at H9c = 159º for symmetry operation *i*: 1-*x*, -*y*, 1-*z*.

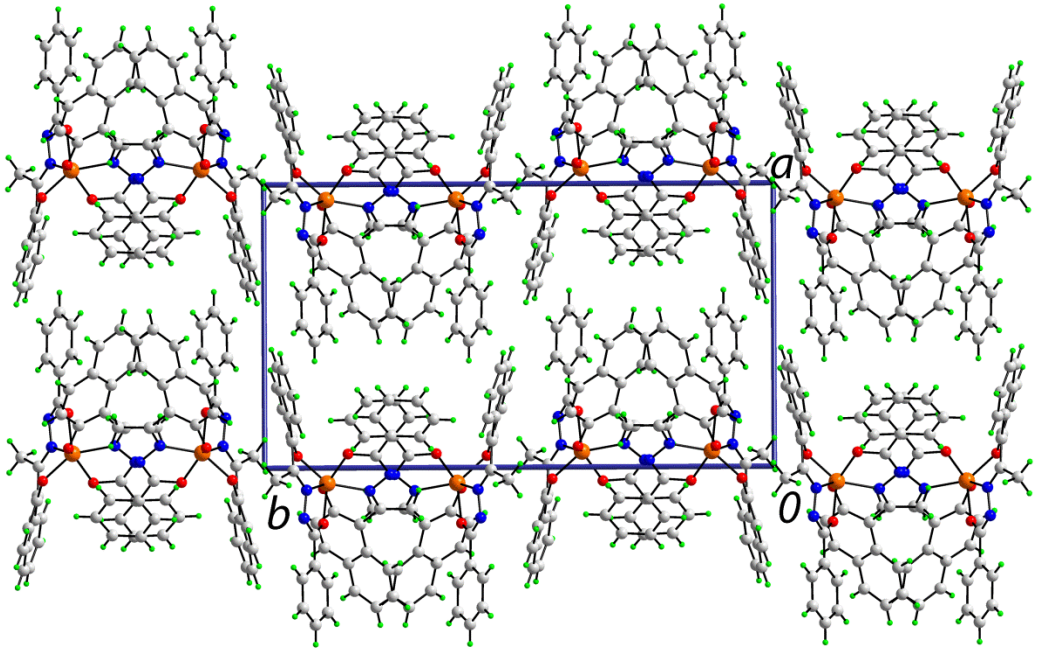

Figure 2.7. View in projection down the *c*-axis of the unit cell contents of of $[V^{IV}(L^3)_2]$ (**3**). No significant intermolecular contacts are apparent.

2.3.3. Spectral Characteristics

2.3.3.1 IR Spectroscopy. The IR data of all the ligands, H_2L^{1-3} and their corresponding metal complexes, **1–3** are given in the experimental section. All the ligands posses a band in the region of 3542–3337 cm^{-1} due to aromatic –OH present in the naphthalene moiety is found absent in the corresponding metal complexes due to the coordination. However, the presence of band at 3427 cm^{-1} in case of complex **2** is due to the –OH group attached to the benzene nucleus of ligand, H_2L^2. Disappearance of bands for –NH and –C=O and appearance of bands in the range 1256–1243 cm^{-1} indicates the enolization of these two groups forming –N=C–O– type of bond. Absence of ν(V=O) bands in the range 1035–935 cm^{-1} clearly indicate the nonoxido nature of the complex.[48]

2.3.3.2. UV Spectroscopy. Electronic spectra of the complexes **1–3** were recorded in CH_2Cl_2, DMF, and different mixture solvents like H_2O + DMF (19:1) and MeOH + DMF (19:1). In all solutions the spectral features are quite similar for all three complexes (**Figures 2.8–2.10**). The spectral data from CH_2Cl_2 are summarized in **Table 2.3** and the representative spectrum is shown in **Figure 2.11**. There are two bands in the 633–501 nm range, among which, the lowest-energy transition band around 633–614 nm is situated in the d−d transition region, but the intensity ($\varepsilon_{max,}$ 16174–10273 $M^{-1}cm^{-1}$) of this band appears too large for a pure d−d transition, for which the intensity is generally very low for vanadium(IV) complexes. The high intensity of these two bands (633–501nm) and analogy with other 'bare' vanadium(IV) complexes[29a,b,c,e,j,h,o,p,x] suggest that these transitions are most reasonably assigned as ligand-to-metal charge transfer in origin. The other bands in the higher energy absorptions (388–229 nm) are likely to be due to ligand centered transitions.[36b] In **1** and **2** the bands are slightly red shifted relative to **3**, presumably a consequence of the electron-releasing $–NH_2$ and –OH substituent on the ligands in **1** and **2,** respectively.[29n]

Table 2.3. Electronic spectra for $[V^{IV}(L^{1-3})_2]$ (1–3) in CH_2Cl_2

Complex	wavelength (nm) (ε_{max} ($M^{-1}cm^{-1}$))
$[V^{IV}(L^1)_2]$, **1**	633 (16174), 509 (13278), 368 (52404), 325 (65737), 265 (80382), 229 (99234)
$[V^{IV}(L^2)_2]$, **2**	619 (13060), 507 (13770), 388 (48743), 312 (54808), 253 (89508), 229 (109781)
$[V^{IV}(L^3)_2]$, **3**	614 (10273), 501 (9508), 361 (29726), 319 (46775), 265 (56666), 229 (72568)

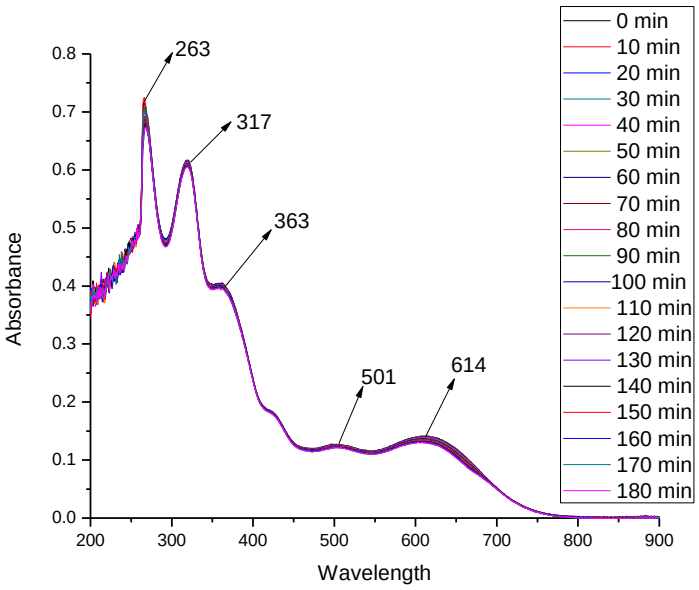

Figure 2.8. Time dependent UV-Vis spectra of $[V^{IV}(L^3)_2]$ (**3**) (1.83 X 10^{-5}M) in DMF as solvent.

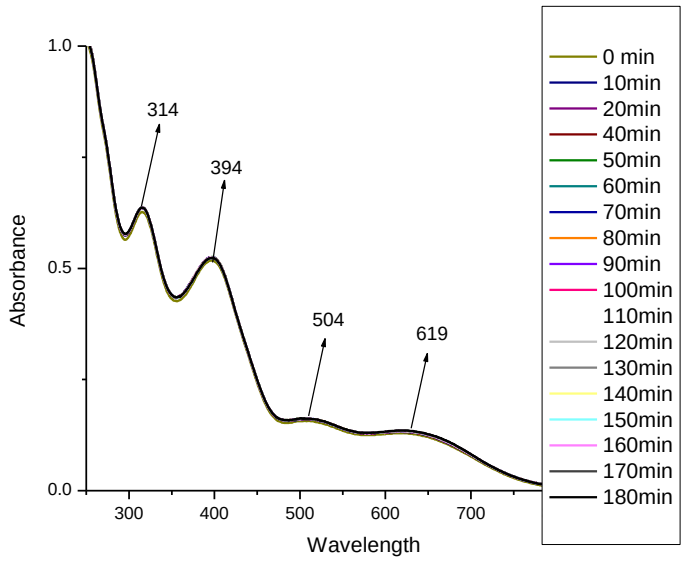

Figure 2.9. Time dependent UV-Vis spectra of $[V^{IV}(L^2)_2]$ (**2**) (2.18 X 10^{-5}M) in solvent mixture (H_2O + DMF) (19:1).

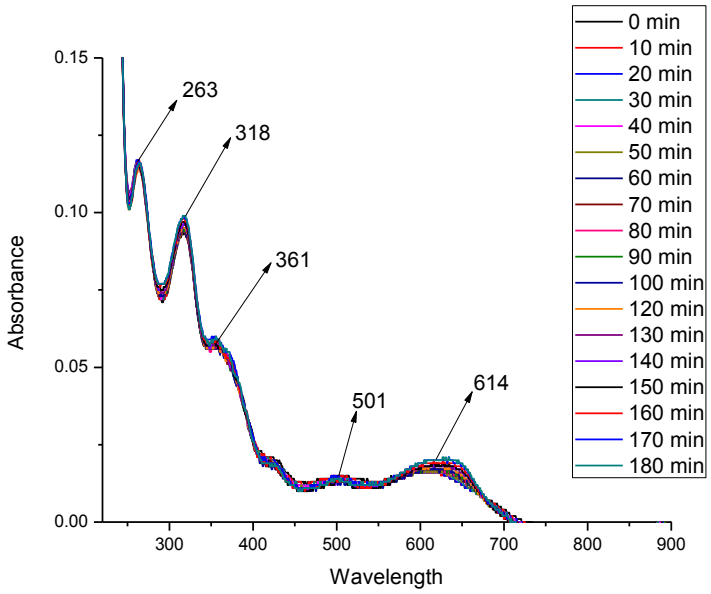

Figure 2.10. Time dependent UV-Vis spectra of $[V^{IV}(L^3)_2]$ (**3**) (2.18 X 10^{-5}M) in solvent mixture (MeOH + DMF) (19:1).

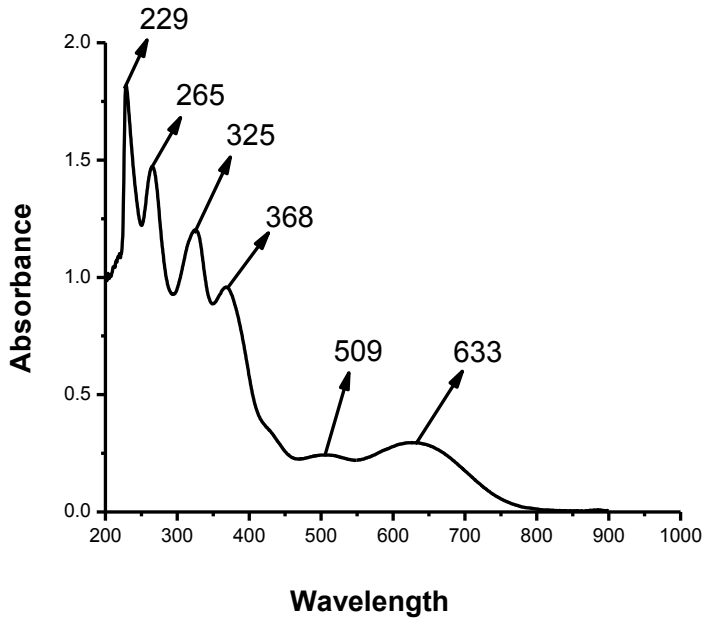

Figure 2.11. UV-Vis spectra of $[V^{IV}(L^1)_2]$ (**1**) (1.83 x 10^{-5} M) in CH_2Cl_2 .

2.3.3.3. NMR Spectroscopy. ^{1}H and ^{13}C NMR of the ligands (H_2L^{1-3}) are recorded in DMSO-d_6 and the data are given in the experimental section. The spectra of the free ligands, (H_2L^{1-3}) exhibit a resonance in the range, δ = 10.35–10.21 ppm due to naphthyl –OH, δ = 10.37–9.17 ppm due to –NH and δ = 2.35–2.32 ppm due to $–CH_3$ protons respectively. All the aromatic protons of the ligands are clearly observed in the expected region, δ = 7.94–6.23 ppm.[36a,b]

From the ^{13}C NMR spectra, it is observed that, signals for (CO–N) and (N=C(Me)) carbon resonates in the downfield region in the range, δ = 161.19–153.71 ppm and δ = 155.89–152.47 ppm respectively whereas the carbon due to the methyl groups ($–CH_3$) are found in the upfield region (δ = 24.30–24.09 ppm). Furthermore appearance of signals in the range δ = 152.50–113.59 ppm due to aromatic carbon confirm the formation of the ligands.[49]

2.3.3.4. ESI mass Spectroscopy. ESI mass spectra of the complexes, **1**–**3** have been recorded in dichloromethane solution. Mass spectral analysis for **3** shows the characteristic molecular ion peak (M^+) at m/z 655.25, whereas for compounds **1** and **2**, ESI-MS peaks are observed at m/z 708.49 [$(M + Na)^+$] and 710.10 [$(M + Na)^+$] respectively. The ESI mass spectra have also been recorded from different solvent mixtures like CH_3CN + CH_2Cl_2 (19:1) and MeOH + DMF (19:1). The results matched well regardless of having been recorded in solutions with coordinating or noncoordinating solvents. The ESI mass data are summarized in experimental section.

2.3.4. Electrochemical Properties. The electrochemical properties of **1**–**3** have been examined in CH_2Cl_2 solution (0.1 M TEAP) by cyclic voltammetry using a Pt working electrode, Pt auxiliary electrode, and an Ag/AgCl reference electrode. The voltammogram pattern is similar for **1**–**3**, which includes both oxidation and reduction process corresponding to one electron transfer. The potential data are listed in **Table 2.4** and **Figure 2.12** depicts a representative voltammogram of **3**. In the anodic region, complexes show a quasi reversible single electron wave (**Figure 2.12a**) at $E_{1/2}$ values within the potential window 1.11 to 1.09 V is assigned to the oxidation of the metal, V(IV)/V(V).[50] In the cathodic region V(IV) is reduced to V(III) showing a quasi reversible single electron wave (**Figure 2.12b**) at $E_{1/2}$ values within the potential window –0.55 to –0.53 V.[51]

Table 2.4. Cyclic voltammetric results for $[V^{IV}(L^{1-3})_2]$ (1–3) at 298 K

Complex	$E^a_{1/2}$ (V)	ΔE^a_P (mV)	$E^c_{1/2}$ (V)	ΔE^c_P (mV)
$[V^{IV}(L^1)_2]$, **1**	1.10	300	– 0.54	240
$[V^{IV}(L^2)_2]$, **2**	1.11	340	– 0.55	270
$[V^{IV}(L^3)_2]$, **3**	1.09	280	– 0.53	220

In CH_2Cl_2 at a scan rate of 100 mV s^{-1}. $E_{1/2} = (E_{pa} + E_{pc})/2$, where E_{pa} and E_{pc} are anodic and cathodic peak potentials vs. Ag/AgCl, respectively. $\Delta E_P = E_{pa} - E_{pc}$.

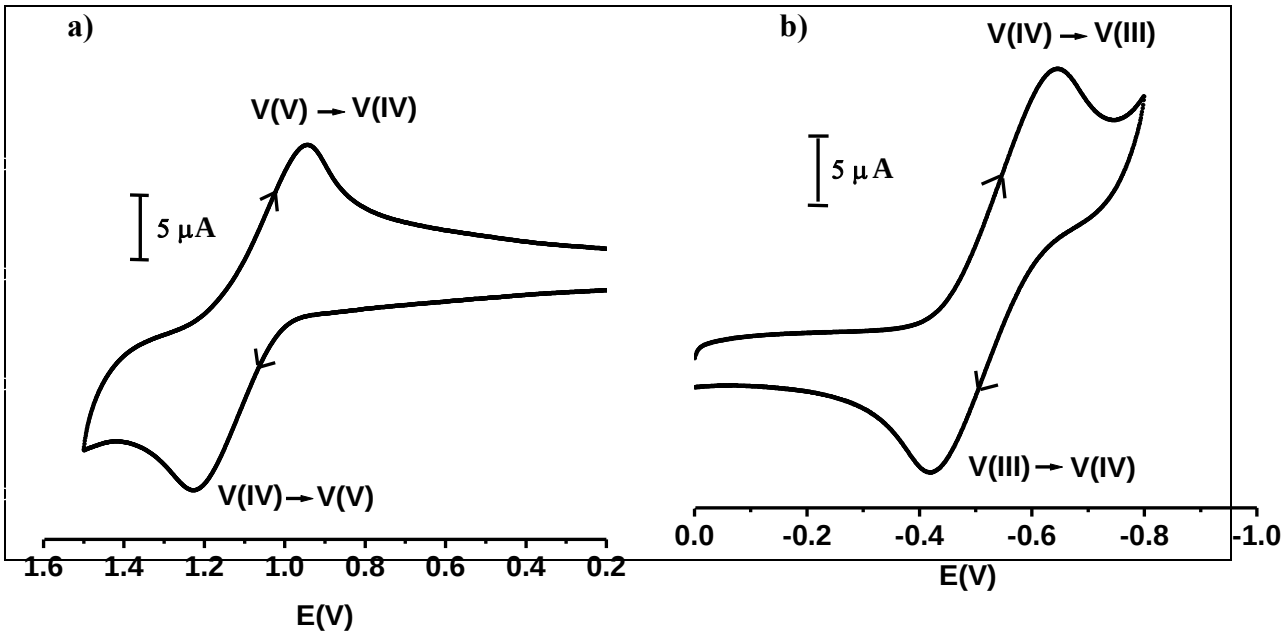

Figure 2.12. Cyclic voltammogram of $[V^{IV}(L^3)_2]$ (**3**) showing (a) oxidation (V(IV) →V(V)) and (b) reduction (V(IV) →V(III)) of the vanadium(IV) centre.

2.3.5. Magnetic Properties. Magnetic susceptibility data for **1**–**3** were collected over the temperature range 2–300 K in an applied magnetic field of 1 T and a representative temperature dependence of the magnetic susceptibility is shown in **Figure 2.13**. At 300 K **1**–**3** have effective magnetic moments (μ_{eff}) of 1.64, 1.66 and 1.68 BM, respectively. These results are typical for a compound with spin ½ per formula unit, suggesting that complexes are monomeric with no or very weak antiferromagnetic interaction between V atoms (intermolecular coupling).[52, 53]

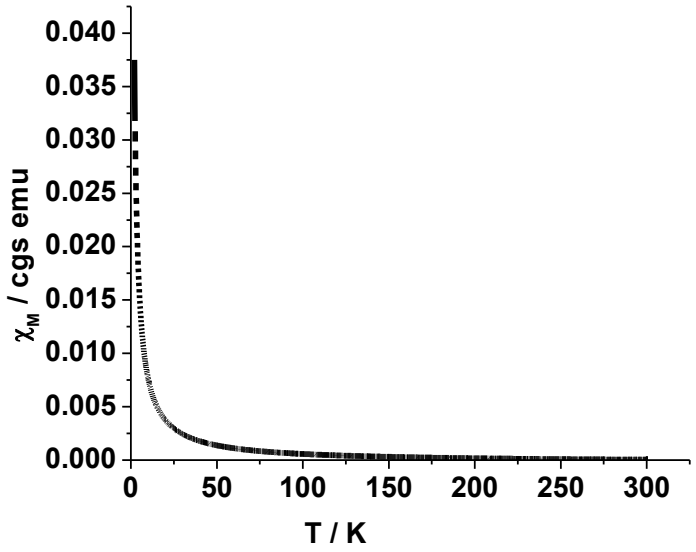

Figure 2.13. Temperature dependence of the magnetic susceptibility of $[V^{IV}(L^3)_2]$ (**3**) at 1 Tesla between 2 and 300 K.

2.3.6. EPR Spectroscopy. X-band EPR spectra of **1**–**3** were recorded in CH_2Cl_2 solution in the frozen state (77 K). The data are listed in **Table 2.5**. A representative frozen solution spectrum for **3** is shown in **Figure 2.14** which reveals well-resolved axial anisotropy with 8-line hyperfine structure, characteristic of a mononuclear vanadium complex with nuclear spin (^{51}V, $I = 7/2$).[54] Corresponding spin-Hamiltonian parameters ($g_{\|}$, 1.948−1.945; $A_{\|}$, 129.43 × 10^{-4} cm^{-1}−126.94 × 10^{-4} cm^{-1}; $g_{\perp}$, 1.996−1.983; $A_{\perp}$, 42.4 × 10^{-4} cm^{-1}−40.8 × 10^{-4} cm^{-1}) are typical of trigonal prismatic oxido vanadium(IV) complexes under comparable ON-containing donor environments.[29a,o] Analysis of the EPR spectra of vanadium(IV) complexes showed that, the anisotropic hyperfine parameters of six-coordinate complexes[35g,54] have significantly lower values compared to the corresponding values obtained with the five-coordinated complexes,[35e,f,36a,55] as is observed in the present case. The EPR spectra have also been recorded from DMF solution and the results matches well with the original spectrum reported above.

Table 2.5. X-band EPR data for $[V^{IV}(L^{1-3})_2]$ (1–3) at 77 K

Complex	$g_{\|}$	$g_{\perp}$	g_{av}	$A_{\|}$ (10^{-4} cm^{-1})	$A_{\perp}$ (10^{-4} cm^{-1})	A_{av} (10^{-4} cm^{-1})
$[V^{IV}(L^1)_2]$, **1**	1.947	1.983	1.971	128.25	41.8	70.61
$[V^{IV}(L^2)_2]$, **2**	1.945	1.991	1.975	129.43	42.4	71.41
$[V^{IV}(L^3)_2]$, **3**	1.948	1.996	1.980	126.94	40.8	69.51

$g_{av} = {}^1/_3 (2\, g_{\perp} + g_{\|})$. $A_{av} = {}^1/_3(2A_{\perp} + A_{\|})$.

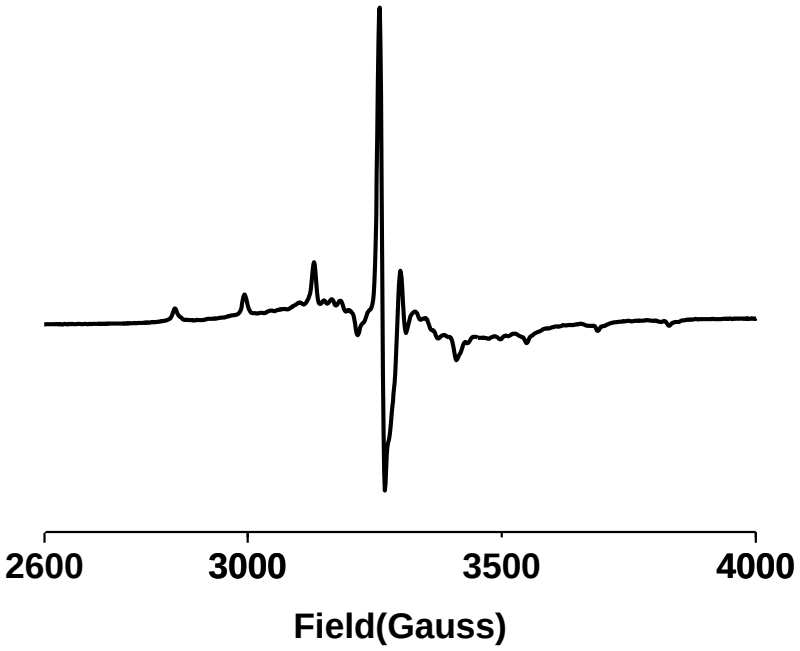

Figure 2.14. Frozen solution X-band EPR spectrum (77 K) in CH_2Cl_2 of complex **3.** Instrument settings: power, – 0.009 dB; modulation, 100 kHz; sweep centre, 2500 G; sweep time, 120 s; sweep width, 2500 G.

2.3.7. In Vitro Insulin Mimetic Activity. Vanadium compounds are known to have insulin mimetic effect.[56] In this study **1**–**3** were tested for their insulin mimetic potential in an *in vitro* glucose uptake assay. In L6 myotubes, a cell line of skeletal muscle origin, glucose uptake in response to insulin stimulation plays a key role in the whole body glucose homeostasis. Glucose transporter (GLUT) 4 is the major glucose transporter of muscle exquisitely regulated by insulin through posttranslational events.[57] The L6 myotubes differentiated from L6 myoblast have the ability to respond to insulin via insulin receptor signaling and translocation of Glut 4 to the plasma membrane. The hyperglycemic condition was created in cell culture by incubating the cells in 25 mM glucose. In the present experiment, **3** at 4μM had a glucose uptake comparable to 2μM insulin, taken as the positive control (**Figure 2.15**). The other two complexes (**1** and **2)** have moderate insulin mimetic activity and $VO(acac)_2$ showed negligible activity at the concentrations tested. In case of **3**, the enhancement of the insulin mimetic activity, with respect to **1** and **2**, might be related with their different structural characteristics, specifically, the lack of hydrogen bonding functionality in **3**. As **3** showed glucose uptake stimulating activity in the myotubes comparable to that of insulin, it is likely that **3** mimics insulin action via insulin receptor signaling with translocation of Glut 4 to the plasma membrane.

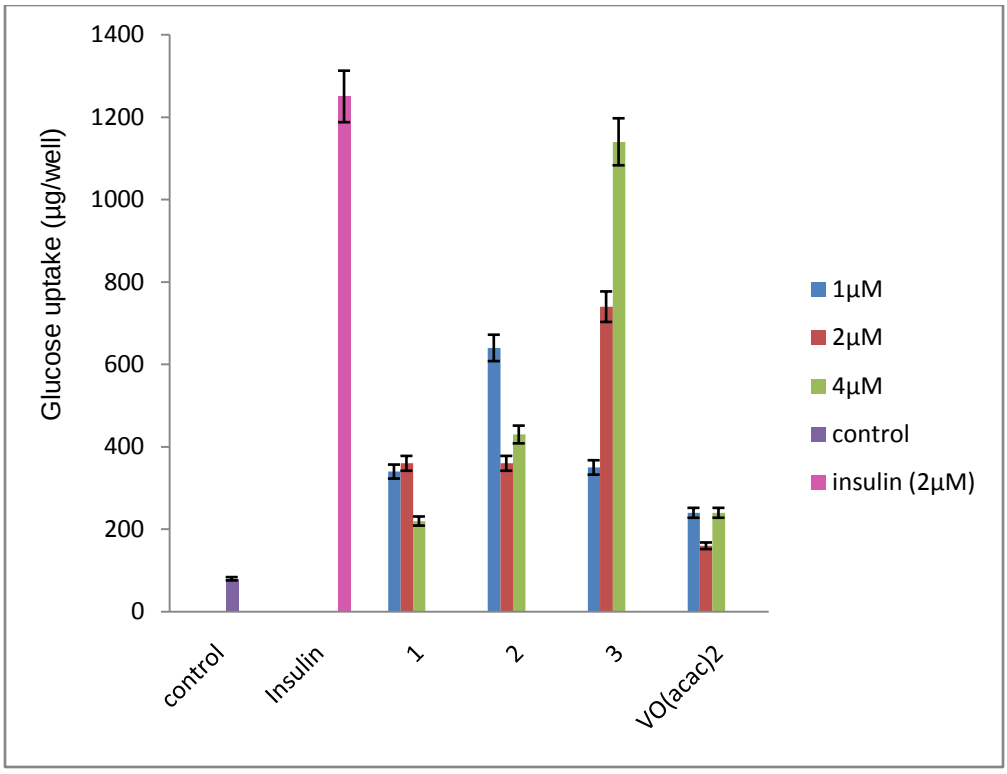

Figure 2.15. Effect of $[V^{IV}(L^{1\text{-}3})_2]$ (**1-3**) on glucose uptake in cultured L6 myotubes under high glucose conditions (25mM Glucose). Three concentrations 1µM, 2µM and 4µM were tested for each complex.The data is indicated as mean ± SEM (n=3). Student's t-Test was used where bars with asterisk show a significant difference (*P< .05) with respect to the untreated control

2.3.8. Inhibition of Cancer Cell Viability. In the present study antiproliferative efficacy of **1**–**3** was assayed by determining the viability of HeLa cells using the MTT assay. The ligands, H_2L^{1-3} and $VO(acac)_2$ gave high IC_{50} values of > 200 μM, whereas **1**–**3** gave values in the range 41–22 μM. In contrast, cisplatin, gefitinib, gemcitabine, 5-fluorouracil and vinorelbine, the most commonly used chemotherapeutic drugs, are comparably effective in HeLa cells with an IC_{50} value of 13, 20, 35, 40 and 48 μM, respectively under similar experimental conditions.[58] The significant decrease in the inhibitory concentration for the ligand compared to the metal complex clearly indicates that incorporation of vanadium in the ligand environment has a marked effect on cytotoxicity. A possible explanation is that by coordination the polarity of the ligand and the central metal ion are reduced through the charge equilibration, which favors permeation of the complexes through the lipid layer of the cell membrane.[59,60] The present results are consistent with the observation that metal complexes can exhibit greater biological activities than the free ligand.[20a]

Comparing the activity of three complexes, the cytotoxicity follows the order **2** > **3** > **1**, which is reflected from their IC_{50} values with dose dependency illustrated in **Figure 2.16**. It is remarkable that **2**, containing the ortho-hydroxy group, is most active suggesting that the electron withdrawing and releasing nature of the ortho-substituent may exert an influence over antiproliferative activity. Specifically, **2** was most cytotoxic, a result correlated with the presence of the electron withdrawing hydroxyl group. On the other hand, presence of an electron donating substituent ($–NH_2$) in the ligand core of **1**, diminishes cytotoxicity which is reflected in its IC_{50} value. For complex **3** the value is in between because of not having an electron withdrawing nor releasing group in the ligand. Very recently the antiproliferative activity of some oxido vanadium(IV) compounds has been reported by Yamaguchi et al. using the similar technique against U937 cells, and the present results are in accordance with the reported values.[61]

2.3.9. Nuclear Staining Assay. To investigate the apoptotic potential of test compounds in HeLa cells, DAPI staining was performed. Chromatin condensation during the process of apoptosis (type I programmed cell death) is a characterizing marker of nuclear alteration. HeLa cells were treated with 35, 20, and 25 μM of **1**, **2**, and **3**, respectively, that is at doses less than their respective IC_{50} values. The cells were incubated for 24 h before DAPI nuclear staining. Cells were examined under fluorescent microscope fitted with a DAPI filter. Control cells (treated with

90% DMF) hardly showed any sort of condensation in comparison to the treated cells, see **Figure 2.17**. All images taken in grayscale demonstrate the brightly condensed chromatin bodies and the nuclear blebbings as marked by arrows in **Figure 2.17**. Besides showing nuclear change, the treated cells exhibited a shrinking morphology, which is another important hallmark of apoptosis.

Compounds	IC_{50} (µM)
1	40.38 ± 1.27
2	21.73 ± 2.89
3	28.84 ± 1.34

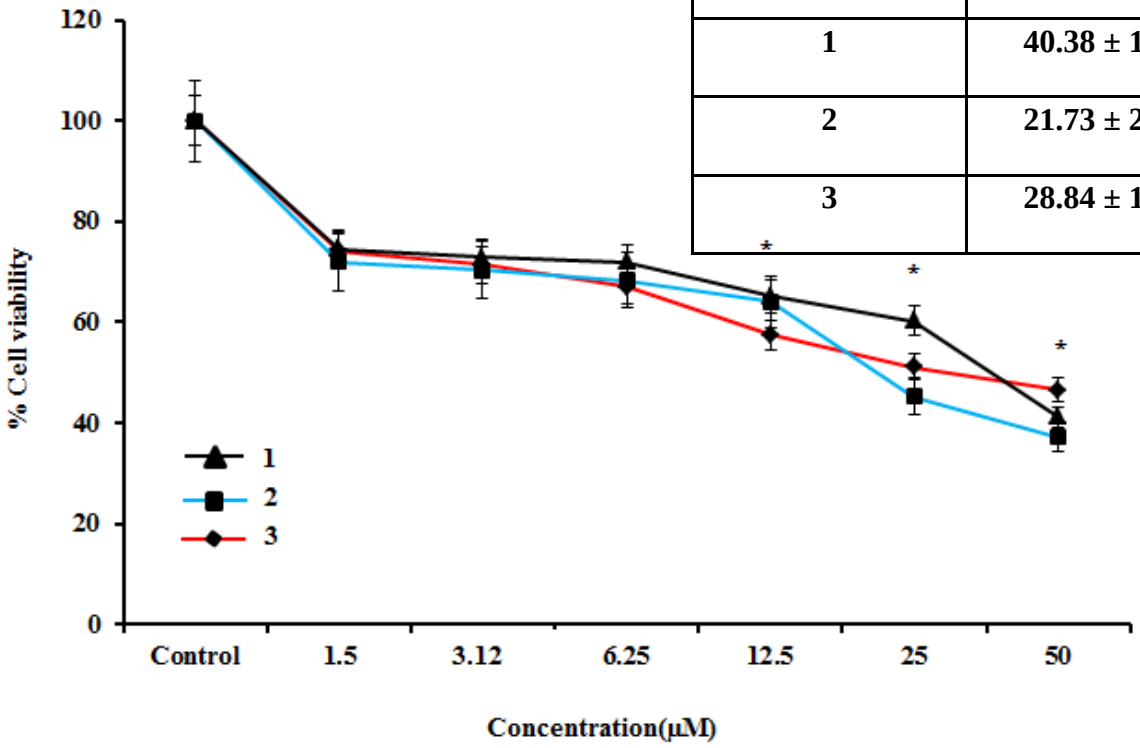

Figure 2.16. Effect of $[V^{IV}(L^{1\text{-}3})_2]$ (**1-3**) on cell viability and growth: Hela cells were treated with different concentrations of the test compound for 72h and then cell viability was measured by MTT assay. Data reported as the mean ± S.D. for *n* = 6 and compared against PBS control by using a Student's *t*-test. (*significant compared to PBS control).

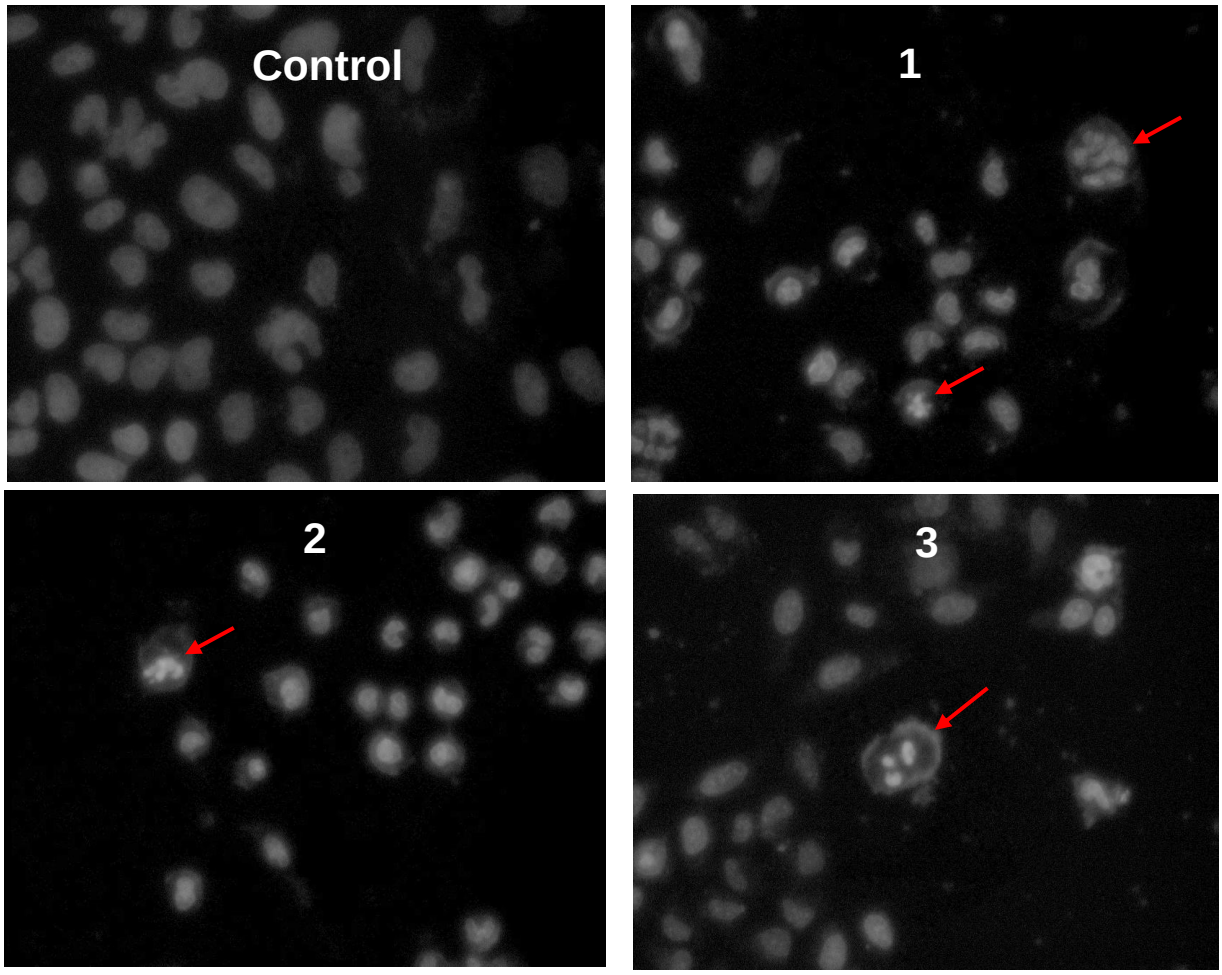

Figure 2.17. Study of apoptosis by morphological changes in nuclei of HeLa cells: After treatment HeLa cells from control and treated group were fixed with 3.7% formaldehyde for 15 min, permeabilized with 0.1% Triton X-100 and stained with 1µg/ml DAPI for 5 min at 37 °C. The cells were then washed with PBS and examined by fluorescence microscopy (Olympus IX 71) (200×). Arrows showing the morphological changes in nuclei of HeLa cells observed on applying drug (**1-3**) in comparison to control.

2.4. CONCLUSION

The following are the salient observations and findings of this work:

(a) Three aroylhydrazone ligands, possessing a rigid bulky 2-hydroxy-1-acetonaphthone core and a selection of anthranil-, salicyl- and benzoyl- hydrazide arms have been synthesized and utilized in the synthesis of the corresponding vanadium complexes. As expected, monomeric, hexacoordinated and bis(tridentate)-vanadium(IV) $[V^{IV}(L)_2]$ complexes were isolated: these do not contain an oxido-group. Stability of the complexes are related to the simultaneous oxido removal and complete charge neutralization as well as the formation of six strong covalent bonds at the V^{4+} center from the hard donor atoms N and O. (b) The importance of the structural and electronic effects arising from the incorporation of a bulky 2-hydroxy-1-acetonaphthone group in the ketone part of aroylhydrazones that can stabilize six-coordinate nonoxido vanadium(IV) complexes has been highlighted, which can be compared with our earlier work on oxido vanadium(V) with a ligand containing ONO donor atoms.[36a,b] (c) Complexes **1**–**3** are highly stable both in the solid state and in solution being resistant to exposure to aerial oxygen for 3–4 days and even purging oxygen into their solutions, a rather unusual phenomenon for "bare" vanadium(IV) or nonoxido vanadium(IV) complexes. (d) EPR and magnetic susceptibility data provide reference values for typical V(IV) sites. Electrochemical results suggest that the electrochemical oxidations and reductions are not ligand-centered but metal-centered generating V^{V} and V^{III} species respectively. (e) All the complexes show *in vitro* insulin mimetic activity against insulin responsive L6 myoblast cells, with complex **3** being the most potent which is comparable to insulin at the complex concentration of 4 μM, while the others have moderate insulin mimetic activity. In addition, the *in vitro* antiproliferative activity of complexes **1**–**3** against HeLa cell line was assayed. The cytotoxicity of the complexes is affected by the various functional groups attached to the benzoylhydrazone derivative and **2** showed considerable antiproliferative activity. It is worth noting that although the structure and chemistry of few nonoxido vanadium(IV) hydrazone complexes has been recently described,[29a,p] the suitability of these and the related nonoxido vanadium(IV) complexes in the study of vanadium insulin mimesis and antiproliferative activity has not been previously described.

2.5. REFERENCES

(1) (a)Rehder, D. *Coord. Chem. Rev.* **1999**, *182*, 297. (b) Rehder, D. *J. Inorg. Biochem.* **2000**, *80*, 133.

(2) Nriagu, J. O. *Advances in Environmental Science and Technology (Vanadium in the Environment)* **1998**, *30*, 1.

(3) (a) Meisch, H. U.; Bielig, H. J. *Basic Res. Cardiol.* **1980**, *75*, 413. (b) Baran, E. J. *Adv. Plant Physiology* **2008**, *10*, 357. (c) Anke, M. *Anales de la Real Academia Nacional de Farmacia* **2004**, *70*, 961.

(4) (a) Cantley, L. C., Jr; Josephson, L.; Warner, R.; Yanagisawa, M.; Lechene, C.; Guidotti, G. *J. Biol. Chem.* **1977**, *252*, 7421. (b) Morsy, M. D.; Abdel-Razek, H. A.; Osman, O. M. *J. Physiol Biochem.* **2011**, *67*, 61.

(5) (a) Rehder, D.; Santonin, G.; Licini, G. M.; Schulzke, C.; Meier, B. *Coord. Chem. Rev.* **2003**, *237*, 53. (b) Plass, W. *Coord. Chem. Rev.* **2003**, *237*, 205. (c) Thompson, K. H.; Orvig, C. *Coord. Chem. Rev*. **2001**, *219*, 1033. (d) Butler, A. *Coord. Chem. Rev.* **1999**, *187*, 17.

(6) (a) Frausto da Silva, J. J. R; Williams, R. J. P. *The Biological Chemistry of the Elements*, 2nd ed.; Oxford University Press: Oxford, U.K., **2001**. (b) Kaim, W.; Schwederski, B. *Bioinorganic Chemistry: Inorganic Elements in the Chemistry of Life*; John Wiley & Sons: Chichester, U. K., **1994**. (c) Eady, R. R. *Coord. Chem. Rev.* **2003**, *237*, 23.

(7) (a) Wei, Y.; Zhang, C.; Zhao, P.; Yang, X.; Wang, K. *J. Inorg. Biochem*. **2011**, 105, 1081. (b) Rehder, D.; Costa Pessoa, J.; Geraldes, C. F. G. C.; Kabanos, T.; Kiss, T.; Meier, B.; Micera, G.; Pettersson, L.; Rangel, M.; Salifoglou, A.; Turel, I.; Wang, D. *J. Biol. Inorg. Chem.* **2002**, *7*, 384. (c) Sutradhar, M.; Barman T. R.; Mukherjee, G.; Kar M.; Saha, S. S.; Drew, M. G. B., Ghosh, S. *Inorg. Chim. Acta* **2011**, *368*, 13. (d) Saltiel, A. R.; Khan, C. R.; *Nature* **2001**, *414*, 799. (e) Noblía, P.; Baran, E. J.; Otero, L.; Gambino, D**.** *Eur. J. Inorg. Chem.* **2004**, 322. (f) Nilsson, J.; Shteinman A. A.; Rehder, D.; Nordlander, E. *J. Inorg. Biochem.* **2011**, *105*, 1795. (g) Willsky, G. R.; Chi, L.-H.; Hu, Z.; Crans, D. C. *Coord. Chem. Rev.* **2011**, *255*, 2258. (h) Rehder, D. *Inorg. Chem. Commun*. **2003**, *6*, 604. (i) Islam, M. N.; Kumbhar, A. A.; Kumbhar, A. S.; Joshi, B. N. *Inorg. Chem*. **2010**, *49*, 8237. (j) Pillai, S. I.; Subramanian, S. P.; Kandaswamy, M. *Eur. J. Med. Chem.* **2013**, *63*, 109.

(8) (a) Shechter, Y.; Karlish, S. J. D. *Nature* **1980**, *284*, 556. (b) Heyliger, C. E.; Tahiliani, A. G.; McNeill, J. H. *Science* **1985**, *227*, 1474.

(9) Ramanadham, S.; Mongold, J. J.; Brownsey, R. W.; Cros, G. H.; McNeill, J. H. *Am. J. Physiol*. **1989**, *257*, H904.

(10) McNeill, J. H.; Yuen, V. G.; Hoveyda, H. R.; Orvig, C. *J. Med. Chem.* **1992**, *35*, 1489.

(11) Schecter, Y.; Meyerovitch, J.; Farfel, Z.; Sack, J.; Bar-Meir, S.; Amir, S.; Degani, H.; Karlish, S. J. D. *Vanadium in Biological Systems*; Kluwer Academic Publishers: Norwell, **1990**; p. 129.

(12) Thompson, K. H.; McNeill, J. H.; Orvig, C. *Topics in Biological Chemistry: Metallopharmaceuticals*; Springer-Verlag: Heidelberg, 1999; Vol. *2*, pp. 139.

(13) (a) Sakurai, H.; Fugono J.; Yasui H. *Mini-Rev. Med. Chem.*, **2004**, *4*, 41. (b) Adachi, Y.; Yoshida, J.; Kodera, Y.; Katoh, A.; Takada, J.; Sakurai, H.; *J. Med. Chem.* **2006**, *49*, 3251. (c) Melchior, M.; Thompson, K. H.; Jong, J. M.; Rettig, S. J.; Shuter, Ed; Yuen, V. G.; Zhou, Y.; McNeill, J. H.; Orvig, C. *Inorg. Chem.* **1999**, *38*, 2288. (d) Yamaguchi, M.; Wakasugi, K.; Saito, R.; Adachi, Y.; Yoshikawa,Y.; Sakurai, H.; Katoh, A. J. *Inorg. Biochem.* **2006**, *100*, 260. (e) Crans, D. C.; Mahroof-Tahir, M.; Johnson, M. D.; Wilkins, P. C.; Yang, L.; Robbins, K.; Johnson, A.; Alfano, J. A.; Godzala, M. E. III; Austin, L. T.; Willsky, G. R. *Inorg. Chim. Acta* **2003**, *356*, 365. (f) Karmaker, S.; Saha, T. K.; Yoshikawa, Y.; Yasui, H.; Sakurai, H. J. *Inorg. Biochem.* **2006**, *100*, 1535.

(14) Thompson, K. H.; Liboiron, B. D.; Sun, Y.; Bellman, K. D. D.; Setyawati, I. A.; Patrick, B. O.; Karunaratme, V.; Rawji, G.; Wheeler, J.; Sutton, K.; Bhanot, S.; Cassidy, C.; McNeill, J. H.; Yuen, V. G.; Orvig, C. *J. Biol. Inorg. Chem.* 2003, *8*, 66.

(15) Rosenberg, B.; Camp, L. V.; Trosko, J. E.; Mansour,V. H. *Nature* **1969**, *222*, 385.

(16) Orvig, C.; Abrams, M. J. *Chem. Rev.* **1999**, *99*, 2201.

(17) Kovala-Demertzi, D.; Boccarelli, A.; Demertzis, M. A.; Coluccia, M. *Chemotherapy* **2007**, *53*, 148.

(18) Sakurai, H.; Kojima, Y.; Yoshikawa, Y.; Kawabe, K.; Yasui, H. *Coord. Chem. Rev*. **2002**, *226*, 187.

(19) Louie, A. Y.; Meade, T. J. *Chem. Rev.* **1999**, *99*, 2711.

(20) (a). Rosu, T.; Pahontu, E.; Pasculescu, S.; Georgescu, R.; Stanica, N.; Curaj, A.; Popescu, A.; Leabu, M.; *Eur. J. Med. Chem.* **2010**, *45*, 1627. (b) Padhye, S.; Afrasiabi, Z.; Sinn, E.; Fok, J.; Mehta, K.; Rath, N. *Inorg. Chem.* **2005**, *44*, 1154. (c) Ali, A. A.; Nimir, H.; Aktas, C.; Huch, V.; Rauch, U.; Schäfer, K. H; Veith, M. *Organometallics* **2012**, *31*, 2256.

(21) Kovala-Demertzi, D.; Papageorgiou, A.; Papathanasis, L.; Alexandratos, A.; Dalezis, P.; Miller, J. R.; Demertzis, M. A. *Eur. J. Med. Chem.* **2009**, *44*, 1296.

(22) Rebolledo, A. P.; Vieites, M.; Gambino, D.; Piro, O. E.; Castellano, E. E.;. Zani, C. L; Souza-Fagundes, E. M.; Teixeira, L. R.; Batista, A. A.; Beraldo, H.; *J. Inorg. Biochem.* **2005**, *99*, 698.

(23) Djordjevic, C. *Metal Ions in Biological Systems* **1995**, *31*, 595.

(24) Sakurai, H.; Tamura, H.; Okatani, K. *Biochem. Biophys. Res. Commun*. **1995**, *206*, 133.

(25) Dong, Y.; Narla, R. K.; Sudbeck, E.; Uckun, F. M. *J. Inorg. Biochem.* **2000**, *78*, 321.

(26) Noleto, G. R.; Petkowicz, C. L. O.; Mercê, A. L. R.; Noseda, M. D.; Méndez-Sánchez, S. C.; Reicher, F.; Oliveira, M. B. M. *J. Inorg. Biochem.* **2009**, *103*, 749.

(27) Sasmal, P. K.; Saha, S.; Majumdar, R.; Dighe, R. R.; Chakravarty, A. R. *Inorg. Chem*. **2010**, *49*, 849.

(28) (*a*) Wilkinson, G., ed.; Gillard, R. D.; McCleverty, J. A. *Comprehensive Coordination Chemistry;* Pergamon Press, Oxford, England, **1987**; Vol. *3*, p. 453. (b) Cotton, F. A.; Wilkinson G. *Advanced Inorganic Chemistry*, 5th edn, John Wiley & Sons, New York, **1988**; p. 665.

(29) (a) Diamantis, A. A.; Snow, M. R.; Vanzo, J. A.; *Chem. Commun.* **1976**, 264. (b) Comba, P.; Engelhardt, L. M.; Harrowfield, J. M.; Lawrance, G. A.; Martin, L. L.; Sargeson, A. M.; White, A. H., *Chem. Commun.* **1985**, 174. (c) Cooper, S. R.; Koh, Y. B.; Raymond, K. N. *J. Am. Chem. Soc.* **1982**, *104*, 5092. (d) Diamantis, A. A.; Manikas, M.; Salam, M.; Snow, M. R.; Tiekink, E. R. T. *Aust. J. Chem.* **1988**, *41*, 453. (e) Auerbach, U.; Della Vedova, B. P. C.; Wieghardt, K.; Nuber, B.; Weiss J. *Chem. Commun.* **1990**, 1004. (f) Kang, B.; Wenig, L.; Liu, H.; Wu, D.; Huang, L.; Lu, C.; Cai, J.; Chen, X.; Lu, J. *Inorg. Chem.* **1990**, *29*, 4873. (g) Kabanos, T. A.; White, A. J. P.; Williams, D. J.; Woolins, J. D. *Chem. Commun.* **1992**, 17. (h) Kabanos, T. A.; Slawin, A. M. Z.; Williams, D. J.; Woolins, J. D. *Dalton Trans.* **1992**, 1423. (i) Bruni, S.; Caneschi, A.; Cariatia, F.; Delfs, C.; Dei, A.; Gatteschi, D. *J. Am. Chem. Soc.* **1994**, *116*, 1388. (j) Neves, A.; Ceccato, A. S.; Vencato, I.; Mascarenhas, Y. P.; Erasmus- Buhr, C. *Chem. Commun.* **1992**, 652. (k) Vergopoulos, V.; Jantzen, S.; Rodewald, D.; Rehder, D. *Chem. Commun.* **1995**, 377. (l) Ludwig, E.; Hefele, H.; Uhlemann, E.; Weller, F.; Kläui, W.; *Z. Anorg. Allg. Chem.* **1995**, *621*, 23. (m) Hefele, H.; Ludwig, E.; Uhlemann, E.; Weller, F. *Z. Anorg. Allg. Chem.*, **1995**, *621*, 1973. (n) Klich, P. R.; Daniher, A. T.; Challen, P. R.; McConville, D. B.; Youngs, W. J. *Inorg. Chem.* **1996**, *35*, 347. (o) Paine, T. K.; Weyhermüller, T.; Slep, L. D.;

Neese, F.; Bill, E.; Bothe, E.; Wieghardt, K.; Chaudhuri, P. *Inorg. Chem.* **2004**, *43*, 7324. (p) Sutradhar, M.; Mukherjee, G.; Drew, M. G. B.; Ghosh S. *Inorg. Chem.* **2007**, *46*, 5069. (q) Farahbakhsh, M.; Schmidt, H.; Rehder, D. *Chem. Commun.* **1998**, 2009. (r) Kajiwara, T.; Wagner, R.; Bill, E.; Weyhermüller, T.; Chaudhuri, P. *Dalton Trans.* **2011**, *40*, 12719. (s) Sanna, D.; Várnagy, K.; Lihi, N.; Micera, G.; Garribba, E.; *Inorg. Chem.* **2013**, *52*, 8202. (t) Stiefel, E. I.; Dori, Z.; Gray, H. B. *J. Am. Chem. Soc.***1967**, *89*, 3353. (u) Raymond, K. N.; Isied, S. S.; Brown, L. D.; Fronczek, F. R.; Nibert, J. H. *J. Am. Chem. Soc.* **1976**, *98*, 1767. (v) Karpishin, T. B.; Stack, T. D. P.; Raymond, K. N. *J. Am. Chem. Soc.* **1993**, *115*, 182. (w) Kondo, M.; Minakoshi, S.; Iwata, K.; Shimizu, T.; Matsuzaka, H.; Kamigata, N.; Kitagawa, S. *Chem. Lett.* **1996**, *25*, 489. (x) Paine, T. K.; Weyhermueller, T.; Bill, E.; Bothe, E.; Chaudhuri, P. *Eur. J. Inorg. Chem.* **2003**, 4299. (y) Morgenstern, B.; Steinhauser, S.; Hegetschweiler, K.; Garribba, E.; Micera, G.; Sanna, D.; Nagy, L. *Inorg. Chem.* **2004**, *43*, 3116. (z) Morgenstern, B.; Kutzky, B.; Neis, C.; Stucky, S.; Hegetschweiler, K.; Garribba, E.; Micera, G. *Inorg. Chem.* **2007**, *46*, 3903.

(30) (a) Bayer, E.; Kneifel, H. *Z. Naturforsch., B: Chem. Sci.* **1972**, *27*, 207. (b) Kneifel, H.; Bayer, E. *J. Am. Chem. Soc.* **1986**, *108*, 3075.

(31) Berry, R. E.; Armstrong, E. M.; Beddoes, R. L.; Collison, D.; Ertok, S. N.; Helliwell, M.; Garner, C. D. *Angew. Chem., Int. Ed.* **1999**, *38*, 795.

(32) Terra, L. H. A.; Areias, M. C.; Gaubeur, I.; Suez-Iha, M. E. V. *Spectrosc. Lett.* **1999**, *32*, 257.

(33) (a) Maurya, M. R.; Agarwal, S.; Abid, M.; Azam, A.; Bader, C.; Ebel, M.; Rehder, D. *Dalton Trans.* **2006**, 937. (b) Savini, L.; Chiasserini, L.; Travagli, V.; Pellerano, C.; Novellino, E. *Eur. J. Med. Chem.* **2004**, *39*, 113. (c) Cui, Z.; Yang, X.; Shi, Y.; Uzawa, H.; Cui, J.; Dohi, H.; Nishida, Y. *Bioorg. Med. Chem. Lett.* **2011**, *21*, 7193.

(34) (a) Cunha, A. C.; Figueiredo, J. M.; Tributino, J. L. M.; Miranda, A. L. P.; Castro H. C.; Zingali, R. B.; Fraga, C. A. M.; Souza, M. C. B. V.; Ferreira, V. F.; Barreiro, E. *J. Bioorg. Med. Chem.* **2003**, *11*, 2051. (b) Easmon, J.; Puerstinger, G.; Thies, K.-S.; Heinisch, G.; Hofmann, J. *J. Med. Chem.* **2006**, *49*, 6343. (c) Chaston, T. B.; Watts, R. N.; Yuan, J.; Richardson, D. R. *Clin Cancer Res* **2004**, *10*, 7365. (d) Braslawsky, G. R.; Edson, M. A.; Pearce, W.; Kaneko, T.; Greenfield, R. S. *Cancer Res.* **1990**, *50*, 6608. (e) Darnell, G.; Richardson, D. R. *Blood* **1999**, *94*, 781. (f) Fan, C. D.; Su, H.; Zhao, J.; Zhao, B. X.; Zhang, S. L.; Miao, J. Y. *Eur. J. Med. Chem.* **2010**, *45*, 1438. (g) Morgan, L. R.; Jursic, B. S.; Hooper, C. L.; Neumann, D. M.; Thangaraj, K.;

LeBlanc, B. *Bioorg. Med. Chem. Lett.* **2002**, *12*, 3407. (h) Dandawate, P.; Khan, E.; Padhye, S.; Gaba, H.; Sinha, S.; Deshpande, J.; Venkateswara S., K.; Khetmalas, M.; Ahmad, A.; Sarkar, F. H. *Bioorg. Med. Chem. Lett.* **2012**, *22*, 3104. (i) Liu, W. Y.; Li, H. Y.; Zhao, B. X.; Shin, D. S.; Lian, S.; Miao, J. Y. *Carbohydr. Res.* **2009**, *344*, 1270. (j) Xia, Y.; Fan, C. D.; Zhao, B. X.; Zhao, J.; Shin, D. S.; Miao, J. Y. *Eur. J. Med. Chem.* **2008**, *43*, 2347. (k) Effenberger, K.; Breyer, S.; Schobert, R. *Eur. J. Med. Chem.* **2010**, *45*, 1947. (l) Hassan, G. S.; Kadry, H. H.; Abou-Seri, S. M.; Ali, M. M.; Mahmoud, A. E. *Bioorg. Med. Chem.* **2011**, *19*, 6808. (m) Tian, F. F.; Li, J. H.; Jiang, F. L.; Han, X. L.; Xiang, C.; Ge, Y. S.; Li, L. L.; Liu, Y. *RSC Advances* **2012**, *2*, 501. (n) Richardson, D. R. *Antimicrob. Agents Chemother.* **1997**, *41*, 2061.

(35) (a) Bhattacharyya, S.; Mukhopadhyay, S.; Samanta, S.; Weakley, T. J. R.; Chaudhury, M. *Inorg. Chem.* **2002**, *41*, 2433. (b) Sutradhar, M.; Mukherjee, G.; Drew M. G. B.; Ghosh, S. *Inorg. Chem.* **2006**, *45*, 5150. (c) Dai, J.; Wang, H. *Polyhedron* **1996**, *15*, 1801. (d) Maurya, R.C.; Rajput, S. *J. Mol. Struct.* **2007**, *833*, 133. (e) Mangalam, N. A.; Sivakumar, S.; Sheeja, S. R.; Kurup, M. R. P.; Tiekink, E. R. T. *Inorg. Chim. Acta* **2009**, *362*, 4191. (f) Maurya, R. C.; Rajput, S.; *J. Mol. Struct.* **2006**, *794*, 24. (g) Lu, L.; Yue, J.; Yuan, C.; Zhu, M.; Han, H.; Liu, Z.; Guo, M. *J. Inorg. Biochem.* **2011**, *105*, 1323. (h) Sarkar, S.; Aydogdu, Y.; Dagdelen, F.; Bhaumik, B. B.; Dey, K. *Mater. Chem. Phys.* **2004**, *88*, 357. (i) Kuriakose, M; Kurup, M. R. P.; Suresh, E. *Polyhedron* **2007**, *26*, 2713. (j) Rahchamani J.; Behzad, M.; Bezaatpour, A.; Jahed, V.; Dutkiewicz, G.; Kubicki, M.; Salehi, M. *Polyhedron* **2011**, *30*, 2611. (k) Tsuchimoto, M.; Kasahara, R.; Nakajima, K.; Kojima, M.; Ohba, S.; *Polyhedron* **1999**, *18*, 3035. (l) Teixeira, M. F. S.; Dockal, E. R.; Cavalheiro, É. T. G. *Sens. Actuators B* **2005**, *106*, 619. (m) Maurya, R. C.; Rajput, S. *Prog. Cryst. Growth Charact. Mater.* **2006**, *52*, 142. (n) Li, L.; Guo, Z.; Zhang, Q.; Xu, T.; Wang, D. *Inorg. Chem. Commun.* **2010**, *13*, 1166. (o) Grivani, G.; Bruno, G.; Rudbari, H. A.; Khalaji, A. D.; Pourteimouri, P. *Inorg. Chem. Commun.* **2012**, *18*, 15. (p) Maurya, M. R., Sikarwar, S., Kumar, M. *Catal. Commun.* **2007**, *8*, 2017. (q) El-Taras, A. A.; EL-Mehasseb, I. M.; Ramadan A. M. *C. R. Chimie* **2012**, *15*, 298. (r) Wang, D.; Ebel, M.; Schulzke, C.; Grüning, C.; Hazari, S. K. S.; Rehder, D. *Eur. J. Inorg. Chem.* **2001**, 935. (s) Maurya, M. R.; Khan, A. A.; Azam, A.; Kumar, A.; Ranjan, S.; Mondal, N.; Pessoa, J. C. *Eur. J. Inorg. Chem.* **2009**, 5377. (t) Teixeir, M. F. S.; Marcolino-Júnior, L. H.; Fatibello-Filhob, O.; Dockal, E. R.; Cavalheiro, É. T. G. *J. Braz. Chem. Soc.*, **2004**, *15*, 803. (u) Alyea, E. C.; Dee, T. D.; Ferguson, G. *J. Crystallogr. Spectro. Res.* **1985**, *15*, 29. (v) Xu, T.; Li, L. Z.; Zhou S. F.; Guo, G. Q.; Niu M. J. *J. Chem.*

Crystallogr. **2005**, *35*, 263. (w) Salavati-Niasari, M.; Ganjali, M. R.; Norouzi, P.; *J. Porous Mater*. **2007**, *14*, 423.

(36) (a) Dinda, R.; Sengupta, P.; Ghosh, S.; Mak, T. C. W. *Inorg. Chem.* **2002**, *41*, 1684. (b) Dinda, R.; Sengupta, P.; Sutradhar, M.; Mak, T. C. W.; Ghosh, S. *Inorg. Chem.* **2008**, *47*, 5634. (c) Dash, S. P.; Pasayat, S.; Bhakat, S.; Dash, H. R.; Das, S.; Butcher, R. J.; Dinda, R. *Polyhedron* **2012**, *31*, 524.

(37) Rowe, R. A.; Jones, M. M. *Inorg, Synth.* **1957**, *5*, 113.

(38) Naskar, S.; Mishra, D.; Butcher, R. J.; Chattopadhyay, S. K. *Polyhedron* **2007**, *26*, 3703.

(39) SMART and SAINT, Bruker AXS Inc.: Madison, WI, **1996**.

(40) Sheldrick, G. M. SADABS. University of Göttingen, **1996**.

(41) Sheldrick, G. M. *Acta Cryst*. **2008**, *A64*, 112.

(42) (a) Farrugia, L. J. *J. Appl. Cryst*. **2012**, *45*, 849. (b) Gans, J.; Shalloway, D. *J. Molec. Graphics Model*. **2001**, *19*, 557. (c) Brandenburg, K. DIAMOND. Crystal Impact GbR, Bonn, Germany, **2006**.

(43) Ha, B. G.; Nagaoka, M.; Yonezawa, T.; Tanabe, R.; Woo, J. T.; Kato, H.; Chung, U.; Yakasaki, K. *J. Nutr. Biochem.* **2012**, *23*, 501.

(44) Bhutia, S. K.; Mallick, S. K.; Stevens, S. M.; Prokai, L.; Vishwanatha, J. K.; Maiti, T. K. *Toxicol in Vitro* **2008**, *22*, 344.

(45) Bhutia, S. K.; Mallick, S. K.; Maiti, S; Maiti, T. K. *Chem Biol Interact.* **2008**, *174*, 11.

(46) Branca, M.; Micera, G.; Dessi, A.; Sanna, D.; Raymond, K. N. *Inorg. Chem.* **1990**, *29*, 1586.

(47) Spek, A. L. *Acta Cryst*. **2009**, *D65*, 148.

(48) (a) Selbin, J. *Chem. Re*v. **1965**, *65*, 153. (b) Selbin, J. *Coord. Chem. Re*v. **1966**, *1*, 293.

(49) Adão, P.; Pessoa, J. C.; Henriques, R. T.; Kuznetsov, M. L.; Avecilla, F.; Maurya, M. R.; Kumar, U.; Correia, I. *Inorg. Chem.* **2009**, *48*, 3542.

(50) Chatterjee, P. B.; Bhattacharya, S.; Audhya, A.; Ki-Young C.; Endo A.; Chaudhury M.; *Inorg. Chem.* **2008**, *47*, 4891.

(51) Mandal, D.; Chaudhury, M. *Struct. Chem.* **2007**, *18*, 187.

(52) Nakai, M.; Yano, S. *J. Inorg. Biochem.* **2004**, *98*, 105.

(53) Pessoa, J. C.; Cavaco, I.; Correia, I. *Inorg. Chim. Acta* **1999**, *293*, 1.

(54) Parihar, S.; Pathan, S.; Jadeja, R. N.; Patel, A.; Gupta, V. K. *Inorg. Chem.* **2012**, *51*, 1152.

(55) Samanta, S.; Ghosh, D.; Mukhopadhyay, S.; Endo, A.; Weakley, T. J. R.; Chaudhury, M. *Inorg. Chem.* **2003**, *42*, 1508.

(56) Islam, M. N.; Kumbhar, A. A.; Kumbhar, A. S.; Zeller M.; Butcher, R. J.; Dusane, M. B.; Joshi, B. N. *Inorg Chem.* **2010**, *49*, 8237.

(57) Ishiki M.; Klip, A. *Endocrinology* **2005**, *146*, 5071.

(58) Ahmed, M.; Jamil, K. *Biology and Medicine*. **2011**, *3*, 60.

(59) Ramadan, A. M. *J. Inorg. Biochem.* **1997**, *65*, 183.

(60) Avaji, P. G.; Kumar, C. H. V.; Patil, S. A.; Shivananda K. N.; Nagaraju C. *Eur. J. Med. Chem.* **2009**, *44*, 3552.

(61) Yamaguchi, T.; Watanabe, S.; Matsumura,Y.; Tokuoka,Y.; Yokoyama, A. *Bioorg. Med. Chem*. **2012**, *20*, 3058

Chapter 3

Oxido vanadium(V) complexes incorporating tridentate aroylhydrazoneoximes: Synthesis, characterizations and antibacterial activity

Chapter 3

Oxido vanadium(V) complexes incorporating tridentate aroylhydrazoneoximes: Synthesis, characterizations and antibacterial activity

ABSTRACT

Some new oxido vanadium(V) complexes [$VOL^{1–3}$(OEt)(EtOH)] (**1**–**3**) have been reported which are obtained from the reaction of the Schiff bases ($H_2L^{1–3}$) (Where H_2L^1= salicylhydrazone of diacetyl monoxime; H_2L^2= 4-methoxy salicylhydrazone of diacetyl monoxime and H_2L^3 = 4-hydroxy salicylhydrazone of diacetyl monoxime) with $VO(acac)_2$ in 1:1 molar ratio. Three 4-R-aroylhydrazoneoximes (**V**) have been used as ligands in the present study, differing in the inductive effect of the substituent R (R = H, OCH_3 and OH), in order to observe their influence, if any, on the redox potentials and biological activity of the complexes. All the synthesized ligands and the metal complexes are successfully characterized by elemental analysis, IR, UV–Vis and NMR spectroscopy. X-ray diffraction study of [VOL^1(OEt)(EtOH)], **1** reveals that the metal centre is in distorted octahedral O_5N coordination spheres where the ONO-donor ligand and the ethoxido group constitute a satisfactory O_3N basal plane. Cyclic voltammetry of the complexes show a quasi-reversible cyclic voltammetric response in the potential range of 0.36–0.29V involving single electron V(V)–V(IV) reduction. The complexes have also been screened for their antibacterial activity against *Escherichia coli*, *Bacillus, Proteus and Klebsiella*. Minimum inhibitory concentration of these complexes and antibacterial activity indicates the compound **1** as the potential lead molecule for drug designing.

3.1. INTRODUCTION

The chemistry of vanadium has become a fascinating area of research in recent time because of the presence of vanadium in metalloenzymes and its medicinal as well as catalytic importance.[1–13] The expanding knowledge of the role of vanadium in biological systems as a therapeutic agent, for example in antitumor and anticancer drugs[14,15] has led to a continuously increasing interest in the coordination chemistry and solution chemistry of this element.

Over the years, oximes have been widely used as very efficient complexing agents in analytical chemistry for isolation, separation and extraction of different metal ions.[16–26] The metal complexes of oxime have also various interesting features[27,28] which include short intramolecular hydrogen bonding and packing configurations, which give rise to unusual optical properties. From the medicinal chemistry, it is found that they served as models for biosystems such as vitamin B_{12}[29] and myocardial perfusion imaging agents.[30] As a ligand, the oxime moiety is potentially ambidentate[16] and can coordinate either through the nitrogen (**I**, **Chart 3.1)**[23–26] or oxygen atom (**II**).[31] The vast literature on structural studies of oxime complexes reveals some interesting features of its coordination behavior. It may coordinate to one metal ion through the nitrogen atom and another metal ion through the oxygen atom (**III**). Thus it can form a $\mu_{1,2}$ (N,O) oximato-bridged extended network.[19-22] In the majority of complexes only the nitrogen atom (**I**) coordinates to the metal center, and the oxygen atom does not take part in coordination. There are quite few examples where both the atoms (oximato nitrogen and oxygen, **IV**) do take part in coordination.[32,33]

On the other hand, hydrazones –NH–N=CRR' (R and R′ = H, alkyl, aryl) are versatile ligands due to their applications in the field of analytical[34] and medicinal chemistry.[35] Hydrazone moieties are the most important pharmacophoric cores of several antiinflammatory, antinociceptive and antiplatelet drugs.[36] It may be relevant to mention here that though the chemistry of aroylhydrazones complexes of many transition metals has been extensively studied,[37-40] that of aroylhydrazoneoximes (**V**) appears to have remained practically unexplored.[41,42]

Keeping this observation in mind and in continuation of our studies on oxido vanadium complexes of hydrazone Schiff base ligands,[43–44] the oxime functionality is incorporated into the

ligand moiety. In this chapter we report the syntheses, X-ray structure and physical properties of some oxido vanadium(V) complexes of aroylhydrazoneoximes with special reference to their antibacterial activity. It is worth mentioning here that, to the best of our knowledge, this report is a rare example[31] of aroylhydrazoneoxime complexes where the oximato oxygen atom coordinates to the metal center, while the nitrogen atom does not take part in coordination.

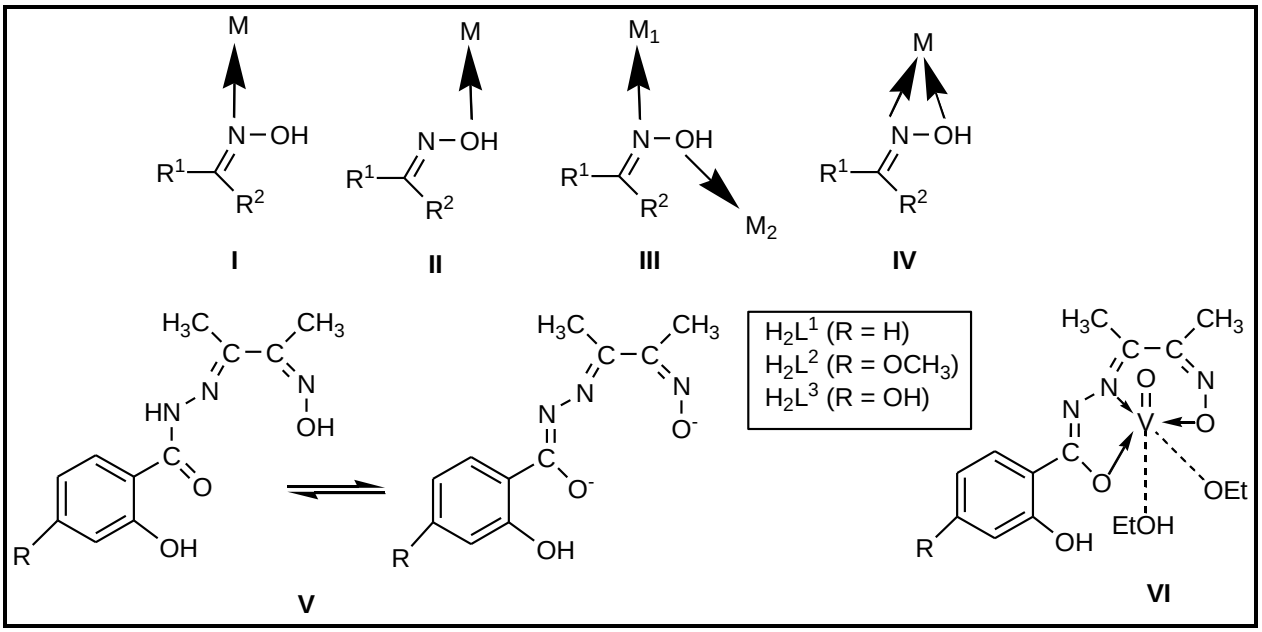

Chart 3.1. Structures **I-VI**

3.2. EXPERIMENTAL SECTION

3.2.1. General Methods and Materials. All chemicals were purchased from commercial sources and used without further purification. [$VO(acac)_2$] was prepared as described in the literature.[45] Reagent grade solvents were dried and distilled prior to use. All other chemicals were reagent grade, available commercially and used as received. Commercially available TBAP (tetra butyl ammonium perchlorate) was properly dried and used as a supporting electrolyte for recording cyclic voltammograms of the complexes. Elemental analyses were performed on a Vario ELcube CHNS Elemental analyzer. IR spectra were recorded on a Perkin-Elmer Spectrum RXI spectrometer. ^1H NMR spectra were recorded with a Bruker Ultrashield 400 MHz spectrometer using $SiMe_4$ as an internal standard. Electronic spectra were recorded on a Lamda25, PerkinElmer spectrophotometer. Magnetic susceptibility was measured with a Sherwood Scintific AUTOMSB sample magnetometer. Electrochemical data were collected using a PAR electrochemical analyzer and a PC-controlled Potentiostat/Galvanostat (PAR 273A) at 298 K in a dry nitrogen atmosphere. Cyclic voltammetry experiments were carried out with a glassy carbon working electrode, platinum counter electrode and Ag/AgCl as reference electrode and TBAP as supporting electrolyte. Antibacterial activity was measured with a PerkinElmer (2030 VICTOR X_3) microtitre plate optical colorimeter (OD_{600}).

3.2.2. Synthesis of Ligands ($H_2L^{1–3}$). Schiff base ligands, $H_2L^{1–3}$ were prepared in 80-90% yield by the condensation of equimolar ratio of 4-substituted salicylhydrazine with diacetyl monoxime in methanol media by a standard procedure.[46] The resulting white compound was filtered, washed thoroughly with ethanol and dried over fused $CaCl_2$.

3.2.3. Synthesis of Complexes [$VO(L^{1–3})(OEt)(EtOH)$] (1-3). To the stirring solution of ligand, H_2L^{1-3} (1.0 mmol) in 20 mL of ethanol, $VO(acac)_2$ (1.0 mmol) was added. The colour changed to brownish red. After 3 h of stirring, the solution was filtered. The filtrate was allowed to stand at room temperature for 4 days, during which crystals, suitable for X-ray analysis were isolated.

[VO(L^1)(OEt)(EtOH)] (1). Yield: 58%. Anal. calc. for $C_{15}H_{22}N_3O_6V$: C, 46.03; H, 5.62; N, 10.74. Found: C, 46.07; H, 5.65; N, 10.79. ^{1}H NMR (DMSO-d_6): δ 2.63 (s, 3H, CH_3C=NN), 2.52 (s, 3H, CH_3C=NO), 7.86 – 6.93 (m, 4H, C_6H_4), 11.42 (s, 1H, OH). ^{51}V NMR (DMSO-d_6): δ –513.

[VO(L^2)(OEt)(EtOH)] (2). Yield: 54%. Anal. calc. for $C_{16}H_{24}N_3O_7V$: C, 45.60; H, 5.70; N, 9.97. Found: C, 45.65; H, 5.73; N, 9.94. ^{1}H NMR (DMSO-d_6): δ 2.68 (s, 3H, CH_3C=NN), 2.53 (s, 3H, CH_3C=NO), 3.71 (s, 3H, CH_3O), 7.94 – 6.83 (m, 3H, C_6H_4), 11.46 (s, 1H, OH). ^{51}V NMR (DMSO-d_6): δ –518.

[VO(L^3)(OEt)(EtOH)] (3). Yield: 61%. Anal. calc. for $C_{15}H_{22}N_3O_7V$: C, 44.22; H, 5.40; N, 10.31. Found: C, 44.27; H, 5.36; N, 10.27. ^{1}H NMR (DMSO-d_6): δ 2.61 (s, 3H, CH_3C=NN), 2.48 (s, 3H, CH_3C=NO), 7.74 – 6.87 (m, 3H, C_6H_4), 9.76 (s, 1H, *p*-Ar–OH), 11.48 (s, 1H, o-Ar–OH). ^{51}V NMR (DMSO-d_6): δ –529.

3.2.4. X-ray Crystallography. A Suitable single crystal of **1** was chosen for X-ray diffraction studies. This compound crystallized in the monoclinic space group P 121/*n*1. The diffraction data for **1** were collected at 295 K with a Bruker AXS Smart CCD diffractometer using graphite monochromated Mo Kα radiation (λ = 0.71073 Å). The following Bruker software packages were used: SMART for collecting frames of data, indexing and determination of lattice parameters, SAINT for integration of intensity of reflections and scaling, SADABS for absorption correction, and SHELXTL for space group and structure determination, and for refinement. The structures were solved by direct methods with SHELX-86 and refined by full-matrix least-squares analysis with SHELXL-97.[47] All the hydrogen atoms were added in their calculated positions using riding models whereas non-hydrogen atoms were refined with anisotropic thermal parameters. Crystallographic data and details of refinement are given in **Table 3.1.**

Table 3.1. Crystallographic data and details of refinement of [VO(L^1)(OEt)(EtOH)] (1).

Empirical formula	$C_{15}H_{22}N_3O_6V$	
Formula weight	391.30	
Temperature	295(2) K	
Wavelength	1.54184 Å	
Crystal system	Monoclinic	
Space group	P 121/*n*1	
Unit cell dimensions	a = 7.06518(10) Å	α= 90°.
	b = 21.9429(3) Å	β= 96.5499(12)°.
	c = 11.80060(13) Å	γ = 90°.
Volume	1817.51(4) $Å^3$	
Z	4	
Density (calculated)	1.430 mg/m^3	
Absorption coefficient	4.887 mm^{-1}	
F(000)	816	
Crystal size	0.54 x 0.24 x 0.17 mm^3	
Theta range for data collection	5.52 – 77.38°.	
Index ranges	$-8 \le h \le 8, -27 \le k \le 26, -14 \le l \le 10$	
Reflections collected	8227	
Independent reflections	3776 [R_{int} = 0.0201]	
Completeness to theta = 67.50°	99.6 %	
Absorption correction	semi-empirical from equivalents	
Max. and min. transmission	1.00000 and 0.19723	
Refinement method	Full-matrix least-squares on F^2	
Data / restraints / parameters	3776 / 10 / 250	
Goodness-of-fit on F^2	1.042	
Final R indices [I>2sigma(I)]	R_1 = 0.0541, wR_2 = 0.1500	
R indices (all data)	R_1 = 0.0604, wR_2 = 0.1563	
Largest diff. peak and hole	0.535 and –0.399 e.$Å^{-3}$	

3.2.5. Antibacterial activity. Antibacterial activity of the compounds (ligands and complexes) was studied against *Escherichia coli (E. coli), Bacillus, Proteus* and *Klebsiella* by determining minimum inhibitory concentration (MIC) following CLSI guidelines of broth micro-dilution method.[48] Briefly, bacterial strains were cultured onto Luria Bertani Agar medium [containing 0.5% peptone, 0.5% yeast extract, 1% NaCl, 1.5% Agar at pH 7.5±0.2]. The stock solution was prepared by dissolving the tested compounds in dimethyl sulfoxide (DMSO). Chloramphenicol, a common antibiotic was used as the positive control and DMSO was used as the negative control. Bacterial cultures were added to the sterilized Mueller Hinton Broth (MHB) [containing 30% beef extract, 1.75% casein acid hydrolysate and 0.15% starch, pH 7.4±0.2]. MIC was determined by using 2 fold serial dilutions in the medium (MHB) containing 1.95-1000 µg/ml of the test compounds. To each well of 96 well microtitre plate, 150µl of medium (MHB) was taken in duplicate, to which 10µl of 0.5 McFarland standard ($1.5x10^8$ CFU/ml) culture pathogens from MHB was added. The inoculated plates were incubated at 37° C for 24h. After incubation, bacterial growth was monitored by measuring the turbidity of the culture by a microtitre plate optical colorimeter (OD_{600}). The MIC was determined as the lowest concentration of compound at which the visible growth of the organisms was completely inhibited.

3.3. RESULT AND DISSCUSSION

3.3.1. Synthesis. Three 4-R-aroylhydrazoneoximes (**V**) have been used in the present study, differing in the inductive effect of the substituent R (R = H, OCH_3 and OH), in order to observe their influence, if any, on the redox potentials and biological activities of the complexes. The reactions of the selected aroylhydrazoneoximes (**V**) with $VO(acac)_2$ proceeded in stirring ethanol and each of these reactions afforded reddish black colored products in decent yields. During this reaction, vanadium is oxidized from its initial +IV state to the +V state. These compounds are highly soluble in aprotic solvents, viz. CH_3CN, DMF or DMSO.

3.3.2. Spectral Characteristics.

Spectral characteristics of **1**–**3** are listed in **Table 3.2**.

3.3.2.1. IR Spectroscopy. The infrared spectra of the complexes display a broad band centred at around 3400 cm^{-1}. This band is possibly due to the O–H stretch of the hydrazine fragment of the ligand. The C=O stretch (1654 cm^{-1}) of the amide functionality[49] in free ligand is found to be absent in the spectra of the complexes, which indicates that the Schiff base is completely deprotonated and acts as a dibasic enolate. The strong and sharp peak displayed by the complexes in the range 1592–1603 cm^{-1} is likely to be associated with the C=N–N=C moiety.[43,44,50] The presence of a strong band in the range 976–985 cm^{-1} is assigned to V=O stretching.[43,44] A representative spectrum of **1** is shown in **Figure 3.1**.

3.3.2.2. UV Spectroscopy. The electronic spectra of the complexes were recorded using acetonitrile solutions. The main features of all the spectra are quite similar. A representative spectrum of **1** is shown in **Figure 3.2**. Three strong absorptions are observed in the wavelength range 403–207 nm. The lower energy absorption at around 390 nm is ascribable to the ligand-to-metal charge transfer transitions where as the higher energy absorptions are likely to be due to ligand centred transitions.[43,44]

Table 3.2. Characteristics IR[a] bands (cm^{-1}) and electronic spectral[b] data [nm (dm^3 mol^{-1} cm^{-1})] for the [VO(L^{1-3})(OEt)(EtOH)] (1–3)

Complex	ν (OH)	ν (C=N)	ν (V=O)	λ_{max} (ε)
[VO(L^1)(OEt)(EtOH)] (**1**)	3434	1592	977	383 (4324); 263 (11190); 221 (14423)
[VO(L^2)(OEt)(EtOH)] (**2**)	3381	1603	985	395 (5212); 278 (13654); 216 (15709)
[VO(L^3)(OEt)(EtOH)] (**3**)	3402	1598	976	403 (4931); 265 (12654); 207 (17809)

[a] In KBr pellet; [b] In CH_3CN

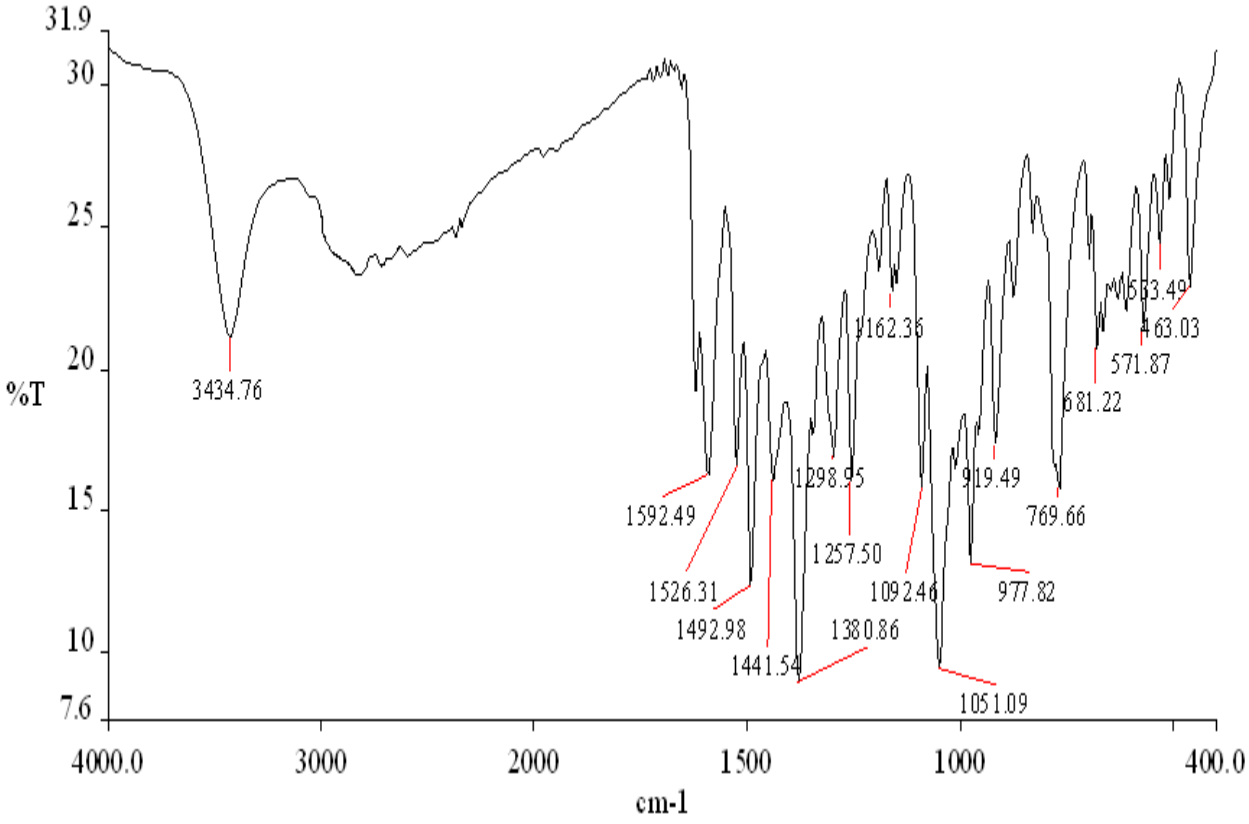

Figure 3.1. IR spectrum of [VO(L^1)(OEt)(EtOH)] **(1)**

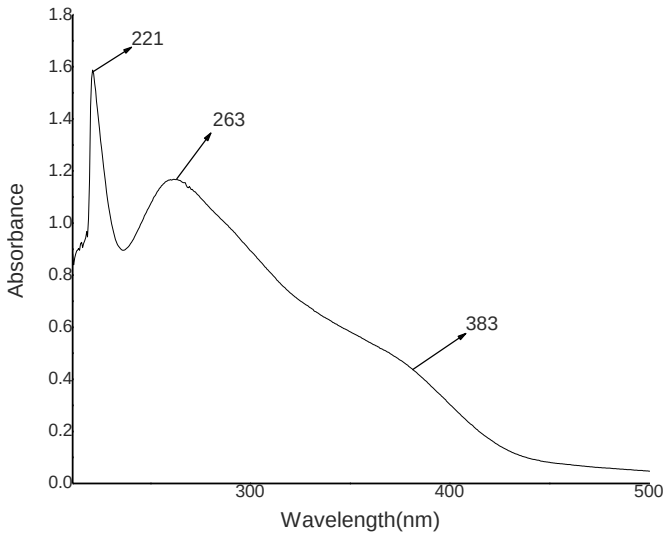

Figure 3.2. UV-Vis spectrum of [VO(L^1)(OEt)(EtOH)] **(1)**

3.3.2.3. NMR Spectroscopy. The ^{1}H NMR spectral data of the free ligands and its corresponding oxido vanadium(V) complexes (**1**–**3**) were recorded using DMSO-d_6. The spectra of the free ligands exhibit two close but separate singlets in the range 11.74–11.53 ppm due to NH and OH (=N–OH) groups, which are absent in the spectra of complexes indicating coordination of these groups to the metal centre. However all the spectra display a singlet in the range 11.42–11.48 ppm, which corresponds to the OH (phenolic) group of the ligand fragment remained uncoordinated in the complexes. Signals for aromatic protons found as multiplets in the 7.94–6.83 ppm range.[46] The protons of the methyl group of the methoxy substituent in [VO(L^2)(OEt)(EtOH)] (**2**) resonate as a singlet at 3.71 ppm and the protons of the hydroxyl substituent at 4- position in [VO(L^3)(OEt)(EtOH)] (**3**) resonate as a singlet at 9.76 ppm.[51] The two methyl groups of the diacetyl monoxime moiety appear as singlets in the range 2.48–2.68 ppm. ^{51}V NMR spectra of **1**–**3** display a singlet at –513, –518 and –529 ppm, respectively. These chemical shifts are usual for complexes containing the monooxido vanadium(V) units.[52]

3.3.3. Electrochemical properties. The electrochemical properties of all the oxido vanadium(V) complexes, **1**–**3** have been examined in CH_3CN solution (0.1 M TBAP) by cyclic voltammetry. All the complexes show a quasi-reversible cyclic voltammetric response in the potential range of 0.36–0.29 V involving single electron V(V)–V(IV) reduction.[44] The one-electron nature of this reduction has been tentatively established by comparing its current height with that of standard ferrocene/ferrocenium couple under the same experimental condition. The potential data of **1**–**3** are listed in **Table 3.3**, and a selected voltammogram is shown in **Figure 3.3**. The potential of V(V)–V(IV) reduction in the 4-R-aroylhydrazoneoxime complexes (**VI**) has been found to be sensitive to the nature of the substituent R in the aroylhydrazone fragment. The potential decreases with increasing electron-releasing character of the substituent R as expected.[53,54]

Table 3.3. Cyclic voltammetric results[a] for [VO(L^{1-3})(OEt)(EtOH)] (1–3) at 298 K

Complex	$E_{1/2}$ (V)	ΔE_P (mV)
[VO(L^1)(OEt)(EtOH)] (**1**)	0.36	91
[VO(L^2)(OEt)(EtOH)] (**2**)	0.31	86
[VO(L^3)(OEt)(EtOH)] (**3**)	0.29	79

[a] In acetonitrile at a scan rate of 50 mVs^{-1}. $E_{1/2} = (E_{pa} + E_{pc})/2$, where E_{pa} and E_{pc} are anodic and cathodic peak potentials vs. Ag/AgCl, respectively. $\Delta E_P = E_{pa} - E_{pc.}$

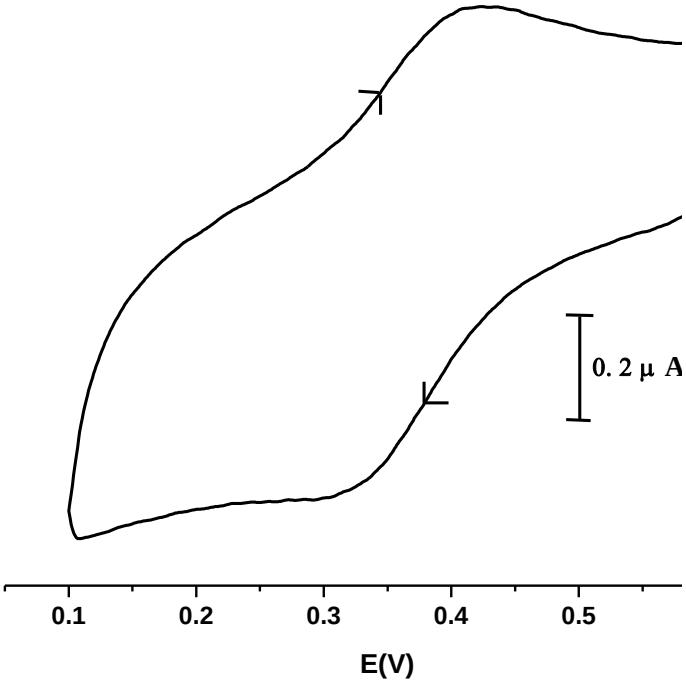

Figure 3.3. Cyclic voltammogram of [VO(L^1)(OEt)(EtOH)] (**1)**, in CH_3CN (0.1 M TBAP); scan rate 50 mV/s, and potentials recorded vs. Ag/AgCl.

3.3.4. Description of Crystal Structure of [VO(L^1)(OEt)(EtOH)] (1). Alhough the preliminary characterization data (microanalytical and spectroscopic) of **1** gave some idea of their composition and about the donor points through which the ligands were attached to the oxido vanadium(V) center, they could not definitely reveal the actual structures, which could only be provided by a structure determination using the single-crystal X-ray diffraction technique. To determine the coordination mode of the aroylhydrazoneoxime ligands in these complexes (**1**–**3**), the structure of a representative member of this family, viz. [VO(L^1)(OEt)(EtOH)], (**1**) was determined. The molecular structure of **1** is shown in **Figure 3.4** and some relevant bond parameters are listed in **Table 3.4**. In the structure the metal centre is in distorted octahedral O_5N coordination spheres. The O,N,O donor ligand and the ethoxido group constitute a satisfactory O_3N basal plane and the oxido group occupies the apical position. Essentially the same arrangement around vanadium has been seen in related systems.[31,44,54] The displacement of the metal centre from the basal plane toward the apical oxido group is 0.2570 (5) Å though the displacement is noticeably small. This small displacement is possibly due to the coordination of the ethanol molecule.[54] The short V–O(4) distance of 1.580(3) Å indicates the presence of a vanadium–oxygen double-bond (V=O), which is commonly found in five- and six-coordinated octahedral complexes of vanadium(IV) and vanadium(V).[43,44,54–57] The five V–O bond lengths are unequal; the V=O bond being the shortest and the V–O [ethanolic oxygen O(6A)] being the longest due to the trans influence of the oxido atom. The V–O bond lengths follow the order V–O (oxido) < V–O (ethoxide) < V–O (oxime) < V–O (enolate) < V–O (ethanolic). This data indicate stronger binding of the alkoxido group compared to those of other bonded oxygen atoms. The V–O bond distance (av. 1.908 A˚) is similar to those reported for V–O bonds in somewhat related systems.[54] The cis bond angles are in the range 74.44(8)–103.71(11)^o while the trans O=V–O (ethanol) bond angle 175.46(11)^o is almost linear as compared to the other two trans angles (149.44 (9)^o and 160.40 (10)^o) (**Table 3.4**). The orientation of the ethoxido ethyl in complex **1** is toward the oxido group side perhaps due to steric constrains imposed by the metal coordinated ethanol (**Figure 3.4)**.

The one-dimensional self-assembling of the molecule [VO(L^1)(OEt)(EtOH)] is shown in **Figure 3.5**. The molecule is found to show both inter and intra molecular hydrogen bonding. Two [VO(L^1)(OEt)(EtOH)] molecules form a dimeric unit via a pair of reciprocal hydrogen bonds between the phenolic oxygen of one molecule with the ethanolic proton of other moiety

forming intermolecular hydrogen bonding. Another hydrogen bonding between N(1) and phenolic hydrogen, H(1), is also observed constituting an intramolecular hydrogen bond. The H-bond parameters are listed in **Table 3.5**.

Structural characterization of complexes **2** & **3** by X-ray crystallography has not been possible, as their single crystals could not be grown. As all three complexes have been synthesized similarly and display similar properties, the other two [VO(L^{2-3})(OEt)(EtOH)] **(2–3)** complexes are assumed to have the same structure as [VO(L^{1})(OEt)(EtOH)] **(1)**. The results of the 1H NMR in DMSO-d_6 and IR in CH_2Cl_2 solution indicate that the structures of complexes **1**–**3** in solution remain the same as those in the solid state.

Table 3.4. Selected bond distances (Å) and angles (°) for [VO(L^{1})(OEt)(EtOH)] (1). The estimated standard deviations are shown in parentheses.

V-O(4)	1.580(3)	V-O(2)	1.984(2)
V-O(5A)	1.774(2)	V-N(2)	2.116(2)
V-O(3)	1.839(2)	V-O(6A)	2.366(2)
O(3)-V-N(2)	81.08(8)	N(2)-V-O(6A)	81.43(9)
O(3)-V-O(2)	149.44(9)	O(2)-V-O(5A)	94.02(10)
O(3)-V-O(5A)	103.71(11)	O(2)-V-O(4)	99.68(12)
O(3)-V-O(4)	100.03(13)	O(2)-V-O(6A)	79.30(10)
O(3)-V-O(6A)	79.20(11)	O(5A)-V-O(3)	103.71(11)
N(2)-V-O(2)	4.44(8)	O(5A)-V-O(6A)	80.86(11)
N(2)-V-O(5A	160.40(10)	O(4)-V-O(6A)	175.46(11)
N(2)-V-O(4)	94.04(10)	O(4)-V-O(5A)	103.64(12)

Table 3.5. Hydrogen bond distances (Å) and angles (°) for [VO(L^1)(OEt)(EtOH)] (1)

D-H...A	d(D-H)	d(H...A)	d(D...A)	<(DHA)
O(1)-H(1)...N(1)	0.82	1.84	2.562(3)	146.3
O(6A)-H(6A)...O(1)#1	0.82	2.35	2.847(3)	119.8

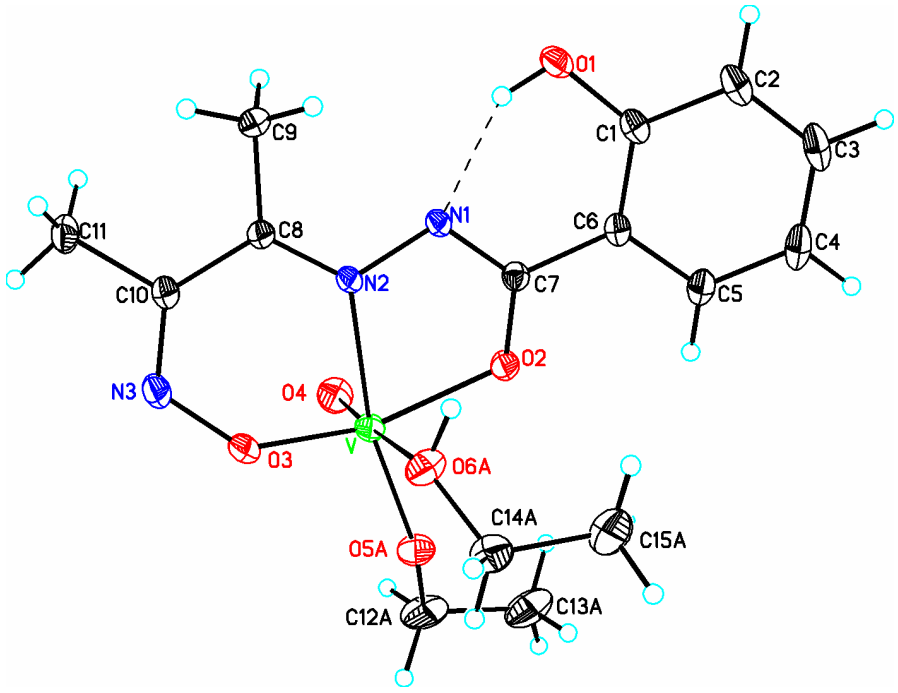

Figure 3.4. ORTEP diagram of [VO(L^1)(OEt)(EtOH)], **1** with atom labeling scheme.

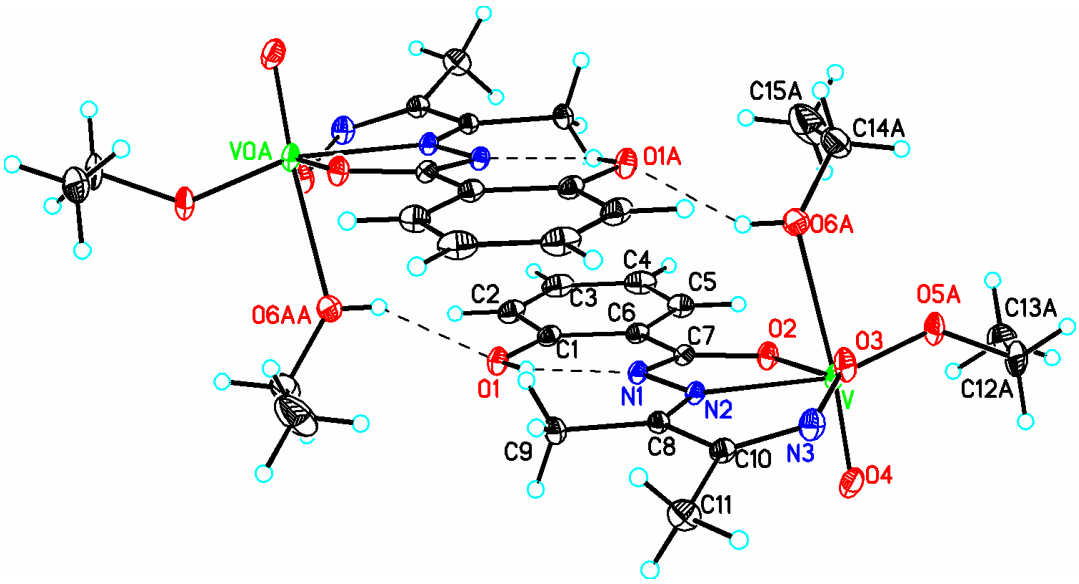

Figure 3.5. Hydrogen bonding diagram of [VO(L^1)(OEt)(EtOH)], **1** with atom labeling scheme.

3.3.5. Antimicrobial activity. In the present study, the synthesized compounds (**1–3**) showed potential antibacterial activity against all the pathogens tested (*Escherichia coli*, *Bacillus*, *Proteus* and *Klebsiella*) and in some cases they showed more promising results by giving the MIC value lesser than the standard drug examined. The biological data (**Table 3.6**) of MIC of the free ligands showed poor activity (MIC = ~ 15.62–500 µg/mL) which is in agreement with the previous results (62.5–250 µg/mL) as reported by Sharma *et al*.[58] following broth micro-dilution method. However, the corresponding oxido vandium(V) complexes (**1–3**) showed much better result with respect to the individual ligands. A possible explanation is that by coordination, the polarity of the ligand and the central metal ion are reduced through the charge equilibration, which favors permeation of the complexes through the lipid layer of the bacterial cell membrane.[59,60] The complex **1** showed the most promising result as compared to the other compounds (**2** and **3**) of this study and similar compounds against same and other pathogens reported by Sharma *et al.*[58] Antibacterial activity of the similar type compounds has also been reported by Chohan et al.[61] and Tahira et al.[62] using agar well diffusion technique against *E. coli*, *Shigella*, *Pseudomonas*, *Salmonella*, *Staphylococcus* and *Bacillus* and the present results are in accordance with the reported values. However, the difference in value may be attributed to the nature of compounds synthesized with different ligands.

Vanadium is a trace element which is essential for higher organisms for their survival where as vanadium(V) complexes are known as potential inhibitors of various enzymes.[63] There are reports of vanadium complexes showing antibacterial, antifungal and anti cancerous properties.[58, 61–63] Hence, the currently synthesized compounds have the potential to be used as an antimicrobial as well as antidiabetic drug. There are also certain draw backs of using vanadium complexes as a therapeutic agent as its toxicity varies with the route of administration and duration; however, there is no report available about its chronic toxicity.[64]

Table 3.6. Antibacterial activity of all the ligands, $H_2L^{1–3}$ and oxido vanadium (V) complexes, [VO($L^{1–3}$)(OEt)(EtOH)] (1–3) *in vitro* MIC in µg $mL^{–1}$

	E.coli	*Bacillus*	*Proteus*	*Klebsiella*
H_2L^1	15.62	31.25	-	-
H_2L^2	125	-	125	500
H_2L^3	125	-	-	125
[VO(L^1)(OEt)(EtOH)] (**1**)	7.81	15.62	15.62	7.81
[VO(L^2)(OEt)(EtOH)] (**2**)	62.50	62.50	31.25	125
[VO(L^3)(OEt)(EtOH)] (**3**)	62.50	31.25	125	62.50
Chloramphenicol	2.00	2.00	6.00	16.00

3.4. CONCLUSION

The present study shows that the 4-R-aroylhydrazoneoximes ligands ($H_2L^{1–3}$, **V**) can bind smoothly to vanadium upon reaction with [$VO(acac)_2$], affording complexes of the type [VO(L)(OEt)(EtOH)], where the oxime oxygen atom coordinates to the metal center, and the nitrogen atom does not take part in coordination (**VI**). All the complexes have been characterized with the help of various spectroscopic techniques and electrochemical measurements. X-ray diffraction measurements of **1**, [$VO(L^1)$(OEt)(EtOH)] have been carried out. The complexes (**1**–**3**) have also been screened for their antibacterial activity against *E. coli, Bacillus, Proteus and Klebsiella*. Minimum inhibitory concentration of these complexes and antibacterial activity indicates the compound **1** as the potential lead molecule for drug designing.

3.5. REFERENCES

(1) Butler, A.; Carrano, C. J. *Coord. Chem. Rev.* **1991**, *109*, 61.

(2) Nielsen, H. F.; Othus, E. O. in: *Vanadium in Biological Systems***,** N. D. Chasteen (Ed), Kluwer Academic Publishers, Dordrecht, The Netherlands, **1990**, 51.

(3) Boyd, D. W.; Kustin, K. Adv. *Inorg. Biochem.* **1984**, *6*, 311.

(4) Kneifel, H.; Bayer, E. *Angew. Chem., Int. Ed. Engl.* **1973**, *85*, 542.

(5) Vilter, H. *Phytochemistry*. **1984**, *23*, 1387.

(6) Butler, A.; Walker, J. V. *Chem. Rev.* **1993**, *93*, 1937.

(7) Weyand, M.; Hecht, H. J.; Kie*β*, M.; Liaud, M. F.; Vilter, H.; Schomburg, D. *J. Mol. Biol.* **1999**, *293*, 595.

(8) Rehder, D.; Santoni, G.; Licini, G. M.; Schulzke, C.; Meier, B. *Coord. Chem. Rev.* **2003**, *237*, 53.

(9) Tsiamis, C.; Voulgaropoulos, B.; Charistos, D.; Voutsas, G. P.; Kavounis, C. A. *Polyhedron.* **2000**, *19*, 2003.

(10) Crans, D. C.; Simone, C. M.; Blanchard, J. S. *J. Am. Chem. Soc.* **1992**, *114*, 4926.

(11) Sigel, H.; Sigel A. (Eds.), *Metal Ions in Biological Systems, Vanadium and its Role in Life*, Marcel Dekker, New York, **1995**, *31*, 779.

(12) Macedo-Ribeiro, S.; Hemrika, W.; Renirie, R.; Wever, R.; Messerschmidt, A. *J. Bio. Inorg. Chem.* **1999**, *4*, 209.

(13) Slebodnick, C.; Hamestra, B. J.; Pecoraro, V. L. *Structure and bonding (Berlin)* **1997**, *89*, 51.

(14) Evangelou, A. E. *Crit. Rev. Oncol. Hematol.* **2002**, *42*, 249.

(15) Köpf-Maier, P. Eur. J. Clin. *Pharmacol.* **1994**, *47*, 1.

(16) Chakravorty, A. *Coord. Chem. Rev.* **1974**, *13*, 1.

(17) Chattopadhyay, S.; Ray, M. S.; Chaudhuri, S.; Mukhopadhyay, G.; Bocelli, G.; Cantoni, A.; Ghosh, A. *Inorg. Chim. Acta* **2006**, *359*, 1367.

(18) Ray, M. S.; Ghosh, A.; Bhattacharya, R.; Mukhopadhyay, G.; Drew, M. G. B.; Ribas, J. *Dalton Trans.* **2004**, 252.

(19) Sreerama, S.; Pal, S. *Inorg. Chem.* **2002**, *41*, 4843.

(20) Datta, D.; Chakravorty, A. *Inorg. Chem.* **1982**, *21*, 363.

(21) Ross, S.; Weyhermüller, T.; Bill, E.; Bothe, E.; Flo¨rke, U.; Wieghardt, K.; Chaudhuri, P. *Eur. J. Inorg. Chem.* **2004**, 984.

(22) Wan, S.; Mori, W.; Yamada, S.; Murahashi, S. I. *Bull. Chem. Soc. Jpn.* **1989**, *62*, 435.

(23) Korvenranta, J.; Saarinen, H.; Näsäkkälä, M. *Inorg. Chem.* **1982**, *21*, 4296.

(24) Mohanty, J. G.; Singh, R. P.; Chakravorty, A. *Inorg. Chem.* **1975**, *14*, 2178.

(25) Mohanty, J. G.; Chakravorty, A. *Inorg. Chem.* **1976**, *15*, 2912.

(26) Lappin, A. G.; Laranjeira, M. C. M.; Peacock, R. D. *Inorg. Chem.* **1983,** *22*, 786.

(27) Gok, Y.; Kantekin, K. *Polyhedron* **1997**, *16*, 2413.

(28) Aly, M. M.; Shatti, N. I. A. *Trans. Met. Chem.* **1998**, *23*, 361.

(29) Hughes, M. N. *The Inorganic Chemistry of Biological Processes,* Wiley, New York, **1981**, 58.

(30) Wolkert, W. A.; Hoffman, T. J. *Chem. Rev.* **1999**, *99*, 2269.

(31) Deng, Z. P.; Gao, S.; Huo, L. H.; Zhao, H. *Acta. Cryst.* **2005**, *E61*, m2214.

(32) Sharma, V.; Sharma, V.; Bohra, R. *Trans. Met. Chem.* **2007**, *32*, 442.

(33) Sharma, V.; Sharma, V.; Bohra, R.; Drake, J. E.; Hursthouse, M. B.; Light, M. E. *Inorg. Chim. Acta* **2007**, *360*, 2009.

(34) Terra, L. H. A.; Areias, M. C.; Gaubeur, I.; Suez-Iha, M. E. V. *Spectrosc. Lett.* **1999**, *32*, 257.

(35) Maurya, M. R.; Agarwal, S.; Abid, M.; Azam, A.; Bader, C.; Ebel, M.; Rehder, D. *Dalton Trans.* **2006**, 937.

(36) Cunha, A. C.; Figueiredo, J. M.; Tributino, J. L. M.; Miranda, A. L. P.; Castro, H. C.; Zingali, R. B.; Fraga, C. A. M.; Souza, M. C. B. V.; Ferreira, V. F.; Barreiro, E. *J. Bioorg. Med. Chem.* **2003**, *11*, 2051.

(37) Iskander, M. F.; El-Sayed, L.; Salem, N. M. H.; Haase, W.; Lindner, H. J.; Foro, S. *Polyhedron* **2004**, *23*, 23.

(38) Ainscough, E. W.; Brodie, A. M.; Denny, W. A.; Finlay, G. J.; Gothe, S. A.; Ranford; J. D., *J. Inorg. Biochem.* **1999**, *77*, 125.

(39) Chaston, T. B.; Richardson, D. R. *J. Biol. Inorg. Chem.* **2003**, *8*, 427.

(40) Bernhardt, P. V.; Chin, P.; Richardson, D. *J. Biol. Inorg. Chem.* **2001**, 6801.

(41) Mostafa, M. M.; Ibrahim, K. M.; Moussa, M. N. H. *Trans. Met. Chem.* **1984**, *9*, 243.

(42) Salem, N. M. H.; El-Sayed, L.; Haase, W.; Iskander, M. F. *J. Coord. Chem.* **2005**, *58*, 1327.

(43) Dinda, R.; Sengupta, P.; Ghosh, S.; Mak. T. C. W. *Inorg. Chem.* **2002**, *41*, 1684.

(44) Dinda, R.; Sengupta, P.; Sutradhar, M.; Mak, T. C. W.; Ghosh, S. *Inorg. Chem.* **2008**, *47* 5634.

(45) Rowe, R. A.; Jones, M. M. *Inorg, Synth.* **1957**, *5*, 113.

(46) Naskar, S.; Mishra, D.; Butcher, R. J.; Chattopadhyay, S. K. *Polyhedron* **2007**, *26*, 3703.

(47) Sheldrick, G. M. SHELX, Programs for Crystal Structure Analysis, University of Göttingen, Germany, **1997**.

(48) Clinical and Laboratory Standards Institute Methods for Dilution Antimicrobial Susceptibility Tests for Bacteria That Grow Aerobically—Seventh Edition: Approved Standard M7-A7. CLSI, Wayne, PA, USA, **2006**.

(49) K. Nakamoto,; in: Infrared and Raman Spectra of Inorganic and Coordination Compounds, Wiley, New York **1986**, 241.

(50) Das, S.; Muthukumaragopal, G. P.; Pal, S. N.; Pal, S. *New J. Chem.* **2003**, *27*, 1102.

(51) Li, D.; Wang, S.; Xu, H.; Yang, Y.; Zeng, S.; Zhao, J.; Wang, D.; Dou, J. *Inorg. Chim. Acta* **2011**, *365*, 85.

(52) Moon, M.; Pyo, M.; Myoung, Y. C.; Ahn, C. II.; Lah, M. S. *Inorg. Chem.* **2001**, *40*, 554.

(53) Halder, S.; Acharyya, R.; Peng, S. M.; Lee, G. H.; Drew, M. G. B.; Bhattacharya, S. *Inorg. Chem.* **2006**, *45*, 9654.

(54) Sarkar, A.; Pal, S. *Inorg. Chim. Acta* **2008**, *361*, 2296.

(55) Glas, H.; HerdTweck, E.; Artus, G. R. J.; Thil, W. R. *Inorg. Chem.* **1998**, *37*, 3644.

(56) Sun, Y.; Melchior, M.; Summers, D. A.; Thompson, R. C.; Retting, S. J.; Orvig, C. *Inorg. Chem.* **1998**, *37*, 3119.

(57) Maurya, M. R.; Khurana, S.; Schulzke, C.; Rehder, D. *Eur. J. Inorg. Chem.* **2001**, 779.

(58) Sharma, N.; Kumari, M.; Kumar, V. *J. Coord. Chem.* **2010**, *63*, 1940.

(59) Ramadan, A. M. *J. Inorg. Biochem.* **1997**, *65*, 183.

(60) Avaji, P. G.; Kumar, C. H. V.; Patil, S. A.; Shivananda, K. N.; Nagaraju, C. *Eur. J. of Med. Chem.* **2009**, *44*, 3552.

(61) Chohan, Z. H.; Sumrra, S. H.; Youssoufi, M. H. *Eur. J. of Med. Chem.* **2010**, *45*, 2739.

(62) Tahira, K.; Ali, S.; Shahzadi, S. *J. Coord. Chem.* **2011**, *64*, 1871.

(63) Prasad, K. S.; Kumar, L. S.; Shekar, S. C.; Prasad, M.; Revanasiddappa, H. D. *Chem. Sci. J.* **2011**, *2011*, CSJ-12.

(64) Katherine, H.; Thompson, J. H.; McNeill, J. H.; Orvig, C. *Chem. Rev.* **1999**, *99*, 2561.

Chapter 4

Study of bio- and catalytic potential of oxidoethoxido vanadium(V) complexes with aroylhydrazones of naphthol-derivative: Special focus on their solution behavior

Chapter 4

Study of bio- and catalytic potential of oxidoethoxido vanadium(V) complexes with aroylhydrazones of naphthol-derivative: Special focus on their solution behavior

ABSTRACT

Four oxidoalkoxido vanadium(V) [$V^{V}O(L^{1–4})OEt$] (**1**–**4**) and one dinuclear oxidoalkoxido mixed-ligand vanadium(V) [{$VO(L^{2})OEt\}_2(Q)$]{Q = 4,4′-bipyridine}(**5**), complexes, taking potentially tridentate binegative aroylhydrazone ligands are reported [where H_2L^1 = anthranylhydrazone of 2-hydroxy-1-napthaldehyde, H_2L^2 = salicylhydrazone of 2-hydroxy-1-napthaldehyde, H_2L^3 = benzoylhydrazone of 2-hydroxy-1-acetonaphthone, H_2L^4 = anthranylhydrazone of 2-hydroxy-1-acetonaphthone]. All the complexes were characterized by elemental analysis as well as various spectroscopic techniques. Single crystal X-ray diffraction crystallography of **1**–**4**, reveals the metal centre is in distorted square pyramidal geometry with O_4N coordination spheres, whereas **5** exhibits a distorted octahedral geometry around the metal center. The solution behavior of the oxidoethoxido vanadium(V) species, **1**–**4** was studied, which indicates the existence of two species (1:1 ratio) in solution. Catalytic potential of **1**–**5**, was tested for the oxidative bromination of styrene, salicylaldehyde and oxidation of methyl phenyl sulphide. In addition, all the complexes (**1**–**5)** showed good DNA binding and photonuclease propensity. Among these, **3** and **4** shows higher binding affinity towards CT-DNA than others.

4.1. INTRODUCTION

The chemistry of vanadium is currently a subject of extensive research, because of its increasingly recognized biochemical importance.[1] Since the discovery by Henze in 1911 of high concentrations of vanadium in the blood of ascidians,[2] it has been identified as an essential element for some important vanadium-containing enzymes, nitrogenase,[3] haloperoxidase,[4] nitrate reductases,[5] and Amavadin,[6] a compound isolated from the mushroom *Amanita muscaria*, that has been shown to contain an octacoordinated V^{4+} ion.[7] A vanadium protein has also been proposed to catalyze the oxidation of NADH.[8] Moreover, several vanadium compounds have been shown to be active as insulin mimetics *in vitro* and *in vivo*,[9] including clinical tests, demonstrating the usability of simple inorganic (vanadyl sulfate, vanadate)[10] and coordination compounds $[VO(maltolato)_2]$[11] for the treatment of diabetes mellitus in humans. The distinct preference of this metal center for O- and/or N-coordination environments, as delineated by EXAFS[12] and crystallographic studies[13] on haloperoxidase, has prompted the synthesis of numerous model vanadium compounds containing O- and N- donor ligands, whose solid state structure, spectroscopic, magnetic, and redox properties have been widely investigated. In contrast, study of solution properties of these, especially the oxidovanadium(V) complexes have so far received only limited attention[14] despite the reported involvement of such species to provide the alternative route for the generation of monooxidobridged binuclear vanadium(V,V) species of the type $(VOL)_2O$. It may also be noted that such binuclear complexes hold the possibility of acting as precursors of mixed-valence V(IV,V) species, which are of current interest.[14b]

Over the past few years, we have been studying the chemistry of oxido-metal complexes including those of vanadium, in N,O-donor environments[14b,15a-c] with electro-generation of mixed-valence divanadium(IV,V) complexes,[14b,15a] and the anti-proliferative, DNA binding, photo-induced DNA cleavage and insulin mimetic activity of variable valence oxido and nonoxido vanadium complexes.[15d,e]

In previous work[14b] our group has described the solution behavior of a mononuclear oxidoalkoxido vanadium(V) complex in chloroform, a non coordinating solvent, where the transformation of a structurally characterized [VO(L)OEt] (H_2L = 2-hydroxybenzaldehydehydrazone of 2-hydroxybenzoylhydrazine) complex to the corresponding

monooxidobridged divanadium(V,V) complex $(VOL)_2O$, and electrogeneration of mixed-valence divanadium(IV,V) species was reported.

In this chapter we now report the synthesis, characterization and biological and catalytic evaluation of five new oxidoethoxido vanadium(V) complex (**1**−**5**) with special emphasis on the solution behavior of monomeric oxidoethoxido vanadium(V) compounds, namely, $[VOL^{1-4}(OEt)]$ (**1**−**4**) in presence of a coordinating solvent, DMSO. Here, NMR (^{1}H, ^{13}C and ^{51}V), solution IR, and ESI-MS solution studies of **1**−**4**, were reported to obtain a detailed understanding of the species existing in solution state, their structure, oxidation states, and their redox properties. Solution studies indicate that two species simultaneously exists in solution. All the complexes (**1**−**5**), were isolated in the solid state and are found to show good catalytic potential for the oxidative bromination of styrene, salicylaldehyde and oxidation of methyl phenyl sulphide. They also show interesting DNA binding and photoinduced DNA cleavage activities.

4.2. EXPERIMENTAL SECTION

4.2.1. General Methods and Materials. All chemicals were purchased from commercial sources and used without further purification. $[VO(acac)_2]$ was prepared as described in the literature.[16] Reagent grade solvents were dried and distilled prior to use. Elemental analyses were performed on a Vario ELcube CHNS Elemental analyzer. IR spectra were recorded on a Perkin-Elmer Spectrum RXI spectrophotometer. ^{1}H and ^{13}C NMR spectra were recorded on a Bruker Ultrashield 400 MHz spectrometer using $SiMe_4$ as an internal standard. Electronic spectra were recorded on a Lamda25, PerkinElmer spectrophotometer. Mass spectra were obtained on a SQ-300 MS instrument operating in ESI mode. The supercoiled (SC) pUC19 DNA was purified from *E. coli* cells with the aid of Gene JET Plasmid Isolation Kit (Thermo Scientific, USA). Calf thymus (CT) DNA was purchased from SRL (India) (biochemistry grade). Agarose (molecular biology grade) was purchased from Sigma Aldrich (USA). A Shimadzu 2010 plus gas-chromatograph fitted with an Rtx-1 capillary column (30 m × 0.25 mm × 0.25 μm) and a FID detector was used to analyze the reaction products and their quantifications were made on the basis of the relative peak area of the respective product. The identity of the products was confirmed using a GC-MS model Perkin-Elmer, Clarus 500 and comparing the fragments of each

product with the library available. The percent conversion of substrate and selectivity of products was calculated from GC data using the formulae:

$$\% \text{ Conversion of substrate } = 100 - \frac{\text{Peak area of a substrate}}{\text{Total area of substrate + products}} \text{ X } 100$$

$$\% \text{ Selectivity of a product} = \frac{\text{Peak area of a product}}{\text{Total area of products}} \text{ X } 100$$

4.2.2. Synthesis of Ligands ($H_2L^{1–4}$). Schiff base ligands, anthranylhydrazone of 2-hydroxy-1-napthaldehyde (H_2L^1), salicylhydrazone of 2-hydroxy-1-napthaldehyde (H_2L^2), benzoylhydrazone of 2-hydroxy-1-acetonaphthone (H_2L^3), and anthranylhydrazone of 2-hydroxy-1-acetonaphthone (H_2L^4) were prepared by the condensation of 2-hydroxy-1-napthaldehyde / 2-hydroxy-1-acetonapthone and the respective acidhydrazide in equimolar ratio in ethanol by a standard procedure.[15d] The resulting white compounds were filtered, washed with ethanol and dried over fused $CaCl_2$. Elemental analysis results, NMR (^1H and ^{13}C) and IR data for all of these verified their preparation.

H_2L^1. Yield: 62%. Anal. Calcd. for $C_{18}H_{15}N_3O_2$: C, 70.81; H, 4.95; N, 13.77. Found: C, 70.77; H, 4.98; N, 13.75. IR (KBr pellet, cm^{-1}): 3472 ν(O–H); 3367 $\nu(NH_2)_s$; 3201 $\nu(NH_2)_{as}$; 3037 ν(N–H); 1637 ν(C=O); 1591 ν(C=N). ^1H NMR (400 MHz, DMSO-d_6): δ 12.97 (s, 1H, naphthyl-OH), 12.04 (s, 1H, NH), 9.47 (s, 1H, HC═N), 8.18–6.64 (m, 10H, Aromatic), 6.61 (s, 2H, NH_2) ppm. ^{13}C NMR (100 MHz, DMSO-d_6): δ 165.12, 158.33, 150.93, 146.33, 133.18, 132.91, 132.07, 129.45, 128.57, 128.25, 128.16, 123.96, 120.88, 119.42, 117.12, 115.14, 112.62, 109.06.

H_2L^2. Yield: 72%. Anal. Calcd. for $C_{18}H_{14}N_2O_3$: C, 70.58; H, 4.61; N, 9.15. Found: C, 70.59; H, 4.58; N, 9.12. IR (KBr pellet, cm^{-1}): 3466 ν(O–H); 3022 ν(N–H); 1621 ν(C=O); 1578 ν(C=N). ^1H NMR (400 MHz, DMSO-d_6): δ 12.74 (s, 1H, naphthyl-OH), 12.07 (s, 1H, NH), 11.87 (s, 1H, OH), 9.54 (s, 1H, HC═N), 8.33–6.62 (m, 10H, Aromatic). ^{13}C NMR (100 MHz, DMSO-d_6): δ 163.72, 158.51, 157.89, 147.44, 133.78, 132.68, 131.44, 128.69, 128.55, 127.57, 127.50, 123.33, 120.73, 118.92, 118.65, 117.05, 115.48, 108.36.

H_2L^3. Yield: 58%. Anal. Calcd. for $C_{19}H_{16}N_2O_2$: C, 74.98; H, 5.29; N, 9.20. Found: C, 74.96; H, 5.32; N, 9.21. IR (KBr pellet, cm^{-1}): 3337 ν(O–H); 3071 ν(N–H); 1659 ν(C=O); 1573 ν(C=N). ^{1}H NMR (400 MHz, DMSO-d_6): δ 10.31 (s, 1H, naphthyl–OH), 9.55 (s, 1H, NH), 7.91–7.27 (m, 11H, Aromatic), 2.34 (s, 3H, CH_3).^{13}C NMR (100 MHz, DMSO-d_6): δ 153.71, 152.63, 134.24, 131.82, 131.51, 130.21, 129.06, 128.76, 128.36, 128.23, 127.86, 127.43, 126.99, 123.67, 123.19, 118.99, 118.71, 113.74, 24.30.

H_2L^4. Yield: 64%. Anal. Calcd. for $C_{19}H_{17}N_3O_2$: C, 71.46; H, 5.36; N, 13.16. Found: C, 71.48; H, 5.37; N, 13.14. IR (KBr pellet, cm^{-1}): 3473 ν(O–H); 3410 $\nu(NH_2)_s$; 3329 $\nu(NH_2)_{as}$; 3221 ν(N–H); 1663 ν(C=O); 1553 ν(C=N). ^{1}H NMR (400 MHz, DMSO-d_6): δ 10.35 (s, 1H, naphthyl–OH), 9.17 (s, 1H, NH), 7.91–6.23 (m, 10H, Aromatic), 6.05 (s, 2H, NH_2), 2.35 (s, 3H, CH_3). ^{13}C NMR (100 MHz, DMSO-d_6): δ 153.98, 152.47, 152.36, 149.84, 132.47, 131.56, 130.22, 129.09, 128.34, 127.98, 127.67, 123.78, 123.14, 118.94, 117.04, 115.46, 114.69, 113.59, 24.15.

4.2.3. Synthesis of Complexes [VO($L^{1–4}$)OEt] (1–4). A general synthetic procedure taking [NH_4VO_3] as metal precursor is described below:

[NH_4VO_3] (1 mmol) was added to a hot solution of appropriate ligand $H_2L^{1–4}$ (1 mmol) in EtOH (20 mL), the color changed instantly to brownish. After 3 h of refluxing, reaction mixture was filtered off, and kept for crystallisation. After 3 to 4 days, crystals of diffraction quality were obtained which were used for X-ray structure determination using single crystal X-ray diffractometer.

[VO(L^1)OEt] (1). Yield: 61%. Anal. Calcd. for $C_{20}H_{18}N_3O_4V$: C, 57.84; H, 4.37; N, 10.12. Found: C, 57.83; H, 4.39; N, 10.08. IR (KBr pellet, cm^{-1}): 3461 $\nu(NH_2)_s$; 3322 $\nu(NH_2)_{as}$; 1595 ν(C=N); 1255 $\nu(C–O)_{enolic}$; 991 ν(V=O). UV–Vis ($CHCl_3$) [λ_{max}, nm (ε, M^{-1} cm^{-1})]: 434 (15257); 336 (19651); 286 (26852); 248 (30614).

[VO(L^2)OEt] (2). Yield: 65%. Anal. Calcd. for $C_{20}H_{17}N_2O_5V$: C, 57.70; H, 4.12; N, 6.73. Found: C, 57.72; H, 4.08; N, 6.77. IR (KBr pellet, cm^{-1}): 3442 (O–H); 1597 ν(C=N); 1254 $\nu(C–O)_{enolic}$; 996 ν(V=O). UV–Vis ($CHCl_3$) [λ_{max}, nm (ε, M^{-1} cm^{-1})]: 425 (12649); 339 (20637); 273 (27392); 245 (27822).

[VO(L^3)OEt] (3). Yield: 66%. Anal. Calcd. for $C_{21}H_{19}N_2O_4V$: C, 60.88; H, 4.62; N, 6.76. Found: C, 60.86; H, 4.58; N, 6.77. IR (KBr pellet, cm^{-1}): 1595 *ν*(C=N); 1239 $\nu(C–O)_{enolic}$; 999 *ν*(V=O). UV–Vis ($CHCl_3$) [λ_{max}, nm (ε, M^{-1} cm^{-1})]: 430 (7003); 343 (14511); 286 (21713); 242 (25207).

[VO(L^4)OEt] (4). Yield: 64%. Anal. Calcd. for $C_{21}H_{20}N_3O_4V$: C, 58.75; H, 4.70; N, 9.79. Found: C, 58.74; H, 4.73; N, 9.78. IR (KBr pellet, cm^{-1}): 1567 *ν*(C=N); 1238 $\nu(C–O)_{enolic}$; 996 *ν*(V=O). UV–Vis ($CHCl_3$) [λ_{max}, nm (ε, M^{-1} cm^{-1})]: 419 (14445); 305 (18634); 277 (24006); 253 (30231).

4.2.4. Synthesis of mixed-ligand complex [{VO(L^2)OEt}$_2$(μ-4,4' bipy)] (5). To the refluxing solution of ligand, H_2L^2 (1 mmol) in 20 mL ethanol, 4,4' bipyridine (0.5 mmol) was added. After 10 mins, NH_4VO_3 (1 mmol) was added to the reaction mixture. The colour changed to brown. After 3 h, the solution was filtered off, and kept for crystallisation. Slow evaporation of the filtrate over 5-6 days, produced crystals of diffraction quality, which were used for X-ray structure determination using single crystal X-ray diffractometer.

[{VO(L^2)OEt}$_2$(μ-4,4' bipy)] (5). Yield: 41%. Anal. Calcd. for $C_{50}H_{42}N_6O_{10}V_2$: C, 60.73; H, 4.28; N, 8.49. Found: C, 60.70; H, 4.24; N, 8.52. IR (KBr pellet, cm^{-1}): 1599 *ν*(C=N), 1252 $\nu(C–O_{enolic})$, 1049 *ν*(N-N), 959 *ν*(V=O). UV–vis ($CHCl_3$) [λ max, nm (ε, M^{-1} cm^{-1})]: 456 (7831); 346 (14651); 281 (12719); 259 (18603). ^{1}H NMR (400 MHz, DMSO-d_6): *δ* 11.59 (s, 1H, OH), 9.89 (s, 1H, CH), 8.70–6.94. (m, 14H, Aromatic), 5.76 (m, 2H, CH_2 (OEt)), 1.62 (t, 3H, CH_3 (OEt)). ^{13}C NMR (100 MHz, DMSO-d_6): *δ* 170.10, 164.33, 159.01, 150.56, 149.27, 145.10, 135.51, 133.50, 132.98, 129.41, 129.17, 128.61, 128.45, 124.32, 122.05, 121.74, 119.61, 119.25, 117.10, 114.69, 111.43, 83.15, 18.60. ^{51}V NMR (DMSO-d_6): *δ* –553.

4.2.5. Solution state Characterization of [VO($L^{1–4}$)OEt] (1–4).

[VO(L^1)OEt] (1). IR ($CHCl_3$, cm^{-1}): 1002, 977 *ν*(V=O), 821 *ν*(V–O–V). ^{1}H NMR (400 MHz, DMSO-d_6): *δ* 9.99 (s, 1H, HC═N), 9.94 (s, 1H, HC═N), 8.59–6.43 (m, 20H, Aromatic), 5.65 (m, 2H, CH_2 (OEt)), 4.32 (s, 2H, NH_2), 3.46 (q, 4H, CH_2 (EtOH)), 1.59 (t, 3H, CH_3 (OEt)), 1.07 (t, 6H, CH_3 (EtOH)). ^{13}C NMR (100 MHz, DMSO-d_6): *δ* 171.22, 170.93, 164.64, 164.46, 164.18, 149.78, 149.65, 148.26, 148.11, 135.71, 135.52, 135.15, 132.91, 132.78, 132. 65, 132.41, 130.97,

130.57, 129.44, 129.34, 128.82, 128.54, 128.48, 124.71, 124.35, 122.45, 122.11, 119.90, 119.03, 116.39, 115.17, 111.82, 111.67, 111.05, 110.36, 81.80, 56.52, 19.03, 18.84. ^{51}V NMR (DMSO-d_6): δ –548, –576. ^{1}H NMR (400 MHz, DMSO-d_6 + EtOH): δ 9.80 (s, 1H, HC═N), 8.49–6.57 (m, 10H, Aromatic), 5.64 (m, 2H, CH_2 (OEt)), 4.33 (s, 20H, NH_2), 3.47 (q, 46H, CH_2 (EtOH)), 1.59 (t, 3H, CH_3 (OEt)), 1.07 (t, 67H, CH_3 (EtOH)). ^{13}C NMR (100 MHz, DMSO-d_6 + EtOH): δ 171.06, 164.22, 149.65, 148.15, 135.04, 132.88, 132.27, 130.54, 129.23, 128.54, 128.39, 124.24, 121.94, 119.79, 116.31, 115.08, 111.65, 111.07, 81.70, 56.54, 18.75, 18.64. ^{51}V NMR (DMSO-d_6 + EtOH): δ –551. ESI-MS (DMSO) : *m/z* 386.16 (100%, $[M - CH_2CH_3]^+$); *m/z* 756.13 (14%, $[V_2O_3(L^1)_2]^+$).

[VO(L^2)OEt] (2). IR ($CHCl_3$, cm^{-1}): 1006, 980 ν(V=O), 823 ν(V–O–V). ^{1}H NMR (400 MHz, DMSO-d_6) δ 11.60 (s, 1H, OH), 11.42 (s, 1H, OH), 10.09 (s, 1H, HC═N), 9.95 (s, 1H, HC═N), 8.65–6.83 (m, 20H, Aromatic), 5.76 (m, 2H, CH_2 (OEt)), 3.44 (q, 4H, CH_2 (EtOH)), 1.61 (t, 3H, CH_3 (OEt)), 1.05 (t, 6H, CH_3 (EtOH)). ^{13}C NMR (100 MHz, DMSO-d_6): δ 169.95, 164.66, 164.29, 158.96, 158.90, 149.52, 136.06, 135.73, 133.98, 133.80, 133.01, 129.72, 129.51, 129.45, 129.34, 128.90, 128.62, 124. 85, 124.53, 122.64, 122.29, 119.76, 119.57, 118.90, 117.31, 114.69, 114.30, 111.62, 111.46, 83.32, 56.50, 19.02, 18.81. ^{51}V NMR (DMSO-d_6): δ –553, –591. ^{1}H NMR (400 MHz, DMSO-d_6 + EtOH,) δ 11.61 (s, 1H, OH), 9.94 (s, 1H, HC═N), 8.56–6.97 (m, 10H, Aromatic), 5.76 (m, 2H, CH_2 (OEt)), 3.45 (q, 46H, CH_2 (EtOH)), 1.62 (t, 3H, CH_3 (OEt)), 1.06 (t, 68H, CH_3 (EtOH)). ^{13}C NMR (100 MHz, DMSO-d_6 + EtOH): δ 170.25, 164.36, 159.04, 149.04, 135.35, 133.31, 132.92, 129.35, 129.05, 128.61, 128.34, 124.18, 121.80, 119.49, 119.05, 116.95, 114.67, 111.41, 83.14, 56.57, 18.25. ^{51}V NMR (DMSO-d_6 + EtOH): δ –553. ESI-MS (DMSO): *m/z* 387.06 (100%, $[M - CH_2CH_3]^+$); *m/z* 758.05 (30%, $[V_2O_3(L^2)_2]^+$).

[VO(L^3)OEt] (3). IR ($CHCl_3$, cm^{-1}): 1004, 966 ν(V=O), 820 ν(V–O–V). ^{1}H NMR (400 MHz, DMSO-d_6) δ 7.98–7.20 (m, 22H, Aromatic), 5.48 (m, 2H, CH_2 (OEt)), 3.45 (q, 4H, CH_2 (EtOH)), 2.92 (s, 3H, CH_3), 2.84 (s, 3H, CH_3), 1.50 (t, 3H, CH_3 (OEt)), 1.06 (t, 6H, CH_3 (EtOH)). ^{13}C NMR (100 MHz, DMSO-d_6): δ 170.91, 170.36, 166.64, 166.47, 166.16, 160.17, 134.85, 134.75, 133.89, 132.13, 132.01, 131.82, 131.77, 130.94, 130.66, 130.01, 129.95, 129.56, 129.35, 128.97, 128.70, 128.61, 128.53, 128.00, 127.58, 126.54, 126.17, 124.99, 124.88, 124.34, 119.50, 118.75, 118.46, 118.17, 118.03, 117.86, 80.23, 56.51, 24.09, 23.84, 19.01, 18.67. ^{51}V NMR (DMSO-d_6): δ –518, –534. ^{1}H NMR (400 MHz, DMSO-d_6 + EtOH) δ 8.09–7.20 (m, 11H, Aromatic), 5.48 (m,

2H, CH_2 (OEt)), 3.46 (q, 56H, CH_2 (EtOH), 2.92 (s, 3H, CH_3), 1.51 (t, 3H, CH_3 (OEt)), 1.06 (t, 83H, CH_3 (EtOH)). ^{13}C NMR (100 MHz, DMSO-d_6 + EtOH): δ 170.87, 166.13, 159.73, 133.80, 131.99, 131.75, 131.69, 129.58, 129.26, 128.86, 128.49, 127.47, 126.10, 124.25, 119.41, 118.16, 80.20, 56.53, 23.68, 18.77, 18.50. ^{51}V NMR (DMSO-d_6 + EtOH): δ –518. ESI-MS (DMSO): *m/z* 385.10 (64%, $[M - CH_2CH_3]^+$); *m/z* 754.19 (100%, $[V_2O_3(L^3)_2]^+$).

[VO(L^4)OEt] (4). IR ($CHCl_3$, cm^{-1}): 1004, 969 ν(V=O), 821 ν(V–O–V). ^{1}H NMR (400 MHz, DMSO-d_6): δ 8.21–6.31 (m, 20H, Aromatic), 5.50 (m, 2H, CH_2 (OEt)), 4.52 (s, 2H, NH_2), 3.48 (q, 4H, CH_2 (EtOH)), 2.95 (s, 3H, CH_3), 2.87 (s, 3H, CH_3), 1.53 (t, 3H, CH_3 (OEt)), 1.08 (t, 6H, CH_3 (EtOH)). ^{13}C NMR (100 MHz, DMSO-d_6): δ 171.89, 171.39, 166.55, 166.22, 166.03, 159.23, 158.05, 150.01 149.87, 134.68, 133.78, 132.85, 132.59, 131.98, 131.72, 130.73, 130.61, 129.93, 129.56, 129.33, 127.99, 127.56, 126.52, 126.16, 124.95, 124.33, 119.51, 118.45, 118. 16, 117.99, 117.89, 116.40, 115.38, 115.13, 111.26, 110.04, 80.15, 56.57, 24.19, 23.96, 19.03, 18.74. ^{51}V NMR (DMSO-d_6): δ –528, –544. ^{1}H NMR (DMSO-d_6+ EtOH, 400 MHz): δ 8.09–6.60 (m, 10H, Aromatic), 5.49 (m, 2H, CH_2 (OEt)), 4.51 (s, 2H, NH_2), 3.50 (q, 48H, CH_2 (EtOH)), 2.86 (s, 3H, CH_3), 1.54 (t, 3H, CH_3 (OEt)), 1.09 (t, 72H, CH_3 (EtOH)). ^{13}C NMR (100 MHz, DMSO-d_6 + EtOH): δ 171.97, 165.94, 158.21, 149.79, 133.63, 132.36, 131.91, 130.51, 129.14, 127.34, 126.02, 124.18, 119.28, 118.09, 116.28, 115.27, 111.23, 80.00, 56.61, 23.64, 18.50, 18.35. ^{51}V NMR (DMSO-d_6+ EtOH): δ –529. ESI-MS (DMSO): *m/z* 400.02 (100%, $[M - CH_2CH_3]^+$); *m/z* 784.30 (50%, $[V_2O_3(L^4)_2]^+$).

4.2.6. X-ray Crystallography. Single crystals of complexes **1**–**5** were mounted on Stoe IPDS 2 diffractometer equipped with an Oxford Cryosystem open flow cryostat, equipped with a graphite monochromator and a Mo Kα radiator (λ) 0.71073 Å. Crystallographic data and details of refinement are given in **Table 4.1**. The unit cell dimensions and intensity data were measured at 200 (2) K. Absorption correction was partially integrated in the data reduction procedure for crystals of **1**–**5**.[17] The intensity data were corrected for Lorentz, polarization and absorption effects. Absorption corrections were applied using SADABS[18] and the structures were solved by direct methods using the program SHELXS-97[19] and refined using least squares with the SHELXL-97[19] software program. Hydrogens were either found or placed in calculated positions and isotropically refined using a riding model. The non-hydrogen atoms were refined anisotropically.

Table 4.1. Crystal data and refinement details for 1–5

Complex	1	2	3	4	5
Empirical formula	$C_{20}H_{18}N_3O_4V$	$C_{20}H_{17}N_2O_5V$	$C_{21}H_{19}N_2O_4V$	$C_{21}H_{20}N_3O_4V$	$C_{50}H_{42}N_6O_{10}V_2$
Formula weight	415.31	416.30	414.32	429.34	988.77
Temperature	293(2) K	293(2) K	293(2) K	200(2) K	293(2) K
Wavelength	0.71073 A	0.71073 A	0.71073 A	0.71073 Å	1.54184 Å
Crystal system	Monoclinic	Monoclinic	Monoclinic	Monoclinic	Tetragonal
Space group	P 21/n	P 21/c	P 21/n	P 21/n	P 4/n
Unit cell dimensions	a = 7.5992(7) A b = 12.7639(11) A c = 19.5684(17) A α = 90 ° β = 90.373(2) ° γ = 90 °	a = 18.249(3) A b = 5.9376(11) A c = 18.227(3) A α = 90 ° β = 110.346(9) ° γ = 90 °	a = 10.109(5) A b = 15.079(8) A c = 13.002(7) A α = 90 ° β = 91.424(9) ° γ= 90 °	a = 10.305(2) Å b = 10.502(2) Å c = 18.603(3) Å α= 90° β= 92.716(16)°. γ = 90°.	a = 21.5608(3) Å b = 21.5608(3) Å c = 10.1344(3) Å α= 90° β= 90° γ = 90°
Volume	1898.0(3) $Å^3$	1851.8(6) $Å^3$	1981.4(18) $Å^3$	2011.0(6) $Å^3$	4711.16(19) $Å^3$
Z	4	4	4	4	4
Density (calculated)	1.453 Mg/m^3	1.493 Mg/m^3	1.389 Mg/m^3	1.418 Mg/m^3	1.394 Mg/m^3
Absorption coefficient	0.554 mm^{-1}	0.571 mm^{-1}	0.529 mm^{-1}	0.526 mm^{-1}	3.872 mm^{-1}
F(000)	856	856	856	888	2040
Theta range for data collection	1.90 to 26.00 °.	2.26 to 26.00 °.	2.07 to 26.00 °	2.192 to 24.995°.	11.203 to 66.586°.
Reflections collected	19292	26070	19369	25232	12627
Independent reflections	3732 [R(int) = 0.0788]	3645 [R(int) = 0.0979]	3894 [R(int) = 0.0399]	3546 [R(int) = 0.1343]	4129 [R(int) = 0.0317]
Completeness to theta = 25.00°	100.0 %	99.9 %	99.7 %	99.9 %	96.6 %
Refinement method	Full-matrix least-squares on F^2	Full-matrix least-squares on F^2	Full-matrix least-squares on F^2	Full-matrix least-squares on F^2	Full-matrix least-squares on F^2
Data / restraints / parameters	3732 / 1 / 262	3645 / 13 / 246	3894 / 13 / 255	3546 / 0 / 267	4129 / 0 / 310
Goodness-of-fit on F^2	1.045	1.056	0.884	0.857	1.011
Final R indices [I>2sigma(I)]	R1 = 0.0939, wR2 = 0.2142	R1 = 0.0831, wR2 = 0.2028	R1 = 0.0464, wR2 = 0.1265	R1 = 0.0489, wR2 = 0.1124	R1 = 0.0457, wR2 = 0.1263
R indices (all data)	R1 = 0.1668, wR2 = 0.2584	R1 = 0.1296, wR2 = 0.2560	R1 = 0.0718, wR2 = 0.1531	R1 = 0.1224, wR2 = 0.1393	R1 = 0.0532, wR2 = 0.1317

4.2.7. Catalytic Reactions.

4.2.7.1. Oxidative bromination of styrene. Complexes **1**–**5**, were used as catalyst precursors to carry out the oxidative bromination of styrene. In a typical reaction, styrene (1.04 g, 10 mmol) was added to an aqueous solution (20 mL) of KBr (3.57 g, 30 mmol), followed by the addition of CH_3CN (25 mL) and 30% aqueous H_2O_2 (3.39 g, 30 mmol) in a 100 mL reaction flask. The catalyst (0.0005g) and 70% $HClO_4$ (2.86g, 5 mmol) were added, and the reaction mixture was stirred at room temperature. Three additional 5 mmol portions of 70% $HClO_4$ were further added after every 15 min with continuous stirring. In all batches, the experimental conditions (e.g., stirring speed, the size of the magnetic bar and reaction flask) were kept as similar as possible. After 1 h, the orange organic layer was separated with a separatory funnel, washed with water and dried. The crude mass was redissolved in CH_3CN; insoluble material, if any, was removed by filtration, and the solvent evaporated. The reaction products were separated by using a silica gel column. Elution of the column with 1% CH_3CN in *n*-hexane first separated a mixture of bromo derivatives followed by 1-phenylethane-1,2- diol. The two bromo derivatives were finally separated from each other with the silica gel column again by eluting with pure *n*-hexane. The identity of all the products was confirmed by GC–MS and ^{1}H NMR spectroscopy.

4.2.7.2. Oxidative bromination of salicylaldehyde. Salicylaldehyde (0.610 g, 5 mmol) was added to an aqueous solution (20 mL) of KBr (1.785 g, 15 mmol), followed by addition of aqueous 30% H_2O_2 (1.14 g, 10 mmol) in a 100 mL reaction flask. The catalyst (0.0005 g) and 70% $HClO_4$ (2.14g, 15 mmol) were added, and the reaction mixture was stirred at room temperature (20 °C). The addition of $HClO_4$, however, in four equal portions during the reaction in 45 min interval was necessary to improve the conversion of the substrate and to avoid decomposition of the catalyst. After 3 h, the separated white products were extracted with CH_2Cl_2 and dried. The crude mass was dissolved in methanol and was subjected to gas chromatography. The identity of the products was confirmed as mentioned above.

4.2.7.3. Oxidation of methyl phenyl sulfide. Methylphenyl sulfide (0.620 g, 5 mmol) and aqueous 30% H_2O_2 (1.14 g, 10 mmol) were dissolved in CH_3CN (5 mL). After addition of 0.001 g catalyst (**1**–**5**) to the above solution, the reaction mixture was stirred at room temperature for 2.5 h. During this period, the reaction products formed were analyzed using gas

chromatography by withdrawing small aliquots after fixed time intervals. The identities of the reaction products were confirmed by GC-MS.

4.2.8. DNA binding experiments.

4.2.8.1. Absorption spectral studies. Binding of the oxidoalkoxido vanadium(V) complexes (**1**–**5)** to calf thymus DNA (CT-DNA) was studied in 10 mM Tris–HCl buffer (pH 8.0) containing 10% DMF. UV-Vis absorption titration experiments were performed by using a fixed concentration of metal complex (25 μM) and varying CT-DNA concentration from 0 to 65 μM. After each addition of CT-DNA (5 μM) to the metal complex, the spectra were recorded after equilibration for 5 min using Perkin Elmer Lamda35 spectrophotometer. The data were then fit to the following equation to obtain binding constant K_b[20]

$$\frac{[\mathrm{DNA}]}{\varepsilon_a - \varepsilon_f} = \frac{[\mathrm{DNA}]}{\varepsilon_b - \varepsilon_f} + \frac{1}{K_b(\varepsilon_b - \varepsilon_f)}; \qquad \text{Eq. 1}$$

where [DNA] is the concentration of DNA base pairs, ε_a, ε_f and ε_b correspond to apparent extinction co-efficient for the complex *i.e.* Abs/[complex] in presence of DNA, in absence of DNA and to fully bound DNA respectively. A plot of [DNA]/(ε_a -ε_f) *vs* [DNA] gave a slope and intercept equal to 1/(ε_b - ε_f) and 1/K_b(ε_b - ε_f), respectively. K_b is calculated from the ratio of the slope to the intercept.

4.2.8.2. Thermal denaturation studies. Thermal denaturation studies of CT-DNA (160 μM) in the absence and presence of complexes (50 μM) were carried out by monitoring the absorbance at 260 nm in the temperature range of 30–90 ^{o}C with a ramp rate of 1 ^{o}C/min in 10 mM Tris-HCl buffer (pH 8.0). The experiments were carried out using a Chirascan CD spectropolarimeter (Applied Photophysics, UK) in absorbance mode equipped with quantum temperature controller. The melting of the double stranded DNA to single stranded DNA was observed with significant hyperchromicity of absorbance at 260 nm. The melting temperature (T_m) was determined from the derivative plot (dA_{260}/dT *vs* T) of the melting profile.[21]

4.2.8.3. Circular dichroism studies. The Circular Dichroism (CD) spectroscopy was studied using Chirascan CD spectropolarimeter (Applied Photophysics, UK) at 25 ^{o}C. CD spectra of CT-DNA (160 μM) in absence and presence of complexes (25 μM) were obtained in the wavelength

range of 240–300 nm in 10 mM Tris-HCl buffer (pH 8.0) using quartz cell with 10 mm path length.[21]

4.2.9. DNA cleavage experiments. For DNA cleavage experiments, 300 ng supercoiled (SC) pUC19 DNA was used and all experiments were carried out in 50 mM Tris-HCl buffer (pH 8.0) containing 10% DMF.

4.2.9.1. Chemical-induced DNA cleavage. For chemical nuclease studies, the reactions were performed in the dark using hydrogen peroxide (0.5 mM) as the oxidising agent in absence and presence of complexes (1 – 500 µM). The solutions were incubated at 37 ^{o}C for 3 h and analysed for DNA cleaved products by agarose gel electrophoresis.

4.2.9.2. Photo-induced DNA cleavage. The effect of oxidoalkoxido vanadium(V) complexes (1 – 500 µM) on the cleavage of supercoiled (SC) pUC19 DNA (300 ng) was studied by agarose gel electrophoresis in 50 mM Tris HCl buffer (pH 8.0) containing 10% DMF. DNA photo cleavage studies were carried out under illuminated conditions using UVA source at 350 nm (Luzchem Photoreactor Model LZC-1, Ontario, Canada) fitted with 14 UVA tubes for 3 h. After photo irradiation, each sample was further incubated for 1.0 h at 37 ^{o}C and analyzed for the photo-cleaved products using gel electrophoresis. The samples after incubation were added to the loading buffer containing 0.25% bromophenol blue and 30% glycerol (2 µL) and the solution was finally loaded on 0.8% agarose gel containing 0.5 µg/mL ethidium bromide (EB). Electrophoresis was carried out for 1.0 h at 90 V in TAE (Tris–acetate EDTA) buffer. DNA cleavage was indicated by the decrease in the supercoiled pUC19 DNA (Form I) and subsequently the formation of nicked circular DNA (Form II) and linearized DNA (Form III). Bands were visualized by UV light (302nm) and photographed. The extent of SC DNA cleavage was measured from the intensities of the bands using UVP (Gel Doc It^2) Gel Documentation System. Due corrections were made for the low level of nicked circular (NC) form of DNA present in the original SC DNA sample and for the low affinity of EB binding to SC compared to NC and linear forms of DNA.[22] The percentage of net DNA cleavage was calculated by the following equation:

$$\text{Net DNA cleavage } \% = \frac{\text{Form IIs} + 2 \times \text{Form IIIs}}{\text{Form Is} + \text{Form IIs} + 2 \times \text{Form IIIs}} - \frac{\text{Form IIc} + 2 \times \text{Form IIIc}}{\text{Form Ic} + \text{Form IIc} + 2 \times \text{Form IIIc}} \qquad \text{Eq.2}$$

The subscripts “s” and “c” refers to the sample and control respectively.[23] Appropriate DNA controls were taken to calculate the net DNA cleavage percent. The observed error in measuring the band intensities ranged between 3% – 6%.

4.3. RESULT AND DISSCUSSION

4.3.1. Synthesis and structure. The four tridentate ligands ($H_2L^{1–4}$), used in this work are given in **Scheme 4.1**. The reaction of NH_4VO_3 with $H_2L^{1–4}$ in a ratio of 1:1 in refluxing ethanol in open air affords the brown colored complexes of composition [VO($L^{1–4}$)OEt] (**1**–**4**) in excellent yields and the same reaction in presence of a co-ligand 4,4'-bipy afford the dimeric product, [{VO(L^2)OEt}$_2$(μ-4,4'-bipy)] **(5)**. These compounds are highly soluble in CH_2Cl_2, DMF and DMSO and sparingly soluble in MeOH, EtOH and CH_3CN. All complexes are diamagnetic and nonconducting in solution. The IR spectrum of complexes **1**−**5**, showed a characteristic V=O stretching band at ~ 999 cm^{-1}.[14b]

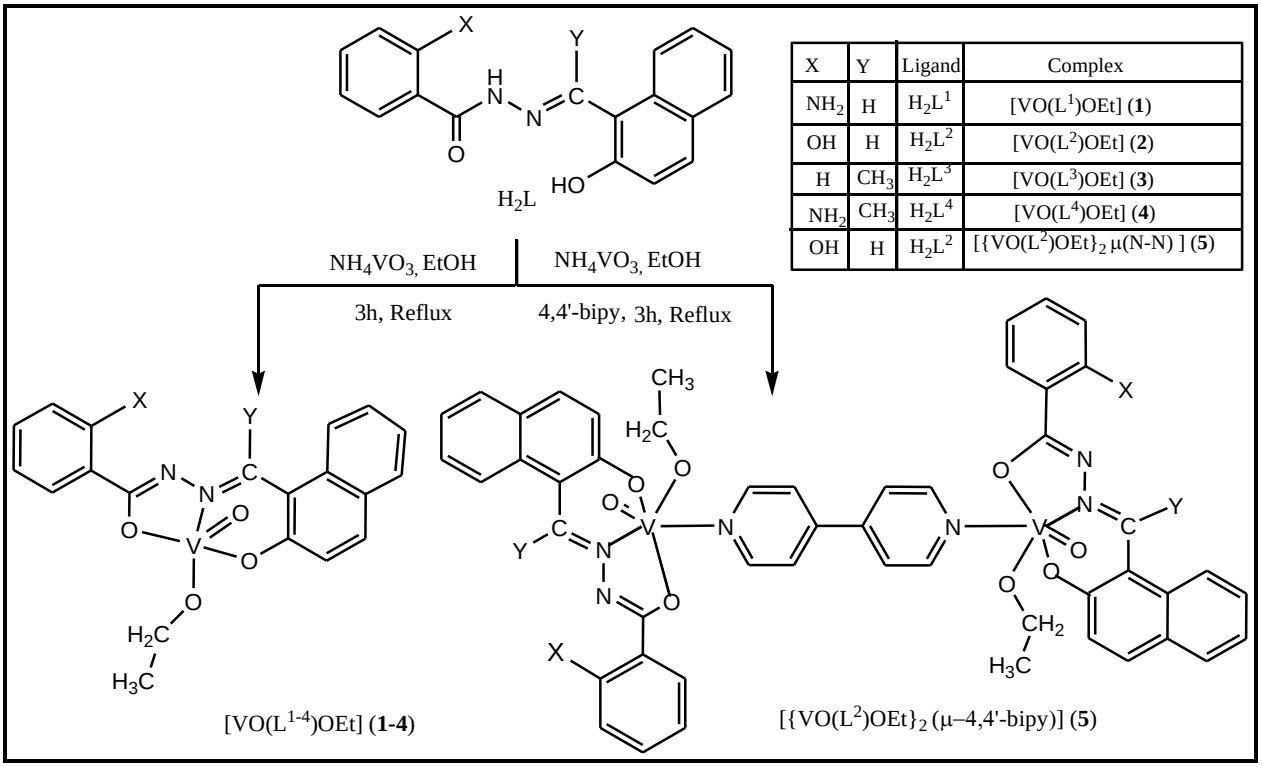

X	Y	Ligand	Complex
NH_2	H	H_2L^1	[VO(L^1)OEt] (**1**)
OH	H	H_2L^2	[VO(L^2)OEt] (**2**)
H	CH_3	H_2L^3	[VO(L^3)OEt] (**3**)
NH_2	CH_3	H_2L^4	[VO(L^4)OEt] (**4**)
OH	H	H_2L^2	[{VO(L^2)OEt}$_2$ μ(N-N)] (**5**)

Scheme 4.1. Schematic diagram of various pathways through which the oxido vanadium(V) complexes (**1**−**5**) were synthesized.

4.3.2. Description of the X-ray structure of complexes (1−5). The observed elemental (C, H, N) analytical data of all the oxidoethoxido vanadium(V) complexes are consistent with their composition. It appears from the formulation of the monomeric complexes that the hydrazones are serving as tridentate ligands in them. Although the preliminary characterization data (microanalysis and IR) indicated the presence of the ligand, oxido group and ethoxido group in the complexes, they could not point to any definite stereochemistry of the complexes, or the coordination mode of H_2L. In order to authenticate the coordination mode of the hydrazones in these complexes, the structure of all the monomeric complexes has been determined by X-ray crystallography. The atom numbering scheme for complexes (**1**−**4**) are given in **Figure 4.1 (a-d)** with the relevant bond distances and angles collected in **Table 4.2**. In complexes (**1**−**4**), the vanadium(V) centre is occupied by O_4N coordination sphere, constituting a square pyramidal structure. The basal plane is made up by the phenolate oxygen, enolic oxygen, imine nitrogen from the ligand and the oxygen from deprotonated alkoxide. The Schiff base ligand forms a six membered and a five membered chelate ring at the V(V) accepter centre with O(1)–V(1)–N(1) and O(2)–V(1)–N(1) bite angles in the range of 82.5(2)−81.6(2)° and 75.1(1)−74.36(7)° respectively. The apical position of square pyramid is occupied by the terminal oxido group O(3). The short V(1)−O(3) distance in the range of 1.606(5)−1.574(4)A° indicates the presence of vanadium oxygen double bond (V=O), which is commonly found in five and six coordinated octahedral complexes[24] of vanadium(IV) and vanadium(V). For all the complexes, the four V−O bond lengths are unequal, the V=O bond being the shortest and V−O (enolate) being the longest. The V−O bond length follows the order, V−O(oxido) < V−O(alkoxido) < V−O(phenolate) < V−O(enolate). These data indicate the stronger binding of alkoxido group compared to those of phenolate and enolate oxygen atom.[24a-b]

The dinuclear complex, **5** (**Figure 4.1(e)**, **Table 4.2**) crystallizes in the tetragonal crystal system with space group, *P4/n* with the molecule sitting across a crystallographic center of inversion. Each half of the dinuclear complex [{VO(L^2)OEt}$_2$(μ-4,4'-bipy)] (**5**), closely resembles the structure of the other half of the complex. The coordination environment around the V(V) center is octahedral and highly distorted. The ligand H_2L^2 is dianionic and tridentate, with its meridionally situated donor sites O(1), N(1), and O(2) lying in the equatorial plane along with the alkoxido oxygen O(4). The chelate bite angles for the five- and six-membered rings have values within the expected ranges [O(2)–V(1)–N(1), 74.87(6)°; O(1)–V(1)–N(1), 82.09(6)°]. The

bond distances about V(1) reveal the magnitude of the distortions, as can be seen in **Table 4.2**. The V–O distances range from 1.601(2) Å for the oxido ligand O(3), located in an axial position, to 1.966(1) Å for the enolate oxygen O(2). The V(1)–O(1) (phenolate) distance is slightly shorter at 1.853(1) Å. The second axial position is occupied by a nitrogen atom of the bridging 4,4'-bipyridine ligand, which is significantly farther from the V center than the other five ligated atoms. V(1)–N(3), at 2.377(2) Å, is undoubtedly the weakest of the six V–L bonds and consequently the most susceptible to ligand exchange.

Table 4.2. Selected bond distances (Å) and angles (^{0}) for 1−5.

	1	**2**	**3**	**4**	**5**
			Distances		
V(1)-O(1)	1.834(4)	1.840(4)	1.835(2)	1.812(3)	1.853(1)
V(1)-O(2)	1.914(4)	1.936(4)	1.908(2)	1.895(3)	1.966(1)
V(1)-O(3)	1.606(5)	1.581(6)	1.587(2)	1.574(4)	1.601(2)
V(1)-O(4)	1.730(7)	1.730(5)	1.753(2)	1.711(4)	1.779(2)
V(1)-N(1)	2.075(5)	2.095(5)	2.093(2)	2.088(3)	2.110(2)
N(1)-N(2)	1.384(6)	1.387(7)	1.395(3)	1.394(5)	1.393(2)
V(1)-N(3)	-	-	-	-	2.377(2)
			Angles		
O(1)-V(1)-O(3)	106.7(2)	105.3(2)	108.11(8)	107.3(2)	100.89(7)
O(1)-V(1)-O(4)	99.4(3)	98.6(2)	99.03(8)	96.8(2)	105.17(6)
O(1)-V(1)-N(1)	82.5(2)	81.6(2)	81.91(7)	82.1(1)	82.09(6)
O(2)-V(1)-O(3)	107.1(2)	104.4(2)	111.68(9)	107.1(2)	97.61(7)
O(2)-V(1)-O(4)	90.2(3)	90.5(2)	89.39(8)	89.1(2)	91.29(6)
O(2)-V(1)-N(1)	74.4(2)	74.7(2)	74.36(7)	75.1(1)	74.87(6)
O(3)-V(1)-O(4)	105.1(3)	108.5(3)	105.20(9)	109.6(2)	102.04(7)
O(3)-V(1)-N(1)	97.0(2)	98.4(2)	97.15(8)	97.4(2)	96.81(7)
O(3)-V(1)-N(3)	-	-	-	-	175.58(7)
O(1)-V(1)-N(3)	-	-	-	-	82.12(6)
O(4)-V(1)-N(3)	-	-	-	-	80.14(6)
O(2)-V(1)-N(3)	-	-	-	-	78.44(6)

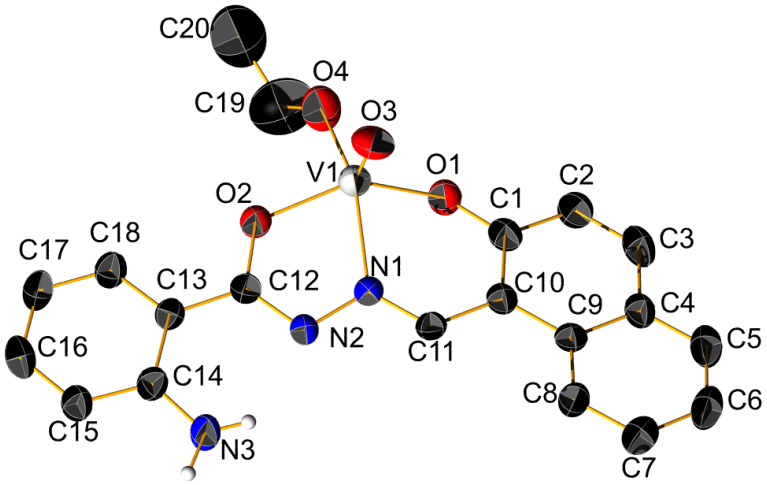
C20
O4
C19
O3
V1
O1
C2
O2
C1
C3
C17
C18
N1
C13
C12
C10
C9
C4
C5
C16
N2
C11
C14
C8
C6
C15
N3
C7

(a)

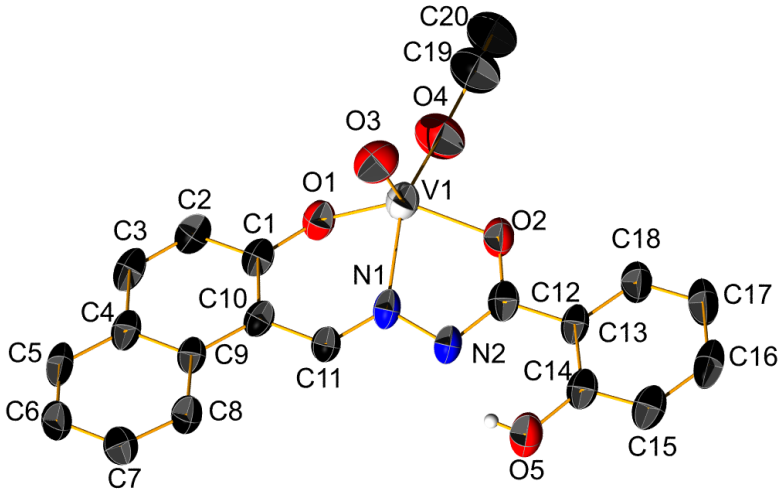
C20
C19
O4
O3
O1
V1
C2
O2
C3
C1
C18
N1
C10
C12
C17
C4
C13
C5
C9
N2
C16
C11
C14
C6
C8
O5
C15
C7

(b)

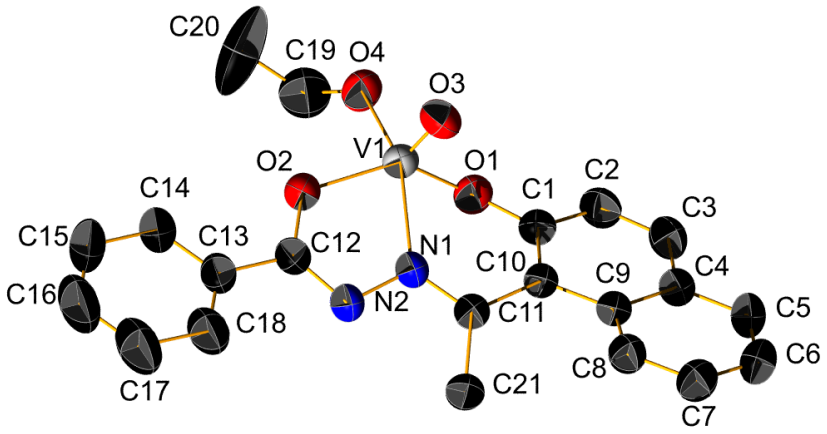
C20
C19
O4
O3
V1
O2
O1
C1
C2
C3
C14
C15
C13
C12
N1
C10
C9
C4
C16
N2
C11
C5
C18
C8
C6
C17
C21
C7

(c)

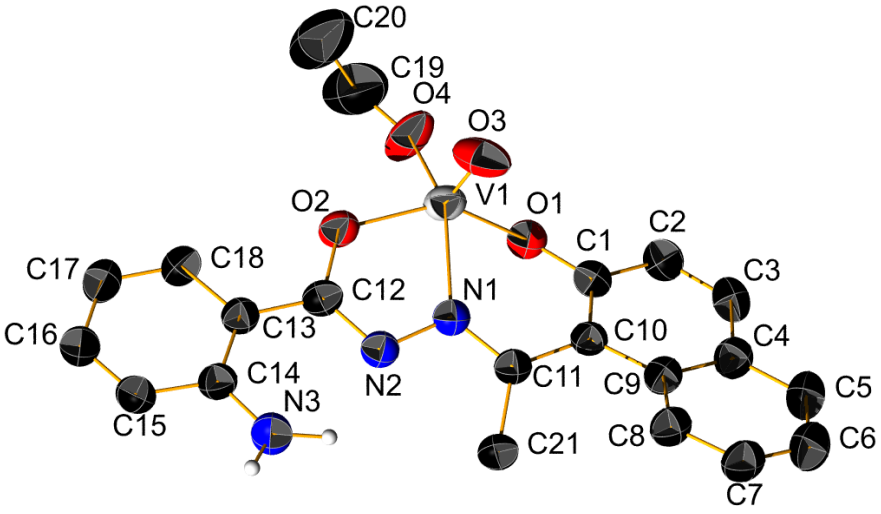
C20
C19
O4
O3
V1
O2
O1
C1
C2
C17
C18
C12
N1
C3
C16
C13
C10
C4
C14
N2
C11
C9
C5
N3
C15
C21
C8
C6
C7

(d)

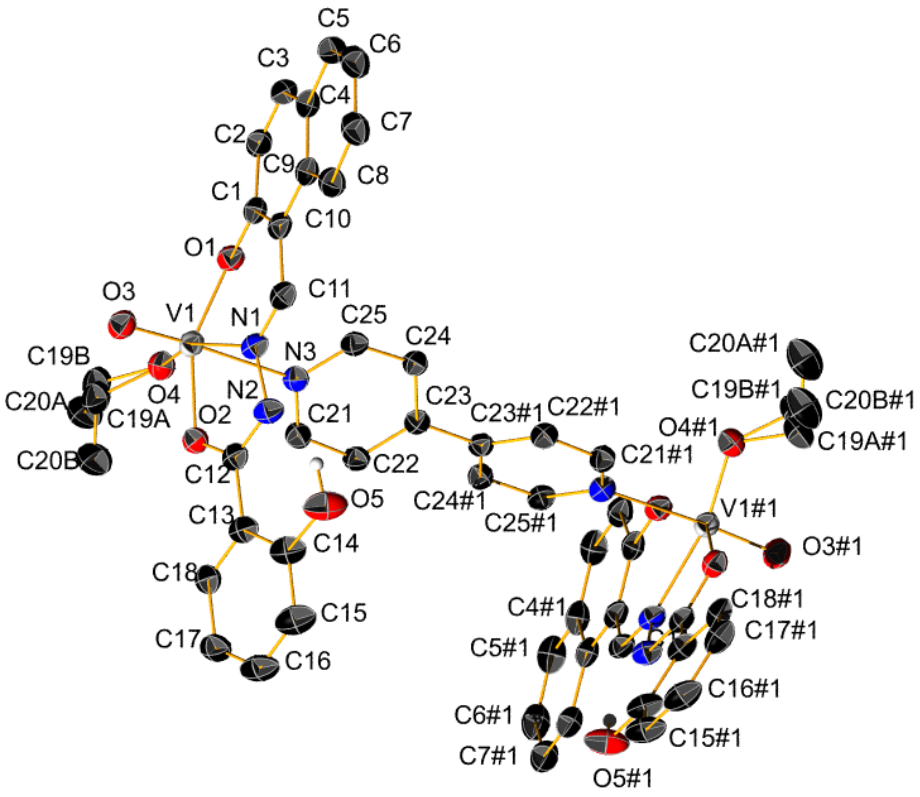

(e)

Figure 4.1. ORTEP diagram of (a) [VO(L^1)OEt] (**1**), (b) [VO(L^2)OEt] (**2**), (c) [VO(L^3)OEt] (**3**), (d) [VO(L^4)OEt] (**4**), (e) [{VO(L^2)OEt}$_2$(μ-4,4'-bipy)] (**5**) .

4.3.3. IR spectroscopy. The IR data of all the ligands, H_2L^{1-4} and their corresponding metal complexes, **1–5** are given in the experimental section. The disappearance of characteristic bands due to –NH and –C=O in the ligand, and the appearance of new bands in the range 1255–1238 cm^{-1} in the complexes **(1–5)**, indicates the enolisation of these two groups forming a =C–O bond sequence. The strong and sharp peak displayed by the complexes in the range 1599–1567 cm^{-1} is likely to be associated with the –C=N–N=C– moiety.[15a,25] The presence of a sharp band in the range 999–959 cm^{-1} is assigned to V=O stretching of an oxidoalkoxido vanadium(V) complex.[15a]

4.3.4. Electronic spectra. The electronic spectra of **1**–**5** were recorded in $CHCl_3$ (1.20×10^{-4} M) and are quite similar. A representative spectrum of **2** is shown in **Figure 4.2**. Strong absorptions in the range 456–419 nm are assignable to the ligand-to-metal charge transfer transitions whereas the bands in the higher energy region (346–242 nm) are likely to be due to ligand centred transitions.[15a,14b]

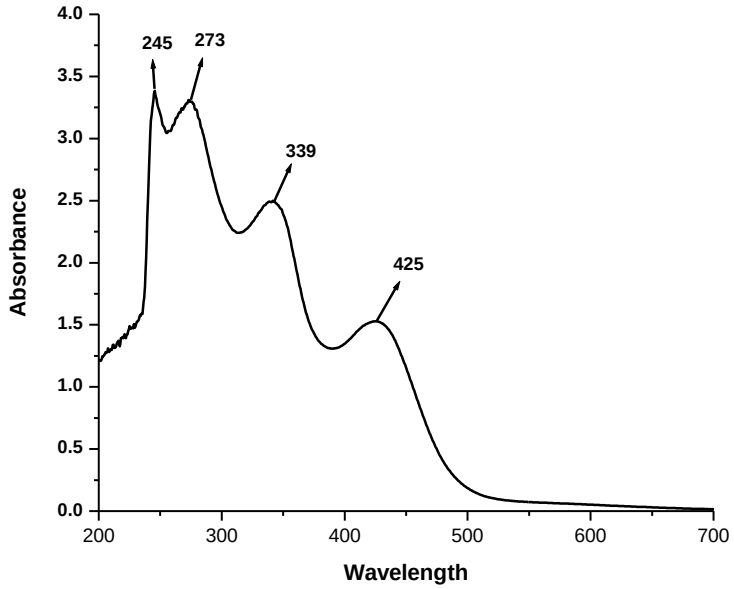

Figure 4.2. UV-Vis spectra of [VO(L^2)OEt] (**2**) (1.20×10^{-4} M) in $CHCl_3$.

4.3.5. Study of Solution behavior of Complexes 1−4. The IR spectrum of all the complexes (**1−4)** in chloroform/DMSO shows two V=O stretch bands in the range 1006–1002 cm^{-1} and 980–966 cm^{-1}, which suggested that two different V=O groups exist in solution.[14b] The representative spectrum is shown in **Figure 4.3**. Another new band corresponding to the *ν*(V–O–V)[14b,15a] mode is also observed at around 821 cm^{-1}, which were absent in the spectrum of **1−4** in the solid state. The IR spectrum in solution pointed to the retention of their mononuclear nature which was in the solid state and simultaneous formation of the corresponding dimeric complexes as a 2nd species. So, these observations suggest that two species may exist in solution and demand proper explanation.

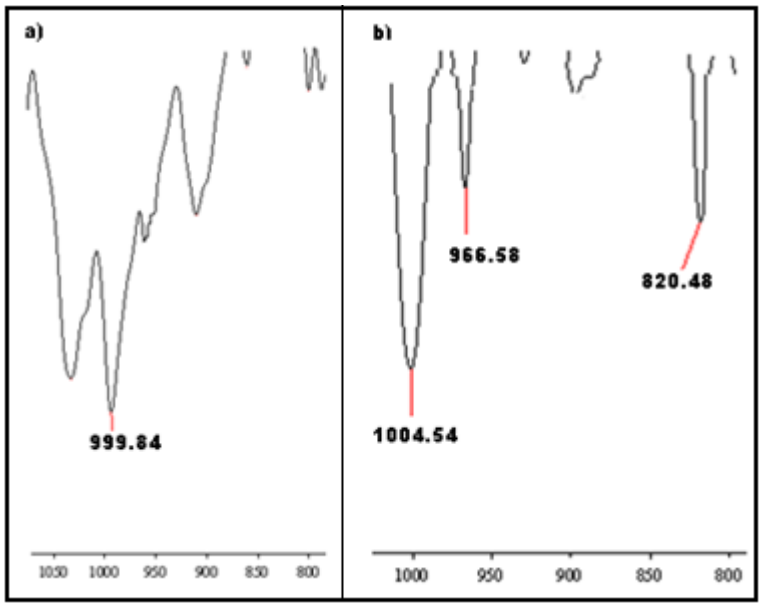

Figure 4.3. FTIR spectra of complex [VO(L^3)OEt] (**3**): a) in solid state b) in $CHCl_3$ solution.

The ^{1}H NMR spectra of the complexes **1−4** in DMSO-d_6 (which contained trace water) yielded two close but separate sets of bands in an approximate 1:1 ratio [**Figures 4.4 (a) and 4.5 (a)**]. The set of sharp ^{1}H NMR signals denoted by the pink rectangles correspond to the monomeric form **M** of the species [VO(L^{1-4})OEt] (**1−4**) which were isolated in the solid state and structurally characterized. The relatively less sharp signals denoted by the blue rectangles were assigned to the other species (let the corresponding 2nd species is a dimer, labeled as **D**). So, the NMR results suggest that two species exist in DMSO solution. The spectrum of **1** and **2** exhibits two sets of CH singlets at 9.99−9.94 ppm (**1**) and 10.09−9.95 ppm (**2**) respectively. The

spectrum of **2** exhibits two sets of OH (phenolic) resonance at 11.60 and 11.42 ppm. The spectrum of **3** and **4** exhibits two sets of CH_3 (methyl) resonance at 2.92−2.84 ppm (**3**) and 2.95−2.87 ppm (**4**). The spectrum of **1** and **4** exhibits a broad signal for two NH_2 group in the range 4.52−4.32 ppm. Finally, the aromatic protons of **1, 2** and **4** (a total of 20) and of **3** (a total of 22) appear in the range 8.65−6.31 ppm. In addition, all the complexes exhibit separate bands corresponding to bound ethoxido in the range, 5.76−5.48 (−CH_2) and 1.61−1.50 (−CH_3) ppm[14a,b,26] and the sharp peaks observed in the range 3.48−3.44 (−CH_2) and 1.08−1.05 (−CH_3) ppm were assigned to free, non-ligated ethanol that is most likely to be formed *in situ* in solution. Though the chemical shifts of the methylene and methyl protons of the ethanol are very close to those of the free ethanol, the alcoholic proton is not detected may be because of less concentration or overlap of the signals.

On addition of few drops of ethanol to the DMSO solution of complexes **1−4**, the 2nd set of bands (blue) disappeared and a clear spectrum resulted [**Figures 4.4 (b) and 4.5 (b)**]. The clear spectrum exhibits only one OH (phenolic) resonance at 11.61 ppm for **2**, one CH proton signal at 9.80 ppm for **1** and 9.94 ppm for **2**, and signals for a total of ten aromatic protons for **1**, **2** and **4** and eleven aromatic protons for **3** in the range 8.56−6.57 ppm. In addition, the coordinated ethoxido bands in the range 5.76−5.48 ppm (−CH_2) ppm and at ~ 1.62−1.51 (−CH_3) ppm[14a,b,26,27] broadened and the free ethanol bands in the range 3.50−3.45 (−CH_2) and 1.09−1.06 (−CH_3) ppm increased.

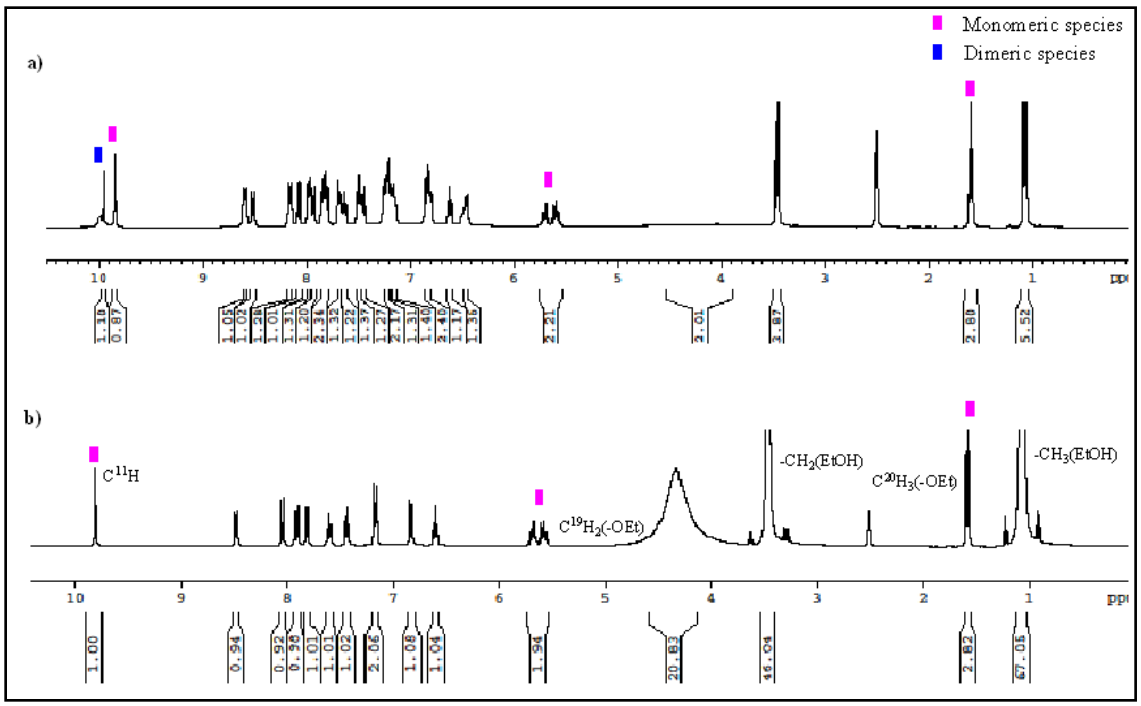

Figure 4.4. Representative ^{1}H NMR spectrum (full range) of [VO(L^{1})OEt] (**1**) in DMSO-d_6: a) before addition of ethanol. b) after addition of ethanol.

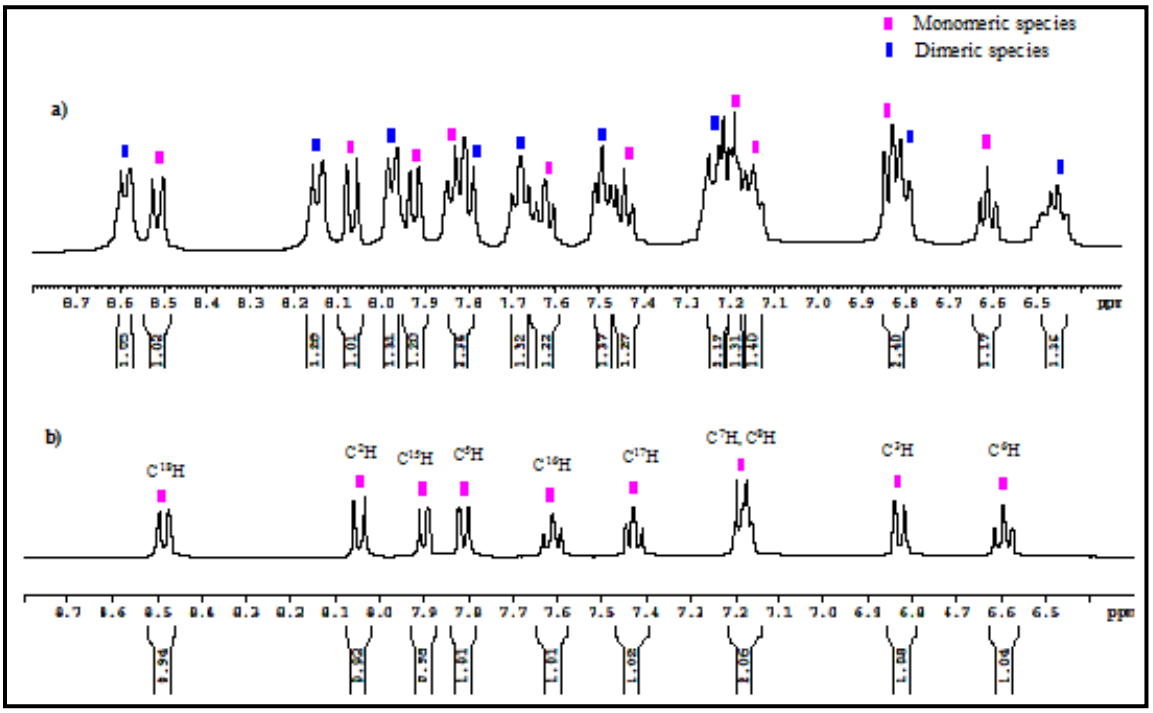

Figure 4.5. Representative ^{1}H NMR spectrum (aromatic region) of [VO(L^{1})OEt] (**1**) in DMSO-d_6: a) before addition of ethanol b) after addition of ethanol.

The ^{13}C (**Figures 4.6** and **4.7**) and ^{51}V (**Figure 4.8**) NMR spectra of complexes **1**−**4**, in DMSO also showed two sets of bands at an approximate ratio of 1:1 and the 2nd set of band (blue) disappeared on addition of small amount of ethanol, as in the case of ^{1}H NMR spectrum.

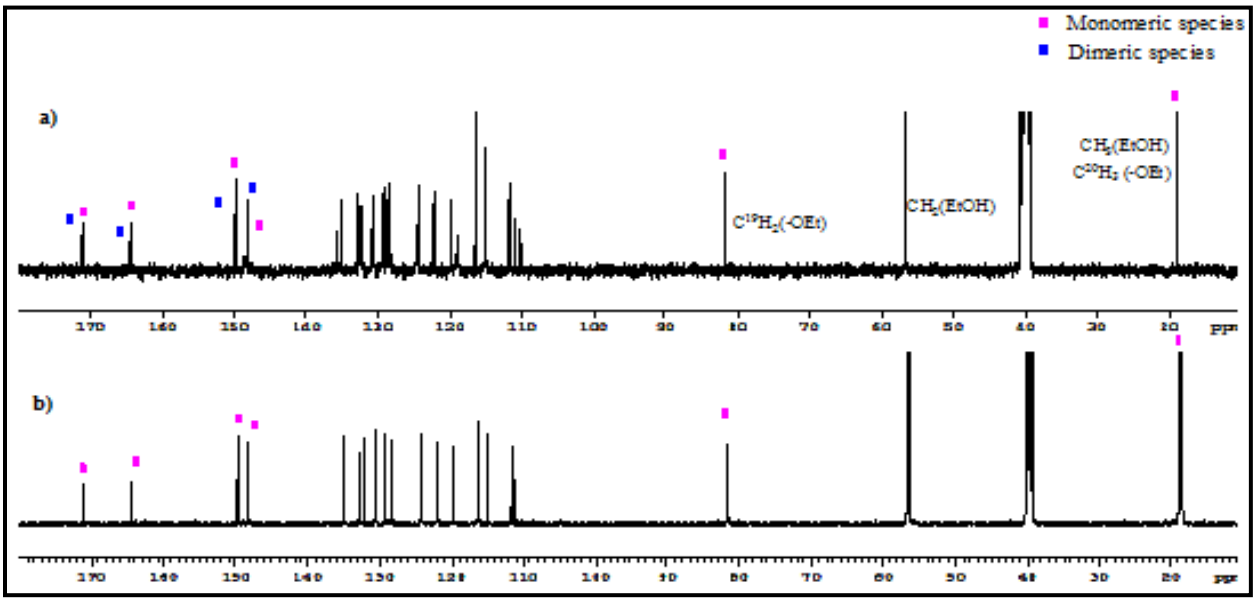

Figure 4.6. Representative ^{13}C NMR spectrum (full range) of [VO(L^{1})OEt] (**1**) in DMSO-d_6: a) before addition of ethanol b) after addition of ethanol.

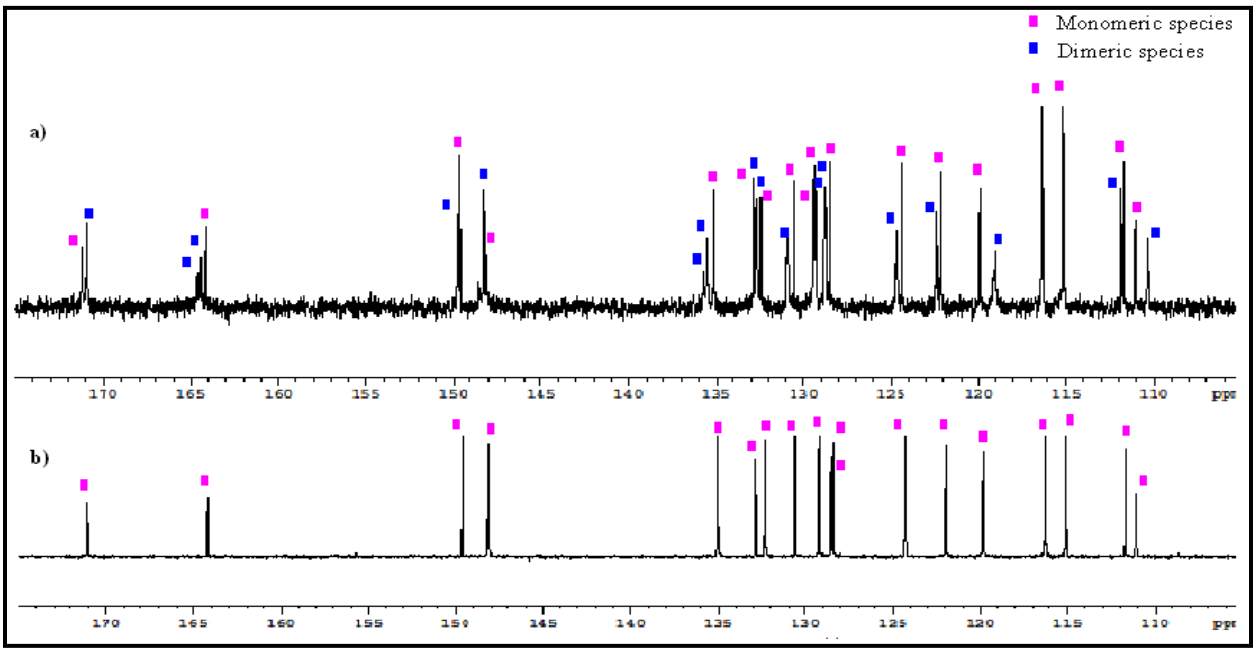

Figure 4.7. Representative ^{13}C NMR spectrum (aromatic region) of [VO(L^{1})OEt] (**1**) in DMSO-d_6: a) before addition of ethanol b) after addition of ethanol.

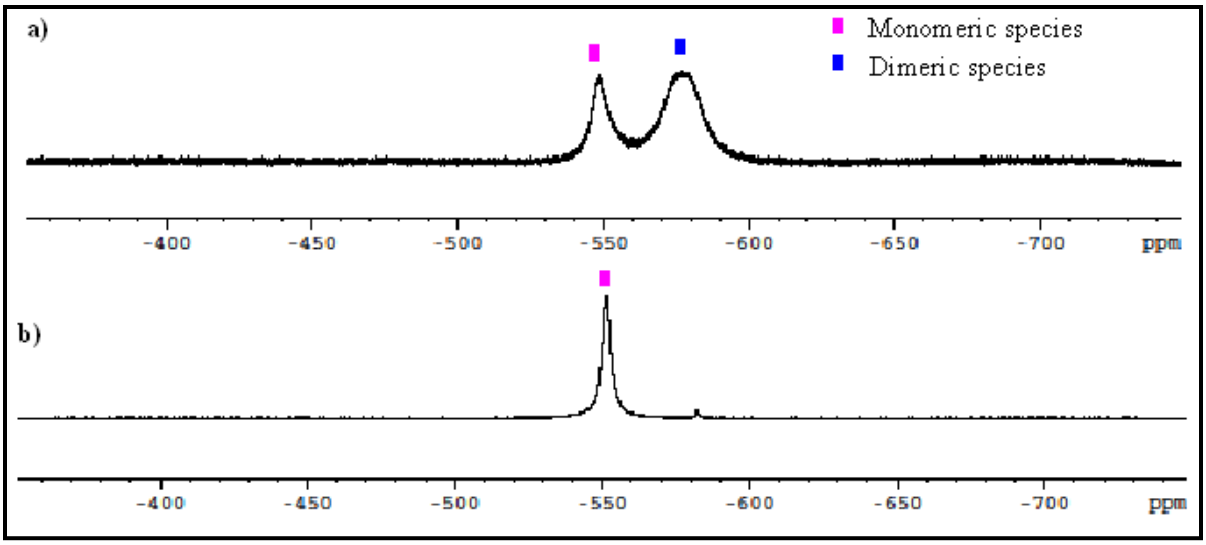

Figure 4.8. Representative ^{51}V NMR spectrum of [VO(L^1)OEt] (**1**) in DMSO-d_6: a) before addition of ethanol b) after addition of ethanol.

Like the solution IR, the NMR (^{1}H, ^{13}C and ^{51}V) results also suggest that two species exist in DMSO solution and whatever the 2nd species (**D**) is, it converts to its monomeric form (**M**) in the presence of a small amount of ethanol.

Glas et al. reported the solution behavior of octahedral monoalkoxido-bound monooxido vanadium(V) complexes with pyrazolylpyridine bidentate chelating ligand and proposed a coordination isomerism for their complexes based on the NMR study.[24a] However, in present study, the vanadium ions are coordinated by a chelating tridentate ligand, so the occurrence of a coordination isomerism is not plausible. Moon et al. also reported[14a] a similar solution behavior of a mononuclear square pyramidal dialkoxido-bound monooxido vanadium(V) complex with a dianionic tridentate chelating ligand and they proposed an intermolecular hydrogen-bonded polymeric form of their oxido vanadium(V) complex may present as minor species in solution. But, they could not produce any conclusive evidence for the final structure of that minor species, so the occurrence of a hydrogen-bonded polymeric structure is excluded.

One of the possible structures for the 2nd species is an alkoxido-bridged dimer.[14c,24b] It is well-known that alkoxides usually form dimeric complexes. However, we could exclude the possibility of an ethoxido-bridged dimer as the 2nd species because there is only one set of bands for a coordinated ethoxido group. If the 2nd species is an ethoxido bridged dimer, there should be another set of bands for two bridging ethoxido groups and as a six coordinated complex the V=O stretching could have been found in lower frequency.[28] So we could exclude the possibility of an alkoxido-bridged dimer as the other (2nd) species. The other possible structure for the 2nd species is a chain structure where a phenolate oxygen atom of the neighboring monomeric species would link vanadium centers of the monomeric species. We could also exclude the possibility of a phenolate-linked chain structure from the evidence that, if phenolate was coordinated to the vanadium ion in the minor species, a phenolate ligand to vanadium metal charge-transfer band would have had to disappear when a small amount of ethanol was added to the chloroform solution of complexes **1**−**4**. However, there were no recognizable changes in the UV-Vis spectrum of complexes **1**−**4** in the chloroform solution were observed after the addition of a small amount of ethanol to the solution. Finally, one of the possible structures for the 2nd species is a μ-oxido dimer. From the IR results in solution, there was a significant change in the V=O stretch of complexes **1**−**4** in chloroform/DMSO solution compared to that of the monomeric species in the solid state and another new band corresponding to the ν(V-O-V)[14b,15a]

mode was observed. This suggests that, with the addition of monomeric species, the corresponding divanadium complexes may exist as a μ-oxido dimer (2nd species) in solution.

To support the above observations, ESI mass spectra of all the complexes (**1**–**4)** were recorded in DMSO solution. The data are summarized in the experimental section. For complexes **1**–**4**, two peaks corresponding to the $[M - CH_2CH_3]^+$ and $[V_2O_3(L^4)_2]^+$ are observed which correspond to the existence of the monomeric and dimeric species respectively. A representative ESI mass spectrum of complex **4** is shown in **Figure 4.9**.

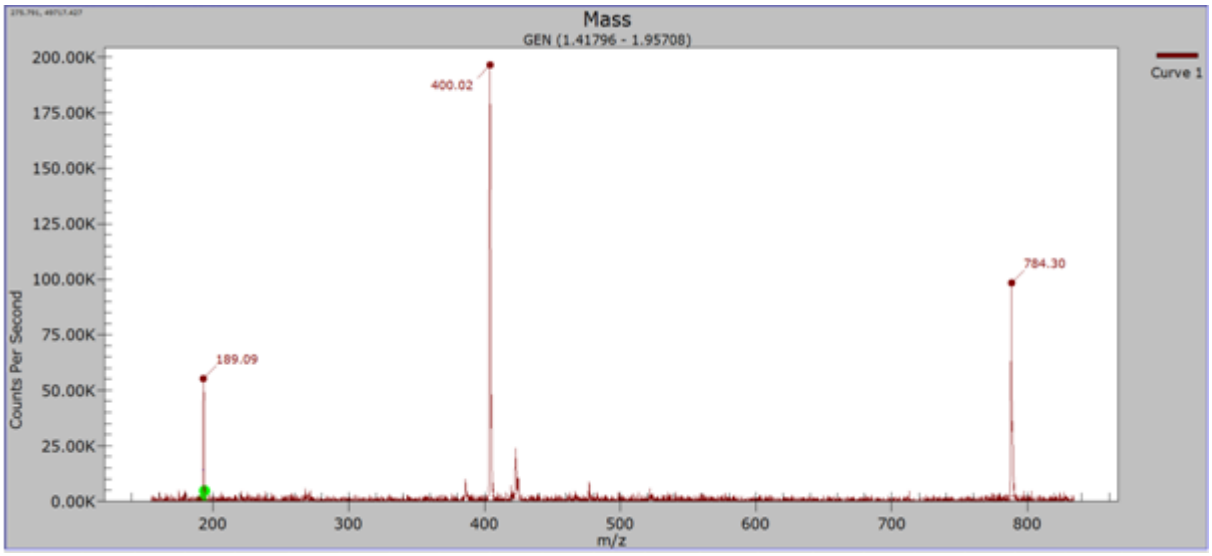

Figure 4.9. ESI mass spectrum of $[VO(L^4)OEt]$ (**4)**.

On the basis of above results, these solution behavior of **1**−**4** can be interpreted as by proposing the following equilibrium (**Chart 4.1**) existing in $CDCl_3$ / DMSO-d_6 containing a little water, which also explains the simultaneous presence of the two species, **M** (monomer, isolated in the solid state and solved by X-ray crystallography) and **D** (2nd species, μ-oxido dimer) in solution.

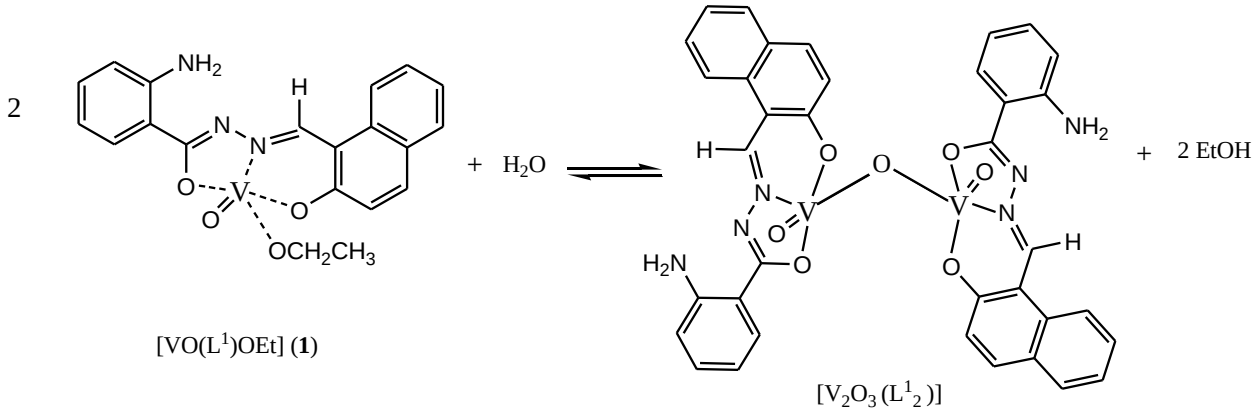

[VO(L[1])OEt] (**1**)

Monomeric form (**M**), isolated in the solid state and solved by X-ray crystallography

[V_2O_3 (L^1_2)]

Dimeric form (**D**), 2nd species generated *insitu* in solution

Chart 4.1. Schematic diagram for the inter-conversion of monomeric and dimeric species in solution taking [VO(L[1])OEt] (**1**) as representative.

Even though no water molecules were observed in the crystal structure of **1**−**4**, it is assumed that the possible water source was either from NMR solvents or from water molecules in the air that were probably physisorbed on the surface of the complexes. The role of water as well as the free ethanol molecules for the existence of the above equilibrium were inferred from the presence of band at ~ 3.73 (br) ppm for H_2O and the sharp peaks at ~ 3.47 and ~ 1.07 ppm for the protons of free, non-ligated ethanol in DMSO-d_6. However, this equilibrium could be shifted more to the left by the addition of ethanol into the NMR sample, which was reflected in the change in NMR spectrum of [VO($L^{1–4}$) OEt] (**1**−**4**).

It is concluded that, on addition of few drops of ethanol into the NMR sample in DMSO-d_6, **1**−**4** retain their structure in which they exist in the solid state and the other (2nd, **D**) species, which were also present in solution, were reconverted into the mononuclear state (**M**). **D** exhibits all the characteristic signals of a μ-oxido binuclear species, which matches well with the similar results reported earlier.[14b]

4.3.6. Catalytic Activity Studies.

4.3.6.1. Oxidative bromination of Styrene. Model vanadium complexes can act as functional models of vanadium-dependent haloperoxidases, in that they catalyse the oxidative bromination of organic substrates in the presence of H_2O_2 and bromide ion.[29-31] During catalytic reaction, vanadium complex reacts with **1** or **2** equivalent of H_2O_2, generates oxido-monoperoxido, $[VO(O_2)]^+$ or oxido-diperoxido, $[VO(O_2)_2]^-$ species which ultimately oxidizes bromide species (to Br_2, and/ or HOBr), the bromination of the substrate then proceeds with the liberation of a proton. The oxidoalkoxido vanadium(V) complexes reported here satisfactorily catalyse the oxidative bromination of styrene.

Oxidative bromination of styrene using these alkoxido vanadium(V) (**1**−**5**) complexes as catalyst precursor in the presence of H_2O_2, KBr and $HClO_4$ gave mainly three products, namely, (a) 1,2-dibromo-1-phenylethane, (b) 2-bromo-1-phenylethane-1-ol and (c) 1-phenylethane-1,2-diol (**Scheme 4.2**). Some minor products (benzaldehyde, styrene epoxide, benzoic acid and 4-bromostyrene) were also detected but their overall percentage was approximately very low (7 %) of the total of the main products. Addition of $HClO_4$ in four equal portions was required to obtain better oxidative bromination. All products were separated/ isolated by column chromatography and the content of each fraction was confirmed by ^{1}H NMR spectroscopy as well as GC–MS.

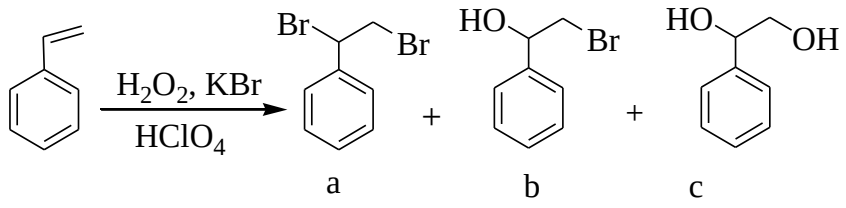

Scheme 4.2. Main products obtained upon oxidative bromination of styrene. (a) 1,2-dibromo-1-phenylethane, (b) 2- bromo-1-phenylethane-1-ol and (c) 1-phenylethane-1,2-diol.

The following parameters were studied to optimize the reaction conditions for the maximum oxidative bromination of styrene considering **3**, as catalyst precursor: (i) amount of catalyst, (ii) amount of KBr (iii) amount of oxidant and (iv) amount of $HClO_4$ while reaction was run at room temperature.

Three different amounts of **3** (0.0005, 0.0010 and 0.0015 g) were used as catalyst precursor while keeping fixed the amounts of styrene (1.04 g, 10 mmol), KBr (1.19 g, 10 mmol), 30% H_2O_2 (1.14 g, 10 mmol) and aqueous 70% $HClO_4$ (1.43 g, 10 mmol) in a CH_3CN/ water (20/5 mL) (entry no.1 to 3 of **Table 4.3**). Additions of $HClO_4$ were made in four equal portions, one immediately after the catalyst precursor (reaction time = 0) and the three other portions with 15 min intervals. A maximum of 21% conversion was obtained after 1 h of reaction with 0.0005 g of catalyst while 0.0010 and 0.0015 g of catalyst did not improve conversion much and gave 23% and 27 % conversion, respectively. Therefore, 0.0005 g of **3** was set as optimum (**Figure 4.10a**).

Similarly, three different substrate-to-KBr ratios were used (entry no. 4 to 5). The initial conversion of 21 % with substrate-to-KBr ratio of 1:1 improved to 38% upon increasing the substrate to KBr ratio to 1:2. This conversion further increased to 69 % at substrate-to-KBr ratio of 1:3. Therefore 3.57 g (30 mmol) of KBr was used for optimization of other conditions (**Figure 4.10b**).

The effect of the amount of oxidant, added as an aqueous 30% H_2O_2 solution, was studied with substrate-to-oxidant ratios of 1:2 and 1:3, for the fixed amount of styrene (1.04 g, 10 mmol), catalyst (0.0005 g), KBr (3.57 g, 30 mmol) and $HClO_4$ (1.43 g, 10 mmol) in CH_3CN/ H_2O (25 mL), and the reaction was monitored at room temperature for 1 h. The conversion increased upon increasing the substrate-to-oxidant ratio, and the substrate-to-oxidant ratio of 1:3 gave 53% conversion of styrene (entry no.6 to7) (**Figure 4.10c**).

To optimize the amount of $HClO_4$, four different amounts of 70% $HClO_4$ were used for fixed amounts of styrene (1.04 g, 10 mmol), catalyst precursor (0.0005 g), KBr (3.57 g, 30 mmol), 30% H_2O_2 (3.39 g, 30 mmol) and CH_3CN/ water (25 mL). Increasing the $HClO_4$ amount from 1.43 g (10 mmol) to 2.86 g (20 mmol) increased the conversion from 53 to 98%. Only a slight improvement in conversion was obtained upon further increasing this amount to 4.29 g (30 mmol) (entry no. 8 to 9). Therefore, 2.86 g (20 mmol) of 70% $HClO_4$ was considered to be adequate to obtain maximum oxidative bromination of styrene (**Figure 4.10d**).

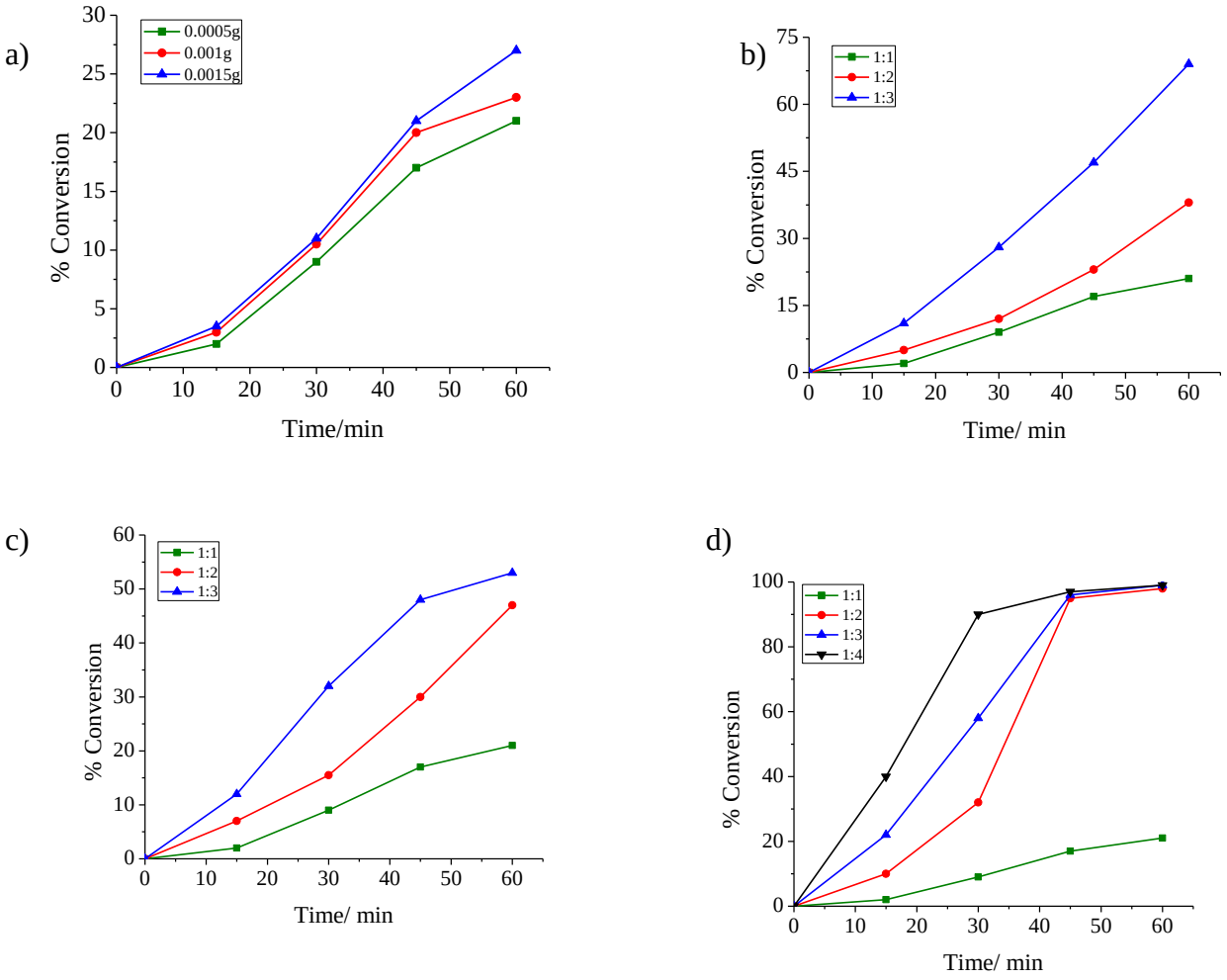

Figure 4.10. (a) Effect of catalyst amount on the oxidative bromination of styrene. Reaction condition: styrene (1.04g, 10 mmol), 30 % aqueous H_2O_2 (1.14, 10 mmol), KBr (1.19 g, 10 mmol) and 70 % aqueous $HClO_4$ (1.43 g, 10 mmol).(b) Effect of KBr amount on the oxidative bromination of styrene. Reaction condition: styrene (1.04 g, 10 mmol), 3 (0.0005g), 30 % aqueous H_2O_2 (1.14,10 mmol), and 70 % aqueous $HClO_4$ (1.43 g, 10 mmol). (c) Effect of oxidant amount on the oxidative bromination of styrene. Reaction condition: styrene (1.04 g, 10 mmol), 3 (0.0005g), KBr (3.57 g, 30 mmol) and 70 % aqueous $HClO_4$ (1.43 g, 10 mmol). (d) Effect of $HClO_4$ amount on the oxidative bromination of styrene. Reaction condition: styrene (1.04 g, 10 mmol), 3 (0.0005g), KBr (3.57 g, 30 mmol) and 30 % aqueous H_2O_2 (3.39, 30 mmol).

Entry 8 of **Table 4.3** presents the optimized reaction conditions for the oxidative bromination of 10 mmol of styrene, which are: catalyst precursor **3** (0.0005 g), 30% aqueous H_2O_2 (3.39 g, 30 mmol), KBr (3.57 g, 30 mmol), 70 % aqueous $HClO_4$ (2.86 g, 20 mmol) (added in four equal portions in 15 min intervals), and CH_3CN/ H_2O (25 mL,) at room temperature for 1 h. Catalytic activities of other complexes (**1**, **2**, **4**, **5**) have also been carried out under similar reaction conditions and are presented in **Table 4.3** (entry no. 11 to 14).

Table 4.3. Conversion of styrene (1.04 g, 10 mmol) using vanadium complexes (1−5), as catalyst in 1 h of reaction time under different reaction conditions

Entry No.	KBr [g (mmol)]	H_2O_2 [g (mmol)]	$HClO_4$ [g (mmol)]	Catalyst [g (mmol)]	TOF [h^{-1}]	Conv. [%]	Mono Bromo	Dibromo	Diol	Other product
1.	1.19 (10)	1.14 (10)	1.43 (10)	0.0005 g	1750	21	14	0	86	0
2	1.19 (10)	1.14 (10)	1.43 (10)	0.001 g	958	23	25	0	74	1
3	1.19 (10)	1.14 (10)	1.43 (10)	0.0015 g	750	27	17	0	82	1
4	2.38 (20)	1.14 (10)	1.43 (10)	0.0005 g	3166	38	13	0	86	1
5	3.57 (30)	1.14 (10)	1.43 (10)	0.0005 g	5750	69	39	0	60	1
6	3.57 (30)	2.27 (20)	1.43 (10)	0.0005 g	3916	47	9	0	90	1
7	3.57 (30)	3.39 (30)	1.43 (10)	0.0005 g	4416	53	11	0	88	1
8	3.57 (30)	3.39 (30)	2.86 (20)	0.0005 g	8167	98	30	2	67	1
9	3.57 (30)	3.39 (30)	4.29 (30)	0.0005 g	8250	99	23	4	69	4
10	3.57 (30)	3.39 (30)	5.72 (40)	0.0005 g	8250	99	17	8	74	1
11[a]	3.57 (30)	3.39 (30)	2.86 (20)	0.0005 g	8000	96	28	1.4	69	1.6
12[b]	3.57 (30)	3.39 (30)	2.86 (20)	0.0005 g	8000	96	28	1.7	67	3.3
13[c]	3.57 (30)	3.39 (30)	2.86 (20)	0.0005 g	8818	97	23	2.3	74	0.7
14[d]	3.57 (30)	3.39 (30)	2.86 (20)	0.0005 g	19600	98	33	2.3	63	1.7
15	3.57 (30)	3.39 (30)	2.86 (20)	blank	-	44	45	0	52	3

a = **1**, b = **2**, c = **4** and d = **5**.

Their catalytic activities are comparable (**Figure 4.11**) and indicated that substituents (-H, -NH_2 and -OH) on the benzene ring have no impact on their catalytic activity. Negative control (entry no. 15) shows under above conditions only 44 % conversion.

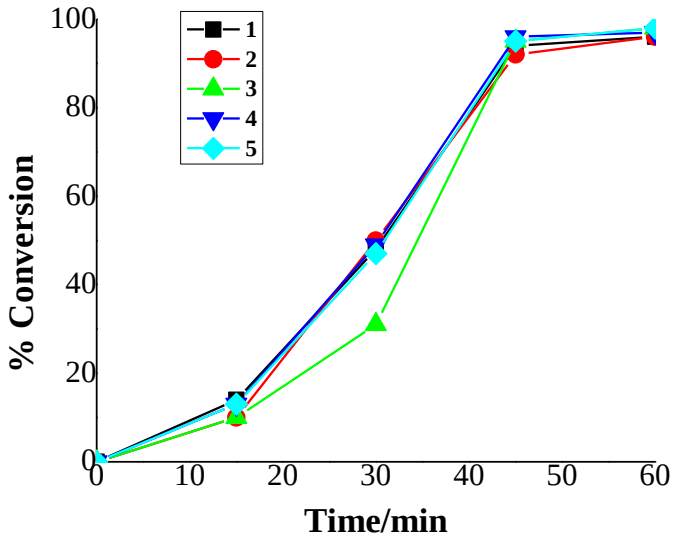

Figure 4.11. Comparison of catalytic efficiency of different catalysts on the oxidative bromination of styrene. Reaction condition: styrene (1.04 g, 10 mmol), catalyst (0.0005g), 30 % aqueous H_2O_2 (3.39, 30 mmol), KBr (3.57 g, 30 mmol) and 70 % aqueous $HClO_4$ (2.86 g, 20 mmol).

Figure 4.12 represents the consumption of styrene and the selectivity of the formation of major products with time for these experimental conditions.

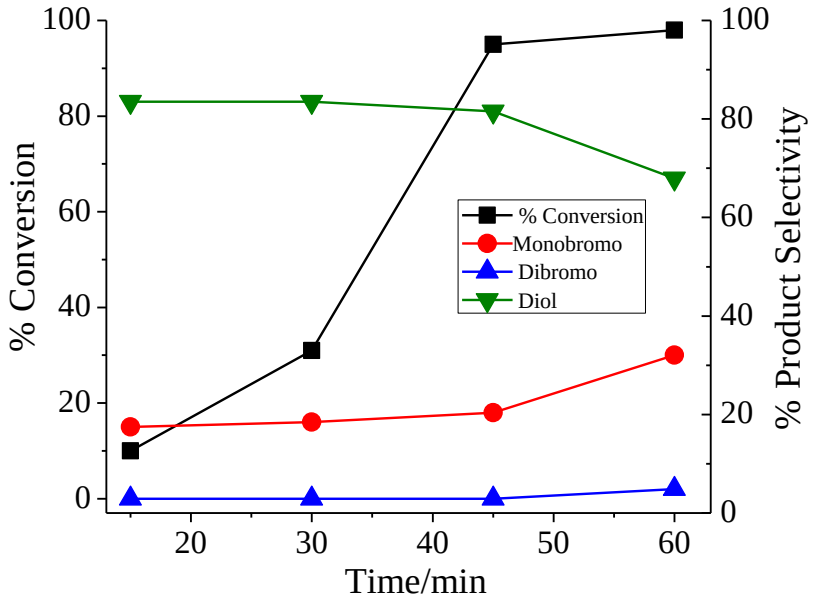

Figure 4.12. Plots showing percentage conversion of styrene and the selectivity of the formation of different reaction products as a function of time. Reaction condition: styrene (1.04 g, 10 mmol), **3** (0.0005g), 30 % aqueous H_2O_2 (3.39, 30 mmol), KBr (3.57 g, 30 mmol) and 70 % aqueous $HClO_4$ (2.86 g, 20 mmol).

4.3.6.2. Oxidative bromination of salicylaldehyde. Vanadium(V) complexes also catalyze the oxidative bromination of salicylaldehyde in the presence of H_2O_2. In the present study, complexes **1**–**5** were used as catalyst precursors with water as solvent. The catalytic oxidative bromination of salicylaldehyde gave 5-bromosalicylaldehyde, 3,5-dibromosalicylaldehyde and 2,4,6-tribromophenol (**Scheme 4.3**).

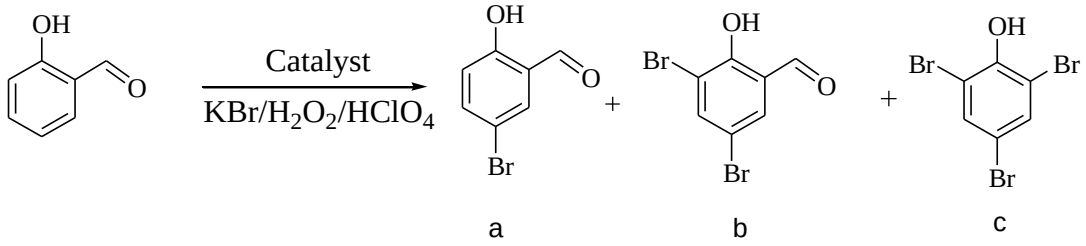

Scheme 4.3. Main products obtained upon oxidative bromination of salicylaldehyde. (a) 5-bromosalicylaldehyde, (b) 3,5-dibromosalicylaldehyde and (c) 2,4,6- tribromophenol.

After carrying out experiments under different conditions (**Table 4.4**), the best suited reaction conditions concluded for the maximum conversion of salicylaldehyde were: salicylaldehyde (0.610 g, 5 mmol), catalyst (0.0005 g), KBr (1.78 g, 15 mmol), aqueous 30% H_2O_2 (1.14 g, 10 mmol), aqueous 70 % $HClO_4$ (2.14g, 15 mmol) and water (20 mL) (entry no. 7, **Table 4.4**); the addition of $HClO_4$, however, in four equal portions during the reaction was necessary to improve the conversion of the substrate and to avoid decomposition of the catalyst. Under the above conditions, a maximum of 99% conversion was achieved with **3** as representative and the selectivity of different products follows the order: 5-bromosalicylaldehyde (74%), 2,4,6-tribromophenol (21%) > 3,5-dibromosalicylaldehyde (5%). **Table 4.5** also provides % conversion of salicylaldehyde and selectivity of products obtained by other catalysts (**1**, **2**, **4**, **5**) under above reaction conditions and is comparable to **3**.

In the absence of the catalyst, the reaction mixture gave only *ca.* 37% conversion of salicylaldehyde with the selectivity order of products: 5-bromosalicylaldehyde (89%) > 2,4,6-tribromophenol (10.5%) > 3,5-dibromosalicylaldehyde (0.5 %)

Table 4.4. Results of oxidative bromination of salicylaldehyde catalyzed by 3 after 3 h of contact time

Entry no.	Catalyst (g)	H_2O_2 (g, mmol)	KBr (g, mmol)	$HClO_4$(g, mmol)	% Conversion
1	0.0005	1.14, 10	1.19, 10	1.43,10	63
2	0.0005	1.14, 10	1.19, 10	2.14, 15	88
3	0.0005	1.14, 10	1.19, 10	2.86, 20	98
4	0.0005	0.57, 05	1.19, 10	2.14, 15	65
5	0.0005	1.71, 15	1.19, 10	2.14, 15	99
6	0.0005	1.14, 10	0.59, 05	2.14, 15	48
7	0.0005	1.14, 10	1.78, 15	2.14, 15	99
8	0.0010	1.14, 10	1.19, 10	1.43,10	68
9	0.0015	1.14, 10	1.19, 10	1.43,10	73

Table 4.5. Effect of different catalysts (1-5) on the oxidative bromination of salicyldehyde, TOF and product selectivity

Catalyst (g)	TOF (h^{-1})	% Conversion	% Selectivity		
			monobromo	Dibromo	Tribromo
1	1375	99	71	0.6	28.4
2	1375	99	68	7	25
3	1375	99	74	5	21
4	1500	99	71	0.5	28.5
5	3300	99	67	3	30

4.3.6.3. Oxidation of methyl phenyl sulfide. Sulfoxides and sulfone, the oxidation product of sulfides, are useful precursors for biologically and chemically important compounds.[32,33] used in various chemical reactions. Vanadium dependent haloperoxidases[1a,34] and model complexes catalyse the oxidation of sulfides (thioethers) to sulfoxides and further to sulfones[30,35] by H_2O_2. Such oxidation of methyl phenyl sulfide was tested using complexes **1**–**5**, as catalyst and corresponding oxidation products were obtained as shown in **Scheme 4.4**.

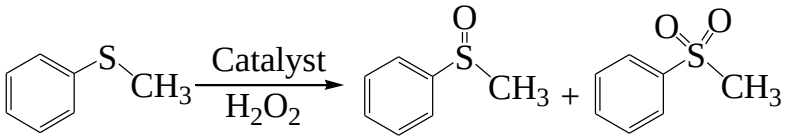

a b

Scheme 4.4. Main products obtained upon oxidation of methyl phenyl sulfide. (a) methyl phenyl sulfoxide (b) methyl phenyl sulfone.

The reaction conditions were optimized for the maximum oxidation of methyl phenyl sulfide by studying three different parameters viz. catalyst (amount of catalyst per mole of methyl phenyl sulfide), the effect of amount of oxidant (moles of H_2O_2 per mole of methyl phenyl sulfide) and and solvent of the reaction mixture in detail. The conversions obtained with all these conditions, plotted as a function of time, are presented in [**Figure 4.13 (a-c)]**. Thus for 5 mmol (0.620 g) of methyl phenyl sulfide, the amount of catalyst (0.0005 g, 0.001 g and 0.0015 g), 30% aqueous H_2O_2 (5, 10 and 15 mmol) and solvent (acetonitrile) volume (5, 10 and 15 mL) were varied and the reaction was carried out at room temperature. **Table 4.6** summarizes all conditions and conversion obtained under particular condition taking **3** as the representative catalyst. The optimized conditions for highest catalytic activity with 94% conversion of methyl phenyl sulfide was concluded as: methyl phenyl sulfide (0.620 g, 5 mmol), **3** (0.001 g), 30% aqueous H_2O_2 (1.14 g, 10 mmol) and CH_3CN (5 mL) [entry no. 2, **Table 4.6**]. Effect of different catalyst (**1**–**5)** on oxidation of methyl phenyl sulfide is presented in **Figure 4.13d**.

The percent conversion of methyl phenyl sulfide under the optimised reaction conditions and the selectivity of reaction products as a function of time is shown in **Figure 4.14**. It is clear from the plot that both the products start to form with the conversion of methyl phenyl sulfide. However, the initial selectivity of 96 % for methyl phenyl sulfoxide at 33.6 % conversion of methyl phenyl

sulfide in the first half an hour starts to decrease and reaches 65 % after 2.5 h of reaction time. Thus, initially formed sulfoxide further reacts with H_2O_2 present in the reaction mixture to give sulfone with 35% selectivity at the end of 2.5 h.

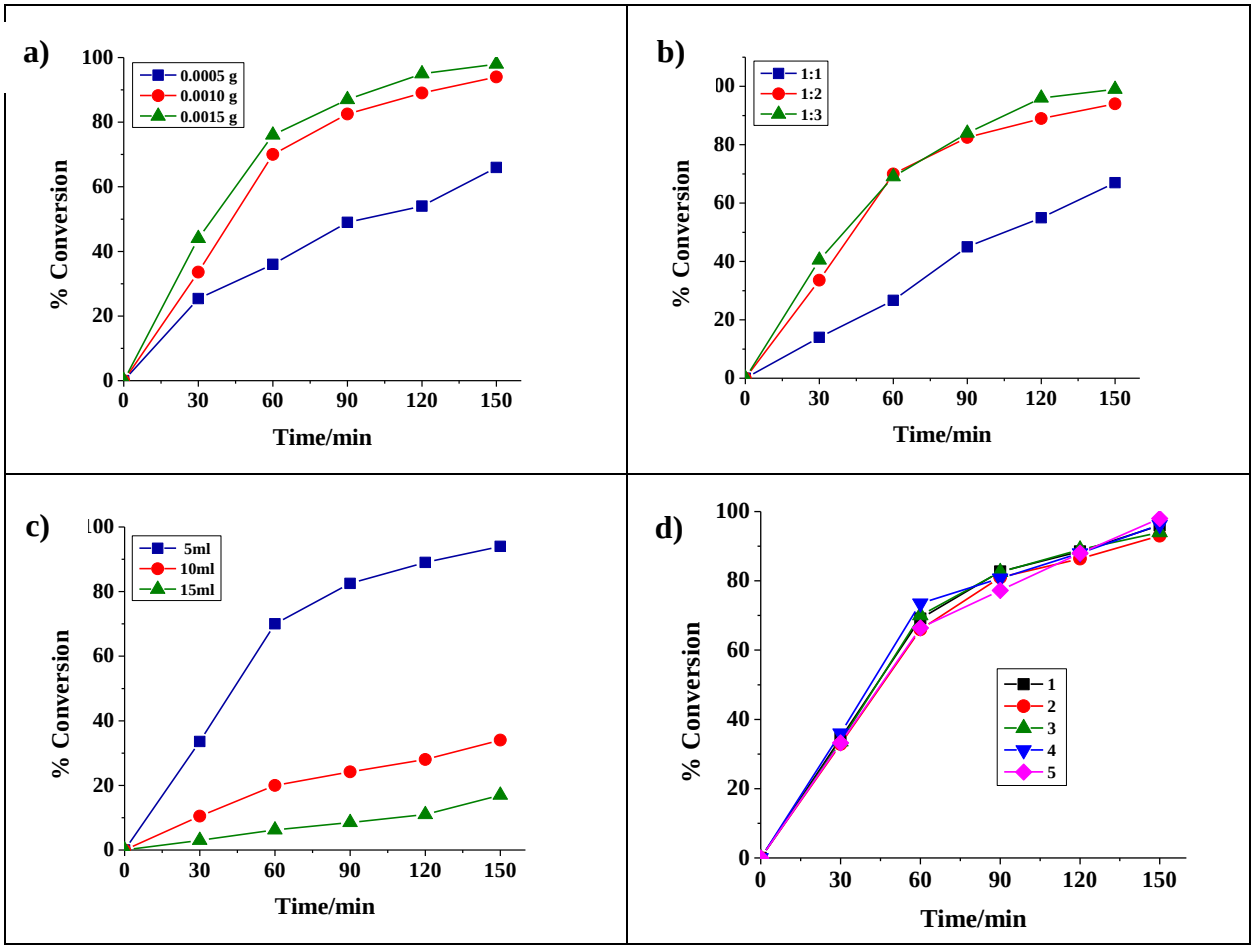

Figure 4.13. (a) Effect of catalyst amount on the oxidation of methyl phenyl sulfide. Reaction conditions: methyl phenyl sulfide (0.620 g, 5 mmol), 30 % H_2O_2 (1.14 g, 10 mmol) and acetonitrile (5 mL). (b) Effect of oxidant amount on the oxidation of methyl phenyl sulfide. Reaction conditions: methyl phenyl sulfide (0.620 g, 5 mmol), catalyst (0.001 g) and acetonitrile (5 mL)**.** (c) Effect of solvent amount on the oxidation of methyl phenyl sulfide. Reaction conditions: methyl phenyl sulfide (0.620 g, 5 mmol), catalyst (0.001 g) and 30 % H_2O_2 (1.14 g, 10 mmol). (d) Effect of different catalyst (**1**–**5**) on oxidation of methyl phenyl sulfide.

Table 4.6. Conversion of methyl phenyl sulfide (0.620 g, 5 mmol) using 3 as catalyst in 2.5 h of reaction time under different reaction conditions

Entry No.	Catalyst [g]	H_2O_2 [g, mmol]	CH_3CN [mL]	Conv. [%]
1	0.0005	1.14, 10	5	66
2	0.0010	1.14, 10	5	94
3	0.0015	1.14, 10	5	98
4	0.0010	0.57, 05	5	67
5	0.0010	1.71, 15	5	99
6	0.0010	1.14, 10	10	34
7	0.0010	1.14, 10	15	17

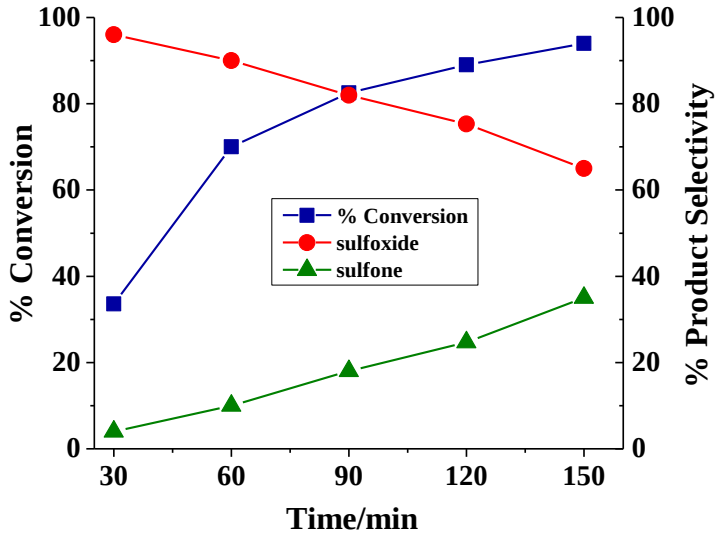

Figure 4.14. Plots showing percentage conversion of methyl phenyl sulfide and the selectivity of the formation of methyl phenyl sulfoxide and methyl phenyl sulfone as a function of time under optimized conditions using **3** as catalyst.

Other catalysts **1**, **2**, **4** and **5**, tested under the above optimized reaction conditions gave maxima of 96%, 93%, 96.2% and 98% conversion, respectively. Thus, amongst the other complexes, the catalytic efficiency varies in the order: **5** > **4** > **1** > **3** > **2**. The selectivity of different products along with the conversion and turn over frequency for these catalysts are presented in **Table 4.7**. It is clear from the table that the selectivity of the formation of methyl phenyl sulfoxide is nearly same in all cases but always higher than methyl phenyl sulfone.

Table 4.7. Oxidation of methyl phenyl sulfide, conversion, TOF and product selectivity using 1–5, as catalyst

Catalyst	TOF [h^{-1}] [a]	Conv. [%]	Selectivity [%][b]	
			mpso	mpsn
1	800	96	63.5	36.5
2	775	93	66.6	33.4
3	783	94	65	35
4	835	96.2	66.7	33.3
5	1960	98	66	34
Blank reaction	-	20	79	21

[a] TOF values calculated at 2.5 h of reaction time. [b] mpso; methyl phenyl sulfoxide; mpsn: methyl phenyl sulfone.

4.3.7. DNA binding studies

4.3.7.1. Absorption spectroscopic studies. DNA binding is a significant factor for chemical and photo-induced DNA cleavage activity of the metal complexes, therefore the binding affinity of the complexes (**1**–**5**) to CT-DNA was studied using various spectral techniques. UV-Vis titration experiments were used to determine the equilibrium binding constant (K_b) of the complexes to CT-DNA (**Table 4.8**). The electronic absorption spectra of **3** and **4** are shown in **Figure 4.15**. Binding of complexes to DNA through intercalation generally leads to hypochromism and bathochromism of the absorption band. This shift is observed due to the strong stacking interaction between the aromatic chromophore of the ligand and the base pairs of the DNA. Minor groove binding of the complexes to DNA results in hyperchromism in absorption intensity, resulting in the unwinding of the DNA double helix as well as its unstacking and concomitant exposure of the bases.[21] Therefore the extent of hypochromism or hyperchromism observed provides a measure of the strength of intercalative binding or minor groove binding of the complexes. All the oxidoalkoxido vanadium(V) complexes **1–5**, exhibited an intense absorption band in the range of 400 – 440 nm which is attributed to ligand to vanadium ($d\pi$) charge transfer (LMCT).[15a] On addition of calf thymus DNA to the complexes, they show a hypochromic shift in the LMCT absorption band which suggests the binding of CT-DNA to the complexes. Interestingly **3** and **4** shows a significant and drastic hypochromism than other complexes, which implies that these two complexes have a higher binding affinity towards CT-DNA than others. Therefore, a decrease in the absorption intensity in the LMCT absorption band due to the addition of CT-DNA to the complexes indicates that there is an interaction/binding between the complexes and CT-DNA.

In order to quantify the binding affinity of the interaction between CT-DNA and each of the complexes **1–5**, the binding constant (K_b) was calculated using Eq. 1 (Experimental Section). The K_b values reported in **Table 4.8** reveal that **3** and **4** are strongly bound with CT-DNA as compared with the others, with binding constant of 7.16×10^5 and 2.73×10^5 M^{-1}, respectively.

Table 4.8. Thermodynamic data for CT-DNA binding with 1–5

Complex	Binding Constant (M^{-1})	ΔT_m (^oC)
1	2.35×10^4	-0.27
2	2.48×10^4	0.15
3	7.16×10^5	-1.46
4	2.73×10^5	-1.11
5	9.29×10^4	0.66

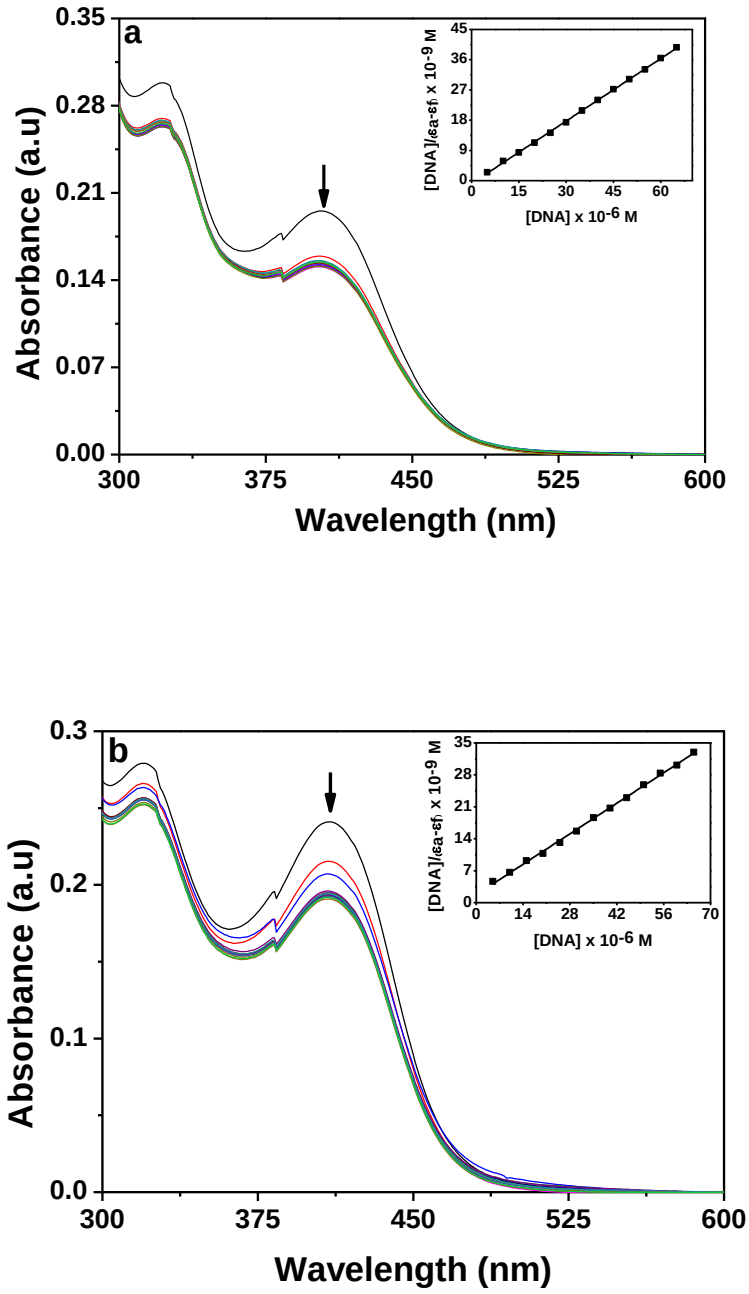

Figure 4.15. Electronic absorption spectra of **3** (a) and **4** (b) (25 μM each) upon the titration of CT-DNA (0 – 65 μM) in 10 mM Tris-HCl buffer (pH 8.0) containing 10% DMF. Arrow shows the changes in absorbance with respect to an increase in the CT-DNA concentration. The inset shows the linear fit of [DNA]/(ε_a - ε_f) vs [DNA] and binding constant (K_b) was calculated using Eq.1.

4.3.7.2. Thermal denaturation studies. To understand the nature of interaction between CT-DNA and these complexes, thermal denaturation experiments were performed. The melting temperature of CT-DNA in absence of any complex is ~65.7 °C which is in good agreement with previous results.[36] The melting temperature of CT-DNA increased very slightly upon interaction with complex **2** and **5** whereas a slight decrease in the melting temperature of CT-DNA was observed upon interaction with complex **1** (**Figure 4.16**, **Table 4.8**). On the other hand a substantial decrease in the melting temperature of CT-DNA was observed when it interacts with complex **3** and **4**. This significant decrease in the melting temperature of CT-DNA may be due to the destabilisation of DNA double helix by these two complexes. A similar kind of property is also shown by well known alkylating agents cisplatin and its derivatives.[37,38] A small shift in the DNA melting temperature suggest that the interaction between the complexes and CT-DNA follows a groove binding mode.

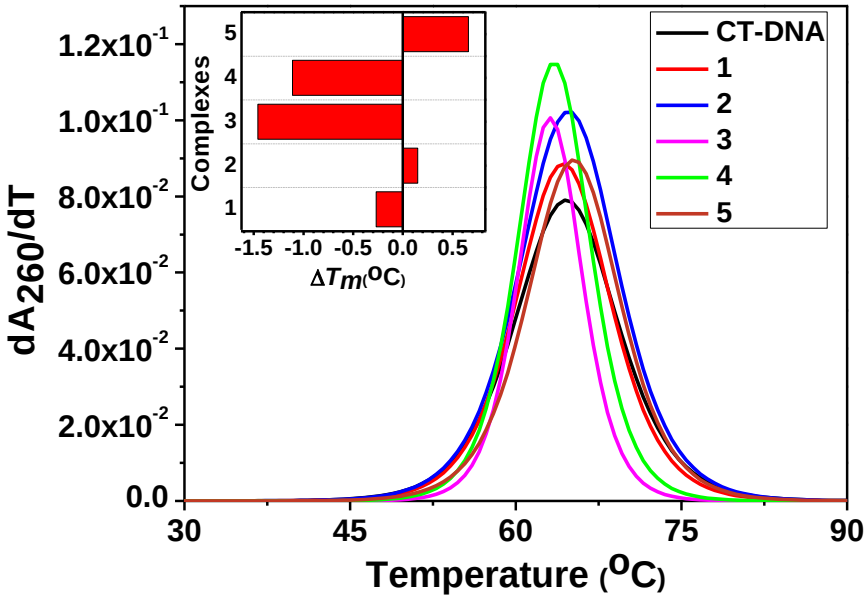

Figure 4.16. Derivative plot of thermal denaturation of CT-DNA (160 μM) in absence and presence of **1**–**5** (50 μM). The experiment was done in 10 mM Tris-HCl buffer (pH 8.0) containing 10% DMF. Inset shows the ΔT_m (^oC) of the complexes as compared to CT-DNA.

4.3.7.3. Circular dichroism studies. The conformational changes in CT-DNA due to interaction with the complexes (**1**–**5**) were monitored using circular dichroism (CD) spectroscopy.[39] The B-conformation of CT-DNA shows two conservative CD bands in the UV region, a positive band at 275 nm due to base stacking and a negative band at 245 nm due to right handed helicity.[39] Groove binding and electrostatic interaction of small molecules shows less or no perturbation on the base stacking and helicity bands whereas an intercalation mode can induce intensity changes of both bands, thus modulating the right handed B-conformation of DNA.[39] The CD spectra of CT-DNA (160 μM) in the presence of the complexes (**1**–**5**) showed an increase in the negative ellipticity at 245 nm as well as an enhanced positive ellipticity at 275 nm (**Figure 4.17**). Therefore, the spectral behavior of the complexes (**1**–**5**) with CT-DNA suggests that the binding of DNA to the complexes follows a minor groove mode of binding, which is in coherence with the results of our absorption studies.

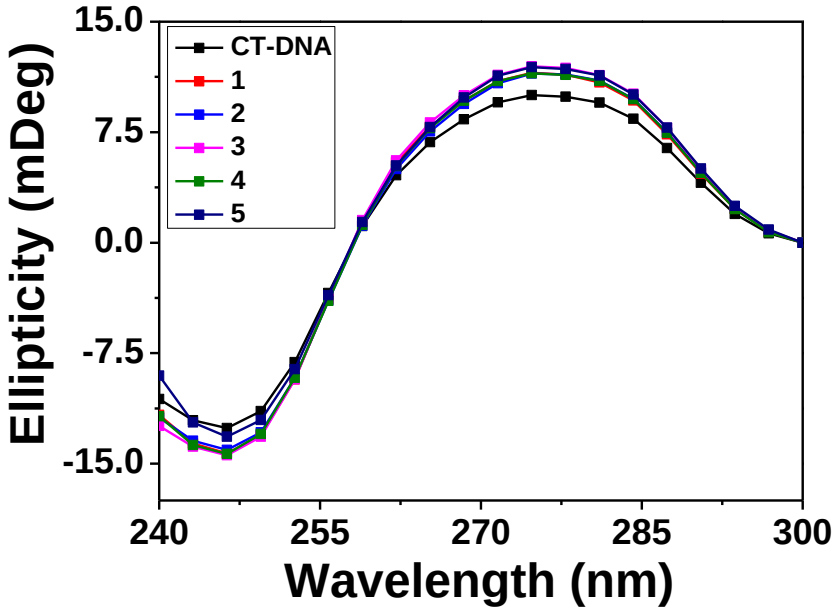

Figure 4.17. Circular dichroism spectra of CT-DNA (160 μM) in the presence and absence of **1-5** (25 μM) in 10 mM Tris-HCl buffer (pH 8.0). The path length of the cuvette was 10 mm.

4.3.8. DNA cleavage studies.

4.3.8.1. Chemical-induced DNA cleavage. The cleavage of supercoiled (SC) pUC19 DNA (300ng) by **1**–**5** (1–500 μM) in the dark was done with the aid of hydrogen peroxide as the oxidising agent. The complexes do not show any apparent DNA cleavage implying no hydrolytic cleavage activity. The lack of chemical nuclease activity may be due to their weak interaction and binding with DNA.

4.3.8.2. Photo-induced DNA cleavage. To investigate whether the DNA binding properties of the complexes were associated with photonuclease activity, a photo-induced nuclease activity assay was performed. Photo-induced DNA nuclease activity of **1**–**5** was studied using supercoiled (SC) pUC19 DNA in 50 mM Tris-HCl buffer (pH 8.0) upon irradiation of UVA light of 350 nm with the aid of gel electrophoresis in the presence and absence of the complexes (**Figure 4.18**). The extent of SC DNA cleavage by the complexes was monitored in a concentration dependent manner as shown in **Figure 4.19**. All the oxidoalkoxido vanadium(V) complexes showed greater than 10% DNA cleavage activity at a concentration of 50 μM (**Figure 4.19**, inset). Among all the complexes, **3** showed the highest DNA cleavage activity of ~20% at a concentration of 50 μM of the complex which correlates well with its DNA binding parameters (**Table 4.8**). Control experiments were suggest that neither DMF (10%) nor the ligands exhibited show photo-induced DNA cleavage activity, which implies that ligands or DMF (10%) alone are cleavage inactive under the similar conditions (**Figure 4.20**).

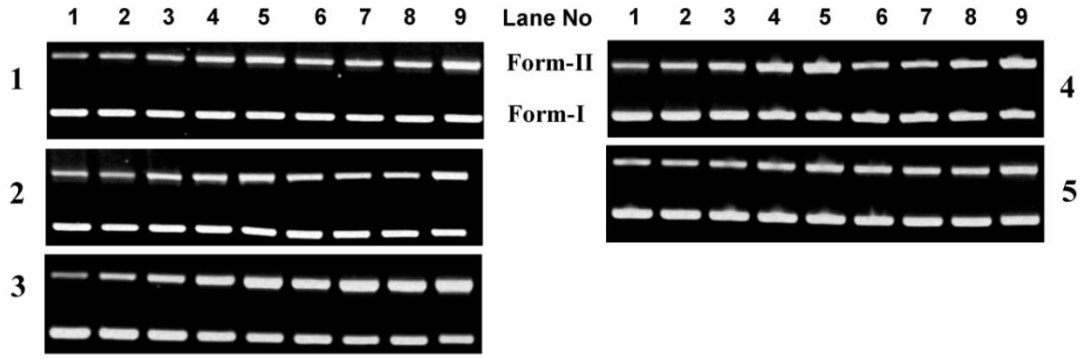

Figure 4.18. Gel diagram showing concentration dependent DNA cleavage by **1**–**5**; 300 ng of SC pUC19 DNA at different concentrations of the complexes [1–500 µM in 50 mM Tris-HCl buffer (pH 8.0) containing 10% DMF] was photo-irradiated with UVA at 350 nm for 3 h. Lanes **1**–**9**: 1, 2.5, 5.0, 7.5, 10, 50, 75, 100 and 500 µM of **1**–**5**.

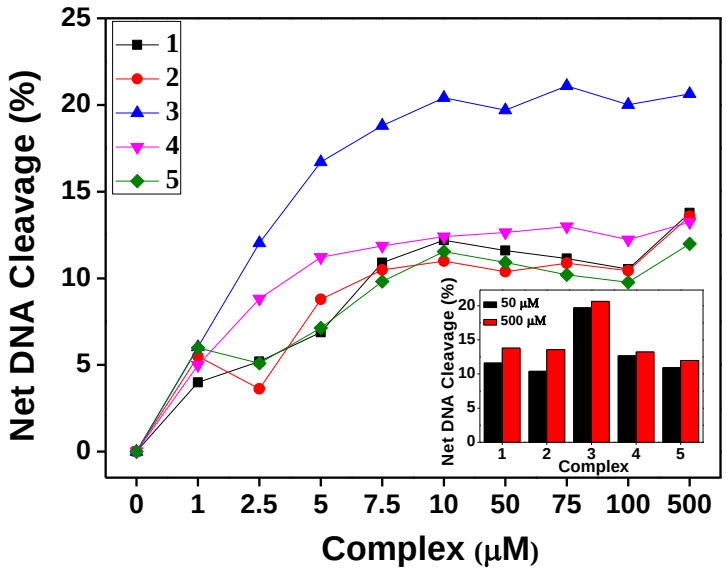

Figure 4.19. Concentration dependent DNA cleavage by **1**–**5**; 300 ng of SC pUC19 DNA at different concentration of the complexes [1–500 µM in 50 mM Tris-HCl buffer (pH 8.0) containing 10% DMF] was photo-irradiated with UVA at 350 nm for 3 h. The net DNA cleavage percent was calculated using Eq.2. Inset shows a bar diagram representation of the net DNA cleavage of different complexes at 50 and 500 µM.

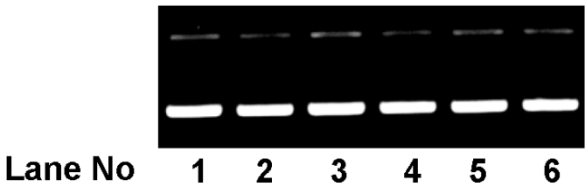

Figure 4.20. Effect of DMF (10%) and ligands on the photo-induced cleavage of SC pUC19 DNA. 300 ng pUC19 DNA with either 10% DMF or various ligands (100 μM) was photo-irradiated with UVA at 350 nm for 3 h. Lane 1, DNA only; Lane 2, DNA in presence of 10% DMF; Lane 3, DNA + H_2L^1; Lane 4, DNA + H_2L^2; Lane 5, DNA + H_2L^3; Lane 6, DNA + H_2L^4.

4.4. CONCLUSION

The following are the salient observations of the present work:

a) Four oxidoethoxido vanadium(V) [$V^{V}O(L^{1\text{-}4})OEt$] (**1**–**4**) and one dinuclear oxidoethoxido mixed-ligand vanadium(V) [{$VO(L^{2})OEt\}_2(Q)$] {Q = 4,4′-bipyridine}(**5**), complexes, taking potentially tridentate binegative aroylhydrazone ligands are reported.

b) All the complexes were characterized by various elemental as well as spectroscopic techniques. Single crystal X-ray diffraction crystallography of **1**–**4** reveals that the metal centre is in distorted square pyramidal geometry with O_4N coordination spheres, whereas **5** exhibits a distorted octahedral geometry around the metal center.

c) The solution behavior of the oxidoethoxido vanadium(V) species, **1**–**4** was studied, which indicates the existence of a new (2^{nd}) species generated *insitu* in solution state. These 2^{nd} species were characterized by spectroscopic techniques (IR, NMR, ESI-MS).

d) Catalytic potential of **1**–**5** was tested for the oxidative bromination of styrene, salicylaldehyde and oxidation of methyl phenyl sulphide and are found to act as efficient catalyst.

e) Complexes **1**–**5**, showed good DNA binding propensity. Their DNA binding activities were investigated using UV-Vis absorption titration, circular dichroism and thermal denaturation studies. The experimental results show that the complexes effectively interact with CT-DNA by an groove binding mode, with binding constants ranging from 10^4−10^5 M^{-1}. Among **1**–**5**, complex **3** and **4** shows higher binding affinity towards CT-DNA than others.

f) In all complexes show moderate photo-induced cleavage of pUC19 supercoiled plasmid DNA with complex **3** showing the highest photo induced DNA cleavage activity of ~20% at a concentration of 50 μM.

4.5. REFERENCES

(1) (a) Rehder, D. *Bioinorganic Vanadium Chemistry*; Wiley: Chichester, UK, **2008**. (b) Kustin, K.; Pesssoa, J. C.; Crans, D. C.; Eds. *Vanadium: The Versatile Metal*; ACS Symposium Series 974; American Chemical Society: Washington, DC, **2007**. (c) Tracey, A. S.; Willsky, G. R.; Takeuchi, E. S. *Vanadium Chemistry, Biochemistry, Pharmacology and Practical Applications*; CRC Press: Boca Raton, FL, **2007**. (d) Crans, D. C.; Smee, J. J.; Gaidamauskas, E.; Yang, L. *Chem. Rev.* **2004**, *104*, 849. (e) Fraústo da Silva, J. J. R.; Williams, R. J. P. *The Biological Chemistry of the Element*; Oxford University Press: Oxford, UK, **2001**. (f) Mueller, A.; Peters, F.; Pope, M. T.; Gatteschi, D. *Chem. Rev.* **1998**, *98*, 849.

(2) Henze, M. *Hoppe-Seyler's* Z. *Physiol. Chem.* **1911**, *72*, 494.

(3) Robson, R. L.; Eady, R. R.; Richardson, T. H.; Miller, R. W.; Hawkins, M.; Postgate, J. R. *Nature (London)* **1986**, *322*, 388.

(4) (a) Viler, H. *Photochemistry* **1984**, *23*, 1387. (b) de Boer, E.; van Kooky, Y.; Tromp, M. G. M.; Plat, H.; Waver, R. *Biochip. Biopsies. Acta* **1986**, *869*, 48. (c) Butler, A.; Walker, J. V. *Chem Rev.* **1993**, *93*, 1937.

(5) Antipov, A. A.; Sorokin, D.Y.; L'Vov, N. P.; Kuenen, J. G. *Biochem. J.* **2003**, *369*, 185.

(6) Kneifel, H.; Bayer, E. *J. Am. Chem. Soc.* **1986**, *108*, 3075.

(7) Berry, R. E.; Armstrong, E. M.; Beddoes, R. L.; Collison, D.; Ertok, S. N.; Helliwell, M.; Garner, C. D. *Angew. Chem., Int. Ed.* **1999**, *38*, 795.

(8) Coulombe, R. A.; Briskin, D. P.; Keller, R. J.; Thornley, W. R.; Sharma, R. P. *Arch. Biochem. Biophys.* **1987**, *255*, 267.

(9) (a) Wei, Y.; Zhang, C.; Zhao, P.; Yang, X.; Wang, K. *J. Inorg. Biochem.* **2011**, *105*, 1081. (b) Rehder, D.; Pessoa, J. C.; Geraldes, C. F. G. C.; Kabanos, T.; Kiss, T.; Meier, B.; Micera, G.; Pettersson, L.; Rangel, M.; Salifoglou, A.; Turel, I.; Wang, D. *J. Biol. Inorg. Chem.* **2002**, *7*, 384. (c) Sutradhar, M.; Barman T. R.; Mukherjee, G.; Kar M.; Saha, S. S.; Drew, M. G. B., Ghosh, S. *Inorg. Chim. Acta* **2011**, *368*, 13. (d) Saltiel, A. R.; Khan, C. R. *Nature* **2001**, *414*, 799. (e) Noblía, P.; Baran, E. J.; Otero, L.; Gambino, D. *Eur. J. Inorg. Chem.* **2004**, 322. (f) Nilsson, J.; Shteinman A. A.; Rehder, D.; Nordlander, E. *J. Inorg. Biochem.* **2011**, *105*, 1795. (g) Willsky, G. R.; Chi, L.-H.; Hu, Z.; Crans, D. C. *Coord. Chem. Rev.* **2011**, *255*, 2258. (h) Rehder, D. *Inorg. Chem. Commun*. **2003**, *6*, 604. (i) Islam, M. N.; Kumbhar, A. A.; Kumbhar, A. S.; Joshi,

B. N. *Inorg. Chem*. **2010**, *49*, 8237. (j) Pillai, S. I.; Subramanian, S. P.; Kandaswamy, M. *Eur. J. Med. Chem.* **2013**, *63*, 109.

(10) Ramanadham, S.; Mongold, J. J.; Brownsey, R. W.; Cros, G. H.; McNeill, J. H. *Am. J. Physiol*. **1989**, *257*, H904.

(11) McNeill, J. H.; Yuen, V. G.; Hoveyda, H. R.; Orvig, C. *J. Med. Chem.* **1992**, *35*, 1489.

(12) Arber, J. M.; deBoer, E.; Garner, C. D.; Hasnain, S. S.; Wever, R. *Biochemistry* **1989**, *28*, 7968.

(13) Messerschmidt, A.; Wever, R. *Proc. Natl. Acad. Sci. U.S.A.* **1996**, *93*, 392.

(14) (a) Moon, M.; Pyo, M.; Myoung, Y. C.; Ahn, C.; Lah, M. S. *Inorg. Chem.* **2001**, *40*, 554. (b) Dinda, R.; Sengupta, P.; Sutradhar, M.; Mak, T. C. W.; Ghosh, S. *Inorg. Chem.* **2008**, *47*, 5634. (c) Asgedom, G.; Sreedhara, A.; Kivikoski, J.; Valkonen, J.; Kolehmainnen, E.; Rao, C. P. *Inorg. Chem*. **1996**, *35*, 5674. (d) Keramidas, A. D.; Miller, S. M.; Anderson, O. P.; Crans, D. C. *J. Am. Chem. Soc.* **1997**, *119*, 8901. (e) Hamstra, B. J.; Houseman, A. L. P.; Colpas, G. J.; Kampf, J. W.; LoBrutto, R.; Frasch, W. D,. Pecoraro, V. L. *Inorg. Chem.* **1997**, *36*, 4866.

(15) (a) Dinda, R.; Sengupta, P.; Ghosh, S.; Mak, T. C. W. *Inorg. Chem.* **2002**, *41*, 1684. (b) Dinda, R.; Majhi, P. K.; Sengupta, P.; Pasayat, S.; Ghosh, S.; *Polyhedron* **2010**, *29*, 248. (c) Dash, S. P.; Pasayat, S.; Bhakat, S.; Dash, H. R.; Das, S.; Butcher, R. J.; Dinda, R. *Polyhedron*, **2012**, *31*, 524. (d) Dash, S. P.; Pasayat, S.; Bhakat, S.; Roy, S.; Dinda, R.; Tiekink, E. R. T.; Mukhopadhyay, S.; Bhutia, S. K.; Hardikar, M. R.; Joshi, B. N.; Patil, Y. P.; Nethaji, M. *Inorg. Chem*. **2013**, *52*, 14096. (e) Dash, S. P.; Panda, A. K.; Pasayat, S.; Dinda, R.; Biswas, A.; Tiekink, E. R. T.; Patil, Y. P.; Nethaji, M.; Kaminsky, W.; Mukhopadhyay, S.; Bhutia, S. K. ***Dalton Trans.*** **2014**, *43*, 10139.

(16) Rowe, R. A.; Jones, M. M. *Inorg, Synth.* **1957**, *5*, 113.

(17) Blanc, E.; Schwarzenbach, D.; Flack, H. D. *J. Appl. Crystallogr.* **1991**, *24*, 1035.

(18) Bruker, SADABS, SAINT, SHELXTL and SMART, Bruker AXS Inc., Madison, Wisconsin, SA, **2003**.

(19) Sheldrick, G. M. *Acta Cryst*. **2008**, *A64*, 112.

(20) Krishnamoorthy, P.; Sathyadevi, P.; Cowley, A. H.; Butorac, R. R.; Dharmaraj, N. *Eur. J. Med.Chem.* **2011**, *46*, 3376.

(21) Kumar, P.; Gorai, S.; Santra, M. K.; Mondal, B.; Manna, D. *Dalton Trans.* **2012**, *41*, 7573.

(22) Sasmal, P. K.; Patra, A. K.; Chakravarty, A. R. *J. Inorg. Biochem.* **2008**, *102*, 1463.

(23) Dai, W. M.; Lai, K. W.; Wu, A.; Hamaguchi, W.; Lee, M. Y.; Zhou, L.; Ishii, A.; Nishimoto, S. *J. Med. Chem.* **2002**, *45*, 758.

(24) (a) Glas, H.; HerdTweck, E.; Artus, G. R. J.; Thil, W. R. *Inorg. Chem.* **1998**, *37*, 3644. (b) Soon, Y.; Melchior, M.; Summers, D. A.; Thompson, R. C.; Retting, S. J.; Orvig, C. *Inorg. Chem.* **1998**, *37*, 3119. (c) Maurya, M. R.; Khurana, S.; Schulzke, C.; Rehder, D. *Eur. J. Inorg. Chem.* **2001**, 779.

(25) Das, S.; Muthukumaragopal, G. P.; Pal, S. N.; Pal, S. *New J. Chem.* **2003**, *27*, 1102.

(26) Jin, Y.; Lee, H.; Pyo, M.; Lah, M. S. *Dalton Trans.* **2005**, 797.

(27) Dutta, S. K.; Kumar, S. B.; Bhattacharyya, S.; Tiekink, E. R. T.; Chaudhury, M. *Inorg. Chem.* **1997**, *36*, 4954.

(28) Li, X.; Lah, M. S.; Pecoraro, V. L. *Inorg. Chem.* **1988**, *27*, 4657.

(29) Chasteen, N. D. in *Biological Magnetic Resonance* (Ed.: J. Reuben), Plenum, New York, **1981**, 53.

(30) Ligtenbarg, A. G. J.; Hage, R.; Feringa, B. L. *Coord. Chem. Rev.* **2003**, *237*, 89.

(31) Colpas, G. J.; Hamstra, B. J.; Kampf, J. W.; Pecoraro, V. L. *J. Am. Chem. Soc.* **1996**, *118*, 3469.

(32) Clark, E.; Kroschwitz, J. I.; Howe-Grant, M. (Eds.), *Encyclopedia of Chemical Technology*, Wiley, New York, **1997**, *23*, 134.

(33) Page, P.C.B. *Organosulfur Chemistry I and II*, Springer, Berlin, **1999**.

(34) ten Brink, H. B.; Schoemaker, H. E.; Wever, R. *Eur. J. Biochem.* **2001**, *268*, 132.

(35) Adao, P.; Pessoa, J. C.; Henriques, R. T.; Kuznetsov, M. L.; Avecilla, F.; Maurya, M. R.; Kumar, U.; Correia, I. *Inorg. Chem.* **2009**, *48*, 3542.

(36) Sasmal, P. K.; Saha, S.; Majumdar, R.; De, S.; Dighe, R. R.; Chakravarty, A. R. *Dalton Trans.* **2010**, *39*, 2147.

(37) Lenglet, G.; David-Cordonnier, M. H. *J Nucleic Acids* **2010,** *2010*.

(38) Poklar, N.; Pilch, D. S.; Lippard, S. J.; Redding, E. A.; Dunham, S. U.; Breslauer, K. J. *Proc. Natl. Acad. Sci. U.S.A.* **1996**, *93*, 7606.

(39) Li, L.; Guo, Q.; Dong, J.; Xu, T.; Li, J. *J. Photochem. Photobiol. B* **2013**, *125*, 56.

Chapter 5

Syntheses and structural investigation of some alkali metal ion-mediated $LV^{V}O_2^-$ (L^{2-} = Tridentate ONO ligands) species: DNA binding, photo-induced DNA cleavage and cytotoxic activities

Chapter 5

Syntheses and structural investigation of some alkali metal ion-mediated $LV^{V}O_2^-$ (L^{2-} = Tridentate ONO ligands) species: DNA binding, photo-induced DNA cleavage and cytotoxic activities

ABSTRACT

Eight, alkali metal ion-mediated dioxido vanadium(V), $[\{V^{V}O_2L^{1-6}\}A(H_2O)_n]_\infty$, complexes for A = Li^+, Na^+, K^+ and Cs^+, containing tridentate aroylhydrazonate ligands coordinating *via* ONO donor atoms, are described. All the synthesised ligands and the metal complexes were successfully characterised by elemental analysis, IR, UV-Vis and NMR spectroscopy. X-ray crystallographic investigation of **3**, **5**–**7** shows the presence of distorted NO_4 coordination geometries for LVO_2^- in each case, and varying μ-oxido and/or μ-aqua bridging with interesting variations correlated with the size of the alkali metal ions: with small Li^+, no bridging-O is found but four ion aggregates are found with Na^+, chains for K^+ and finally, layers for Cs^+. Two (**5**) or three-dimensional (**3**, **6** and **7**) architectures are consolidated by hydrogen bonding. The dioxido vanadium(V) complexes were found to exhibit DNA binding activity due to their interaction with CT-DNA by the groove binding mode, with binding constants ranging from $10^3 - 10^4$ M^{-1}. Complexes **1**–**8** were also tested for DNA nuclease activity against pUC19 plasmid DNA which showed that **6** and **7** had the best DNA binding and photonuclease activity; these results support their good protein binding and cleavage activity with binding constants ranging from $10^4 - 10^5$ M^{-1}. Finally, the *in vitro* antiproliferative activity of all complexes was assayed against the HeLa cell line. Some of the complexes (**2**, **5**, **6** and **7**) show considerable activity compared to commonly use chemotherapeutic drugs. The variation in cytotoxicity of the complexes is influenced by the various functional groups attached to the aroylhydrazone derivative.

5.1. INTRODUCTION

Metal-based anticancer drug discovery is at the forefront of pharmaceutical research. Metal complexes which can efficiently bind and cleave DNA under physiological conditions are considered as potential candidates for use as therapeutic agents in medicinal applications and for genomic research.[1–6] Therefore, attempts are being made to replace the most successful anti-cancer drug cisplatin with suitable alternatives and hence numerous transition metal complexes have been synthesised and tested for their anti-cancer activities. Among the transition metals, the coordination chemistry of the vanadium attracts increasing interest because of the use of many vanadium complexes as models for the biological functions of vanadium,[7–10] such as haloperoxidation,[11] phosphorylation,[12] insulin mimicking,[13–17] nitrogen fixation,[18] tumour growth inhibition and prophylaxis against carcinogenesis.[19] This bioelement takes part in various DNA maintenance reactions and thereby prevents genomic instability which otherwise leads to cancer.[20,21] Vanadium complexes could also suppress the growth and spread of existing tumours by inhibiting tumour cell proliferation, inducing apoptosis and limiting the invasion and metastatic potential of neoplastic cells. Moreover, it has been found that oxido vanadium complexes that efficiently interact with DNA also show antitrypanosomatid activity.[21-23] Thus, the DNA-binding, DNA photocleavage and anti-proliferative activity of oxidometal complexes based on vanadium and multifunctional ligands have been of recent interest.[24]

Additionally, in recent times a new area of research involving the design and synthesis of extended frameworks *via* supramolecular interactions has emerged. Hydrogen bonding interactions have been particularly explored in the context of molecular recognition and engineering of molecular solids.[25] Many studies have focused on the use of monovalent alkali metals as a source of counter ion for the formation of polymeric aggregates,[26] featuring channels or sheets of metal ions and which may have potential to act as ionic conductors,[27] charge storage materials as well as biomimetic models.[28] In most of these cases the water molecules are present as part of aquated A^+ ions (A = alkali metal), and play a vital role in holding the components of the assembly together through hydrogen bonding networks and thereby enhancing the stability through charge neutralisation. In the context of the present study it is relevant to mention that although the pharmacological activity of many vanadium-hydrazone complexes has been studied[21-23] and the syntheses and structural investigation of alkali metal ion-mediated $LV^VO_2^-$

complexes have been reported previously,[26b,c,h,i] the study of pharmacological activity of the latter has yet to be explored.

Hydrazones, –NH–N=CRR' (R and R′ = H, alkyl, aryl), are versatile ligands and have applications in the fields of analytical[29] and medicinal chemistry.[30] Hydrazone moieties are important pharmacophoric cores of several anti-cancer, anti-inflammatory, anti-nociceptive and anti-platelet drugs.[31] Moreover, the electronic effects of hydrazone complexes are also important in the design of complexes with better DNA-binding and cleaving characteristics.[32] In addition, the presence of a rigid aromatic system in the Schiff base structure gives rise to particular spectroscopic properties, which makes it a potential probe for nucleic acids. Recently, reports on vanadium hydrazone complexes with potential biological properties have appeared.[33] In this context, the utilisation of the intercalating aroylhydrazone moiety when coordinated to vanadium might accentuate the biochemical activity of the derived hybrid molecules, which may lead to efficient DNA binding and cleavage. As the complexes cause photocleavage of DNA and exhibit photocytotoxic properties, these are established as important potential chemotherapeutic agents.[23,34] In short, the new oxido vanadium complexes may prove to be a promising and attractive approach in the search for new potential drugs for the treatment of cancer.

For the past few years, we have been studying the chemistry of oxido-metal complexes including those of vanadium, in N,O-donor environments[35] along with electro-generation of mixed-valence divanadium(IV,V),[35a,b] and some highly stable nonoxido vanadium(IV) complexes.[36] Although many hydrazone complexes exhibit good biological activities, their water-solubility is still unsatisfactory, which may restrict their application. Hence, it seemed of interest to synthesise some new water-soluble dioxido-metal complexes of hydrazones which may have significant pharmacological effects.

In previous studies it was found a change in the substituent in the hydrazone moiety changed bio-activity.[36] In connection with that, in the present chapter the syntheses, structural investigation and pharmacological activities of some water-soluble alkali metal (Li^+, Na^+, K^+ and Cs^+) ion-mediated dioxido vanadium(V) hydrazone complexes, with varying substitution, that show interesting DNA binding, photo-induced DNA cleavage and cytotoxicity profiles activities, is reported. The interaction of these complexes with calf-thymus DNA (CT-DNA) was investigated

using UV-Vis absorption titration, circular dichroism and thermal denaturation studies. Their photo-cleavage reactions with pUC19 supercoiled plasmid DNA were investigated by gel electrophoresis, and for **6** and **7**, the protein binding and cleavage activity were also tested. In addition, the cytotoxicity of the new complexes against the HeLa cell line was assessed by the MTT assay.

5.2. EXPERIMENTAL SECTION

5.2.1. General Methods and Materials. All chemicals were purchased from commercial sources and used without further purification. $[VO(acac)_2]$ was prepared as described in the literature.[37] MTT (3-[4,5-Dimethylthiazol-2-yl]-2,5-diphenyltetrazolium) and DAPI (4′,6-diamidino-2-phenylindole dihydrochloride) were purchased from Sigma Aldrich (USA). Minimal essential medium (MEM) was purchased from Gibco, India. Reagent grade solvents were dried and distilled prior to use. The supercoiled (SC) pUC19 DNA was purified from *E. coli* cells with the aid of GeneJET Plasmid Isolation Kit (Thermo Scientific, USA). Calf thymus (CT) DNA was purchased from SRL (India) (biochemistry grade). Agarose (molecular biology grade) and bovine serum albumin (BSA) was purchased from Sigma Aldrich (USA). Elemental analyses were performed on a Vario ELcube CHNS Elemental analyzer and IR spectra were recorded on a Perkin-Elmer Spectrum RXI spectrophotometer. ^1H and ^{13}C NMR spectra were recorded with a Bruker Ultrashield 400 MHz spectrometer using $SiMe_4$ as the internal standard. Electronic spectra were recorded on a Perkin-Elmer Lamda25 spectrophotometer.

5.2.2. Synthesis of Ligands ($H_2L^{1–6}$). Schiff base ligands, H_2L^{1-6} were prepared in good yield by the condensation of acid hydrazide with the corresponding carbonyl compound in equimolar ratio in ethanol by a standard procedure.[38] The resulting white compounds were filtered, washed with ethanol and dried over fused $CaCl_2$. Elemental analysis results, NMR (^1H and ^{13}C) and IR data for all of these verified their preparation.

H_2L^1. Yield: 68%. Anal. Calcd for $C_{15}H_{14}N_2O_3$: C, 66.65; H, 5.22; N, 10.36. Found C, 66.63; H, 5.27; N, 10.38. FTIR (KBr pellet, cm^{-1}): 3303 ν(O–H), 3053 ν(N–H), 1627 ν(C=O), 1615 ν(C=N), 1580 ν(C=C/aromatic). ^1H NMR (400 MHz, DMSO-d_6): δ 13.18 (s, 1H, OH), 12.10 (s, 1H, OH), 11.55 (s, 1H, NH), 8.00–6.88 (m, 8H, C_6H_4), 2.42 (s, 3H, CH_3). ^{13}C NMR (100 MHz, DMSO-d_6): δ 162.69, 159.04, 157.11, 156.37, 134.22, 131.73, 131.02, 128.94, 120.23, 119.67, 119.11, 117.76, 117.66, 117.36, 13.62.

H_2L^2. Yield: 64%. Anal. Calcd for $C_{14}H_{12}N_2O_3$: C, 65.61; H, 4.72; N, 10.93. Found C, 65.63; H, 4.74; N, 10.89. FTIR (KBr pellet, cm^{-1}): 3383 ν(O–H), 3102 ν(N–H), 1629 ν(C=O), 1619 ν(C=N), 1573 ν(C=C/aromatic). ^1H NMR (400 MHz, DMSO-d_6): δ 12.05 (s, 1H, OH), 11.79 (s, 1H, OH), 11.22 (s, 1H, NH), 8.68 (s, 1H, CH), 7.91–6.90 (m, 8H, C_6H_4). ^{13}C NMR (100 MHz,

DMSO-d_6): δ 164.99, 159.50, 157.99, 149.48, 134.44, 132.08, 130.55, 129.95, 129.27, 119.85, 117.76, 117.33, 116.92, 116.06.

H_2L^3. Yield: 64%. Anal. Calcd for $C_{15}H_{14}N_2O_2$: C, 70.85; H, 5.54; N, 11.01. Found C, 70.82; H, 5.56; N, 11.02. FTIR (KBr pellet, cm^{-1}): 3341 ν(O–H), 3216 ν(N–H), 1650 ν(C=O), 1606 ν(C=N), 1579 ν(C=C/aromatic). ^{1}H NMR (400 MHz, DMSO-d_6): δ 13.45 (s, 1H, OH), 11.37 (s, 1H, NH), 7.99–6.91 (m, 9H, C_6H_4), 2.46 (s, 3H, CH_3). ^{13}C NMR (100 MHz, DMSO-d_6): δ 164.92, 159.29, 158.62, 133.47, 132.40, 131.72, 128.94, 128.86, 128.58, 119.91, 118.99, 117.80, 14.48.

H_2L^4. Yield: 69%. Anal. Calcd for $C_{14}H_{13}N_3O_2$: C, 65.87; H, 5.13; N, 16.46. Found C, 65.88; H, 5.11; N, 16.50. FTIR (KBr pellet, cm^{-1}): 3218 ν(O–H), 3099 ν(N–H), 1679 ν(C=O), 1607 ν(C=N), 1574 ν(C=C/aromatic). ^{1}H NMR (400 MHz, DMSO-d_6): δ 13.32 (s, 1H, OH), 11.72 (s, 1H, NH), 8.20–6.89 (m, 8H, C_6H_4), 2.42 (s, 3H, CH_3). ^{13}C NMR (100 MHz, DMSO-d_6): δ 163.40, 160.01, 159.21, 150.56, 140.84, 132.05, 129.19, 122.84, 122.63, 122.43, 119.68, 119.10, 117.82, 14.78.

H_2L^5. Yield: 62%. Anal. Calcd for $C_{13}H_{11}N_3O_2$: C, 64.72; H, 4.59; N, 17.41. Found C, 64.68; H, 4.58; N, 17.45. FTIR (KBr pellet, cm^{-1}): 3167 ν(O–H), 3002 ν(N–H), 1683 ν(C=O), 1612 ν(C=N), 1567 ν(C=C/aromatic). ^{1}H NMR (400 MHz, DMSO-d_6): δ 12.33 (s, 1H, OH), 11.14 (s, 1H, NH), 8.69 (s, 1H, CH), 8.80–6.89 (m, 8H, C_6H_4). ^{13}C NMR (100 MHz, DMSO-d_6): δ 161.83, 157.96, 150.81, 150.11, 149.56, 140.40, 132.19, 129.76, 123.17, 121.98, 119.88, 119.09, 116.90.

H_2L^6. Yield: 63%. Anal. Calcd for $C_{15}H_{15}N_3O_2$: C 66.90; H, 5.61; N, 15.60. Found C, 66.89; H, 5.62; N, 15.63. FTIR (KBr pellet, cm^{-1}): 3476 ν(O–H), 3364 $\nu(N–H_2)_s$, 3207 $\nu(N–H_2)_{as}$, 3028 ν(N–H), 1627 ν(C=O), 1611 ν(C=N), 1573 ν(C=C/aromatic). ^{1}H NMR (400 MHz, DMSO-d_6): δ 13.55 (s, 1H, OH), 11.09 (s, 1H, NH), 7.68–6.61 (m, 8H, C_6H_4), 2.48 (s, 3H, CH_3). ^{13}C NMR (100 MHz, DMSO-d_6): δ 166.68, 159.23, 157.52, 150.49, 133.10, 131.54, 129.64, 128.78, 119.99, 118.95, 117.77, 116.89, 115.30, 113.61, 14.35.

5.2.3. Synthesis of complexes [{VO_2L^{1-6}}$A(H_2O)_n]_\infty$ (1–8). To the (1 mmol) sample of ligand $H_2L^{1–6}$ in 20 mL of ethanol, alkali metal carbonate (1 mmol) dissolved in 5 mL of water was added. The white suspension turned yellowish. The mixture was refluxed for 5 min to give a clear yellow solution. Thereafter a sample of $[VO(acac)_2]$ (1 mmol) was added under refluxing conditions. After 1h, the resulting deep-yellow solution was filtered and slow evaporation of the filtrate over 4–5 days produced thin yellow or orange crystals. The crystals were filtered and washed with ethanol. Elemental analysis results, NMR (^{1}H, ^{13}C, ^{51}V), UV-Vis and IR data for all of these verified their preparation.

[{VO_2L^1}$Li(H_2O)_3]_\infty$ (1). Yield: 63%. Anal. Calcd for $C_{15}H_{18}LiN_2O_8V$: C, 43.70; H, 4.40; N, 6.79. Found: C, 43.67; H, 4.42; N, 6.78. FTIR (KBr pellet, cm^{-1}): 3400 ν(O–H), 1603 ν(C=N), 1261 $\nu(C–O)_{enolic}$, 947, 901 ν(V=O). UV–Vis (DMF) [λ_{max}, nm (ε, M^{-1} cm^{-1})]: 410 (25410), 365 (33650), 278 (39321). ^{1}H NMR (400 MHz, DMSO-d_6): δ 12.58 (s, 1H, OH), 7.87–6.83 (m, 8H, C_6H_4), 2.73 (s, 3H, CH_3). ^{13}C NMR (100 MHz, DMSO-d_6): δ 170.16, 164.98, 161.96, 159.42, 133.23, 132.79, 130.20, 129.43, 122.36, 120.55, 119.15, 118.00, 116.96, 116.16, 17.12. ^{51}V NMR (DMSO-d_6): δ –542.

[{VO_2L^1}$K(H_2O)_2]_\infty$ (2). Yield: 67%. Anal. Calcd for $C_{15}H_{16}KN_2O_7V$: C, 42.26; H, 3.78; N, 6.57. Found C, 42.24; H, 3.81; N, 6.55. FTIR (KBr pellet, cm^{-1}): 3590 ν(O–H), 1599 ν(C=N), 1253 $\nu(C–O)_{enolic}$, 921, 903 ν(V=O). UV–Vis (DMF) [λ_{max}, nm (ε, M^{-1} cm^{-1})]: 408 (23910), 323 (38209), 265 (43120). ^{1}H NMR (400 MHz, DMSO-d_6): δ 12.58 (s, 1H, OH), 7.83–6.84 (m, 8H, C_6H_4), 2.73 (s, 3H, CH_3). ^{13}C NMR (100 MHz, DMSO-d_6): δ 170.14, 165.04, 161.90, 159.42, 133.18, 132.71, 130.18, 129.47, 122.33, 120.61, 119.08, 117.88, 117.66, 116.19, 17.10. ^{51}V NMR (DMSO-d_6): δ –540.

[{VO_2L^2}$Li(H_2O)_{4.5}]_\infty$ (3). Yield: 63%. Anal. Calcd for $C_{28}H_{38}Li_2N_4O_{19}V_2$: C, 39.54; H, 4.50; N, 6.58. Found C, 39.51; H, 4.49; N, 6.60. FTIR (KBr pellet, cm^{-1}): 3457 ν(O–H), 1606 ν(C=N), 1228 $\nu(C–O)_{enolic}$, 929, 905 ν(V=O). UV–Vis (DMF) [λ_{max}, nm (ε, M^{-1} cm^{-1})]: 406 (30600), 336 (44480), 265 (46680). ^{1}H NMR (400 MHz, DMSO-d_6): δ 12.21 (s, 1H, OH), 9.09 (s, 1H, CH), 7.83–6.80 (m, 8H, C_6H_4). ^{13}C NMR (100 MHz, DMSO-d_6): δ 170.73, 165.19, 159.03, 156.78, 134.20, 133.24, 133.15, 129.46, 120.06, 119.16, 117.52, 116.97, 115.94. ^{51}V NMR (DMSO-d_6): δ –539.

[{VO_2L^2}$Cs(H_2O)_3]_\infty$ (4). Yield: 69%. Anal. Calcd for $C_{14}H_{16}CsN_2O_8V$: C, 32.08; H, 3.07; N, 5.34. Found C, 32.04; H, 3.10; N, 5.35. FTIR (KBr pellet, cm^{-1}): 3488 *v*(O–H), 1607 *v*(C=N), 1227 $v(C–O)_{enolic}$, 920, 899 *v*(V=O). UV–Vis (DMF) [λ_{max}, nm (ε, M^{-1} cm^{-1})]: 403 (24160), 337 (33200), 266 (35600). ^{1}H NMR (400 MHz, DMSO-d_6): *δ* 12.21 (s, 1H, OH), 9.11 (s, 1H, CH), 7.85–6.81 (m, 8H, C_6H_4). ^{13}C NMR (100 MHz, DMSO-d_6): *δ* 170.74, 165.12, 159.04, 156.83, 134.23, 133.26, 133.16, 129.50, 120.08, 119.18, 117.61, 116.99, 115.93. ^{51}V NMR (DMSO-d_6): *δ* –539.

[{VO_2L^3}$Cs(H_2O)_2]_\infty$ (5). Yield: 61%. Anal. Calcd for $C_{15}H_{14}CsN_2O_5V$: C, 37.06; H, 2.90; N, 5.76. Found C, 37.03; H, 2.91; N, 5.79. FTIR (KBr pellet, cm^{-1}): 3562 *v*(O–H), 1599 *v*(C=N), 1243 $v(C–O)_{enolic}$, 946, 900 *v*(V=O). UV–Vis (DMF) [λ_{max}, nm (ε, M^{-1} cm^{-1})]: 390 (11240), 317 (16200), 266 (19280). ^{1}H NMR (400 MHz, DMSO-d_6): *δ* 8.07–6.81 (m, 9H, C_6H_4), 2.87 (s, 3H, CH_3). ^{13}C NMR (100 MHz, DMSO-d_6): *δ* 168.76, 164.27, 162.11, 133.36, 131.82, 130.60, 129.60, 128.30, 128.11, 127.92, 122.48, 120.04, 117.39, 16.26. ^{51}V NMR (DMSO-d_6): *δ* –534.

[{VO_2L^4}$K(H_2O)_2]_\infty$ (6). Yield: 63%. Anal. Calcd for $C_{14}H_{15}KN_3O_6V$: C, 40.88; H, 3.67; N, 10.21. Found C, 40.85; H, 3.66; N, 10.24. FTIR (KBr pellet, cm^{-1}): 3429 *v*(O–H), 1601 *v*(C=N), 1248 $v(C–O)_{enolic}$, 943, 907 *v*(V=O). UV–Vis (DMF) [λ_{max}, nm (ε, M^{-1} cm^{-1})]: 395 (36920), 322 (45840), 268 (50760). ^{1}H NMR (400 MHz, DMSO-d_6): *δ* 8.71–6.82 (m, 8H, C_6H_4), 2.89 (s, 3H, CH_3). ^{13}C NMR (100 MHz, DMSO-d_6): *δ* 167.26, 165.01, 164.25, 150.49, 141.19, 132.60, 130.19, 122.58, 122.15, 120.58, 117.78, 16.68. ^{51}V NMR (DMSO-d_6): *δ* –533.

[{VO_2L^5}$Na(H_2O)_4]_\infty$ (7). Yield: 60%. Anal. Calcd for $C_{13}H_{17}N_3NaO_8V$: C, 37.42; H, 4.10; N, 10.07. Found C, 37.47; H, 4.13; N, 10.04. FTIR (KBr pellet, cm^{-1}): 3531 *v*(O–H), 1614 *v*(C=N), 1223, $v(C–O)_{enolic}$, 926, 907 *v*(V=O). UV–Vis (DMF) [λ_{max}, nm (ε, M^{-1} cm^{-1})]: 410 (65240), 328 (77920), 268 (87560). ^{1}H NMR (400 MHz, DMSO-d_6): *δ* 9.05 (s, 1H, CH), 8.69–6.78 (m, 8H, C_6H_4). ^{13}C NMR (100 MHz, DMSO-d_6): *δ* 168.32, 165.44, 157.83, 150.52, 140.59, 134.15, 133.34, 122.02, 120.11, 117.33. ^{51}V NMR (DMSO-d_6): *δ* –531.

[{VO_2L^6}$Cs(H_2O)_3]_\infty$ (8). Yield: 65%. Anal. Calcd for $C_{15}H_{19}CsN_3O_7V$: C, 33.54; H, 3.56; N, 7.82. Found C, 33.56; H, 3.52; N, 7.85. FTIR (KBr pellet, cm^{-1}): 3454 *v*(O–H), 3365 $v(NH_2)_s$, 3237 $v(NH_2)_{as}$, 1597 *v*(C=N), 1253 $v(C–O)_{enolic}$, 932, 897 *v*(V=O). UV–Vis (DMF) [λ_{max}, nm (ε, M^{-1} cm^{-1})]: 398 (15780), 320 (21718). 258 (28242). ^{1}H NMR (400 MHz, DMSO-d_6): *δ* 7.83–

6.84 (m, 8H, C_6H_4), 2.73 (s, 3H, CH_3). ^{13}C NMR (100 MHz, DMSO-d_6): δ 170.76, 164.81, 160.67, 149.45, 132.02, 131.60, 129.87, 122.86, 120.44, 117.56, 116.80, 115.19, 114.99, 113.74, 17.20. ^{51}V NMR (DMSO-d_6): δ –540.

5.2.4. X-ray Crystallography. Intensity data for **3**, **5-7** were collected on a Bruker APEXII diffractometer equipped with a CCD area detector and graphite-monochromated Mo Kα radiation (λ = 0.71069 Å). Crystal data and refinement details are given in **Table 5.1**. Data reduction and empirical absorption correction, based on the multi-scan method, was by standard methods.[39] The structures were solved by direct methods using SHELXS97[2] and refinement (anisotropic displacement parameters and C-bound hydrogen atoms in idealised positions) of each structure was carried out on F^2 by using full-matrix least-squares procedures.[40] Based on hydrogen bonding considerations, the hydroxyl- and water-H atoms in **3** were included in their idealised positions. The water-H atoms in **5** and **7** were located from the respective difference Fourier maps and refined with the distance restraint O−H = 0.84±0.01 Å. The water-H atoms in **6** were located in the case of the O1w water molecule but not for O2w. For the latter, the H atoms were placed based on stereochemical grounds and all refined with the distance restraint O−H = 0.84±0.01 Å. While the O1w molecule formed the anticipated hydrogen bonding interactions, the same was not true for the O2w water molecule which exists in a pocket, forming O...O separations in the range 2.852(4) to 3.364(2) Å with four putative hydrogen bond acceptors as detailed in **Table 5.2**. Therefore, it was concluded that the O2w-bound hydrogen atoms are disordered over several positions. Molecular structure diagrams, showing the atom labelling schemes, were drawn with 50% (**6** and **7**) or 70% (**3** and **5**) displacement ellipsoids using ORTEP-3 for Windows,[41] the overlay diagrams were drawn with QMol[42] and the remaining crystallographic figures were drawn with DIAMOND.[43] Data manipulation and interpretation were accomplished using WinGX[3] and PLATON.[44]

Table 5.1. Crystal data and refinement details for 3, 5–7

	3	**5**	**6**	**7**
Empirical formula	Li_2, $2(C_{14}H_{10}N_2O_5V)$, $9H_2O$	Cs, $C_{15}H_{12}N_2O_4V$, H_2O	K, $C_{14}H_{11}N_3O_4V$, $2H_2O$	Na, $C_{13}H_9N_3O_4V$, $4H_2O$
Formula weight	850.38	486.13	411.33	417.23
Crystal size (mm)	0.15 × 0.15 × 0.60	0.04 × 0.07 × 0.30	0.03 × 0.05 × 0.32	0.03 × 0.04 × 0.27
Crystal morphology, colour	Prism, orange	Prism, yellow	Prism, yellow	Prism, yellow
Temperature (K)	100(2)	100(2)	293(2)	293(2)
Crystal system	Triclinic	Monoclinic	Orthorhombic	Triclinic
Space group	$P\bar{1}$	$P2_1/c$	*Pbca*	$P\bar{1}$
a (Å)	6.8227(2)	15.430(2)	11.6880(4)	7.7429(8)
b (Å)	15.4441(6)	7.1128(10)	8.2858(2)	10.3131(10)
c (Å)	18.3454(7)	30.505(4)	34.9484(11)	12.0373(13)
α (°)	67.969(2)	90	90	109.590(6)
β (°)	80.954(2)	98.682(8)	90	104.363(5)
γ (°)	89.346(2)	90	90	92.983(5)
V (Å^3)	1767.24(11)	3309.5(8)	3384.56(18)	867.59(15)
Z	2	8	8	2
D_x (g cm^{-3})	1.598	1.951	1.614	1.597
μ (mm^{-1})	0.616	2.795	0.868	0.644
θ range (°)	2.2–28.5	1.8–28.4	2.1–30.6	1.9–30.7
Reflections measured	24488	107431	63472	17852
Independent reflections; R_{int}	8797; 0.026	8117; 0.049	5179; 0.070	5283; 0.028
Reflections with $I > 2\sigma(I)$	7372	6866	3225	4107
Number of parameters	498	447	239	259
$R(F)$ [$I > 2\sigma(I)$ reflns]	0.036	0.028	0.046	0.042
a, *b* in wghting scheme	0.054, 0.949	0.019, 5.712	0.040, 1.998	0.057, 0.095
$wR(F^2)$ (all data)	0.102	0.059	0.109	0.111
$\Delta\rho_{max,\ min}$ (e Å^{-3})	0.54, -0.50	0.95, -0.92	0.43, -0.48	0.39, -0.27

Table 5.2. Summary of intermolecular interactions (A–H…B; Å, º) operating in the crystal structures of 3, 5-7.[a]

A	H	B	A–H	H…B	A…B	A–H…B	Symmetry
3							
O1	H1O	N1	0.84	1.83	2.567(2)	146	*x*, *y*, *z*
O6	H6O	N3	0.84	1.83	2.571(2)	146	*x*, *y*, *z*
O1W	H1W1	O9	0.80	1.93	2.7126(19)	167	*x*, *y*, *z*
O1W	H1W2	O5	0.80	2.01	2.7486(19)	153	*x*, *y*, -1+*z*
O2W	H2W1	O3	0.80	2.09	2.886(2)	173	-1+*x*, *y*, -1+*z*
O2W	H2W2	O8W	0.80	2.04	2.817(2)	165	-1+*x*, *y*, *z*
O3W	H3W1	O7	0.80	2.24	2.972(2)	152	1-*x*, 1-*y*, -*z*
O3W	H3W1	O10	0.80	2.46	3.108(2)	139	1-*x*, 1-*y*, -*z*
O3W	H3W2	O9W	0.80	1.99	2.774(2)	165	*x*, *y*, *z*
O4W	H4W1	O8	0.80	2.06	2.831(2)	163	-1+*x*, *y*, *z*
O4W	H4W2	O7	0.80	2.31	3.088(2)	165	*x*, *y*, *z*
O5W	H5W1	O8W	0.80	1.97	2.736(2)	159	-1+*x*, *y*, *z*
O5W	H5W2	O2	0.80	2.14	2.937(2)	171	1-*x*, -*y*, 1-*z*
O6W	H6W1	O2	0.80	2.06	2.8552(19)	169	*x*, *y*, -1+*z*
O6W	H6W2	O3	0.80	2.39	3.079(2)	145	-1+*x*, *y*, -1+*z*
O6W	H6W2	O4	0.80	2.36	3.0187(19)	140	-1+*x*, *y*, -1+*z*
O7W	H7W1	O4	0.80	1.95	2.744(2)	173	*x*, *y*, -1+*z*
O7W	H7W2	O6W	0.80	2.04	2.825(2)	166	1-*x*, -*y*, -*z*
O8W	H8W1	O8	0.80	2.41	3.073(2)	141	*x*, *y*, *z*
O8W	H8W1	O9	0.80	2.27	2.959(2)	145	*x*, *y*, *z*
O8W	H8W2	O7W	0.80	1.97	2.760(2)	169	*x*, *y*, *z*
O9W	H9W1	O10	0.80	1.97	2.767(2)	178	*x*, *y*, *z*
O9W	H9W2	O2W	0.80	1.99	2.785(2)	171	1+*x*, *y*, *z*
C8	H8	O6	0.95	2.35	3.274(2)	165	1+*x*, *y*, *z*
C22	H22	O1	0.95	2.30	3.240(2)	168	*x*, *y*, *z*

5

O1W	H1W1	O2	0.84(2)	2.43(3)	3.038(3)	130(2)	*x*, *y*, *z*
O1W	H1W1	O4	0.84(2)	2.48(2)	3.274(3)	159(2)	*x*, *y*, *z*
O1W	H1W2	O4	0.84(3)	1.89(2)	2.723(3)	170(3)	1-*x*, 1-*y*, 1-*z*
O2W	H2W1	O6	0.85(3)	1.96(3)	2.776(3)	160(3)	-*x*, -1-*y*, 1-*z*
O2W	H2W2	O7	0.85(3)	2.15(3)	2.986(3)	171(2)	*x*, -1+*y*, *z*

6

O1W	H1W1	O1	0.85(3)	2.11(4)	2.931(3)	162(3)	½-*x*, ½+*y*, *z*
O1W	H1W2	N1	0.837(18)	2.01(2)	2.815(3)	162(4)	1-*x*, -*y*, -*z*
C5	H5	O4	0.93	2.54	3.439(3)	164	1-*x*, -*y*, -*z*
C7'	H72	Cg1	0.96	2.56	3.477(3)	159	1½-*x*, - ½+*y*, *z*
O2W	H2W2	O3	0.863(14)	2.44(5)	2.852(4)	110(4)	½-*x*, ½+*y*, *z*

The O2W-water molecule atom lies in a pocket comprising the O3 atom, see above, and the O1W (separation 3.313(2) Å), O3 (3.261(2) Å) and O4 (3.364(2) Å) atoms.

Cg1 is the centroid of the (C8-C13) ring

7

O1W	H1W1	O1	0.82(3)	2.17(3)	2.975(2)	165(2)	*x*, *y*, *z*
O1W	H1W2	O4W	0.83(3)	1.97(3)	2.787(2)	166(3)	1-*x*, -*y*, 2-*z*
O2W	H2W1	O3	0.84(3)	2.08(3)	2.885(2)	162(3)	-1+*x*, *y*, *z*
O2W	H2W2	O4W	0.83(3)	1.98(3)	2.809(2)	173(3)	*x*, *y*, *z*
O3W	H3W1	O2W	0.83(3)	2.24(3)	3.015(3)	156(3)	-*x*, -*y*, 2-*z*
O3W	H3W2	N2	0.83(3)	2.26(3)	2.991(3)	147(3)	1-*x*, 1-*y*, 2-*z*
O4W	H4W1	N1	0.834(13)	1.982(13)	2.808(2)	171(2)	-1+*x*, -1+*y*, -1+*z*
O4W	H4W2	O2	0.84(2)	2.06(2)	2.876(2)	166(2)	*x*, *y*, *z*

5.2.5. DNA binding experiments.

5.2.5.1. Absorption spectral studies. Binding of the dioxido vanadium(V) complexes to calf thymus (CT) DNA was studied in 10 mM Tris–HCl buffer (pH 8.0) containing 10% DMF. UV-Vis absorption titration experiments were performed with Perkin-Elmer Lamda35 spectrophotometer using a fixed concentration of metal complex (25 μM) but variable nucleotide concentrations ranging from 0 to 100 μM. After each addition of DNA (10 μM) to the metal complex, the readings were noted. The data were then fit to the following equation to obtain binding constant K_b[45]

$$\frac{[DNA]}{\varepsilon_a - \varepsilon_f} = \frac{[DNA]}{\varepsilon_b - \varepsilon_f} + \frac{1}{K_b(\varepsilon_b - \varepsilon_f)}; \qquad \textbf{Eq. 1}$$

where [DNA] is the concentration of DNA base pairs, ε_a, ε_f and ε_b correspond to apparent extinction co-efficient for the complex *i.e.* Abs/[complex] in presence of DNA, in absence of DNA and to fully bound DNA respectively. A plot of [DNA]/(ε_a - ε_f) *vs* [DNA] gave a slope and the intercept equal to 1/(ε_b - ε_f) and 1/K_b(ε_b - ε_f), respectively. The binding constant K_b is calculated from the ratio of the slope to the intercept. Binding of ligands to CT-DNA was also studied. In order to find out the binding constant (K_b) of "ligand-DNA interaction", a fixed concentration of ligand [25 μM in 10 mM Tris–HCl buffer (pH 8.0) containing 10% DMF] was titrated with variable DNA concentration ranging from 0 to 350 μM.

5.2.5.2. Thermal denaturation studies. Thermal denaturation studies of CT-DNA (160 μM) in the absence and presence of complexes (100 μM) were carried out by monitoring the absorbance at 260 nm in the temperature range of 30-90 ^oC with a ramp rate of 1 ^oC/min in 10 mM Tris-HCl buffer (pH 8.0). The experiments were carried out using a Chirascan CD spectropolarimeter (Applied Photophysics, UK) in absorbance mode equipped with quantum temperature controller. The melting of the double stranded DNA to single stranded DNA was observed with significant hyperchromicity of absorbance at 260 nm. The melting temperature (T_m) was determined from the derivative plot (dA_{260}/dT *vs* T) of the melting profile.[46]

5.2.5.3. Circular dichroism studies. The Circular Dichroism (CD) spectroscopy was studied using Chirascan CD spectropolarimeter (Applied Photophysics, UK) at 25 ^oC. CD spectra of CT-DNA (160 μM) in absence and presence of complexes (300 μM) were obtained in the

wavelength range of 240–400 nm in 10 mM Tris-HCl buffer (pH 8.0) using quartz cell with 2 mm path length.[46]

5.2.6. DNA cleavage experiments.

For DNA cleavage experiments, 300 ng supercoiled (SC) pUC19 DNA was used and all experiments were carried out in 50 mM Tris-HCl buffer (pH 8.0) containing 10% DMF. The photo-induced DNA cleavage experiments were also carried out in 10 mM phosphate buffer (pH 7.8) containing 1 % DMF or 10 mM Tris-HCl buffer (pH 8.0) containing 1% DMF.

5.2.6.1. Chemical-induced DNA cleavage. For chemical nuclease studies, the reactions were performed in the dark using hydrogen peroxide (0.5 mM) as the oxidising agent in absence and presence of complexes (1 – 500 μM). The solutions were incubated at 37 ^{o}C for 3 h and analysed for DNA cleaved products by agarose gel electrophoresis.

5.2.6.2. Photo-induced DNA cleavage. The effect of complexes (1 – 500 μM) on the cleavage of supercoiled (SC) pUC19 DNA (300 ng) was studied by agarose gel electrophoresis in 50 mM Tris HCl buffer (pH 8.0). DNA photocleavage studies were carried out under illuminated conditions using UVA source at 350 nm (Luzchem Photoreactor Model LZC-1, Ontario, Canada) fitted with 14 UVA tubes for 3 h. After photo irradiation, each sample was further incubated for 1.0 h at 37 ^{o}C and analyzed for the photo-cleaved products using gel electrophoresis. The samples after incubation were added to the loading buffer containing 0.25% bromophenol blue and 30% glycerol (2 μL) and the solution was finally loaded on 0.8% agarose gel containing 0.5 μg/mL ethidium bromide (EB). Electrophoresis was carried out for 1.0 h at 90 V in TAE (Tris–acetate EDTA) buffer. DNA cleavage was indicated by the decrease in the supercoiled pUC19 DNA (Form I) and subsequently the formation of nicked circular DNA (Form II) and linearised DNA (Form III). Bands were visualised by UV light (302nm) and photographed. The extent of SC DNA cleavage was measured from the intensities of the bands using UVP (Gel Doc It^2) Gel Documentation System. Due corrections were made for the low level of nicked circular (NC) form of DNA present in the original SC DNA sample and for the low affinity of EB binding to SC compared to NC and linear forms of DNA.[47] The percentage of net DNA cleavage was calculated by the following equation:

$$\text{Net DNA cleavage \%} = \frac{\text{Form IIs} + 2 \times \text{Form IIIs}}{\text{Form Is} + \text{Form IIs} + 2 \times \text{Form IIIs}} - \frac{\text{Form IIc} + 2 \times \text{Form IIIc}}{\text{Form Ic} + \text{Form IIc} + 2 \times \text{Form IIIc}} \qquad \textbf{Eq.2}$$

The subscripts "s" and "c" refers to the sample and control respectively.[48] Appropriate DNA controls were taken to calculate the net DNA cleavage percent. The observed error in measuring the band intensities ranged between 3% - 6%. The mechanistic studies were done using different additives (sodium azide, L-histidine, KI and D-mannitol, each 0.5 mM) prior to the addition of the complex.

5.2.7. Protein binding and cleavage experiments.

5.2.7.1. Bovine serum albumin (BSA) interaction studies. The protein binding study was performed by tryptophan fluorescence quenching experiments using BSA (2 μM) as a substrate in 10 mM Tris-HCl buffer (pH 8.0) using Fluoromax 4P spectrofluorimeter (Horiba Jobin Mayer, USA). The quenching of the emission intensity of tryptophan residues of BSA at 344 nm (excitation at 295 nm) was monitored with increasing complex concentration [0 – 20 μM in 10 mM Tris-HCl buffer (pH 8.0) containing 1% DMF].[49] Stern-Volmer plots and Scatchard analysis were done using corrected fluorescence data taking into account the effect of dilution. Linear fit of the data using the Stern-Volmer
equation,

$$\frac{F_0}{F} = 1 + K_{SV}[Q] \qquad \textbf{Eq.3}$$

and the Scatchard equation,

$$\log\left[\frac{F_0 - F}{F}\right] = \log K_{BSA} + n \log[Q] \qquad \textbf{Eq.4}$$

where F_0 and F are the emission intensity of BSA in absence and in presence of the quencher (complexes) concentration [Q] respectively, gave the Stern-Volmer quenching constant (K_{SV}), the binding constant (K_{BSA}) and the number of binding sites (n).[45]

5.2.7.2. BSA photo-induced cleavage studies. Freshly prepared solution of BSA in 10 mM Tris-HCl buffer (pH 8.0) was used for photochemical protein cleavage studies. BSA (5 μM) solution in absence and presence of complexes [1 – 500 μM in 10 mM Tris-HCl buffer (pH 8.0) containing 1% DMF] was photo-irradiated using UVA source at 350 nm (Luzchem Photoreactor Model LZC-1, Ontario, Canada) fitted with 14 UVA tubes (84 W) for 90 min. The irradiated

samples (20 μL) were dissolved in loading buffer (20 μL) containing SDS (7% w/v), glycerol (4% w/v), Tris-HCl buffer (50 mM, pH 6.8), mercaptoethanol (2% v/v) and bromophenol blue (0.01% w/v). The samples were then heat denatured at 100 ^{o}C for 5 min and loaded onto a 12% SDS PAGE separating gel. The gel electrophoresis was done at 60 V until the dye passed into the separating gel from the stacking (5 %) gel, and then the voltage was increased to 120 V. The gels were run for 2 h, stained with Coomassie Brilliant Blue R-250 solution (acetic acid: methanol: water = 1 : 5 : 4 v/v) and destained with water:methanol:acetic acid mixture (5 : 4 : 1 *v/v*). The gels after destaining, were photographed by using the UVP (Gel Doc It^2) Gel Documentation System. Molecular weight markers were used in each gel to calibrate the molecular weight of BSA.[49] We also studied the BSA cleavage activity in dark as well as in presence of UV-A light (84 W) for all the complexes with a molar ratio of BSA to complex 1:20.

5.2.8. Cytotoxicity Studies

5.2.8.1. MTT assay. Human cervical cells HeLa were obtained from National Centre of Cell Science (NCCS), Pune, India, and were maintained in minimal essential medium supplemented with 10% fetal bovine serum, penicillin-streptomycin solution and incubated at 37 °C in 5% CO_2 and 95% humidified incubator. HeLa cells were harvested from maintenance cultures in logarithmic phase, after counting in a hemocytometer using trypan blue solution. The cell concentration was adjusted to 5x10^4 cells/ml and the cells were plated in a 96 well flat bottom culture plate and incubated for 72 h with various concentrations of the test complexes which were dissolved in a 10% (v/v) DMF solution. The effect of the drugs on the cancer cell viability was studied using MTT dye reduction assay by measuring the optical density at 595 nm using micro-plate reader spectrophotometer (Perkin-Elmer 2030).[50] A 10% (v/v) DMF solution which was used to dissolve the drugs was used in the control group treatment.

5.2.8.2. Nuclear Staining. Nuclear staining using DAPI stain was performed according to the method previously described.[51] Briefly, HeLa cells either treated or untreated with test compounds were smeared on a clean glass slide, cells were fixed with 3.7% formaldehyde for 15 min, permeabilised with 0.1% Triton X-100 and stained with 1 μg/ml DAPI for 5 min at 37 °C. 10% DMF solution which was used to dissolve the drugs was also used in control group treatment. The cells were then washed with PBS and examined by fluorescence microscopy

(Olympus IX 71) to ascertain any condensation or fragmentation of the nuclei indicating cells undergoing apoptosis.

5.3. RESULT AND DISSCUSSION

5.3.1. Synthesis. Eight dioxidovanadium(V) complexes $[\{V^{V}O_2L^{1\text{-}6}\}A(H_2O)_n]_{\infty}$ (**1**–**8**) have been prepared (**Scheme 5.1**) in the present study by taking six different aroyl hydrazones as ligands, with varying substitution in their hydrazone moieties, in order to observe their influence on the pharmacological activities of the complexes. Reactions of the selected aroylhydrazones with $VO(acac)_2$ along with alkali metal carbonate proceed in refluxing ethanol / water afforded yellow or orange products in good yields. These compounds are highly soluble in protic, *viz*. water, ethanol and methanol, as well as in aprotic solvents, *viz*. CH_3CN, DMF and DMSO. Alternatively, these complexes can also be synthesised using acetonitrile / water as solvent.

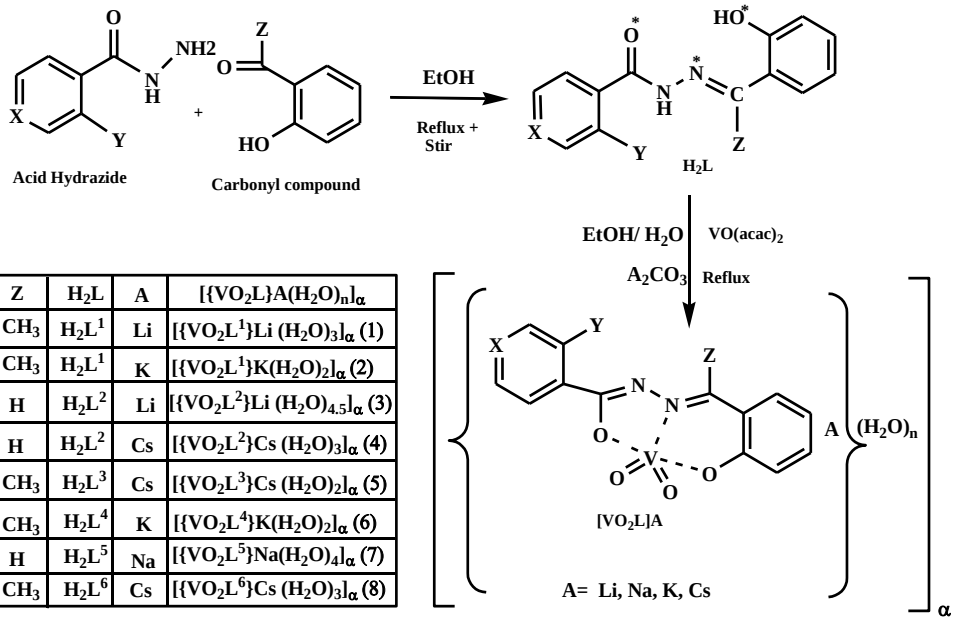

X	Y	Z	H_2L	A	$[\{VO_2L\}A(H_2O)_n]_{\alpha}$
C	OH	CH_3	H_2L^1	Li	$[\{VO_2L^1\}Li(H_2O)_3]_{\alpha}$ (1)
C	OH	CH_3	H_2L^1	K	$[\{VO_2L^1\}K(H_2O)_2]_{\alpha}$ (2)
C	OH	H	H_2L^2	Li	$[\{VO_2L^2\}Li(H_2O)_{4.5}]_{\alpha}$ (3)
C	OH	H	H_2L^2	Cs	$[\{VO_2L^2\}Cs(H_2O)_3]_{\alpha}$ (4)
C	H	CH_3	H_2L^3	Cs	$[\{VO_2L^3\}Cs(H_2O)_2]_{\alpha}$ (5)
N	H	CH_3	H_2L^4	K	$[\{VO_2L^4\}K(H_2O)_2]_{\alpha}$ (6)
N	H	H	H_2L^5	Na	$[\{VO_2L^5\}Na(H_2O)_4]_{\alpha}$ (7)
C	NH_2	CH_3	H_2L^6	Cs	$[\{VO_2L^6\}Cs(H_2O)_3]_{\alpha}$ (8)

Scheme 5.1. Schematic diagram of various pathways through which the dioxido vanadium(V) complexes $[\{V^{V}O_2L^{1\text{-}6}\}A(H_2O)_n]_{\infty}$ (**1**–**8**) were synthesised.

5.3.2. Spectral Characteristics

The spectral (IR, UV-Vis and NMR) data of all the ligands, H_2L^{1-6} and their corresponding dioxido vanadium(V) complexes, **1–8**, are given in the Experimental Section.

5.3.2.1. IR Spectroscopy. The infrared spectra of all the complexes, display a broad band in the range 3590–3400 cm^{-1}, due to the O–H stretch of the coordinated water molecules which form extensive hydrogen bonding interactions. The disappearance of characteristic bands due to –NH and –C=O in the ligand spectra, and the appearance of new bands in the range 1261–1223 cm^{-1} in the complexes indicates the enolisation of these two groups forming a –N=C–O bond sequence. The strong and sharp peak displayed by the complexes in the range 1614–1597 cm^{-1} is likely to be associated with the –C=N–N=C– moiety.[35a,b,52] The presence of two strong bands in the range 947–897 cm^{-1} is assigned to V=O stretching,[26h,i] which clearly indicates the dioxido nature of the complexes. A representative spectrum of complex **6** is shown in **Figure 5.1**.

5.3.2.2. UV Spectroscopy. The electronic spectra of the complexes **1–8** were recorded in DMF at 25 μM concentration, and are quite similar for all eight complexes. A representative spectrum of complex **7** is shown in **Figure 5.2.** The strong absorptions are observed in the wavelength range 410–390 nm are assignable to the ligand-to-metal charge transfer transitions whereas the other bands in the higher energy region (365–258 nm) are likely to be due to ligand centred transitions.[35a,b]

5.3.2.3. NMR Spectroscopy. The ^{1}H and ^{13}C NMR data of the free ligands (H_2L^{1-6}) and corresponding dioxido vanadium(V) complexes (**1–8**) were recorded using DMSO-d_6 and the data are given in the Experimental Section. The spectra of all the ligands exhibit resonances in the range δ = 13.55–11.79 ppm due to phenyl–OH and δ = 11.72–11.09 ppm due to –NH, which disappear in the spectra of the complexes confirming deprotonation and complexation of the ligands. The presence of resonances in the range δ = 12.58–12.21 ppm in complexes **1–4** is due to the uncoordinated –OH present in the hydrazide part of the ligand. Complexes **3**, **4** and **7** possess a resonance in the range δ = 9.11–9.05 ppm, and complexes **1**, **2**, **5**, **6** and **8** display a singlet in the range δ = 2.89–2.73 ppm due to –CH and $–CH_3$ group, respectively. All the

aromatic protons of the complexes are clearly observed in the expected region, δ = 8.71–6.78 ppm.[35a,b] A representative ^{1}H NMR spectrum of complex **6** is shown in **Figure 5.3.**

The ^{51}V NMR spectra of **1**–**8** each displays a singlet in the range δ = –542.22 to –531.87 ppm. These chemical shifts are usual for complexes containing the dioxido vanadium(V) complexes.[53]

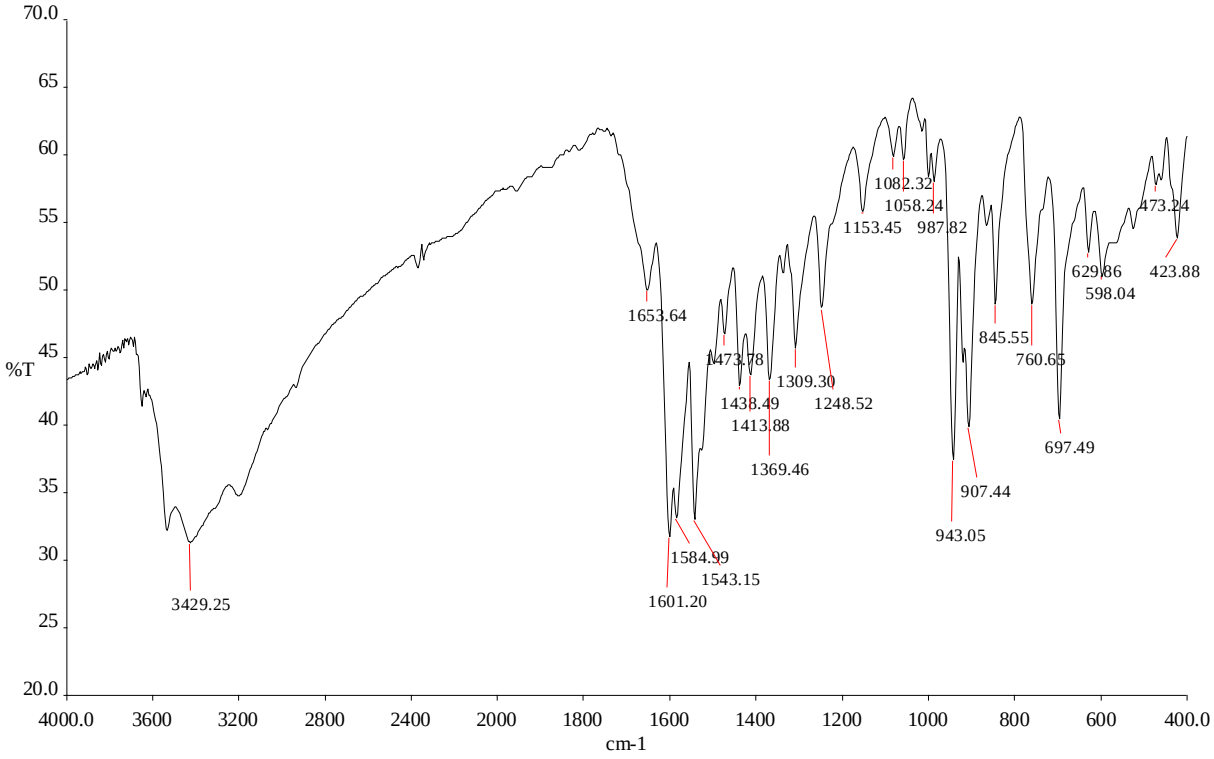

Figure 5.1. FTIR spectra of $[\{VO_2L^4\}K(H_2O)_2]_\infty$ **(6)**

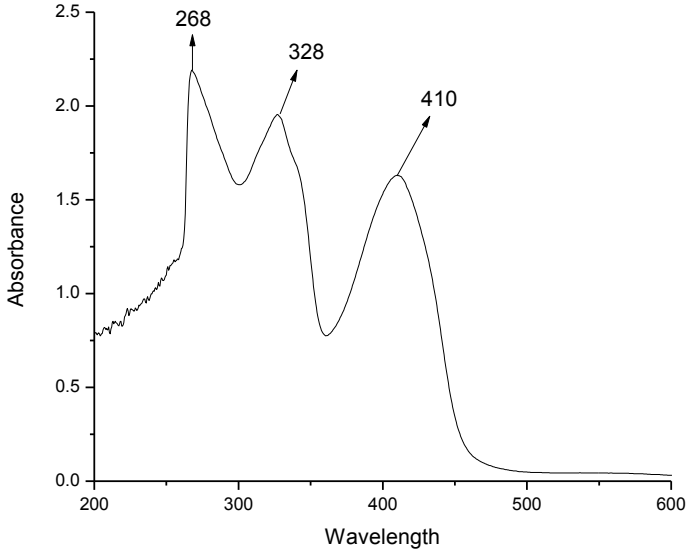

Figure 5.2. Electronic absorption spectra of $[\{VO_2L^5\}Na(H_2O)_4]_\infty$ **(7)** in DMF.

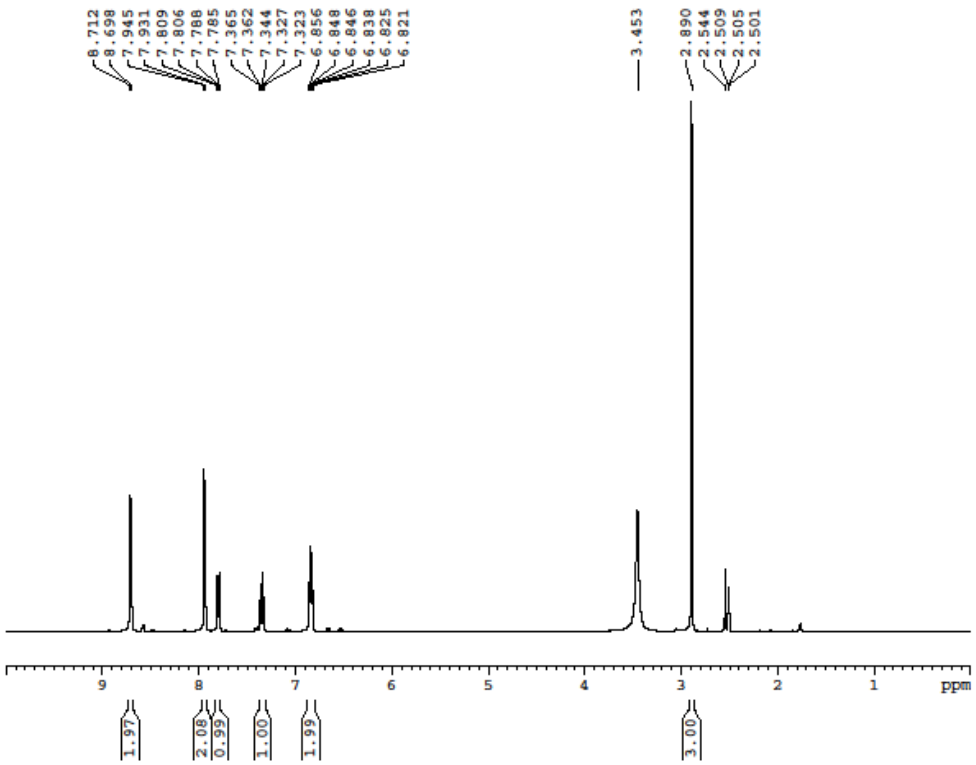

Figure 5.3. ^{1}H NMR spectra of $[\{VO_2L^4\}K(H_2O)_2]_\infty$ **(6)** in DMSO-d_6.

5.3.3. Description of the X-ray structure of complexes. The crystal and molecular structures of **3**, **5**–**7** have been determined and reveal a wide variety of structural motifs dependent in the main on the type of cation and presence of water (coordinated or lattice). The common feature of the structures is the presence of five-coordinate vanadium within NO_4 donor sets which define coordination geometries between the extremes of square pyramidal and trigonal bipyramidal.

The asymmetric unit of **3** comprises two complex anions, two Li^+ cations and nine water molecules, **Figure 5.4**. selected geometric parameters are given in the caption. Seven of the water molecules coordinate to Li^+ cations. The molecular structures of the anions are quite similar as seen from the overlay diagram (**Figure 5.5**) and feature five-coordinate vanadium atoms, being coordinated by a dinegative, tridentate ligand and two oxido-O atoms. The status of the Schiff base ligand as 2-hydroxy-*N*-(2-oxidobenzylidene)benzenecarbohydrazonate, *i.e.* an azo ligand, is confirmed by the C=N bond lengths, **Figure 5.4**. Based on τ values of 0.51 (V1-containing anion) and 0.47 (V2), the resulting NO_4 donor set defines a geometry intermediate between square pyramidal (ideal value of $\tau = 0.0$) and trigonal bipyramidal ($\tau = 1.0$).[54] The five- and six-membered chelate rings are practically planar with r.m.s. deviations of the atoms comprising these being 0.013 Å (0.008) and 0.031 Å (0.036), respectively; values for the V2-containg anion are given in parenthesis. Co-planarity between the five-membered ring and attached hydroxyphenyl ring (dihedral angles = 3.48(8) and 1.95(8)º, respectively) is ensured by an intramolecular O–H...N hydrogen bond (**Table 5.2**). This planarity extends throughout the anion as seen in the dihedral angles between the terminal rings of 5.37(9) and 2.69(9)º, respectively. According to a search of the Cambridge Structural Database (CSD),[55] the specific anion in **3** has been characterised as a variety of vanadium salts and adopt very similar molecular conformations.[56]

The Li^+ cations are bridged by a water molecule and each of their tetrahedral coordination geometries is completed by three additional water molecules. The components of the crystal structure are connected into supramolecular layers in the *ab*-plane by an extensive network of O–H...O hydrogen bonds involving all but the hydroxyl-O atoms (**Figure 5.6a**); geometric data defining the intermolecular interactions for **3**, **5-7** are collated in **Table 5.2**. The Schiff base ligands project to either side of the layers and associate *via* significant C−H...O(hydroxyl) hydrogen bonds to consolidate the three-dimensional crystal packing (**Table 5.2** and **Figure 5.6b**).

The asymmetric unit of **5** comprises two Cs^+ cations, two complex anions and two aqua ligands, **Figure 5.7**. By contrast to the other structures described herein, both the five- and six-membered rings deviate significantly from planarity, with the former adopting an envelope conformation with the V1 or V2 atom being the flap atom. The six-membered rings adopt half-chair conformations with the V1 atom lying 0.566(3) Å above the plane of the remaining five atoms comprising the chelate ring (r.m.s. deviation = 0.0461 Å); the corresponding values for the V2-containing anion are 0.840(3) and 0.0487 Å, respectively. The two anions adopt distinct conformations (**Figure 5.8**) with the differences best reflected in the dihedral angles between the five-membered and attached phenyl ring of 8.34(13) and 18.54(13)°, respectively. The values of τ compute to 0.04 and 0.21, consistent with descriptions of the coordination geometry being based on a square pyramid.[54] The same anion as found in **5** has been described in the literature as its anhydrous diethylammonium salt.[57] Underscoring the flexibility of coordination modes exhibited by these Schiff base ligands, in the ammonium salt the five-membered ring is very close to planar and the six-membered ring has a half-chair conformation with the phenoxide-O atom lying above the plane of the remaining atoms.[57]

The Cs1 cation is in a highly distorted eight-coordinate environment whereas the Cs2 cation is in a seven-coordinate geometry resembling closely a square anti-prism but with one site vacant. The μ-O bridging leads to a layer in the *ab*-plane as illustrated in **Figure 5.9a**. The layers are also stabilised by an extensive network of O–H…O hydrogen bonds (**Table 5.2**) and stack along the *c*-axis with no specific interactions between them (**Figure 5.9b**).

For **6**, the asymmetric unit comprises a K^+ cation, a complex anion and two coordinated water molecules, **Figure 5.10**. The introduction of a methyl group into the backbone of the ONO-coordinating tridentate ligand of **3** introduces a change in the configuration of the six-membered chelate ring. Thus, while the five-membered ring is planar (r.m.s. deviation = 0.028 Å), the conformation of the six-membered ring is based on a screw-boat. This has the result that overall the dianion exhibits a twist as seen in the dihedral angle of 11.12(12)º between the terminal rings. The value of τ is 0.14, suggesting a coordination geometry approaching square pyramidal.[54] There are no V-containing precedents featuring this Schiff base ligand in the crystallographic literature.[55]

The cation in **6** is coordinated by the two water molecules comprising the asymmetric unit, **Figure 5.10**, and direct links between this and the anion are afforded by oxido bridges. The

oxido-O4 and phenoxide-O2 atoms also link symmetry related cations, which in turn are bridged by two water molecules with the result that the K^+ cation is eight-coordinate within an O_8 donor set (range of K−O bond lengths: 2.7176(17) to 3.107(3) Å). The coordination geometry is based on a heavily distorted square anti-prism with each face defined by two oxido- and two water-O atoms. The K−O bridging leads to a supramolecular zigzag chain oriented along the *b*-axis, **Figure 5.11**. Chains are linked into a three-dimensional architecture by water-O-H...O(phenoxide), N(pyridyl) hydrogen bonds as well as phenyl-C-H...O(oxido) and methyl-C-H...π(arene) interactions, as illustrated in **Figure 5.12**; **Table 5.2** for parameters. In this scheme, the O2w molecule does not form significant hydrogen bonding interactions, most likely as the hydrogen atoms are disordered in a pocket defined by four possible hydrogen atom acceptors, see Experimental Section and **Table 5.2**. It is noted that all four oxygen atoms in the pocket belong to a single supramolecular chain indicating that any putative hydrogen bonds formed by the O2w molecule would contribute primarily to the stability of the chain.

The asymmetric unit of **7** comprises a Na^+ cation, a complex anion, three coordinated water molecules and a water molecule of hydration, **Figure 5.13**. The anion exhibits the similar features as described for **3**. The r.m.s. deviations for the five- and six-membered chelate rings are 0.036 and 0.045 Å, respectively. A small twist is noted between the five-membered ring and attached pyridyl ring, *i.e*. 9.33(9)º, so that the ligand is no longer planar; the dihedral angle between the terminal rings is 8.42(10)º. The value of τ is computed to be 0.41, indicating a coordination geometry intermediate between square pyramidal and trigonal pyramidal.[54] There is only one precedent in the crystallographic literature[55] for a vanadium complex of the Schiff base ligand in **7**. In this single molecule structure, the charge balance is achieved by protonation at the pyridyl-N atom,[58] *i.e.* the Schiff base ligand is present as a zwitterion.

The ions in **7** are connected into a centrosymmetric four-component aggregate *via* oxido-O bridges whereby the O3 atom connects to one Na cation and the O4 atom bridges two Na cations, **Figure 5.14**. In this way, the Na cation achieves a coordination number of six based on an octahedral O_6 donor set, range of Na−O bond lengths = 2.2904(18) to 2.7277(19) Å. A supramolecular layer in the *ab*-plane is formed by O−H...O hydrogen bonds as well as an O−H...N hydrogen bond involving the non-coordinating azo-N3 atom, **Figure 5.15a** (**Table 5.2**). Layers are connected along the *c*-axis by water-O−H...N(pyridyl) hydrogen bonds, **Figure 5.15b**.

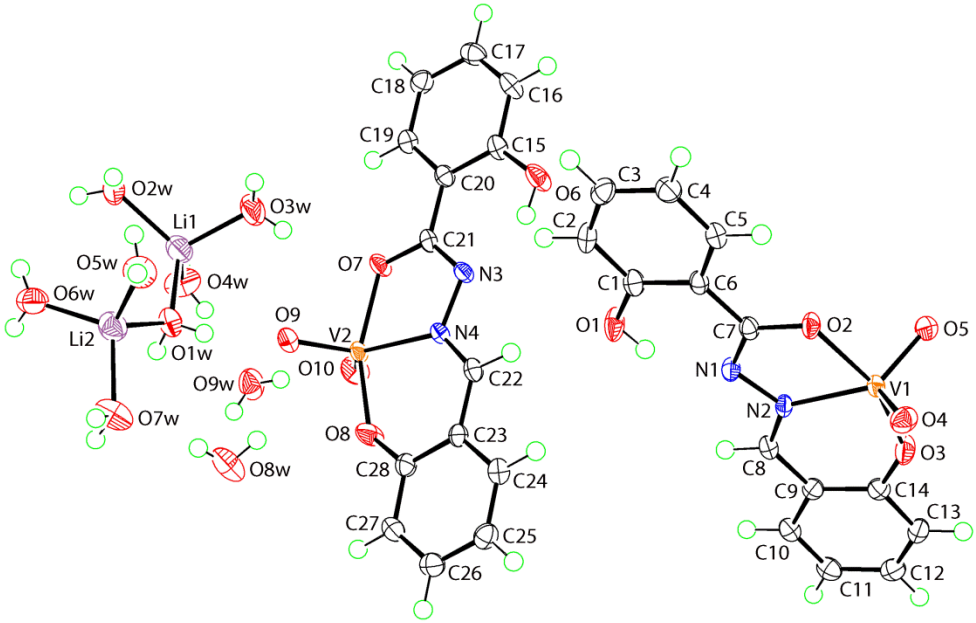

Figure 5.4. Perspective view of the components of the crystallographic asymmetric unit of $[\{VO_2L^2\}Li(H_2O)_{4.5}]_\infty$ (**3**). V1–O2 2.0028(12), V1–O3 1.9119(13), V1–O4 1.6330(13), V1–O5 1.6238(13), V1–N2 2.1121(14), N1–N2 1.3994(19), N1–C7 1.302(2), N2–C8 1.298(2), V2–O7 1.9771(12), V2–O8 1.9109(13), V2–O9 1.6284(13), V2–O10 1.6343(13), V2–N4 2.1163(14), N3–N4 1.3975(19), N3–C21 1.301(2), N4–C22 1.297(2) Å; O2–V1–O3 157.54(5), O7–V2–O8 156.95(5)º.

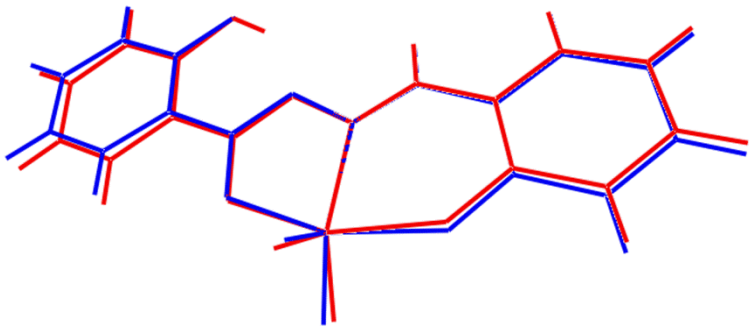

Figure 5.5. Overlay diagram of the two independent complex anions in $[\{VO_2L^2\}Li(H_2O)_{4.5}]_\infty$ (**3**). Molecules have been superimposed so that the five-membered chelate rings involving the V1 (red image) and V2 (blue image) atoms are superimposed.

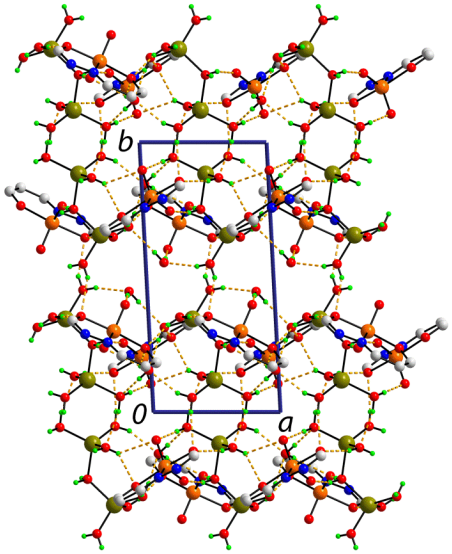

(a)

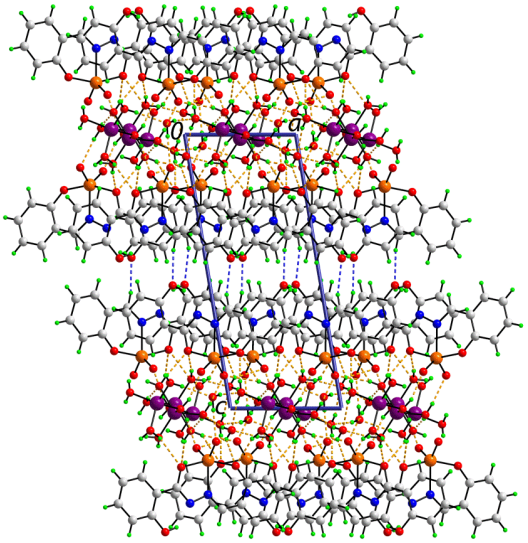

(b)

Figure 5.6. (a) A view of the supramolecular layer in the *ab*-plane in $[\{VO_2L^2\}Li(H_2O)_{4.5}]_\infty$ (**3**) sustained by an extensive network of O−H...O hydrogen bonds shown as orange dashed lines. For clarity, only the chelate rings of the anions are illustrated, and (b) Unit cell contents for **3** viewed in projection down the *b*-axis. The O−H...O and C−H...O(hydroxy) hydrogen bonds are shown as orange and blue dashed lines, respectively.

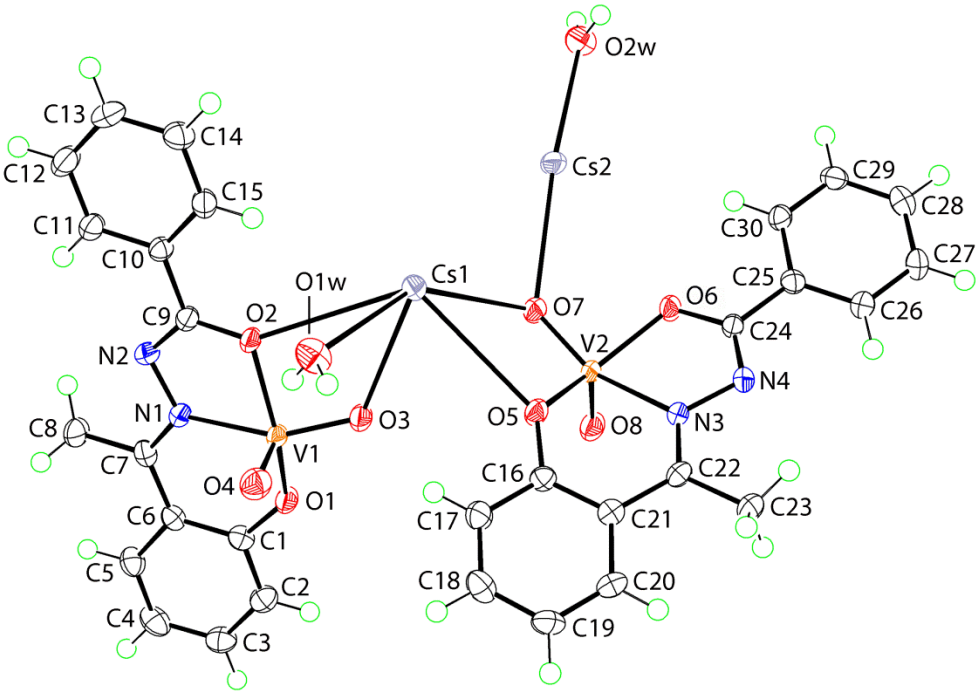

Figure 5.7. Perspective view of the components of the crystallographic asymmetric unit of $[\{VO_2L^3\}Cs(H_2O)_2]_\infty$ (**5**). Selected geometric parameters: V1–O1 1.892(2), V1–O2 1.9656(19), V1–O3 1.6352(19), V1–O4 1.634(2), V1–N1 2.149(2), N1–N2 1.399(3), N1–C7 1.305(4), N2–C9 1.298(4), V2–O5 1.883(2), V2–O6 1.9631(19), V2–O7 1.6534(19), V2–O8 1.618(2), V2–N3 2.162(2), N3–N4 1.402(3), N3–C22 1.299(3), N4–C24 1.295(4), O3…Cs1 2.923(2), O4…Cs1^{i} 3.302(2), O7…Cs1 3.019(2), O3…Cs2^{i} 3.014(2), O7…Cs2 2.9900(19), O8 …Cs2^{i} 3.292(2) and O8…Cs2^{ii} 3.473(2) Å. Symmetry operation *i*: *x*, 1+*y*, *z*, and *ii*: -*x*, -*y*, 1-*z*.

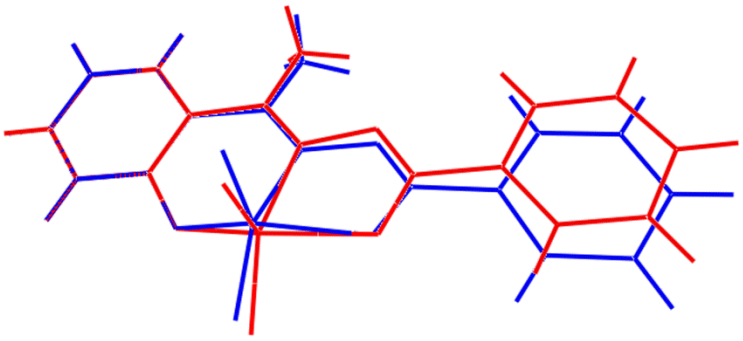

Figure 5.8. Overlay diagram of the two independent complex anions in $[\{VO_2L^3\}Cs(H_2O)_2]_\infty$ (**5**). Molecules have been superimposed so that the C1-C6 ring (red image) and C16-C21 ring (blue image) are superimposed.

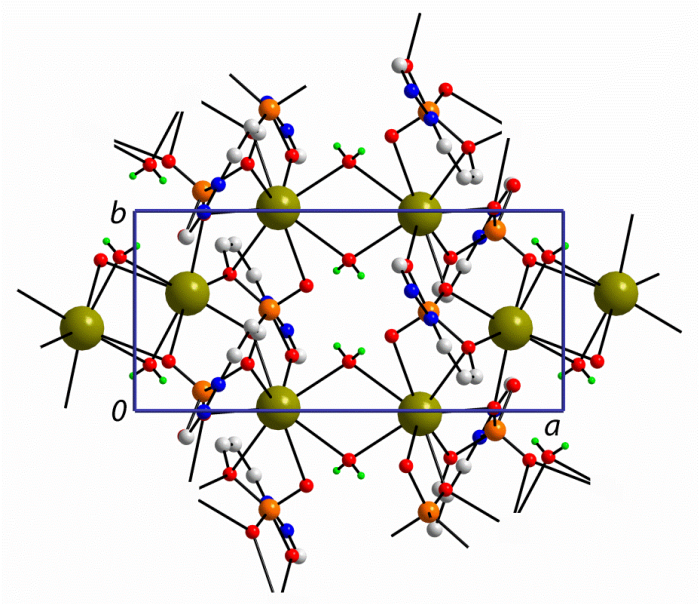

(a)

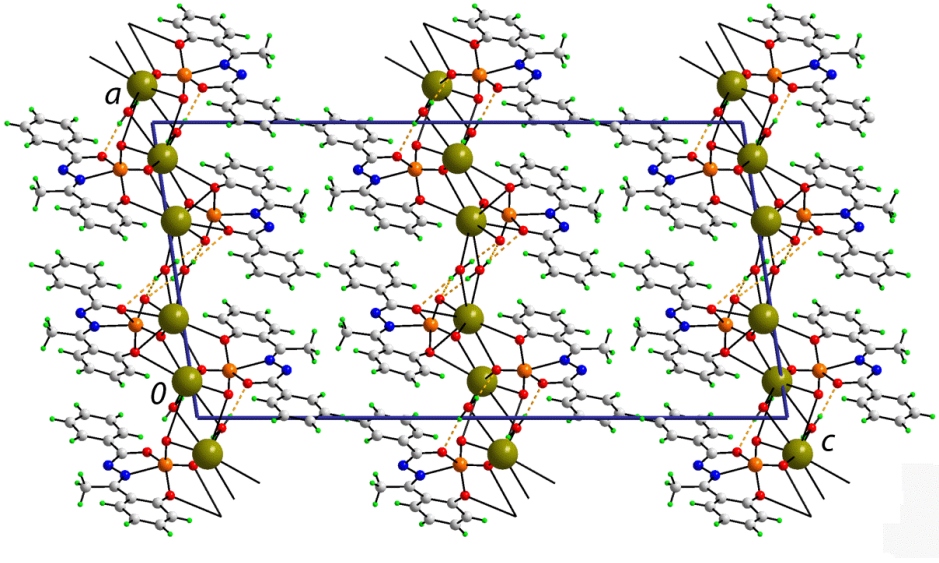

(b)

Figure 5.9. (a) Crystal packing in $[\{VO_2L^3\}Cs(H_2O)_2]_\infty$ (**5**): Layer in the *ab*-plane mediated by μ-O bridges. For clarity, only the chelate rings of the anions are illustrated, and (b) Unit cell contents for **5** viewed in projection down the *b*-axis. The O−H...O hydrogen bonds are shown as orange dashed lines.

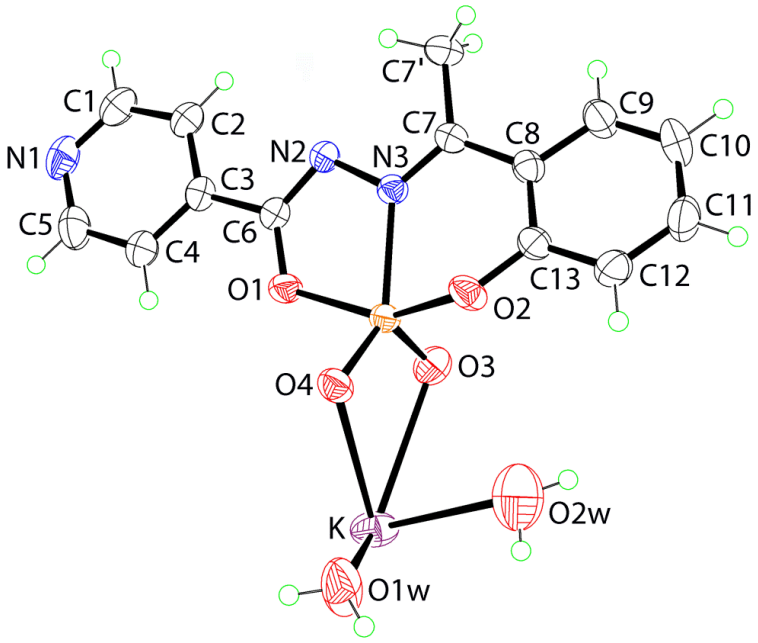

Figure 5.10. Perspective view of the components of the crystallographic asymmetric unit of $[\{VO_2L^4\}K(H_2O)_2]_\infty$ (**6**). Selected geometric parameters: V1–O1 1.9668(16), V1–O2 1.8926(16), V1–O3 1.6174(17), V1–O4 1.6350(16), V1–N3 2.1552(19), N2–N3 1.409(2), N2–C6 1.291(3), N3–C7 1.306(3), O3…K 2.9383(19), O4…K 2.8330(18) and $O4^i$…K 2.7178(17) Å. Symmetry operation *i*: ½-*x*, -½+*y*, *z*.

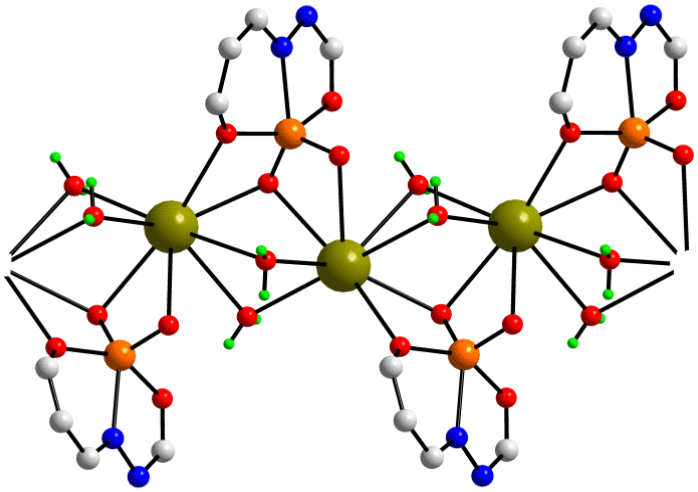

Figure 5.11. Crystal packing in $[\{VO_2L^4\}K(H_2O)_2]_\infty$ (**6**): Zigzag chain along the *b*-axis mediated by μ-O bridging. For clarity, only the chelate rings of the anions are illustrated.

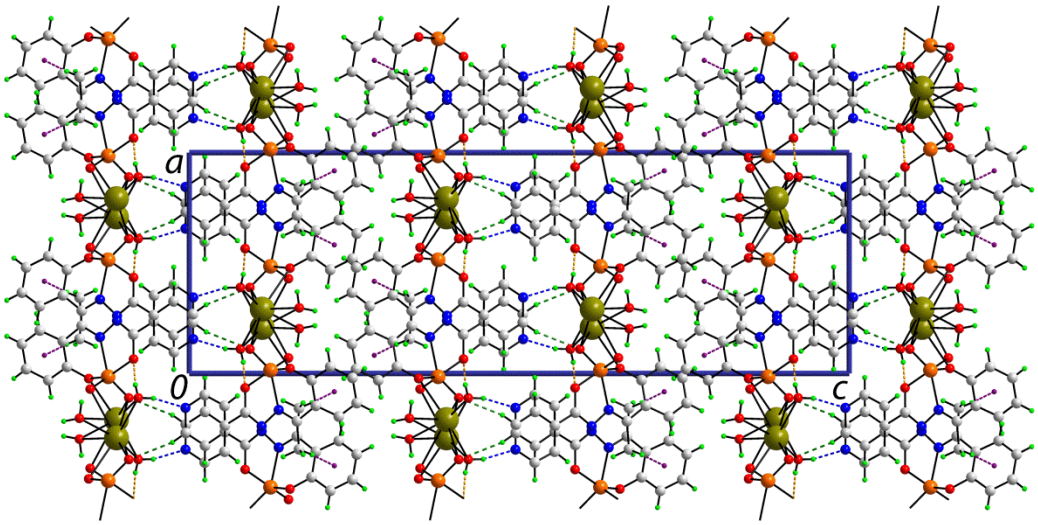

Figure 5.12. Crystal packing in $[\{VO_2L^4\}K(H_2O)_2]_\infty$ (**6**): View in projection down the *b*-axis showing the unit cell contents. The O−H...O, O−H...N, C−H...O and C−H...π interactions are shown as orange, blue, green and purple dashed lines, respectively.

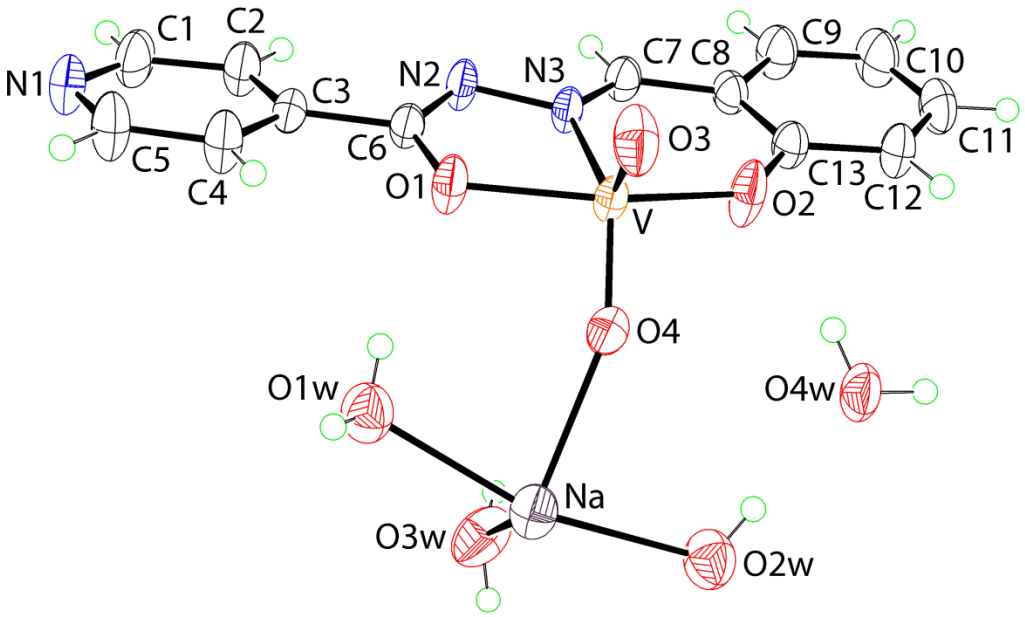

Figure 5.13. Perspective view of the components of the crystallographic asymmetric unit of $[\{VO_2L^5\}Na(H_2O)_4]_\infty$ (**7**). Selected geometric parameters: V1–O1 1.9884(12), V1–O2 1.9027(13), V1–O3 1.6183(14), V1–O4 1.6263(14), V1–N3 2.1236(14), N2–N3 1.4067(18), N2–C6 1.291(2), N3–C7 1.293(2), O4…Na 2.3889(16), O3…Na^i 2.7274(19) and O4…Na^i 2.5576(18) Å. Symmetry operation *i*: 1-*x*, -*y*, 2-*z*.

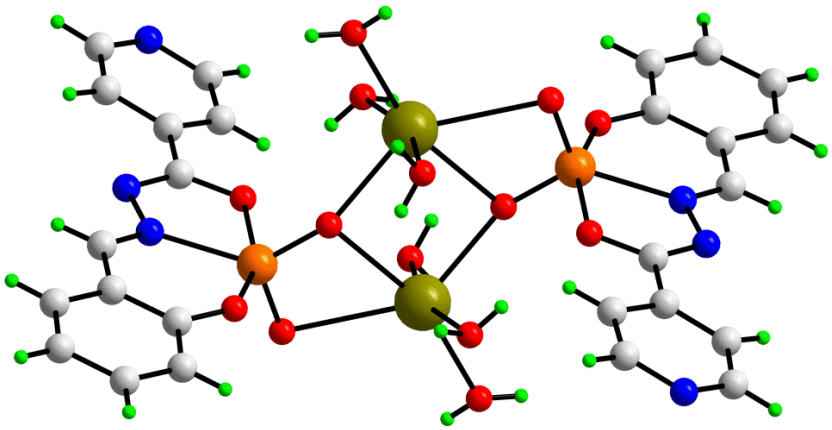

Figure 5.14. Crystal packing in $[\{VO_2L^5\}Na(H_2O)_4]_\infty$ (**7**): Centrosymmetric four-ion aggregate mediated by μ-O bridging.

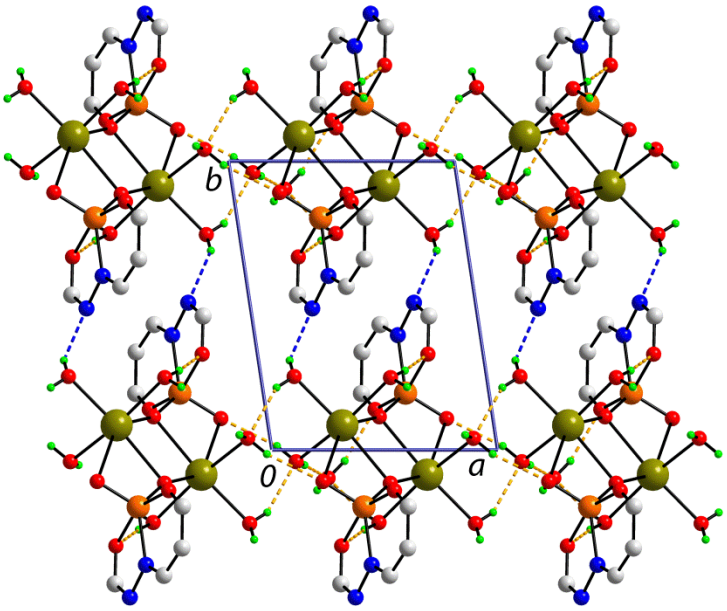

(a)

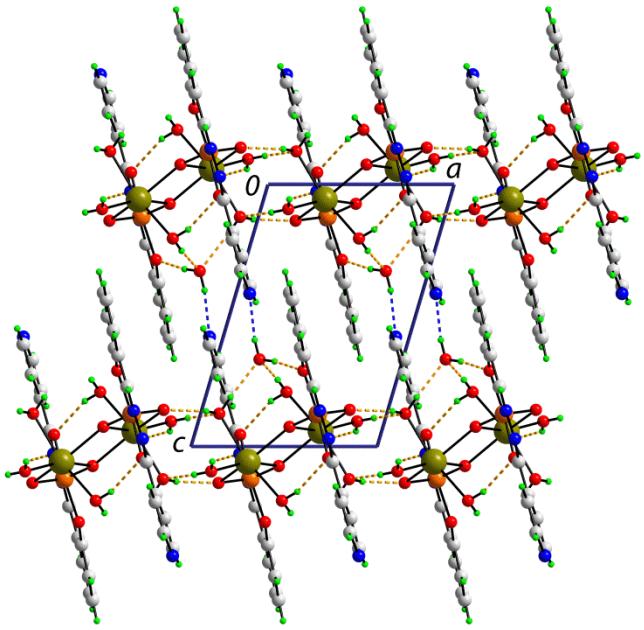

(b)

Figure 5.15. Crystal packing in $[\{VO_2L^5\}Na(H_2O)_4]_\infty$ (**7**): (a) Layer in the *ab*-plane sustained by O−H...O and O−H...N hydrogen bonds shown as orange and blue dashed lines, respectively. For clarity, only the chelate rings of the anions are illustrated, and (b) Unit cell contents viewed in projection down the *b*-axis.

5.3.4. DNA binding studies

5.3.4.1. Absorption spectroscopic studies. DNA binding is an important parameter for chemical- and photo-induced DNA cleavage activity of the metal complexes, therefore the binding affinity of the complexes **1**–**8** to CT-DNA was studied using various spectral techniques. UV-Vis titration experiments were carried out to determine the equilibrium binding constant (K_b) of the complexes to CT-DNA (**Table 5.3**). The electronic absorption spectra of **6** and **7** are shown in **Figure 5.16**. Binding of complexes to DNA through intercalation generally leads to hypochromism and bathochromism of the absorption band. This shift is observed due to the strong stacking interaction between the aromatic chromophore of the ligand and the base pairs of the DNA. Minor groove binding of the complexes to DNA results in hyperchromism in absorption intensity, resulting in the unwinding of the DNA double helix as well as its unstacking and concomitant exposure of the bases.[46] Therefore the extent of hypochromism or hyperchromism observed provides a measure of the strength of intercalative binding or minor groove binding of the complexes. The UV-Vis spectra of the complexes in the absence and presence of CT-DNA (at a constant complex concentration of 25 μM) exhibited a hypochromic shift around ~260 nm (**Figure 5.16**), which indicates that there is an interaction/binding between the complexes and CT-DNA.

In order to quantify the binding affinity of the interaction between CT-DNA and each of **1–8**, the binding constant (K_b) was calculated using Eq. 1 (Experimental Section). The K_b values were reported in **Table 5.3**. Complexes **6** and **7** showed higher K_b values among all the complexes, *i.e.* 3.34×10^4 and 6.88×10^4 M^{-1}, respectively. The binding propensities of ligands to CT-DNA were also estimated. All the ligands showed DNA binding affinity yielding K_b values ~10^3 M^{-1} (**Table 5.4**).

Table 5.3. Thermodynamic data for CT-DNA binding with $[\{V^{V}O_2L^{1-6}\}A(H_2O)_n]_{\infty}$ (1–8)

Complex	Binding Constant (K_b) [a] (M^{-1})	ΔT_m [b] (^oC)
1	1.23×10^4	0.75
2	5.5×10^3	1.30
3	1.67×10^4	1.63
4	2.41×10^4	1.31
5	7.6×10^3	1.15
6	3.34×10^4	1.95
7	6.88×10^4	2.09
8	1.11×10^4	1.03

[a]DNA binding constant by UV-vis spectral method. [b] Change in the melting temperature of CT- DNA

Table 5.4. Binding Constant (K_b) values for the interaction of CT-DNA with ligands

Complex	Binding Constant (K_b) [a] (M^{-1})
$\mathbf{H_2L^1}$	1.29×10^3
$\mathbf{H_2L^2}$	7.74×10^3
$\mathbf{H_2L^3}$	8.79×10^3
$\mathbf{H_2L^4}$	3.82×10^3
$\mathbf{H_2L^5}$	1.09×10^3
$\mathbf{H_2L^6}$	4.57×10^3

[a]DNA binding constant by UV-vis spectral method.

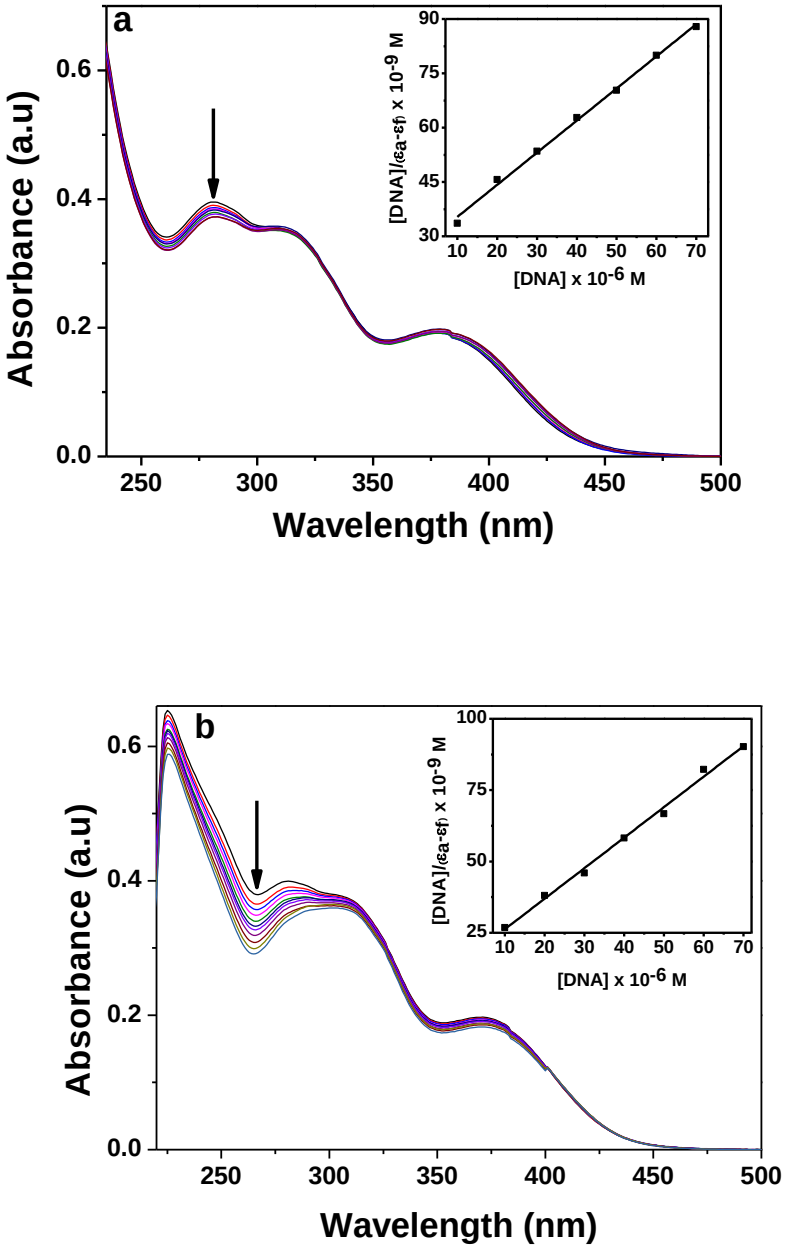

Figure 5.16. Electronic absorption spectra of **6** (a) and **7** (b) (25 μM each) upon the titration of CT-DNA (0 – 100 μM) in 10 mM Tris-HCl buffer (pH 8.0) containing 10% DMF. Arrow shows the changes in absorbance with respect to an increase in the CT-DNA concentration. The inset shows the linear fit of [DNA]/(ε_a - ε_f) vs [DNA] and binding constant (K_b) was calculated using Eq.1.

5.3.4.2. Thermal denaturation studies. To understand the nature of interaction between CT-DNA and these complexes, thermal denaturation experiments were performed.[46] The melting temperature of CT-DNA (T_m) increased very slightly upon interaction with complexes **1**-**8** (**Table 5.3**, **Figure 5.17**). The shift of DNA melting temperature (ΔT_m) for the interaction between CT-DNA and complexes **6** and **7** was greater among eight synthesised dioxido vanadium complexes i.e ~ 2 ^{0}C. The low ΔT_m values for **1**-**8** suggests groove binding of the complexes to CT-DNA rather than an intercalative mode of binding to DNA which usually gives a large positive ΔT_m value.[59,60]

5.3.4.3. Circular dichroism studies. The conformational changes in CT-DNA due to interaction with the complexes were monitored using circular dichroism (CD) spectroscopy.[61] The B-conformation of CT-DNA shows two conservative CD bands in the UV region, a positive band at 275 nm due to base stacking and a negative band at 245 nm due to right handed helicity.[61] Groove binding and electrostatic interaction of small molecules shows less or no perturbation on the base stacking and helicity bands whereas an intercalation mode can induce intensity changes of both bands, thus modulating the right handed B-conformation of DNA.[61] The CD spectra of CT-DNA (160 μM) in the presence of the complexes showed very marginal changes, with a slight increase in the negative ellipticity at 245 nm for all the complexes except for **8** which exhibited a slight decrease in negative ellipticity. (**Figure 5.18**). The positive band at 275 nm did not show any significant change in intensity. The results of CD spectra indicate that there is an interaction between complexes with CT-DNA.

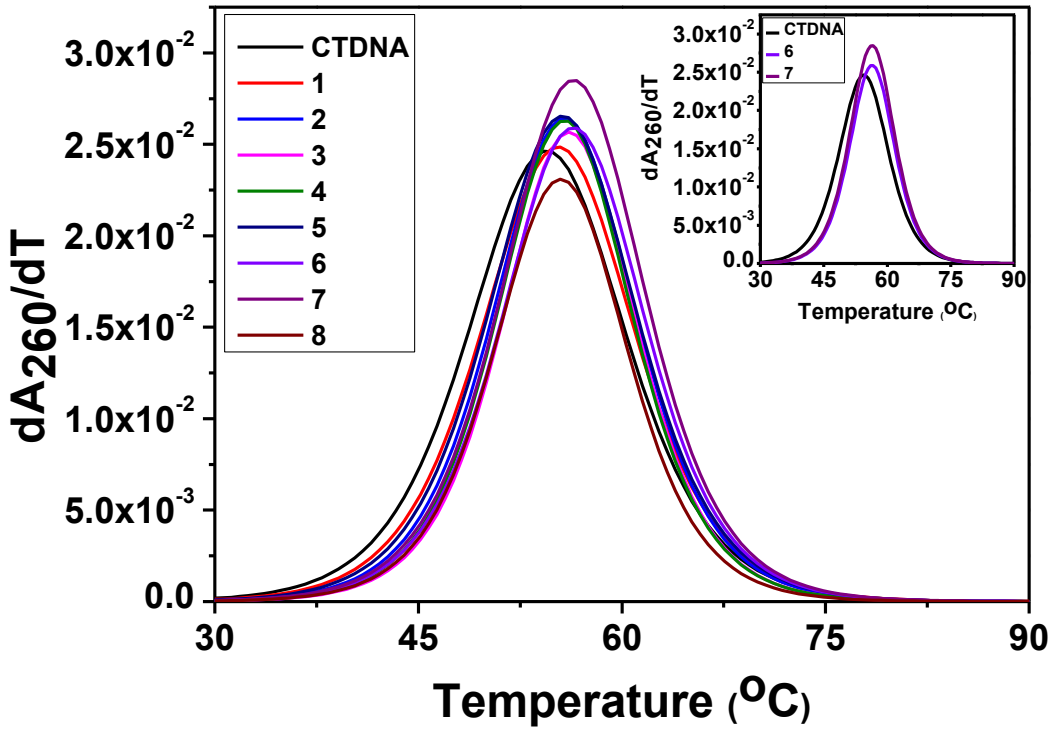

Figure 5.17. Derivative plot of thermal denaturation of CT-DNA (160 μM) in absence and presence of **1**–**8** (100 μM). The experiment was done in 10 mM Tris-HCl buffer (pH 8.0) containing 10% DMF. Inset shows the thermal denaturation derivate plot for **6** and **7** which showed ~ 2 ^{o}C shift in T_m as compared to CT-DNA.

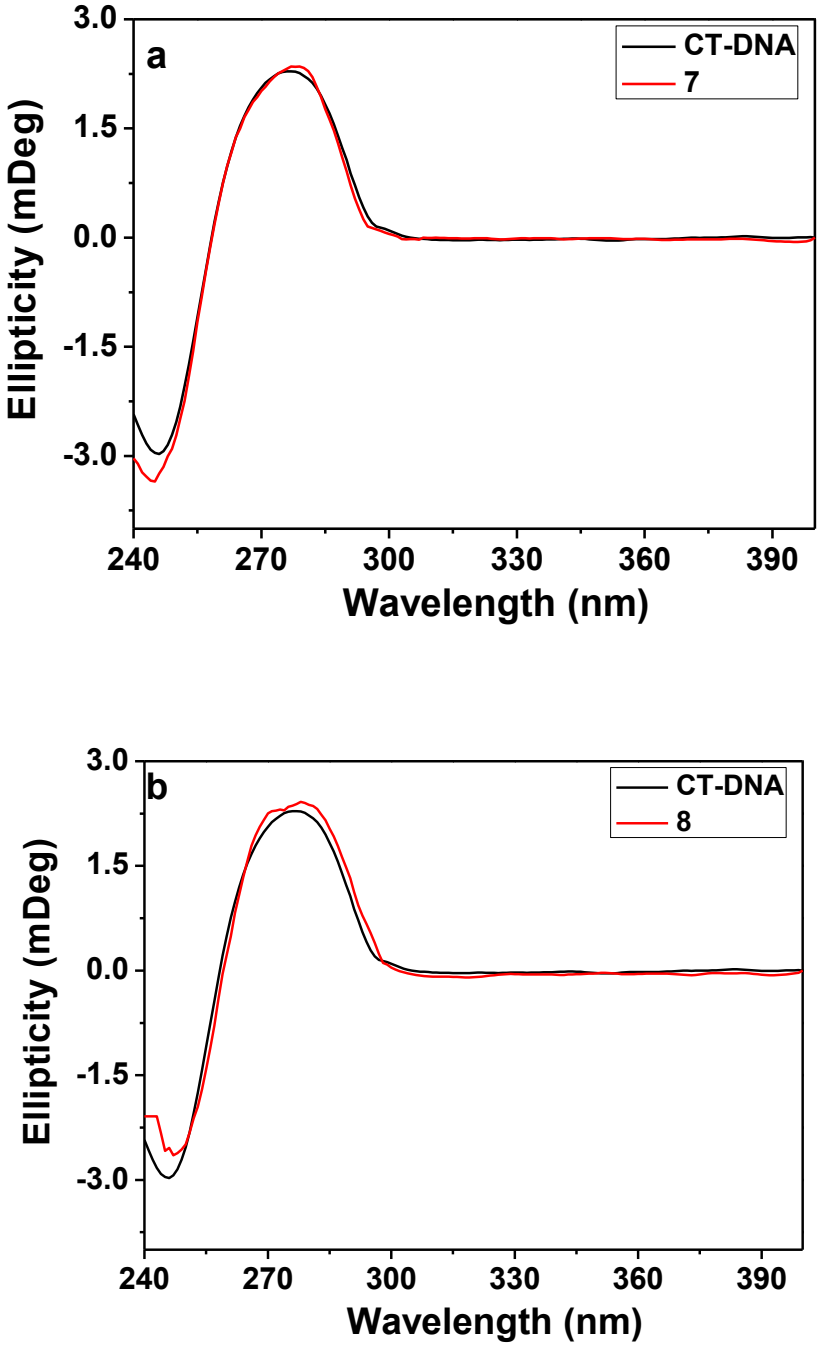

Figure 5.18. Circular dichroism spectra of CT-DNA (160 μM) in the presence and absence of **7 (**a) and **8** (b) in 10 mM Tris-HCl buffer (pH 8.0). The path length of the cuvette was 2 mm.

5.3.5. DNA cleavage studies.

5.3.5.1. Chemical-induced DNA cleavage. The cleavage of supercoiled (SC) pUC19 DNA (300ng) by **1**–**8** (1–500 μM) in the dark using hydrogen peroxide as the oxidising agent was studied. The complexes do not show any apparent DNA cleavage implying no hydrolytic cleavage activity. The lack of chemical nuclease activity may be due to their weak interaction and binding with DNA.

5.3.5.2. Photo-induced DNA cleavage. To investigate whether the DNA binding properties of the complexes were associated with photonuclease activity, a photo-induced nuclease activity assay was performed. Photo-induced DNA nuclease activity of **1**–**8** was studied using supercoiled (SC) pUC19 DNA in 50 mM Tris-HCl buffer (pH 8.0) upon irradiation of UVA light of 350 nm with the aid of gel electrophoresis in the presence and absence of the complexes (**Figure 5.19**). The extent of SC DNA cleavage by the complexes was monitored in a concentration-dependent manner as shown in (**Figure 5.20**). All of the complexes (except **3**) exhibited more than 10% enhanced photo-induced DNA cleavage activity at a complex concentration of 10 μM (**Figure 5.20**, inset). The cleavage activity is saturated for each of the complexes at a concentration of 100 μM and the highest nuclease activity of 33 and 39 %, at a 100 μM complex concentration, was conferred by **6** and **7**, respectively, which correlates well with their DNA binding parameters (**Figure 5.20**, inset and **Table 5.3**). All the complexes exhibited almost similar cleavage even in solutions having low DMF concentrations, *i.e.* 1% DMF (v/v). Butenko et al reported that organic buffers such as tris, MOPS, HEPES, *etc*. suppressed the nuclease activity of some vanadium complexes.[62] In the same paper, they demonstrated that these complexes exhibited more nuclease activity in phosphate buffer compared to that of organic buffers listed above. Thus, we also performed the photo-induced DNA cleavage activity of **1**–**8** in 10 mM phosphate buffer (pH 7.8) containing 1% DMF . We found that buffer had no effect on the photo-nuclease activity of these complexes. They exhibited almost similar activity even when we used phosphate buffer instead of tris buffer. Since, we worked with buffer solutions having basic pH (>7.5), this may be ruled out the influence of tris buffer on the photo-nuclease activity of these dioxidovanadium complexes. Control experiments suggest that neither DMF (10%) nor the ligands show any photo-induced DNA cleavage activity, which implies that, the ligands or DMF alone are cleavage inactive under similar conditions.

In order to understand the mechanistic pathway involved in the DNA cleavage reactions, we systematically investigated the photo-induced DNA cleavage activity in presence of various additives. The DNA cleavage reaction involving molecular oxygen can proceed in two mechanistic pathways, namely, a type-II process involving singlet oxygen species ($^1O_2$) or by a photo-redox pathway involving reactive hydroxyl radicals (OH).[49] For the present mechanistic studies NaN_3 and L–histidine were used as singlet oxygen quenchers, and KI and D-mannitol were employed as hydroxyl radical quenchers. The addition of singlet oxygen quenchers like NaN_3 partially inhibited the DNA cleavage activity of **6** and **7** among the series, whereas the other singlet oxygen quencher L-histidine did not inhibit DNA cleavage activity of any complex. Similarly, the hydroxyl radical scavenger KI showed moderate inhibition of photo-induced DNA cleavage activity for **6** and **7**, whereas the other hydroxyl radical scavenger, D-mannitol did not inhibit the DNA cleavage activity of any complex (**Figure 5.21**). These results suggest that **6** and **7** exhibit photo-induced DNA cleavage activity *via* both singlet oxygen and hydroxyl radical pathways. Although the other complexes showed slight inhibition of DNA cleavage activity in presence of various additives, the mechanistic pathway followed could not be stated with certainty.

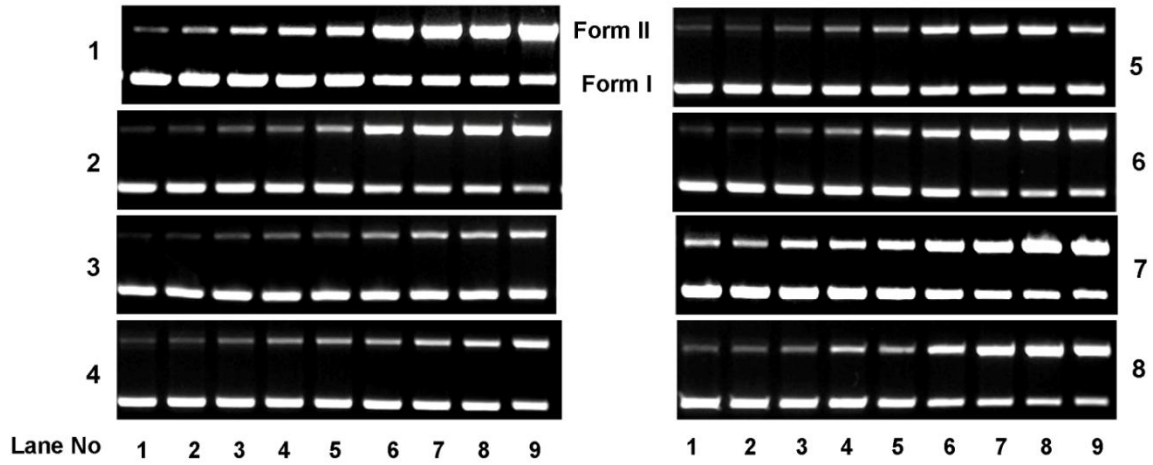

Figure 5.19. Gel diagram showing concentration dependent DNA cleavage by **1**–**8**; 300 ng of SC pUC19 DNA at different concentrations of the complexes [1–500 µM in 50 mM Tris-HCl buffer (pH 8.0) containing 10% DMF] was photo-irradiated with UVA at 350 nm for 3 h. Lanes **1**–**9**: 1, 2.5, 5.0, 7.5, 10, 50, 75, 100 and 500 µM of **1**–**8**. .

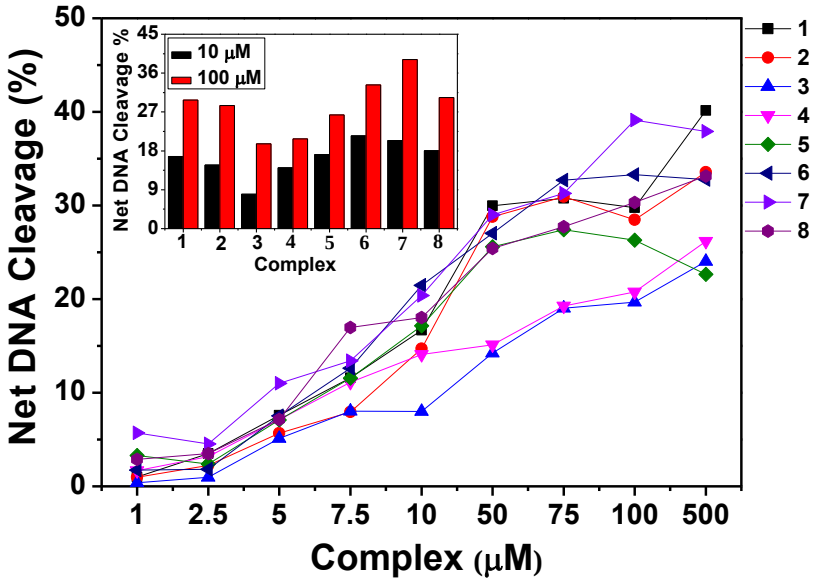

Figure 5.20. Concentration dependent DNA cleavage by **1**–**8**; 300 ng of SC pUC19 DNA at different concentration of the complexes [1–500 µM in 50 mM Tris-HCl buffer (pH 8.0) containing 10% DMF] was photo-irradiated with UVA at 350 nm for 3 h. The net DNA cleavage percent was calculated using Eq.2. Inset shows a bar diagram representation of the net DNA cleavage of different complexes at 10 and 100 µM.

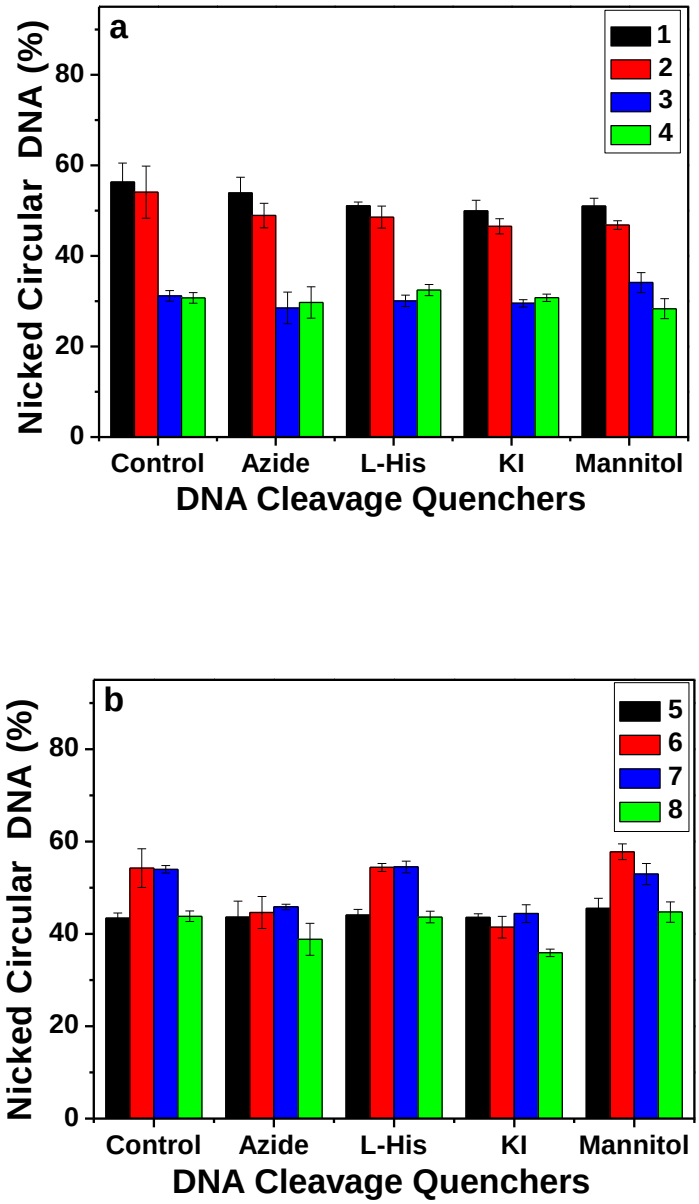

Figure 5.21. Cleavage of SC pUC19 DNA by **1**–**4** (a) and **5**–**8** (b) in presence of various additives in 50mM Tris-HCl buffer (pH 8.0) containing 10% DMF. SC pUC19 DNA (300 ng) in the presence of various additives was photo-irradiated at 350 nm for 3 h with **1**-**8** (100 µM). The additive concentrations were: sodium azide (0.5 mM), L-histidine (0.5 mM), KI (0.5 mM) and D-mannitol (0.5 mM).

5.3.6. Protein binding and cleavage experiments.

5.3.6.1. Bovine Serum Albumin (BSA) binding studies. As **6** and **7** revealed good binding propensities towards CT-DNA and showed better photo-induced DNA cleavage activity, the investigation of the interaction of these two complexes with bovine serum albumin (BSA) was undertaken. Qualitative analysis of the interaction of the complexes with BSA was studied by examining the quenching of tryptophan fluorescence emission spectra of BSA in presence of **6** and **7**. The fluorescence of the protein is specifically caused by three amino acid residues namely tryptophan, tyrosine and phenylalanine. The sequence analysis of BSA reveals the presence of two tryptophan residues and exhibits tryptophan fluorescence at an excitation of 295 nm with an emission maximum at 344 nm. The interaction with BSA was followed by monitoring the quenching of tryptophan fluorescence upon the addition of **6** and **7**. The effect of increasing concentration of **6** and **7** on the fluorescence emission of BSA is shown in **Figure 5.22**. The intrinsic tryptophan fluorescence intensity of BSA is found to quench gradually on increasing the complex concentration (**Figure 5.22**). The Stern-Volmer quenching constant (K_{SV}) was calculated using **Eq. 3** (Experimental Section). The quenching constants for **6** and **7** are 2.52 $\times 10^4$ and 2.72 $\times 10^5$ M^{-1}, respectively, (**Table 5.5**) which reveals that **7**, has ~10 fold greater quenching ability than **6.** The extent of quenching of the fluorescence intensity confers a measure of association of the complex with BSA. Small molecules bind independently to a set of sites in a protein molecule and the equilibrium between the free and the bound molecule is given by the Scatchard equation[45] (**Eq. 4**). The binding constant (K_{BSA}) and the number of binding sites (*n*) were obtained from the plot of log $\left[\frac{F_0 - F}{F}\right]$ *vs* log [Q] (**Table 5.5**). Both complexes interact with BSA in a 1:1 stoichiometry, although the binding affinity of complex **7** towards BSA is greater than for complex **6**.

5.3.6.2. BSA cleavage activity. Since both the complexes exhibited good binding affinity towards BSA, their protein cleavage activity by photo-induced BSA cleavage assay was investigated. The photo-induced BSA cleavage activity of these two complexes in UVA light of 350 nm was carried out using 5 μM of BSA in 10 mM Tris-HCl buffer (pH 8.0) monitored by SDS-PAGE gel electrophoresis in the presence and absence of **6** and **7**. A 100 μM solution of **6** and **7** showed more than 75% cleavage of BSA (5 μM) with a photo-irradiation of 90 min (**Figure 5.23** (**a, b**), lane 8) which suggests that both the complexes have similar photo-induced

BSA cleavage activity. At this same molar ratio of BSA to complex, all other complexes also exhibited similar kind of photo-induced BSA cleavage activity, whereas all the complexes (**1**−**8**) failed to show any cleavage of BSA in the dark. Moreover, the densitometry analysis of photo-induced BSA cleavage experiments revealed that ~ 33-36% BSA cleavage occurred even at 1:1 molar ratio of BSA to complex (**Figure 5.23c**).

Table 5.5. BSA Binding parameters of 6 and 7

Complex	Stern Volmer Constant (K_{SV}) (M^{-1})	Binding Constant (K_{BSA}) (M^{-1})	Number of Binding Sites (*n*)
6	$2.52 \pm 0.11 \times 10^4$	$3.12 \pm 0.13 \times 10^4$	0.81 ± 0.11
7	$2.72 \pm 0.15 \times 10^5$	$4.12 \pm 0.18 \times 10^5$	1.04 ± 0.07

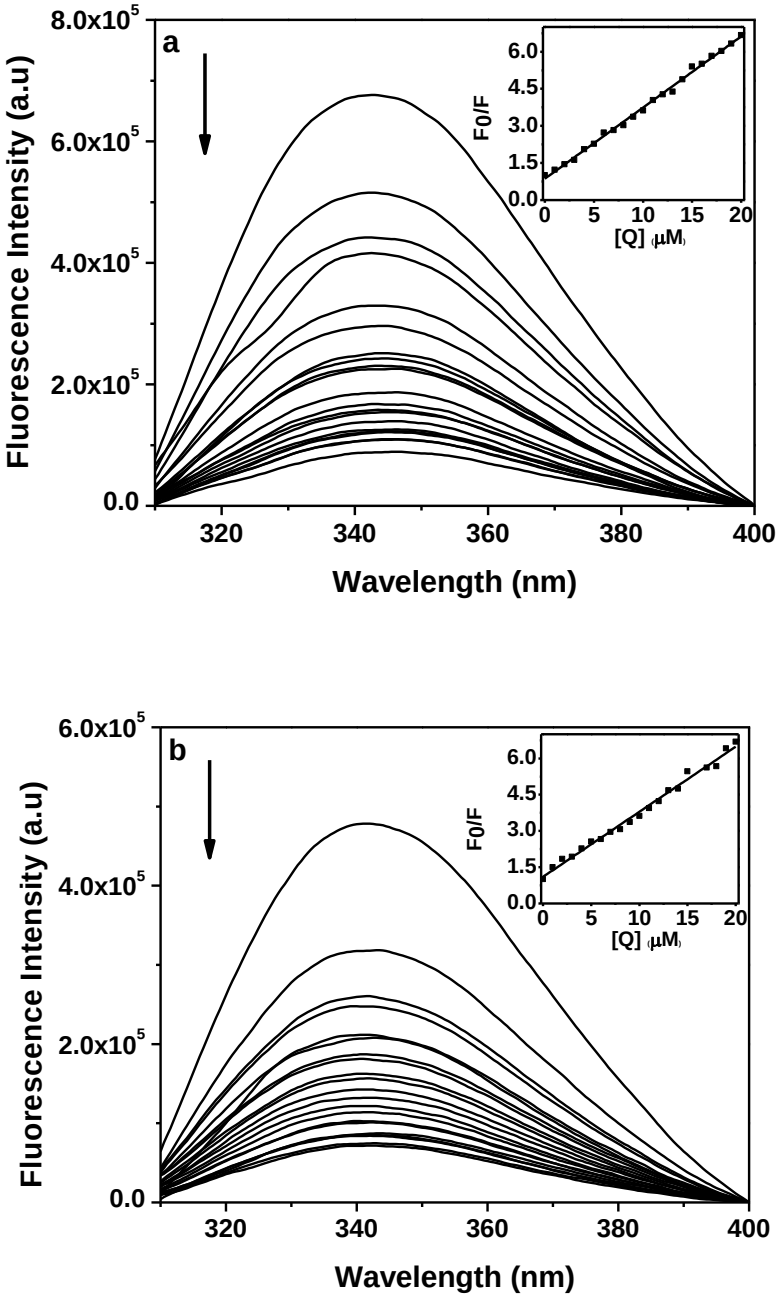

Figure 5.22. Intrinsic tryptophan fluorescence spectra of BSA (2 μM) in presence of complex **6** (a) and **7** (b) (0–20 μM in 10 mM Tris-HCl buffer (pH 8.0) containing 1% DMF). Tryptophan fluorescence spectra were recorded in the range 310–400 nm at 25 °C. The excitation wavelength was 295 nm. Arrow indicates the effect of increasing concentration of complexes on the tryptophan fluorescence emission of BSA. The inset shows the linear fit of F_0/F *vs* [complex] and Stern-Volmer quenching constant (K_{SV}) was calculated using Eq.3.

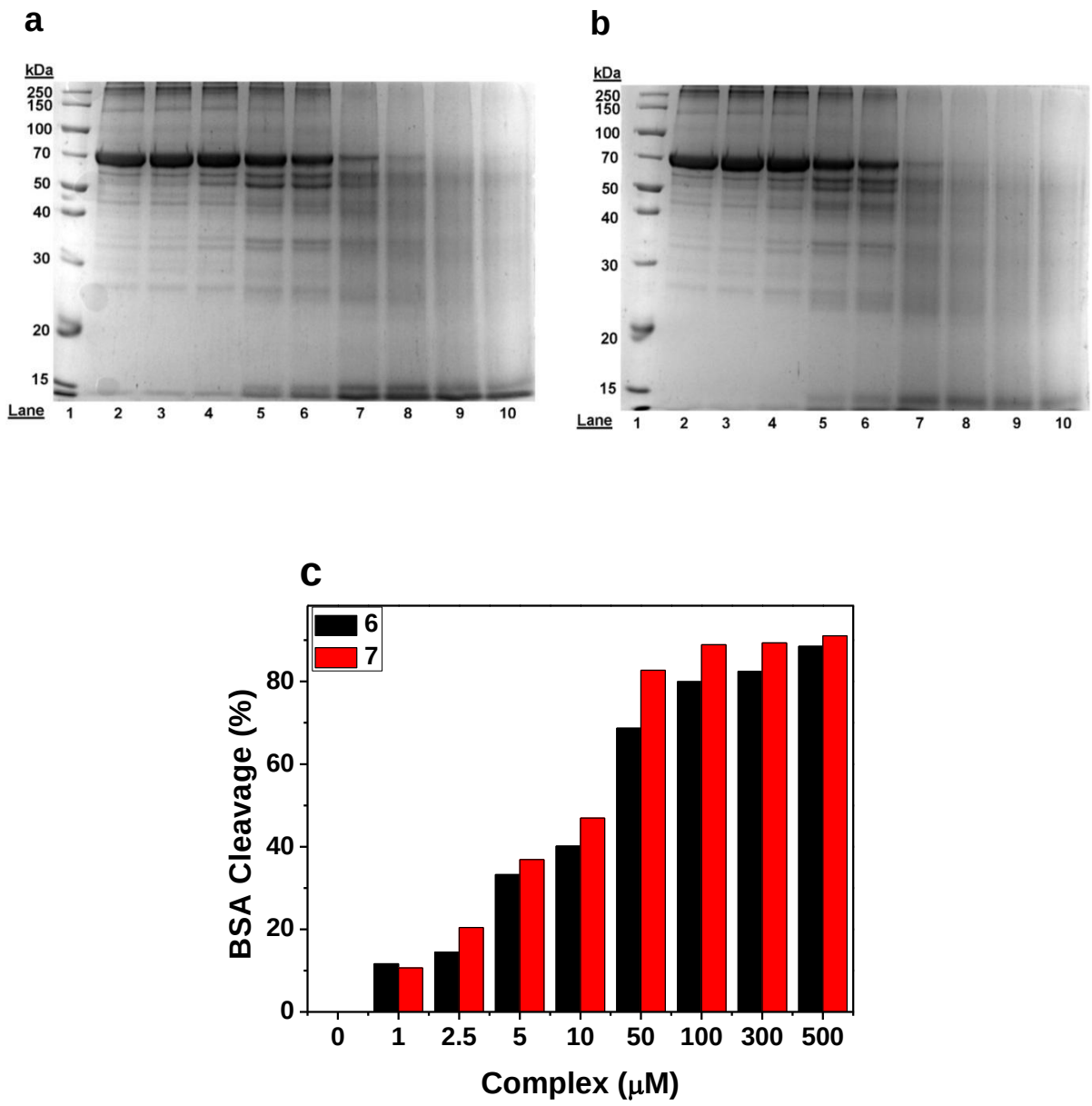

Figure 5.23. SDS-PAGE profile of concentration dependent photo-induced cleavage of BSA (5 μM) in UVA light of 350 nm by **6** (a) and **7** (b) in 10 mM Tris-HCl buffer (pH 8.0) containing 1% DMF. Lane 1, Molecular marker; Lane 2, BSA only; Lane 3, BSA + complex (1 μM); Lane 4, BSA + complex (2.5 μM); Lane 5, BSA + complex (5 μM); Lane 6, BSA + complex (10 μM); Lane 7, BSA + complex (50 μM); Lane 8, BSA + complex (100 μM); Lane 9, BSA + complex (300 μM); Lane 10, BSA + complex (500 μM). (c) Net BSA cleavage percent of concentration dependent photo-induced cleavage of BSA (5 μM) in UVA light of 350 nm (84 W) by **6** and **7**.

5.3.7. Cytotoxicity Studies

5.3.7.1. MTT assay. In the present study, antiproliferative efficacy of **1**–**8** was assayed by determining the viability of HeLa cells using the MTT assay. The ligands, H_2L^{1-6} and $VO(acac)_2$ gave high IC_{50} values of > 200 μM, whereas **1**–**8** gave values in the range 45–17 μM (**Table 5.6**). By contrast, cisplatin, gefitinib, gemcitabine, 5-fluorouracil and vinorelbine, commonly used chemotherapeutic drugs, are comparably effective in HeLa cells with an IC_{50} value of 13, 20, 35, 40 and 48 μM, respectively, under the same experimental conditions.[63] The significant decrease in the inhibitory ability of the ligands as well as their lower binding affinity to CT-DNA compared to their metal complexes clearly indicates that incorporation of vanadium has a marked effect on cytotoxicity. A possible explanation is that by coordination, the polarity of the ligand and the central metal ion are reduced through the charge equilibration, which favours permeation of the complexes through the lipid layer of the cell membrane.[64,65] The results of DNA binding/cleavage ability for the ligands have been considered and are consistent with the observation that metal complexes can exhibit greater biological activities than the free ligands.[66]

Within the series **1**–**8**, the cytotoxicities of **2**, **5**, **6** and **7** are almost similar whereas those of **6** and **7** are greater as reflected from their IC_{50} values, **Table 5.6**, with their dose dependency illustrated in **Figure 5.24**. The variation in results of cytotoxicity of the complexes may be affected by the various functional groups attached to the aroylhydrazone derivative. Very recently, the antiproliferative activity of some vanadium compounds reported by Yamaguchi *et al.*[67] and us[36] using U937 cells and HeLa cells, respectively, and the present results are in accordance with the reported values.

5.3.7.2. Nuclear Staining Assay. To investigate the apoptotic potential of test compounds in HeLa cells, DAPI staining was performed. Chromatin condensation during the process of apoptosis (type I programmed cell death) is a characterising marker of nuclear alteration. HeLa cells were treated with 40, 15, 20, 30, 18, 15, 12 and 30 μM of complexes **1**–**8**, respectively. The cells were incubated for 24 h before DAPI nuclear staining. Cells were examined under fluorescent microscope fitted with a DAPI filter. Control cells (treated with 10% (v/v) DMF) hardly showed any sort of condensation in comparison to the treated cells, as shown in **Figure 5.25**. All images taken in grayscale demonstrate the brightly condensed chromatin bodies and the nuclear blebbings as marked by arrows in **Figure 5.25**. Besides showing nuclear change, the

treated cells exhibited a shrinking morphology, which is another important hallmark of apoptosis.

Table 5.6. Cytotoxic scores for 1–8 in HeLa cancer cells

Complex	IC_{50} (μM)
1	44.96±3.98
2	20.56±4.58
3	24.25±3.74
4	33.25±2.9
5	23.18±3.66
6	18.96±4.09
7	17.23±3.24
8	37.45±4.26

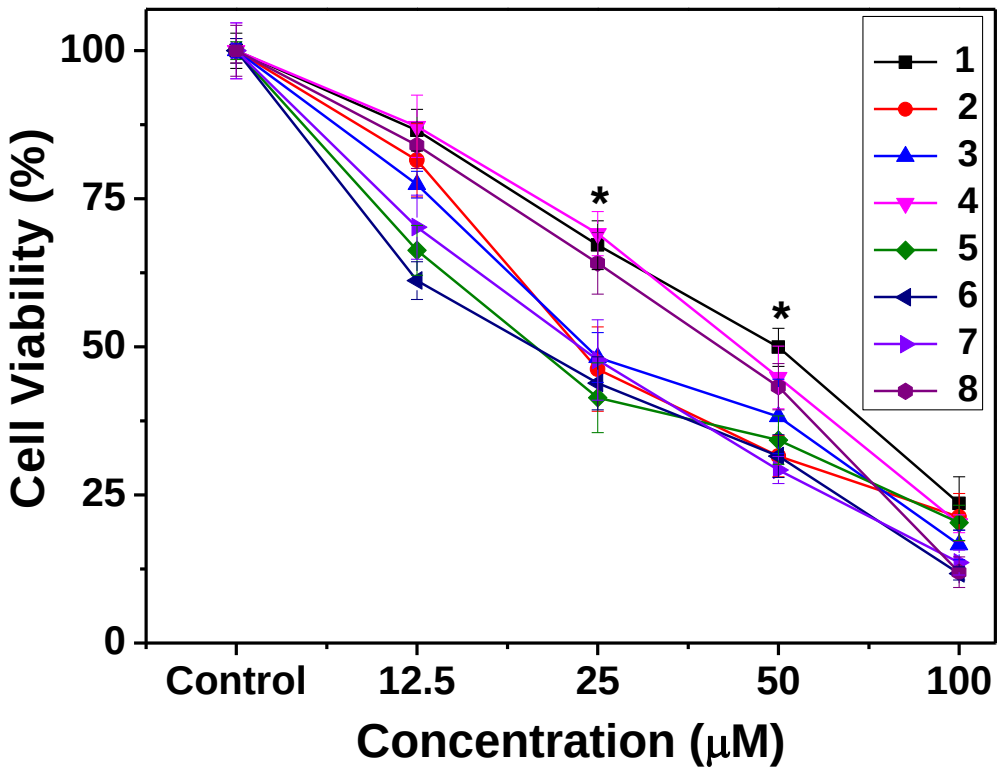

Figure 5.24. Effect of **1**–**8** on cell viability and growth: HeLa cells were treated with different concentrations of the test compound for 72 h and then cell viability was measured by MTT assay. Data reported as the mean ± S.D. for n = 6 and compared against 10% (v/v) DMF treated control by using a Student's t-test. (*significant compared to control).

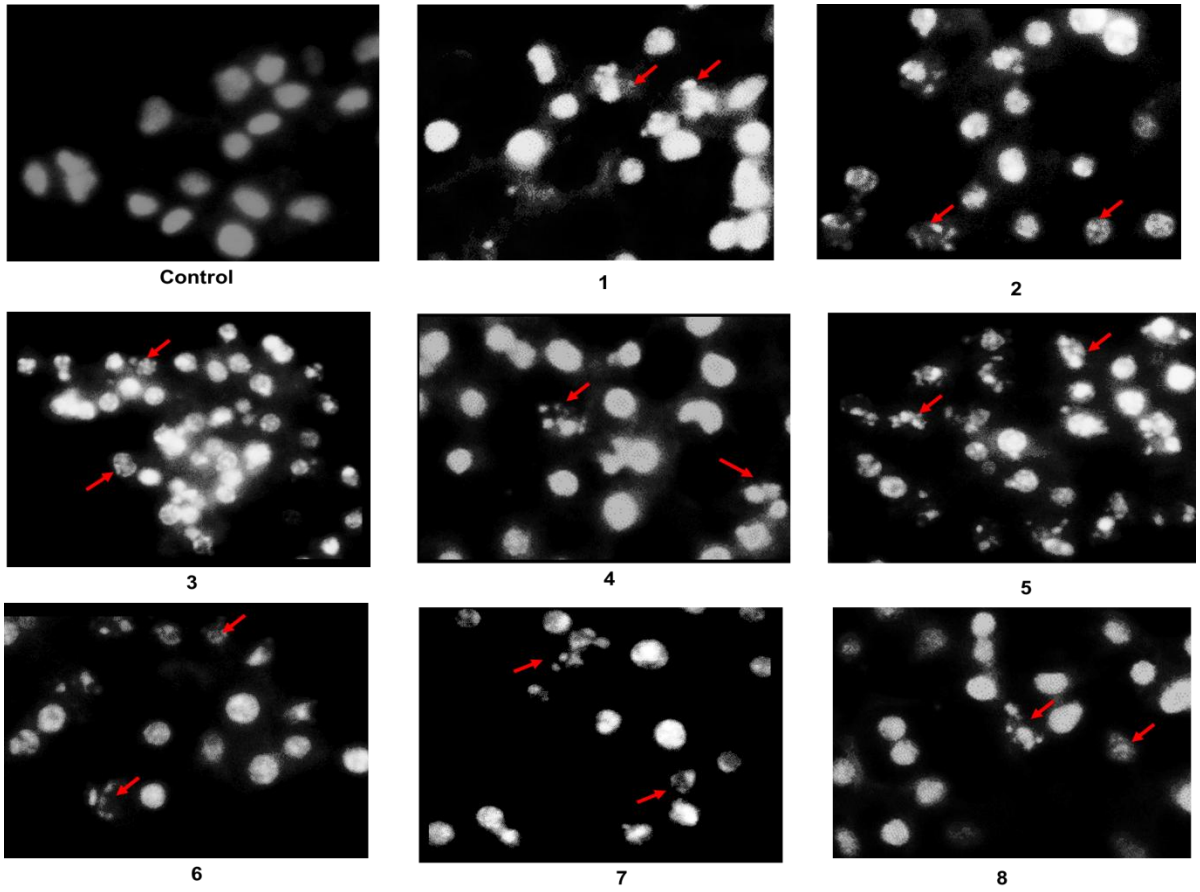

Figure 5.25. Study of apoptosis by morphological changes in nuclei of HeLa cells: HeLa cells, from control and treated groups, were fixed with 3.7% formaldehyde for 15 min, permeabilised with 0.1% Triton X-100 and stained with 1 µg/ml DAPI for 5 min at 37 °C. The cells were then washed with PBS and examined by fluorescence microscopy (Olympus IX 71) (200×). HeLa cells were treated with 40, 15, 20, 30, 18, 15, 12 and 30 µM of complexes **1**–**8**, respectively. Arrows showing the morphological changes in nuclei of HeLa cells observed on applying **1**–**8** in comparison to the control group treated with 10% (v/v) DMF.

5.4. CONCLUSION

The following are the salient observations of the present work: A series of dioxido vanadium(V) complexes (**1**−**8**) with tridentate aroylhydrazonates containing ONO donor atom form polymeric extended structures incorporating various alkali metal ion. The vanadium anions in **3**, **5**–**7** have been shown by X-ray crystallography to be five-coordinated within NO_4 donor sets tending towards square pyramidal. The primary influence of the cations is related to size so that with small Li^+, no bridging-O is found between the constituent ions but four-ion aggregates are found with Na^+, chains for K^+ and finally, layers for Cs^+. Strong electrostatic and hydrogen bonding interactions play the central role in stabilizing these extended structures in the solid-state.

Complexes **1**–**8** demonstrated moderate DNA binding propensity. Their DNA binding activities were investigated using UV-Vis absorption titration, circular dichroism and thermal denaturation studies. The experimental results show the complexes moderately interact with CT-DNA probably by groove binding mode, with binding constants ranging from 10^3–10^4 M^{-1}. All complexes also show efficient photo-induced cleavage of pUC19 supercoiled plasmid DNA. Among **1**–**8**, complexes **6** and **7** showed the best CT-DNA binding properties. Moreover, these two complexes exhibited greater cleavage activity of pUC19 DNA under photolytic conditions probably *via* both singlet oxygen and hydroxyl radical pathways. Complexes **6** and **7** also exhibit good binding affinity in the range of 10^4–10^5 M^{-1} towards BSA. Both complexes also showed efficient photo-induced BSA cleavage activity. The results obtained are significant in the context that vanadium complexes showing only DNA photo-cleavage activity but no chemical nuclease activity are sparse. The *in vitro* antiproliferative activity of complexes **1**−**8** against HeLa cell line was assayed. Among the complexes, **2**, **5**, **6** and **7** show considerable activity compared to commonly used chemotherapeutic drugs and the variation of cytotoxicity of the complexes may be affected by the various functional groups attached to the aroylhydrazone derivative whereby it may be globally stated that **6** and **7** are more potent against the HeLa cell line. The results of DNA binding, photo-induced DNA cleavage and antiproliferative activity of the new dioxidovanadium(V) complexes of aroylhydrazones reported in this paper reveals that the pharmacological activities of these complexes can be fine-tuned by changing the substituent on the hydrazone residue. It is important to mention that the alkali metal ions variation in **1**−**8** may have some influence on the results of pharmacological activity but their precise role remains unknown. Further work is in progress to identify the reasons. The results obtained from the

present dioxidovanadium(V) complexes are of importance for the development of metal-based agents for anti-cancer applications. Further work is in progress to better identify the mechanism of action and to prepare more potent related compounds for the treatment of cancer.

5.5. REFERENCES

(1) Rosenberg, B.; VamCamp, L.; Trosko J. E.; Mansour, V. H. *Nature* **1969**, *222*, 385.

(2) Zelenko, O.; Gallagher, J.; Xu, Y.; Sigman, D. S. *Inorg. Chem.* **1998**, *37*, 2198.

(3) Wu, Z.; Liu, Q.; Liang, X.; Yang, X.; Wang, N.; Wang, X.; Sun, H.; Lu, Y.; Guo, Z. *J. Biol. Inorg. Chem.* **2009**, ***14***, 1313.

(4) Raja, D. S.; Bhuvanesh, N. S. P.; Natarajan, K. *Dalton Trans.* **2012**, *41*, 4365.

(5) Qiao, X.; Ma, Z. Y.; Xie, C. Z.; Xue, F.; Zhang, Y. W.; Xu, J. Y.; Qiang, Z. Y.; Lou, J. S.; Chen, G. J.; Yan, S. P. *J. Biol. Inorg. Chem.* **2011**, *105*, 728.

(6) Bednarski, P. J.; Mackay, F. S.; Sadler, P. J. *Anticancer Agents Med. Chem.* **2007**, *7*, 75.

(7) In: Sigel, H.; Sigel, A. (Eds.), *Vanadium and its Role in Life, Metal Ions in Biological Systems*, vol. 31, Marcel Dekker, New York, **1995**.

(8) Crans, D. C.; Smee, J. J.; Gaidamauskas, E.; Yang, L. *Chem. Rev.* **2004**, *104*, 849.

(9) Tracey, A. S.; Willsky G. R.; Takeuchi, E. S. *Vanadium Chemistry, Biochemistry, Pharmacology and Practical Applications*, CRC Press, Boca Raton, **2007**.

(10) Rehder, D. *Bioinorganic Vanadium Chemistry, John Wiley & Sons*, Chichester, **2008**.

(11) Butler. A.; Walker, J. V. *Chem. Rev.* **1993**, *93*, 1937.

(12) Cornman, C. R.; Zovinka, E. P.; Meixner, M. H. *Inorg. Chem.* **1995**, *34*, 5099.

(13) Thompson, K. H.; McNeill, J. H.; Orvig, C. *Chem. Rev.* **1999**, *99*, 2561.

(14) Thompson,K. H.; Liboiron, B. D.; Sun, Y.; Bellman, K. D. D.; Karunaratne, V.; Rawji, G.; Wheeler, J.; Sutton, K.; Bhanot, S.; Cassidy, S. B. C.; McNeill, J. H.; Yuen, V. G.; Orvig, C. *J. Biol. Inorg. Chem.* **2003**, *8*, 66.

(15) Yasui, H.; Adachi, Y.; Katoh, A.; Sakurai, H. *J. Biol. Inorg. Chem.* **2007**, *12*, 843.

(16) Shechter, Y.; Goldwaser, I.; Mironchik, M.; Fridkin, M.; Gefel, D. *Coord. Chem. Rev.* **2003**, *237*, 3.

(17) Bastos, A. M. B.; da Silva, J. G.; Maia, P. I. S.; Deflon, V. M.; Batista, A. A.; Ferreira, A. V. M.; Botion, L. M.; Niquet, E.; Beraldo, H. *Polyhedron* **2008**, *27*, 1787.

(18) Eady, R. R. *Coord. Chem. Rev.* **2003**, *237*, 23.

(19) Sasmal, P. K.; Patra, A. K.; Chakravarty, A. R. *J. Inorg. Biochem.* **2008**, *102*, 1463.

(20) Mendes, I. C.; Botion, L. M.; Ferreira, A. V. M.; *Inorg. Chim. Acta.* **2009**, *362*, 414.

(21) Benítez, J.; Guggeri, L.; Tomaz, I.; Pessoa, J. C.; Moreno, V.; Lorenzo, J.; Avilés, F. X.; Garat, B.; Gambino, D. *J. Inorg. Biochem.* **2009**, *103*, 1386.

(22) Benítez, J.; Guggeri, L.; Tomaz, I.; Arrambide, G.; Navarro, M.; Pessoa, J. C.; Garat, B.; Gambino, D. *J. Inorg. Biochem.* **2009**, *103*, 609.

(23) Benítez, J.; Becco, L.; Correia, I.; Leal, S. M.; Guiset, H.; Pessoa, J. C.; Tanco, S.; Escobar, P.; Moreno, V.; Garat, B.; Gambino, D. *J. Inorg. Biochem.* **2011**, *105*, 303.

(24) (a) Andrezalova, L.; Gbelcova, H.; Durăckova, *Z. J. Trace Elem. Med. Biol.* **2013**, *27*, 21. (b) Chohan, Z. H.; Sumrra, S. H.; Youssoufi, M. H.; Hadda, T. B. *Eur. J. Med. Chem.* **2010**, *45*, 2739. (c) Lu, J.; Guo, H.; Zeng, X.; Zhang, Y.; Zhao, P.; Jiang, J.; Zang, L. *J. Inorg. Biochem.* **2012**, *112*, 39. (d) Yamaguchi, T.; Watanabe, S.; Matsumura, Y.; Tokuoka, Y.; Yokoyama, A. *Bioorg. Med. Chem.* **2012**, *20*, 3058.

(25) (a) Braga, D.; Grepioni, F.; Desiraju, G. R. *Chem. Rev.* **1998**, *98*, 1375. (b) Braga, D.; Grepioni, F. *Coord. Chem. Rev.* **1999**, *183*, 19. (c) Braga, D.; Grepioni, F. *Acc. Chem. Res.* **2000**, *33*, 601.

(26) (a) Dutta, S.; Basu, P.; Chakravorty, A. *Inorg. Chem.* **1993**, *32*, 5343. (b) S. K. Dutta,; Samanta, S.; Mukhopadhyay, S.; Burckel, P.; Pinkerton, A.; Choudhry, M. *Inorg. Chem.* **2002**, *41*, 2946. (c) Samanta, S.; Mukhopadhyay, S.; Mandal, D.; Butcher, R. J.; Choudhry, M. *Inorg. Chem.* **2003**, *42*, 6284. (d) Doble, D. M. J.; Blake, A. J.; Li, W. S.; Schroder, M. *Dalton Trans.* **2001**, 3137. (e) Ling Pan, C.; Qing Xu, J.; Hua Li, G.; Bing Cui, X.; Ye, L.; Yang, G. Di. *Dalton Trans.* **2003**, 517. (f) Zhu, H.; Chen, C.; Zhang, X.; Liu, Q.; Liao, D.; Li, L. *Inorg. Chim. Acta* **2002**, *328*, 96. (g) Przybylski, W.; Grybos´, R.; Rehder, D.; Ebel, M.; Grzywa, M.; Łasocha, W.; Lewinski, K.; Szklarzewicz, J. T. *Polyhedron* **2009**, *28*, 1429. (h) Dinda, R.; Majhi, P. K.; Sengupta, P.; Pasayat, S.; Ghosh, S. *Polyhedron* **2010**, *29*, 248. (i) Hazra, A.; Gupta, S.; Roy, S.; Mandal, T. N.; Das, K.; Konar, S.; Jana, A.; Ray, S.; Butcher, R. J.; Kar, S. K. *Polyhedron* **2011**, *30*, 187.

(27) Bruce, P. G. Solid State Electrochemistry, Cambridge University Press, Cambridge, **1993**.

(28) Pregel, M. J.; Jullien, L.; Lehn, J. M. *Angew. Chem. Int. Ed. Engl.* **1992**, *31*, 637.

(29) Terra, L. H. A.; Areias, M. C.; Gaubeur, I.; Suez-Iha, M. E. V. *Spectrosc. Lett.* **1999**, *32*, 257.

(30) (a) Maurya, M. R.; Agarwal, S.; Abid, M.; Azam, A.; Bader, C.; Ebel, M.; Rehder, D. *Dalton Trans.* **2006**, 937. (b) Savini, L.; Chiasserini, L.; Travagli, V.; Pellerano, C.; Novellino, E. *Eur. J. Med. Chem.* **2004**, *39*, 113. (c) Cui, Z.; Yang, X.; Shi, Y.; Uzawa, H.; Cui, J.; Dohi, H.; Nishida, Y. *Bioorg. Med. Chem. Lett.* **2011**, *21*, 7193.

(31) (a) Cunha, A. C.; Figueiredo, J. M.; Tributino, J. L. M.; Miranda, A. L. P.; Castro, H. C.; Zingali, R. B.; Fraga, C. A. M.; Souza, M. C. B. V.; Ferreira, V. F.; Barreiro, E. *J. Bioorg. Med. Chem.* **2003**, *11*, 2051. (b) Easmon, J.; Puerstinger, G.; Thies, K. S.; Heinisch, G.; Hofmann, J. *J. Med. Chem.* **2006**, *49*, 6343. (c) Chaston, T. B.; Watts, R. N.; Yuan, J.; Richardson, D. R. *Clin. Cancer Res.* **2004**, *10*, 7365.

(32) (a) Raja, D. S.; Bhuvanesh, N. S. P.; Natarajan, K. *J. Biol. Inorg. Chem.* **2012**, *17*, 223. (b) Chaston, T. B.; Richardson, D. R. *J. Biol. Inorg. Chem.* **2003**, *8*, 427. (c) Wang, Q.; Yang, Z. Y; Qi, G. F; Qin, D. D. *Biometals*, **2009**, *22*, 927. (d) Yang, Z. Y.; Wang, B. D.; Li, Y. H. *J. Organomet. Chem*. **2006**, *691*, 4159. (e) Wang, B. D.; Yang, Z. Y.; Crewdson P.; Wang, D. Q. *J. Inorg. Biochem.* **2007**, *101*, 1492. (f) Li, T. R.; Yang, Z. Y.; Wang, B. D.; Qin, D. D. *Eur. J. Med. Chem.* **2008**, *43*, 1688. (g) Wang, Q.; Yang, Z. Y.; Qi, G. F.; Qin, D. D. *Eur. J. Med. Chem.* **2009**, *44*, 2425.

(33) (a) Maurya, M. R.; Khan, A. A.; Azam, A.; Kumar, A.; Ranjan, S.; Mondal, N.; Pessoa, J. C. *Eur. J. Inorg. Chem.* **2009**, 5377. (b) Maurya, M. R.; Khan, A. A.; Azam, A.; Ranjan, S.; Mondal, N.; Kumar, A.; Avecilla, F.; Pessoa, J. C. *Dalton Trans.* **2010**, *39*, 1345. (c) Benítez, J.; de Queiroz, A. C.; Correia, I.; Alves, M. A.; Alexandre-Moreira, M. S.; Barreiro, E. J.; Lima, L. M.; Varela, J.; González, M.; Cerecetto, H.; Moreno, V.; Pessoa, J. C.; Gambino, D. *Eur. J. Med. Chem.* **2013**, *62*, 20.

(34) (a) Crans, D. C.; Smee, J. J.; Gaidamauskas, E.; Yang, L. *Chem. Rev.* **2004**, *104*, 849. (b) Nunes, G. G.; Bonatto, A. C.; de Albuquerque, C. G.; Barison, A.; Ribeiro, R. R.; Back, D. F.; Andrade, A. V. C.; de Sa´, E. L.; de Pedrosa, F. O.; Soares, J. F.; de Souza, E. M. *J. Inorg. Biochem.* **2012**, *108*, 36. (c) Tudor, R.; Maria, N.; Simona, P.; Elena, P.; Donald, P.; Aurelian, G. *Eur. J. Med. Chem.* **2010**, *45*, 774. (d) Sumrra, S. H.; Chohan, Z. H. *Spectrochim. Acta, Part A*, **2012**, *98*, 53. (d) Raja, D. S.; Bhuvanesh, N. S. P.; Natarajan, K.; *Inorg. Chim. Acta* **2012**, *385*, 81. (e) Bishayee, A.; Waghray, A.; Patel, M. A. *Cancer Lett.* **2010,** *294*, 1. (f) Liao, X.; Lu, J.; Ying, P.; Zhao, P.; Bai, Y.; Li, W.; Liu, M. *J. Biol. Inorg. Chem.* **2013**, *18*, 975.

(35) (a) Dinda, R.; Sengupta, P.; Ghosh, S.; Mak, T. C. W. *Inorg. Chem.* **2002**, *41*, 1684. (b) Dinda, R.; Sengupta, P.; Sutradhar, M.; Mak, T. C. W.; Ghosh, S. *Inorg. Chem.* **2008**, *47*, 5634. (c) Dash, S. P.; Pasayat, S.; Bhakat, S.;. Dash, H. R; Das, S.; Butcher, R. J.; Dinda, R. *Polyhedron* **2012**, *31*, 524.

(36) Dash, S. P.; Pasayat, S.; Bhakat, S.; Roy, S.; Dinda, R.; Tiekink, E. R. T.; Mukhopadhyay, S.; Bhutia, S. K.; Hardikar, M. R.; Joshi, B. N.; Patil, Y. P.; Nethaji, M. *Inorg. Chem*. **2013**, *52*, 14096.

(37) Rowe, R. A.; Jones, M. M. *Inorg. Synth*. **1957**, *5*, 113.

(38) Naskar, S.; Mishra, D.; Butcher, R. J.; Chattopadhyay, S. K. *Polyhedron* **2007**, *26*, 3703.

(39) Bruker. APEX2 (version 2.1-4), SAINT (version 7.34A) and SADABS (version 2007/4), BrukerAXS Inc, Madison, Wisconsin, USA. **2007**.

(40) G. M. Sheldrick,; *Acta Crystallogr*. *Sect. A, Foundat. Crystallogr.* **2008**, *64*, 112.

(41) Farrugia, L. J. *J. Appl. Crystallogr*. **2013**, *45*, 849.

(42) Gans, J.; Shalloway, D. *J. Molec. Graphics Model*. **2001**, *19*, 557.

(43) *DIAMOND, Visual Crystal Structure Information System, Version 3.1*, CRYSTAL IMPACT, Postfach 1251, D-53002 Bonn, Germany, **2006**.

(44) Spek, A. L. *Acta Crystallogr. Sect. D, Biol. Crystallogr*. **2009**, *65*, 148.

(45) Krishnamoorthy, P.; Sathyadevi, P.; Cowley, A. H.; Butorac R. R.; Dharmaraj, N. *Eur. J. Med. Chem.* **2011**, *46*, 3376.

(46) Kumar, P.; Gorai, S.; Santra, M. K.; Mondal, B.; Manna, D. *Dalton Trans.* **2012**, *41*, 7573.

(47) Sasmal, P. K.; Patra, A. K.; Chakravarty, A. R. *J. Inorg. Biochem.* **2008**, *102*, 1463.

(48) Dai, W. M.; Lai, K. W.; Wu, A.; Hamaguchi, W.; Lee, M. Y.; Zhou, L.; Ishii, A.; Nishimoto, S. *J. Med. Chem.* **2002**, *45*, 758.

(49) Sasmal, P. K.; Saha, S.; Majumdar, R.; De, S.; Dighe, R. R.; Chakravarty, A. R. *Dalton Trans.* **2010**, *39*, 2147.

(50) Bhutia, S. K.; Mallick, S. K.; Stevens, S. M.; Prokai, L.; Vishwanatha, J. K.; Maiti, T. K. *Toxicol. Vitro* **2008**, *22*, 344.

(51) Mukhopadhyay, S.; Panda, P. K.; Behera, B.; Das, C. K.; Hassan, M. K.; Das, D. N.; Sinha, N.; Bissoyi, A.; Pramanik, K.; Maiti, T. K.; Bhutia. S. K. *Food Chem. Toxicol.* **2014**, *64*, 369.

(52) Das, S.; Muthukumaragopal, G. P.; Pal, S. N.; Pal, S. *New J. Chem.* **2003**, *27*, 1102.

(53) (a) Maurya, M. R.; Kumar, A.; Ebel, M.; Rehder, D. *Inorg. Chem.* **2006**, *45*, 5924. (b) Maurya, M. R.; Haldar, C.; Kumar, A.; Kuznetsov, M. L.; Avecilla, F.; Pessoa, J. C. *Dalton Trans.* **2013**, *42*, 11941.

(54) Addison, A. W.; T. N. Rao,; J. Reedijk,; van Rijn, J.; Verschoor, G. C. *Dalton Trans*. **1984**, 1349.

(55) Allen, F. H. *Acta Crystallogr. Sect. B: Struct. Sci*. **2002**, *58*, 380.

(56) (a) Sutradhar, M.; Mukherjee, G.; Drew, M. G. B.; Ghosh, S. *Inorg. Chem*. **2006**, *45*, 5150. (b) Sutradhar, M.; Barman, T. R.; Mukherjee, G.; Drew, M. G. B.; Ghosh, S. *Polyhedron* **2012**, *34*, 92.

(57) Mondal, B.; Drew, M. G. B.; Ghosh, T. *Inorg. Chim. Acta* **2010**, *363*, 2296.

(58) Shahverdizadeh, G. H.; Ng, S. W.; Tiekink, E. R. T.; Mirtamizdoust, B. *Acta Crystallogr. Sect. E: Struct. Rep. Online* **2012**, *68*, m236.

(59) An, Y.; Liu, S. D.; Deng, S. Y.; Ji, L. N.; Mao, Z. W. *J. Inorg. Biochem.* **2006**, *100*, 1586.

(60) Banerjee, S.; Hussain, A.; Prasad, P.; Khan, I.; Banik, B.; Kondaiah, P.; Chakravarty, A. R. *Eur. J. Inorg. Chem.* **2012**, 3899.

(61) Li, L.; Guo, Q.; Dong, J.; Xu, T.; Li, J. *J. Photochem. Photobiol. B*, **2013**, *125*, 56.

(62) Butenko, N.; Tomaz, A. I.; Nouri, O.; Escribano, E.; Moreno,V.; Gama, S.; Ribeiro, V.; Telo, J. P.; Pesssoa, J. C.; Cavaco, I. *J. Inorg. Biochem.* **2009**, *103*, 622.

(63) Ahmed, M.; Jamil, K. *Biol. Med*. **2011**, *3*, 60.

(64) Ramadan, A. M.; *J. Inorg. Biochem.* **1997**, *65*, 183.

(65) Avaji, P. G.; Kumar, C. H. V.; Patil, S. A.; Shivananda, K. N.; Nagaraju, C. *Eur. J. Med. Chem.* **2009**, *44*, 3552.

(66) Rosu, T.; Pahontu, E.; Pasculescu, S.; Georgescu, R.; Stanica, N.; Curaj, A.; Popescu, A.; Leabu, M. *Eur. J. Med. Chem.* **2010**, *45*, 1627.

(67) Yamaguchi, T.; Watanabe, S.; Matsumura, Y.; Tokuoka, Y.; Yokoyama, A. *Bioorg. Med. Chem*. **2012**, *20*, 3058.

Chapter 6

Oxido vanadium(V) complexes of aroylhydrazones containing bioactive heterocycles: Synthesis, characterisation and study of DNA binding, photo-induced DNA cleavage and cytotoxic activities

Chapter 6

Oxido vanadium(V) complexes of aroylhydrazones containing bioactive heterocycles: Synthesis, characterisation and study of DNA binding, photo-induced DNA cleavage and cytotoxic activities

ABSTRACT

Four neutral oxido vanadium(V) complexes $[VO_2L^1]$ (**1**), $[VO_2L^2]$ (**2**), $[VOL^3(OEt)]$ (**3**) and $[VOL^4(OEt)EtOH]$ (**4**) [where HL^1= 2-thiophenoylhydrazone of 2-acetylpyridine, HL^2= 2-amino benzoylhydrazone of 2-benzoyl pyridine, H_2L^3= isonicotinoylhydrazone of 2-hydroxy acetophenone, H_2L^4= 2-furoylhydrazone of 2-hydroxy-1-napthaldehyde] with a bioactive hydrazone scaffold containing furan, thiophene and pyridine-residues have been synthesised. All complexes were thoroughly characterised by various spectroscopic (IR, UV-Vis, NMR and ESI-MS) and single crystal X-ray diffraction techniques. Crystallography establishes five-coordinate geometries, distorted toward square pyramidal for each of **1** and **2**, based on a tridentate-ONN coordinating anion and two oxido-O atoms. The dianion in **3** is tetradentate, coordinating one V atom as for **1** and **2**, and bridging another via the pyridyl-N atom, and the N_2O_4 octahedral coordination geometry is completed by oxido- and ethanolate-O atoms. The result of the V–N bridging is a helical coordination polymer. An NO_5 octahedral geometry is found in **4** defined by a tridentate-ONO anion, as well as oxido-, ethanolate- and ethanol-O atoms. Biological studies reveal that **1**–**4** have DNA binding propensity and show these to interact with CT-DNA by a minor groove binding mode, with binding constants ranging from 10^3–10^5 M^{-1}. All complexes show good photo-induced cleavage of pUC19 supercoiled plasmid DNA with **3** showing the highest photo-induced DNA cleavage activity of ~ 65%. Additionally, **1**–**4** are cytotoxic against the human cervical cancer cell line (HeLa) following the order **4** > **2** > **3** > **1** with IC_{50} values ranging from 10 to 20 μM.

6.1. INTRODUCTION

Metal complexes bearing a heterocyclic moiety open a new era of pharmaceutical research since their presence moderates not only physicochemical properties but also enhances medicinal properties.[1–4] Isoxazoles, pyrroles, and pyrazoles are well-known examples of heteroaromatic organic compounds associated with diverse biological properties. Hence, it is not surprising there are several reports in the literature where metal complexes have had their physicochemical and pharmacological properties influenced by the presence of biologically active heterocycles containing nitrogen.[5–7] In this context, thiophene,[8] furan,[9] and pyridine[10] moieties are especially regarded as desirable, due to their widespread use as a scaffold in medicinal chemistry.

Metal coordination is one of the most efficient strategies in the design of repository, slow-release or long-acting drugs.[11]It was the discovery of cisplatin that gave momentum to metal-based drug research.[12] Despite its tremendous success as an anti-cancer drug, its use is restricted due to serious side-effects, general toxicity, and acquired drug resistance.[13–16] Therefore, considerable effort is being made to synthesise new metal-based drugs that effectively and specifically target cancer cells while minimising toxic side effects. Among transition metals, vanadium complexes have attracted significant attention owing to their diversified applications as models for the biological functions of vanadium,[17–20] such as haloperoxidation,[21] phosphorylation,[22] insulin mimicking,[23–26] nitrogen fixation,[27] tumour growth inhibition and prophylaxis against carcinogenesis.[28] These complexes have also numerous applications in DNA binding, cleavage and have shown the ability to act as anti-proliferative agents.[29–32]

Hydrazones, –NH–N=CRR' (R and R′ = H, alkyl, aryl), are versatile ligands and have applications in the fields of analytical[33] and medicinal chemistry.[34] Hydrazone moieties are important pharmacophoric cores of several anticancer, anti-inflammatory, anti-nociceptive and anti-platelet drugs.[35] Moreover, the electronic properties of hydrazone complexes are also important in the design of complexes with better DNA-binding and cleavage characteristics.[36] Hydrazones in combination to heterocycles display a broad range of biological activity.[37–39] Examples of hydrazide and hydrazone derivatives containing bioactive heterocycles demonstrating medicinal properties are presented in **Chart 6.1**.[40–44] There are a handful reports in the literature on metal complexes having hydrazone ligands where a heterocyclic moiety

enhances the pharmacological activity of these complexes.[45] However, to date, analogous vanadium complexes, and especially the study of their pharmacological activity, is still scarce and needs to be explored.[46]

Considering the interesting pharmacological properties of ligand systems containing bioactive heterocycles and as a part of our studies on design and synthesis of novel vanadium complexes with potential pharmaceutical activities,[32,47] in this chapter we now focus our attention on the synthesis of some new oxido vanadium complexes with a bioactive hydrazone scaffold containing furan, thiophene and pyridine residues. These show interesting DNA binding, photo-induced DNA cleavage and cytotoxicity profiles. The interaction of the complexes with calf-thymus DNA (CT-DNA) was also investigated using UV-Vis absorption titration and thermal denaturation studies. Their photo-cleavage reactions with pUC19 supercoiled plasmid DNA were investigated by gel electrophoresis. In addition, the cytotoxicity of the complexes against the cervical cancer cell line (HeLa) was assessed by the MTT assay.

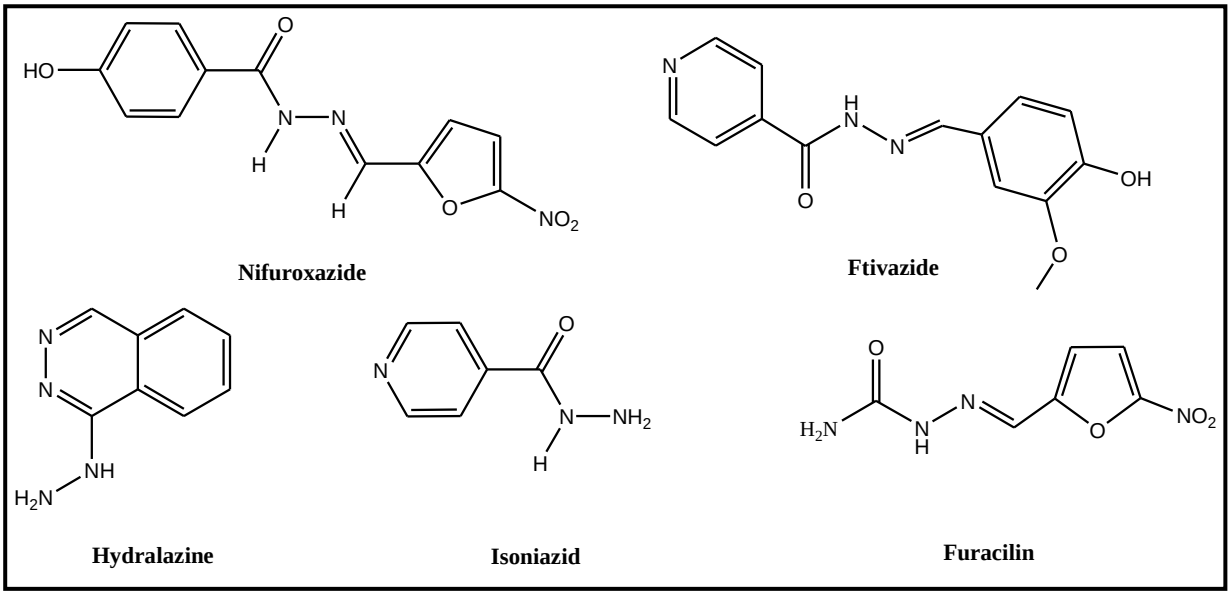

Chart 6.1. Chemical structures of some hydrazide and hydrazone derivatives demonstrating pharmacological activities.

6.2. EXPERIMENTAL SECTION

6.2.1. General Methods and Materials. All chemicals were purchased from commercial sources and used without further purification. The $VO(acac)_2$ complex was prepared as described in the literature.[48] MTT (3-[4,5-Dimethylthiazol-2-yl]-2,5-diphenyltetrazolium) and DAPI (4′,6-diamidino-2-phenylindole dihydrochloride) were purchased from Sigma Aldrich (USA). Minimal essential medium (MEM) was purchased from Gibco, India. Reagent grade solvents were dried and distilled prior to use. The supercoiled (SC) pUC19 DNA was purified from E. coli cells with the aid of GeneJET Plasmid Isolation Kit (Thermo Scientific, USA). Biochemistry grade calf thymus (CT) DNA was purchased from SRL (India). Molecular biology grade agarose was purchased from Sigma Aldrich (USA). Elemental analyses were performed on a Vario ELcube CHNS Elemental analyser and IR spectra were recorded on a Perkin-Elmer Spectrum RXI spectrophotometer. ^{1}H and ^{13}C NMR spectra were recorded with a Bruker Ultrashield 400 MHz spectrometer using $SiMe_4$ as the internal standard. Electronic spectra were recorded on a Perkin-Elmer Lamda25 spectrophotometer.

6.2.2. Synthesis of Ligands (HL^{1-2}, $H_2L^{3–4}$) Schiff base ligands, HL^1 and $H_2L^{3–4}$, were prepared by condensation of acid hydrazides (10 mmol) and the corresponding carbonyl compound (10 mmol) in stirring ethanol (15 mL) for 3 h following a standard procedure.[47] HL^2 was prepared by condensation of 2-amino benzoylhydrazide with 2-benzoyl pyridine in refluxing methanol for 5 h. The resulting white compound was filtered, washed with ethanol and dried over fused $CaCl_2$. The synthesised ligands are shown in **Scheme 6.1**.

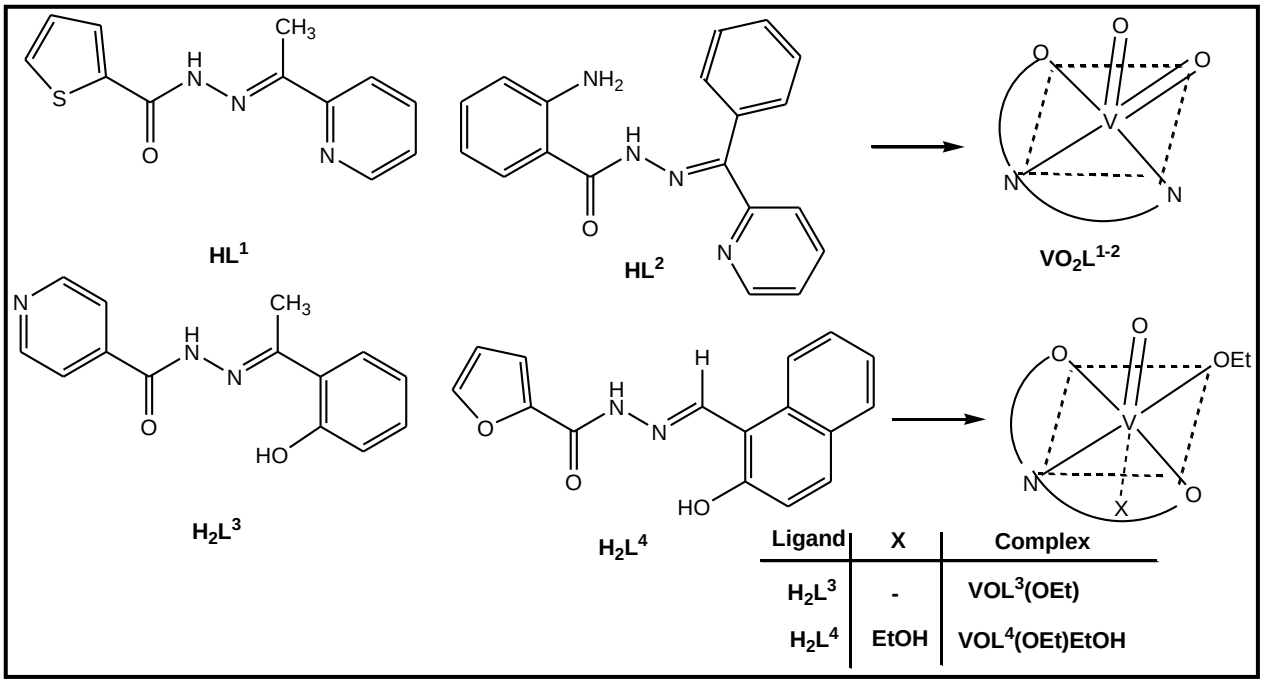

Scheme 6.1. Schematic diagram of ligand molecules and composition of the complexes.

HL^1. Yield: 74%. Anal. Calcd for $C_{12}H_{11}N_3OS$: C, 58.76; H, 4.52; N, 17.13; S, 13.07. Found: C, 58.79; H, 4.48; N, 17.11; S, 13.05. IR (KBr pellet, cm^{-1}): 3164 ν(N–H), 1647 ν(C=O), 1572 ν(C=N). ^{1}H NMR (400 MHz, DMSO-d_6): δ 11.09 (s, 1H, NH), 8.61–7.20 (m, 7H, aromatic), 2.45 (s, 3H, CH_3). ^{13}C NMR (100 MHz, DMSO-d_6): δ 162.55, 155.32, 150.79, 149.12, 137.10, 135.59, 133.33, 127.16, 125.23, 124.45, 121.25, 12.88.

HL^2. Yield: 78%. Anal. Calcd for $C_{19}H_{16}N_4O$: C, 72.14; H, 5.10; N, 17.71. Found: C, 72.15; H, 5.11; N, 17.69. IR (KBr pellet, cm^{-1}): 3472 $(NH_2)_{sym}$, 3354 $\nu(NH_2)_{asym}$, 3048 ν(N–H), 1654 ν(C=O), 1576 ν(C=N). ^{1}H NMR (400 MHz, DMSO-d_6): δ 14.50 (s, 1H, NH), 8.91–6.63 (m, 13H, aromatic), 6.56 (s, 2H, NH_2). ^{13}C NMR (100 MHz, DMSO-d_6): δ 157.07, 155.75, 153.94, 153.81, 152.27, 143.60, 142.78, 141.95, 138.00, 134.30, 134.12, 134.05, 133.64, 132.51, 131.38, 130.09, 122.24, 120.67, 117.91.

H_2L^3. Yield: 69%. Anal. Calcd for $C_{14}H_{13}N_3O_2$: C, 65.87; H, 5.13; N, 16.46. Found: C, 65.88; H, 5.11; N, 16.50. IR (KBr pellet, cm^{-1}): 3368 ν(O–H), 3151 ν(N–H), 1678 ν(C=O), 1607 ν(C=N). ^{1}H NMR (400 MHz, DMSO-d_6): δ 13.32 (s, 1H, OH), 11.72 (s, 1H, NH), 8.20–6.89 (m, 8H, aromatic), 2.42 (s, 3H, CH_3). ^{13}C NMR (100 MHz, DMSO-d_6): δ 163.40, 160.01, 159.21, 150.56, 140.84, 132.05, 129.19, 122.84, 122.63, 122.43, 119.68, 119.10, 117.82, 14.78.

H_2L^4. Yield: 71%. Anal. Calcd. for $C_{16}H_{12}N_2O_3$: C, 68.57; H, 4.32; N, 9.99. Found: C, 68.59; H, 4.34; N, 9.96. IR (KBr pellet, cm^{-1}): 3445 ν(O–H), 3172 ν(N–H), 1640 ν(C=O), 1603 ν(C=N). ^{1}H NMR (400 MHz, DMSO-d_6): δ 12.72 (s, 1H, OH), 12.26 (s, 1H, NH), 9.51 (s, 1H, CH), 8.21–6.71 (m, 9H, aroamtic). ^{13}C NMR (100 MHz, DMSO-d_6): δ 158.43, 154.24, 147.54, 146.70, 146.50, 133.20, 132.10, 129.37, 128.26, 128.16, 123.96, 121.04, 119.29, 115.95, 112.75, 109.00.

6.2.3. Synthesis of complexes (1–4).

6.2.3.1. Synthesis of $[VO_2L^1]$ (1). To a hot solution of HL^1 (1 mmol) in methanol (30 mL), $VO(acac)_2$ (1 mmol) in DMF (5 mL) was added, the colour changed instantly to green-brown. After 6 h of reflux, the solution was cooled, filtered and kept for crystallisation. Slow evaporation of the filtrate over 4 days produced yellow crystals.

[VO_2L^1] (1). Yield: 63%. Anal. Calcd for $C_{12}H_{10}N_3O_3SV$: C, 44.05; H, 3.08; N, 12.84; S, 9.80. Found: C, 44.06; H, 3.05; N, 12.83; S, 9.81. IR (KBr pellet, cm^{-1}): 1600 ν(C=N), 1255 $\nu(C–O)_{enolic}$, 1036 ν(N–N), 946 ν(V=O). UV–Vis (DMF) [λ_{max}, nm (ε, M^{-1} cm^{-1})]: 399 (14121), 277 (8371). ^{1}H NMR (400 MHz, DMSO-d_6): δ 8.81–7.22 (m, 7H, aromatic), 2.72 (s, 3H, CH_3). ^{13}C NMR (100 MHz, DMSO-d_6): δ 171.54, 165.30, 159.69, 152.14, 148.11, 145.19, 144.33, 132.16, 127.23, 126.40, 124.22, 13.48. ^{51}V NMR (DMSO-d_6): δ –507.

6.2.3.2. Synthesis of [VO_2L^2] (2). To a hot solution of HL^2 (1 mmol) in ethanol (30 mL), $VO(acac)_2$ (1 mmol) was added, the colour changed instantly to orange. After 5 h of reflux, the solution was cooled, filtered off and kept for crystallisation. Slow evaporation of the filtrate over 4 days produced orange crystals.

[VO_2L^2] (2). Yield: 68%. Anal. Calcd for $C_{19}H_{15}N_4O_3V$: C, 57.30; H, 3.80; N, 14.07. Found: C, 57.31; H, 3.84; N, 14.08. IR (KBr pellet, cm^{-1}): 3393 $\nu(NH_2)_{sym}$, 3284 $\nu(NH_2)_{asym}$, 1594 ν(C=N), 1255 $\nu(C–O)_{enolic}$, 1028 ν(N–N), 943 ν(V=O). UV–Vis (DMF) [λ_{max}, nm (ε, M^{-1} cm^{-1})]: 460 (8945), 298 (11114), 258 (12770). ^{1}H NMR (400 MHz, DMSO-d_6): δ 8.93–6.53 (m, 13H, aromatic), 6.73 (s, 2H, NH_2). ^{13}C NMR (100 MHz, DMSO-d_6): δ 178.68, 158.22, 155.08, 154.13, 150.71, 143.56, 134.04, 131.61, 130.99, 129.96, 129.32, 129.21, 127.12, 116.69, 115.45, 110.75. ^{51}V NMR (DMSO-d_6): δ –512.

6.2.3.3. Synthesis of [VOL^3(OEt)] (3). To the (1 mmol) sample of ligand H_2L^3 in ethanol (20 mL), $VO(acac)_2$ (1 mmol) was added under refluxing conditions. After 3 h, the resulting deep-brown solution was filtered and slow evaporation of the filtrate over 4–5 days produced brown crystals. The crystals were filtered and washed with ethanol.

[VOL^3(OEt)] (3). Yield: 64%. Anal. Calcd for $C_{16}H_{16}N_3O_4V$: C, 52.61; H, 4.42; N, 11.50. Found: C, 52.63; H, 4.44; N, 11.48. IR (KBr pellet, cm^{-1}): 1601 ν(C=N), 1239 $\nu(C–O)_{enolic}$, 1037 ν(N–N), 964 ν(V=O). UV–Vis (DMF) [λ_{max}, nm (ε, M^{-1} cm^{-1})]: 399 (7783), 326 (18601), 267 (22547). ^{1}H NMR (400 MHz, DMSO-d_6): δ 8.75–6.92 (m, 8H, aromatic), 5.59 (m, 2H, CH_2(OEt)), 1.54 (t, 3H, CH_3(OEt)), 2.93 (s, 3H, CH_3). ^{13}C NMR (100 MHz, DMSO-d_6): δ 167.52, 164.69, 164.32, 161.80, 150.22, 140.15, 133.79, 130.69, 123.00, 122.51, 120.72, 117.00, 82.18, 56.50, 18.98, 17.32. ^{51}V NMR (DMSO-d_6): δ –541.

6.2.3.4. Synthesis of [VOL^4(OEt)EtOH)] (**4**)**.** Complex **4** was prepared similarly to **3**, replacing H_2L^3 by H_2L^4.

[VOL^4(OEt)EtOH)] (4). Yield: 69%. Anal. Calcd for $C_{20}H_{21}N_2O_6V$: C, 55.05; H, 4.85; N, 6.42. Found: C, 55.02; H, 4.86; N, 6.38. IR (KBr pellet, cm^{-1}): 1611 ν(C=N), 1238 $\nu(C–O)_{enolic}$, 1052 ν(N–N), 998 ν(V=O). UV–Vis (DMF) [λ_{max}, nm (ε, M^{-1} cm^{-1})]: 436 (7621), 326 (8168), 284 (11506), 260 (13128). ^{1}H NMR (400 MHz, DMSO-d_6): δ 9.61(s, 1H, CH), 8.40–6.65 (m, 9H, aromatic), 5.67 (m, 2H, CH_2(OEt)), 3.45 (q, 2H, CH_2(EtOH)), 1.55 (t, 3H, CH_3(OEt)), 1.06 (t, 3H, CH_3(EtOH)). ^{13}C NMR (100 MHz, DMSO-d_6): δ 164.45, 163.24, 148.60, 146.19, 145.88, 135.40, 132.74, 129.24, 128.70, 128.61, 124.43, 121.75, 119.55, 115.27, 112.53, 111.50, 74.38, 56.61, 48.94, 18.57. ^{51}V NMR (DMSO-d_6): δ –537.

6.2.4. X-ray Crystallography. Intensity data for **1**, **2** and **4** were collected on a Bruker APEXII diffractometer equipped with a CCD area detector and graphite-monochromated Mo Kα radiation (λ = 0.71069 Å), and those for **3** were measured on an Oxford Difftaction Xcalibur Ruby Gemini system employing graphite-monochromated Cu Kα radiation (λ = 1.54178 Å). Data reduction and empirical absorption correction, based on the multi-scan method, was by standard methods.[49,50] The structures were solved by direct methods using SHELXS97[51] through the WinGX Interface[52] and refinement (anisotropic displacement parameters, C-bound hydrogen atoms in idealised positions and a weighting scheme of the form $w = 1/[\sigma^2(F_o^2) + aP^2 + bP]$ where $P = (F_o^2 + 2F_c^2)/3$) of each structure was carried out on F^2 by full-matrix least-squares procedures.[51] The amine-H atoms in **2** were located from a difference Fourier map and refined with the distance restraint N−H = 0.88±0.01 Å. The thienyl ring in **1** was found to be disordered over two coplanar dispositions of opposite orientation: the major component refined to a site occupancy factor of 0.836(2). For **1**, the maximum and minimum residual electron density peaks of 1.03 and 0.41 e Å^{-3}, respectively, were located 0.78 and 0.51 Å, respectively, from the V atom. The absolute structure of **3** was determined on the basis of 539 Friedel pairs included in the data set; the value of the Flack parameter[53] was 0.012(6). Crystal data and refinement details are given in **Table 6.1**. The molecular structures shown in **Figures 6.1**, **6.2**, **6.4**,**6.5** were drawn with 70% (35% for **2**) displacement ellipsoids.[52] The overlay diagrams shown in the were drawn

with QMol,[54] and the crystal packing diagrams with DIAMOND.[55] Data interpretation was accomplished using PLATON.[56]

Table 6.1. Crystallographic and refinement details for 1–4.

Compound	**1**	**2**	**3**	**4**
Formula	$C_{12}H_{10}N_3O_3SV$	$C_{19}H_{15}N_4O_3V$	$C_{16}H_{16}N_3O_4V$	$C_{20}H_{21}N_2O_6V$
Formula weight	327.23	398.29	365.26	436.33
Crystal colour/habit	Orange prism	Dark-red prism	Black prism	Red needle
Crystal dimensions/mm	0.11 x 0.15 x 0.20	0.14 x 0.17 x 0.34	0.06 x 0.11 x 0.25	0.03 x 0.07 x 0.40
Temperature/K	100	100	293	293
Crystal system	monoclinic	triclinic	orthorhombic	monoclinic
Space group	$P2_1/c$	$P\bar{1}$	$Pna2_1$	$C2/c$
a/Å	7.1876(3)	7.2745(2)	12.4265(2)	41.893(4)
b/Å	10.6882(4)	14.3309(3)	10.8273(2)	8.7854(10)
c/Å	16.6167(6)	16.7694(4)	12.0750(2)	21.729(2)
a/°	90	87.92(10)	90	90
β/°	92.567(2)	80.07(10)	90	98.017(5)
γ/°	90	83.41(10)	90	90
V/Å^3	1275.26(9)	1710.41(7)	1624.64(5)	7919.2(14)
Z	4	4	4	16
D_c/g cm^{-3}	1.704	1.547	1.493	1.464
F(000)	664	816	752	3616
μ/mm^{-1}	0.951	0.609	5.339	0.541
Measured data	43228	29305	4415	114454
θ range/°	2.3–27.5	1.9–27.5	5.4–77.5	1.9–25.6
Unique data	2933	7826	2329	7421
Observed data [$I \geq 2.0\sigma(I)$]	2760	6698	2119	5085
R, obs. data; all data	0.028; 0.030	0.033; 0.040	0.030; 0.033	0.045; 0.80
a, b in weighting scheme	0.035, 1.109	0.046, 0.865	0.061, 0	0.052, 15.124
R_w, obs. data; all data	0.075; 0.076	0.086; 0.091	0.081; 0.082	0.106, 0.130
Residual electron density peaks/e Å^3	1.03, -0.41	0.39, -0.42	0.22, -0.22	0.65, -0.39

6.2.5. DNA binding experiments.

6.2.5.1. Absorption spectral studies. Binding of the oxido vanadium(V) complexes to calf thymus (CT) DNA was carried out as previously described.[47] The UV-Vis titration experiments were performed using a fixed concentration of metal complex (25 μM) but variable CT-DNA concentrations ranging from 0 to 70 μM in 10 mM Tris–HCl buffer (pH 8.0) containing 1% DMF. Binding of ligands to CT-DNA was also studied. For this, a fixed concentration of ligand [25 μM in 10 mM Tris–HCl buffer (pH 8.0) containing 1% DMF] was titrated with variable DNA concentration ranging from 0 to 350 μM.

6.2.5.2. Thermal denaturation studies. Thermal denaturation studies of CT-DNA (160 μM) in the absence and presence of complexes (150 μM) were carried out by monitoring the absorbance at 260 nm in the temperature range of 30–90 ^{o}C with a ramp rate of 1 ^{o}C/min in 10 mM Tris-HCl buffer (pH 8.0) containing 1% DMF. The experiments were carried out using a Chirascan CD spectropolarimeter (Applied Photophysics, UK) in absorbance mode equipped with peltier temperature controller. The melting temperature (T_m) was determined from the derivative plot (dA_{260}/dT vs T) of the melting profile.[57]

6.2.6. DNA cleavage experiments.

For DNA cleavage experiments, 300 ng supercoiled (SC) pUC19 DNA was used and all experiments were carried out in 50 mM Tris-HCl buffer (pH 8.0) containing 1% DMF and 10 mM phosphate buffer (pH 7.8) containing 1% DMF.

6.2.6.1. Chemical-induced DNA cleavage. For chemical nuclease studies, the reactions were performed in the dark using hydrogen peroxide (0.5 mM) as the oxidising agent in the absence and presence of complexes (1-500 μM). The solutions were incubated at 37 ºC for 3 h and analysed for DNA cleaved products by agarose gel electrophoresis.

6.2.6.2. Photo-induced DNA cleavage. The photo-induced DNA cleavage activity was done as described previously.[47] The photolytic DNA cleavage experiments were carried out on supercoiled (SC) pUC19 DNA (300 ng) with complexes (1-500 μM) in 50 mM Tris HCl buffer (pH 8.0) containing 1% DMF and in 10 mM phosphate buffer (pH 7.8) containing 1% DMF. The extent of DNA cleavage was measured from the intensities of the bands using UVP Gel

Documentation System. The observed error in measuring the band intensities ranged between 3-6%. The mechanistic studies were performed using four different additives: two are singlet oxygen quenchers (sodium azide and L-histidine) and two are hydroxyl radical quenchers (KI and D-mannitol) prior to the addition of the complex. The concentration of each additive was 0.5 mM.

6.2.7. Cytotoxicity Studies

6.2.7.1. MTT assay. Human cervical cancer cells (HeLa) were obtained from National Centre of Cell Science (NCCS), Pune, India, and were maintained in minimal essential medium supplemented with 10% fetal bovine serum, penicillin-streptomycin solution and incubated at 37 °C in 5% CO_2 and 95% humidified incubator. HeLa cells were harvested from maintenance cultures in logarithmic phase, after counting in a hemocytometer using trypan blue solution. The cell concentration was adjusted to $5x10^4$ cells/ml and the cells were plated in a 96 well flat bottom culture plate and incubated for 72 h with various concentrations of the test complexes which were dissolved in a 10% (v/v) DMF solution. The effect of the drugs on the cancer cell viability was studied using MTT dye reduction assay by measuring the optical density at 595 nm using microplate reader spectrophotometer (Perkin-Elmer 2030).[58] A 10% (v/v) DMF solution which was used to dissolve the drugs was used in the control group treatment.

6.2.7.2. Nuclear Staining. Nuclear staining using DAPI stain was performed according to the method previously described.[59] Briefly, HeLa cells either treated or untreated with test compounds were smeared on a clean glass slide, cells were fixed with 3.7% formaldehyde for 15 min, permeabilised with 0.1% Triton X-100 and stained with 1 μg/ml DAPI for 5 min at 37 °C. 10% DMF solution which was used to dissolve the drugs was also used in control group treatment. The cells were then washed with PBS and examined by fluorescence microscopy (Olympus IX 71) to ascertain any condensation or fragmentation of the nuclei indicating cells undergoing apoptosis.

6.3. RESULT AND DISSCUSSION

6.3.1. Synthesis. Four oxido vanadium(V) complexes (**1**–**4**) have been prepared using different aroylhydrazones as ligands (**Scheme 6.1**), i.e. with varying heterocycle-derivatives in their hydrazone moieties, in order to observe their influence on the pharmacological activities of the resultant complexes. Reactions of the selected aroylhydrazones with $VO(acac)_2$ proceed in refluxing ethanol / DMF+MeOH to afford crystalline products in good yields. These complexes are highly soluble in aprotic solvents, viz. DMF and DMSO.

6.3.2. Spectral Characteristics. The spectral (IR, UV-Vis and NMR) data of $HL^{1–2}$, $H_2L^{3–4}$ and their corresponding oxido vanadium(V) complexes (**1–4**) are given in the Experimental Section.

6.3.2.1. IR Spectroscopy. The disappearance of characteristic bands due –NH and –C=O in the respective ligand spectra, and the appearance of new bands in the range 1255–1238 cm^{-1} in the spectra of the resulting complexes indicates the enolisation of these two groups to form a –N=C–O bond sequence. The strong and sharp peak displayed by the complexes in the range 1611–1594 cm^{-1} is likely to be associated with the –C=N–N=C– moiety.[60,61] The presence of broad bands at 946 and 943 cm^{-1} for **1** and **2**, respectively, is assigned to V=O stretching,[47,62] which indicates the presence of dioxido group in the complexes whereas a sharp band in the range 998–964 cm^{-1} is assigned to V=O stretching of a oxidoalkoxido vanadium(V) complex, as for **3** and **4**.[60a]

6.3.2.2. UV Spectroscopy. The electronic spectra of **1**–**4** were recorded in DMF (1.48×10^{-4} M) and are similar. Strong absorptions in the range 460–399 nm are assignable to the ligand-to-metal charge transfer transitions whereas the bands in the higher energy region (326–258 nm) are likely to be due to ligand centred transitions.[60a,b]

6.3.2.3. NMR Spectroscopy. The ^1H and ^{13}C NMR data of $HL^{1–2}$, $H_2L^{3–4}$ and **1**–**4** were recorded in DMSO-d_6. The spectra of $HL^{1–2}$ and $H_2L^{3–4}$ exhibit resonances due to –NH in the range 14.50–11.09 ppm. These disappear in the spectra of the complexes confirming enolisation of the ligands. For **3** and **4**, the absence of signals in the range 13.32–12.72 ppm indicates deprotonation of the –OH groups and its coordination to the vanadium centre after metallation. Complexes **1** and **3** each displays a singlet in the range δ = 2.93–2.72 ppm due to $–CH_3$ protons. Complexes **3** and **4** exhibit separate resonances corresponding to bound ethanolate at 5.59 and

5.67 ppm due to $–CH_2$ and 1.54 and 1.55 ppm due to $–CH_3$, respectively.[60b,63,64] In addition, **4**, exhibits a quartet at 3.45 ppm due to $–CH_2$ and a triplet at 1.06 ppm due to $–CH_3$, respectively which indicates the presence of the coordinated ethanol group. Finally, **4** displays a resonance at $\delta = 9.61$ ppm ascribed to –CH.

The ^{51}V NMR spectra of **1**–**4** each displays a singlet in the range $\delta = –541$ to –507 ppm. These chemical shifts are usual for complexes containing oxido vanadium(V) species.[65]

6.3.3. Description of the X-ray structure of complexes 1-4.

6.3.3.1. Structural commentary. Crystal structures were obtained for each of **1**–**4** and these are discussed in turn below. The selected geometric parameters are listed in **Table 6.2**.

6.3.3.2. Molecular structures. In $[VO_2L^1]$ (**1**), **Figure 6.1**, the penta-coordinated vanadium atom is bound by a tridentate uninegative anion, coordinating via enolate-O, azo-N and pyridyl-N atoms, and two oxido-O atoms. Confirmation that the multidentate ligand is functioning as a 2-acetylpyridine 2-thiophenoylhydrazone is found in the magnitudes of the two C=N bond lengths, **Table 6.2**; a similar mode of coordination for this specific anion toward vanadium was found in a seven-coordinated species where one oxido-O atom is replaced by peroxo- and methanol-O atoms.[66] The resulting N_2O_3 donor set in **1** is distorted toward square pyramidal based on a τ value of 0.30 which compares to ideal values of 0.0 and 1.0 for square pyramidal and trigonal bipyramidal geometries, respectively.[67] Each five-membered chelate ring is planar with r.m.s. deviations of 0.021 and 0.023 Å for the (V1,O1,N2,N3,C7) and (V1,N1,N2,C1,C6) rings, respectively, and the dihedral angle between them is 1.91(6)º. The dihedral angle between the terminal pyridyl and thienyl (major component) rings is 4.96(19)º suggesting that the entire ligand is approximately planar. The overall molecular structure in **1** matches closely to the most relevant structure available for comparison, namely the furanyl derivative, which exhibits crystallographically imposed mirror symmetry with the tridentate ligand lying on the plane.[68]
The molecular structures of the two independent molecules comprising the asymmetric unit of $[VO_2L^2]$ (**2**) are shown in **Figure 6.2** and **Figure 6.3a**, and these are similar to that just described for **1** except that the methyl and thienyl groups in **1** have been substituted by phenyl and anilinyl groups, respectively. The uninegative, tridentate ligand adopts a similar mode of coordination as just described for **1** in each molecule of **2**. The independent molecules differ most notably in the

relative orientations of the phenyl and anilinyl substituents as highlighted in the overlay diagram, **Figure 6.3b**, and quantified in the dihedral angles formed between the pyridyl and each of the phenyl and anilinyl rings of 54.39(8) and 23.36(8)º, respectively, for the first independent molecule in **2**, and 47.77(7) and 6.18(8)º for the second molecule. From these data, the tridentate ligand in the second molecule adopts a more planar conformation cf. the first independent molecule. The five-membered chelate rings in each molecule are almost planar with the r.m.s. deviations for (V1,O1,N2,N3,C7) and (V1,N1,N2,C1,C6) rings being 0.046 and 0.009 Å for the first molecule, respectively, and 0.044 and 0.028 Å for the second molecule, respectively. The values of τ calculated for the two independent molecules are 0.35 and 0.28, respectively, again indicating a distortion toward a square pyramidal geometry. Each molecule features an intramolecular N–H...N hydrogen bond which closes an S(6) loop.[69] The analogous ligand where the phenyl group has been substituted for a methyl group has been characterised in two crystal structures, i.e. mononuclear cobalt[70] and uranium[71] complexes, each with a nearly planar conformation of the tridentate ligand.

An increase in coordination number at vanadium in [VOL^3(OEt)] (**3**), **Figure 6.4**, is evident owing to the formation of intermolecular V–N1(pyridyl) bonds. The vanadium atom is coordinated by the enolate-O1, phenoxide-O2 and azo-N2 atoms of the dinegative ligand, as well as oxido-O3, ethanolate-O4 and bridging pyridyl-N1 atoms; the dianion is therefore, tetradentate. The result of the V–N bridging is the formation of a supramolecular helical chain along the c-axis, **Figure. 6.4b**. The N_2O_4 donor set defines a distorted octahedral geometry with the twist angle between the trigonal faces defined by the O1,O4,N1 atoms and the O2,O3,N2 atoms being approximately 51º, cf. 60º for an ideal octahedron and 0º for an ideal trigonal prism. While the five-membered chelate ring is essentially planar, r.m.s. deviation = 0.033 Å, the six-membered chelate ring is best described as being based on a half-chair conformation with the vanadium atom lying 0.812(3) Å out of the plane defined by the remaining chelate atoms, i.e. O2,N2,C1,C6,C7, which have a r.m.s. deviation of 0.0787 Å from their least-squares plane. There are no literature precedents for crystal structures containing the ligand as found in **3**.

The fourth structure, [VOL^4(OEt)EtOH)] (**4)**, is illustrated in **Figure 6.5** and **Figure 6.6a**, as the asymmetric unit comprises two independent complex molecules; for the second independent molecule, the ethanol molecule is statistically disordered over two positions (**Figure 6.6a**). The

overlay diagram of the two independent molecules with the moleculeis shown in **Figure 6.6b.** The coordination geometry is based on an octahedral NO_5 donor set defined by enolate-O1, azo-N2 and naphthyl-oxide-O2 atoms of the tridentate dinegative anion, as well as oxido-O4, ethanolate-O5 and ethanol-O6 atoms. The V=O4 bond lengths in **4** are the shortest across the series owing to the trans disposition of the oxido-O to the relatively weakly bound ethanol molecules. Each five-membered chelate ring is planar but the six-membered rings are best described as having half-chair conformations with the O2 atom lying 0.454(3) Å out of the plane defined by the remaining five atoms (r.m.s. deviation = 0.1037 Å); the equivalent values for the V2-molecule are 0.348(3) and 0.0826 Å, respectively. The dihedral angle between the chelate rings for the V1-containing molecule is 6.88(18)º, and this opens up to 10.06(12)º for the species with V2. Overall, the multidentate ligand exhibits a small twist as seen in the dihedral angles formed between the outermost ring of the naphthalyl system and furanyl group of 13.90(19)º (V1) and 10.42(18)º (V2). A search of the Cambridge Structural Database[72] revealed 42 vanadium-containing structures with an NO_5 donor set defined by the same donor atoms as for **4**. In each structure there was a trans arrangement of oxido-O and ethanol-O atoms as well as between ethanolate-O and nitrogen donor atoms. The most closely related structure is one where the furanyl group has been replaced by a 3-pyridyl ring and the N1-imine C atom carries a methyl group.[73] In the latter, the tridentate ligand has a decidedly curved conformation with the dihedral angle between the terminal rings being 34.56(7)°.

6.3.3.3. Supramolecular features. In the absence of functional groups capable of hydrogen bonding, the most significant intermolecular interactions operating in the structure of **1** are of the type π…π and C–H…O. The former connect molecules into centrosymmetric dimers via interactions involving the thienyl and pyridyl rings. These are connected into a three-dimensional architecture via pyridyl-C–H interacting with a bifurcated oxido-O3 atom. A view of the unit cell contents for **1** is given in **Figure 6.7** and full geometric details describing the aforementioned interactions are collected in the figure caption.

The most prominent feature of the crystal packing in $[VO_2L^2]$ (**2**) is the formation of N–H…O hydrogen bonds between the amino-H and oxido-O atoms so that supramolecular chains aligned along [101] are formed comprising alternating V1- and V2-containing molecules, **Figure 6.8a**.

These are linked by a network of C–H…O interactions involving anilinyl-, methyl-, phenyl- and pyridyl-H as donors and oxido-O as acceptors, see **Figure 6.8b** for geometric data.

In the crystal structure of [VOL^3(OEt)] (**3**), the coordination polymers are connected into a supramolecular layer in the ac-plane with the links being of the type C–H…π(chelate) ring with the latter comprising the (V,O1,N2,N3,C8) atoms of the five-membered ring, see **Figure 6.9a.** for geometric data. Such C–H…π(chelate) ring interactions are relatively rare, or more likely not always recognised, but are increasingly attracting attention in the crystallographic literature.[74–76] The layers stack along the b-axis in an ...ABA... pattern with no specific interactions between them, see **Figure 6.9b.**

Finally, in the crystal packing of [VOL^4(OEt)EtOH)] (**4)**, each of the two independent molecules comprising the asymmetric unit self-associate via methanol-O–H...N1(imine) hydrogen bonds to form two-molecule aggregates and 10-membered $\{...HOVN_2\}_2$ supramolecular synthons, see **Figure 6.10** (**a,b**). Within the dimeric aggregates there are also π...π interactions between the thienyl and inner ring of the naphthalyl group. The dimers stack into columns aligned along the b-axis, so that layers of alternating V1- and V2-containg molecules stack along the a-axis. In the layers comprising V2-containing molecules, naphthalyl-C–H...O(naphthalyl) interactions stabilise the architecture but there are no specific interactions between V1-containing dimers or between layers, **Figure 6.10c**.

Table 6.2. Selected bond lengths and angles (Å, º) for 1–4.

Complex	**1**	**2a**	**2b**	**3**[a]	**4a**	**4b**[b]
Parameter						
V–O1	1.9684(11)	1.9458(12)	1.9604(12)	1.969(2)	1.958(2)	1.938(2)
V–O2	1.6213(12)	1.6196(13)	1.6203(12)	1.859(2)	1.856(2)	1.848(2)
V–O3	1.6196(13)	1.6206(13)	1.6171(12)	1.594(2)	–	–
V–O4	–	–	–	1.777(2)	1.577(2)	1.575(3)
V–O5	–	–	–	–	1.775(2)	1.753(2)
V–O6	–	–	–	–	2.325(2)	2.46(3)
V–N1	2.1112(13)	2.0939(15)	2.1015(14)	2.434(2)	–	–
V–N2	2.1200(13)	2.1067(14)	2.1200(14)	2.141(2)	2.111(2)	2.109(2)
V–N3	–	–	–	–	–	–
N2–N3	1.3840(18)	1.381(2)	1.3786(19)	1.400(3)	1.392(3)	1.395(3)
C=N1	–	–	–	–	1.299(4)	1.297(4)
C=N2	1.291(2)	1.303(2)	1.304(2)	1.298(4)	1.285(4)	1.283(4)
C=N3	1.312(2)	1.324(2)	1.325(2)	1.297(4)	–	–
O1–V–O2	102.55(6)	103.92(6)	101.83(6)	149.59(9)	150.57(9)	151.97(10)
O1–V–O3	102.16(6)	104.12(6)	102.57(6)	100.86(11)	–	–
O2–V–O3	109.99(7)	109.89(7)	109.15(7)	99.62(11)	–	–
O4–V–O6	–	–	–	–	177.03(10)	171.5(6)
O1–V–N1	146.50(5)	147.47(6)	146.72(5)	79.19(9)	–	–
O3–V–N1	97.60(6)	95.25(6)	97.00(6)	178.81(11)	–	–
O4–V–N2	–	–	–	163.35(9)	93.61(11)	96.30(11)
O5–V–N2	–	–	–	–	163.36(11)	157.32(12)
N1–V–N2	73.08(5)	73.32(6)	72.94(5)	85.55(9)	–	–

a The N1 atom in **3** is related by the symmetry operation 2-x, 2-y, ½+z.

b For the second component of the disordered ethanol molecule in **4**, the V2–O6b bond length is 2.52(3) Å and the O4a–V2–O6b bond angle is 174.8(6)º.

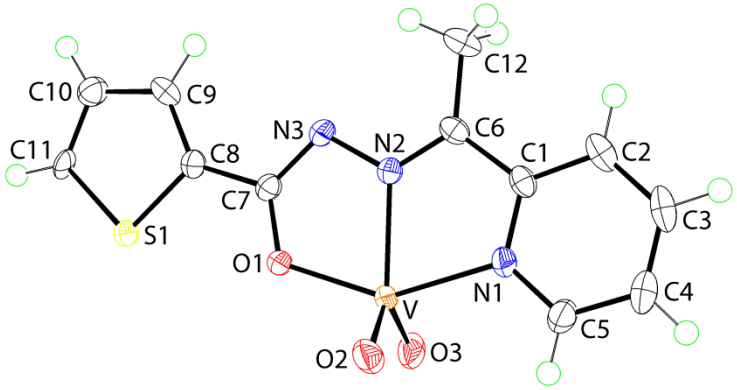

Figure 6.1. The molecular structure of $[VO_2L^1]$ (**1**), showing the atom-labelling scheme and 70% displacement ellipsoids. Only the major component of the disordered thienyl ring is shown.

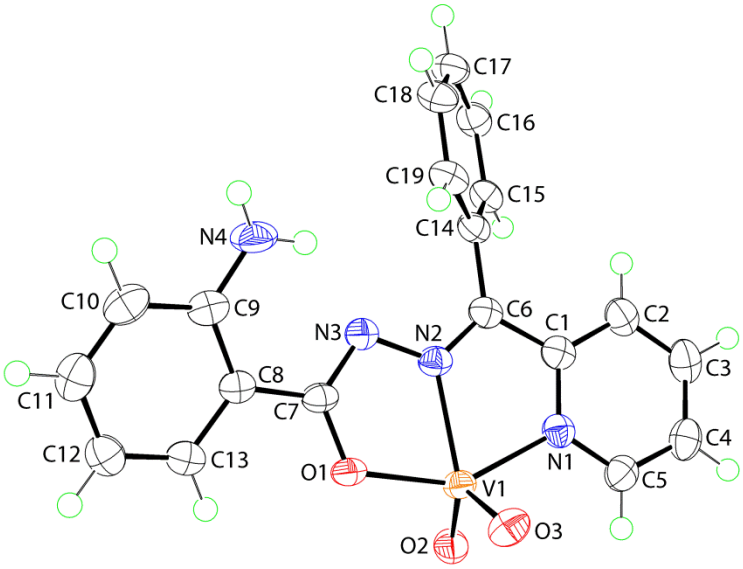

Figure 6.2. The molecular structure of one of the two independent molecules comprising the asymmetric unit of $[VO_2L^2]$ (**2**), showing atom-labelling scheme and 70% displacement ellipsoids

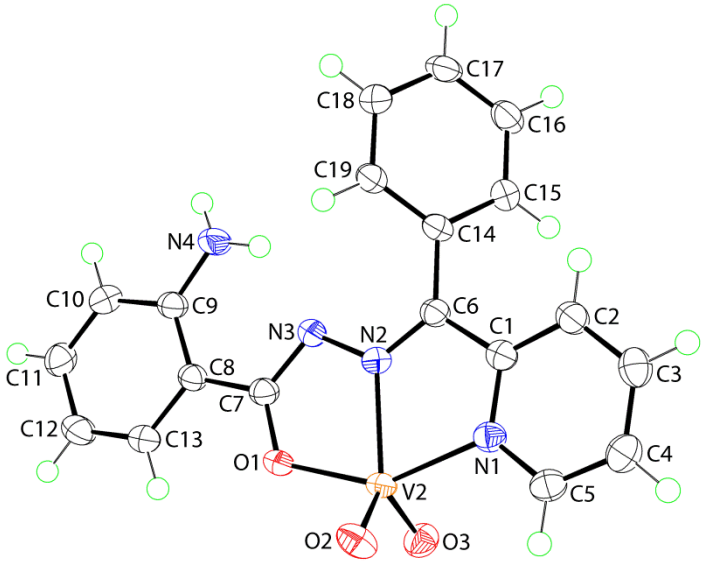

(a)

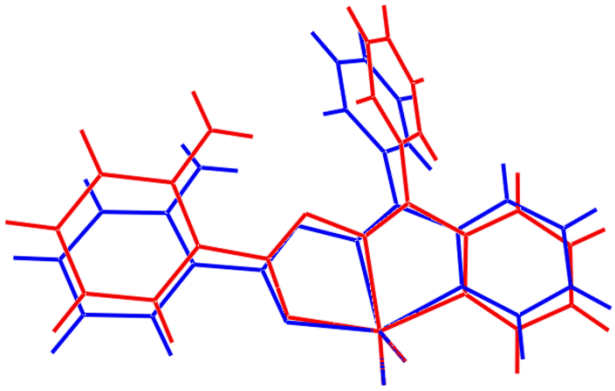

(b)

Figure 6.3. (a) The molecular structure of the second of the two independent molecules comprising the asymmetric unit of $[VO_2L^2]$ (**2**) showing the atom-labelling scheme and 70% displacement ellipsoids. Atoms are further designated with a suffix "a"; and (b) overlay diagram of the two independent molecules with the molecule containing the V1 atom shown in red. The molecules have been overlapped so that the $V(=O)_2$ units are superimposed.

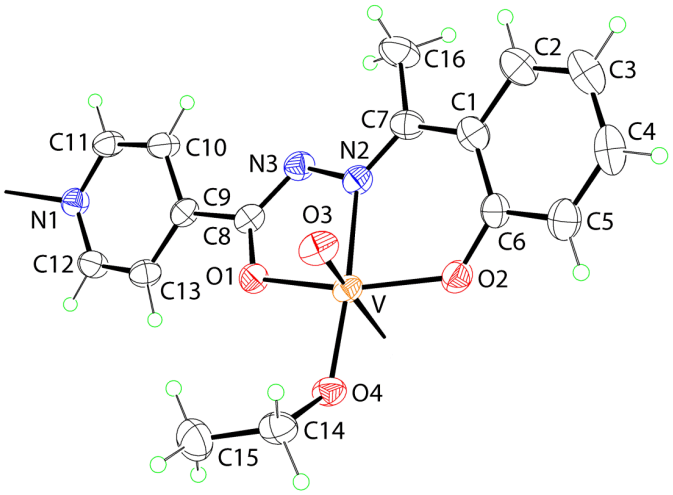

(a)

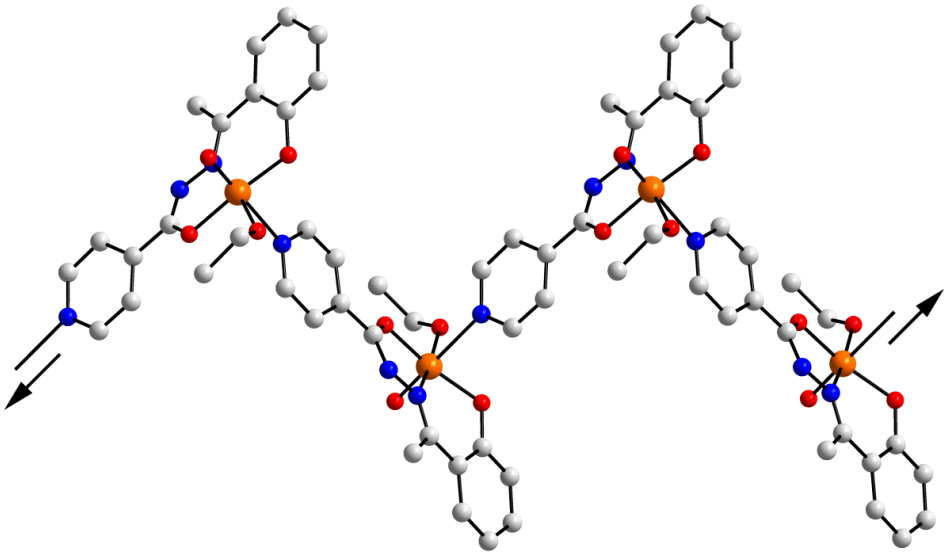

(b)

Figure 6.4. (a) The asymmetric unit in [VOL^{3}(OEt)] (**3**), showing the atom-labelling scheme and 35% displacement ellipsoids. The coordination geometry of the vanadium atom has been extended to indicate the V−N1 bonds that generate the helical polymer along the c-axis, shown in (b).

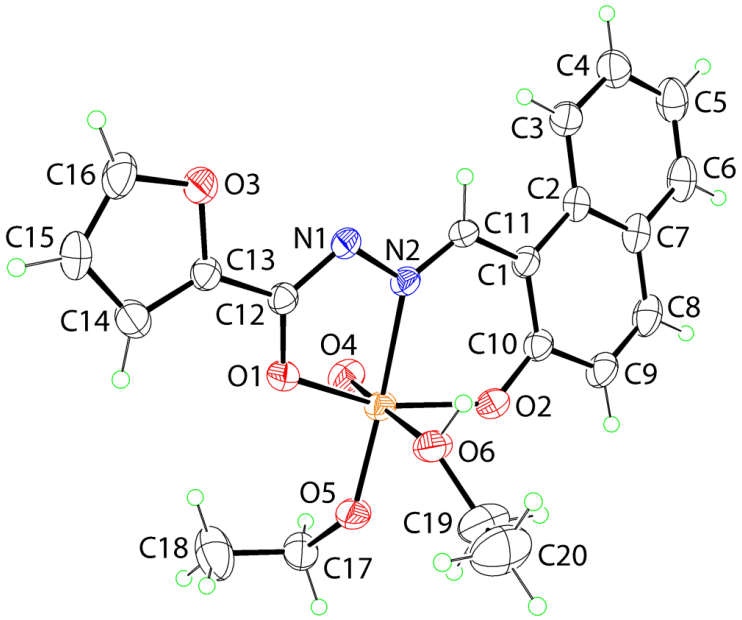

Figure 6.5. The molecular structure of one of the two independent molecules comprising the asymmetric unit of [VOL^4(OEt)EtOH)] (**4**), showing atom-labelling scheme and 70% displacement ellipsoids.

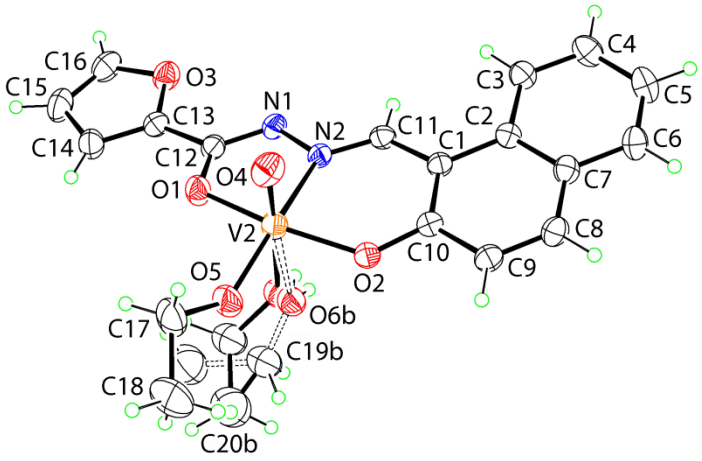

(a)

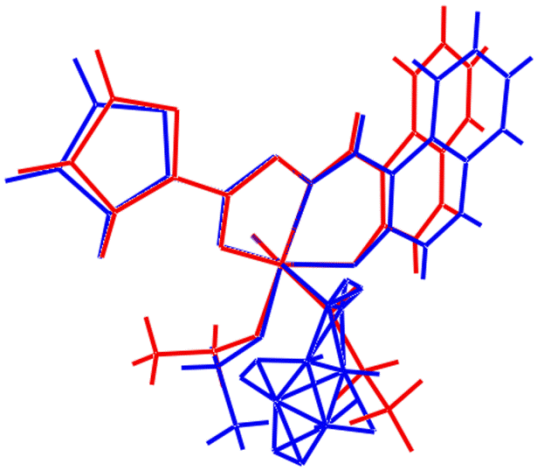

(b)

Figure 6.6. (a) The molecular structure of the second of the two independent molecules comprising the asymmetric unit of [VOL^4(OEt)EtOH)] (**4)** showing the atom-labelling scheme and 70% displacement ellipsoids. Atoms are further designated with a suffix "a". The coordinated ethanol molecule is statistically disordered over two positions. The atoms comprising the second orientation of the disordered ethanol molecule are additionally labelled with a suffix "b" and are highlighted with dashed bonds; and (b) overlay diagram of the two independent molecules with the molecule containing the V1 atom shown in red; the inverted V2-containing molecule is shown for a better match. The molecules have been overlapped so that the V, O4 and N2 atoms are superimposed.

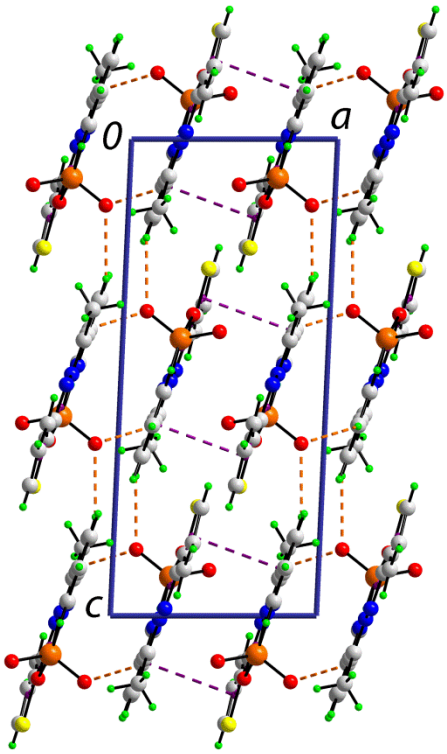

Figure 6.7. A view of the unit cell contents for $[VO_2L^1]$ (**1**) in projection down the b-axis. The C–H…O [C2–H2...O3^{i} = 2.57 Å, C2...O3^{i} = 3.413(2) Å, angle at H2 = 147° for symmetry operation i: x, ½-y, -½+z; and C4–H4...O3^{ii} = 2.53 Å, C4...O3^{ii} = 3.183(2) Å, angle at H4 = 126° for ii: 2-x, 1-y, -z] and π…π interactions [Cg(S1,C8-C11)…Cg(N1,C1-C5)^{iii} = 3.625(2) Å, angle of inclination = 4.96(19)° for iii: 1-x, -y, -z] are shown as orange and purple dashed lines, respectively. The 2-thienyl ring is disordered over two co-planar conformations and the complementary Cg(S1b,C8b-C11b)…Cg(N1,C1-C5)^{iii} separation is 3.666(12) Å and the angle of inclination is 4.3(12)º.

(a)

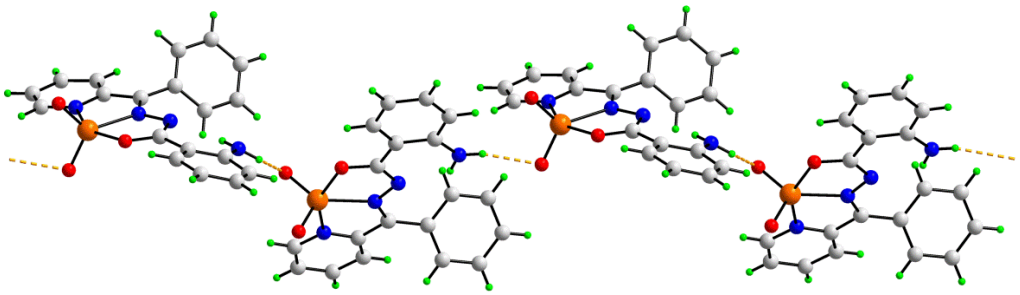

(b)

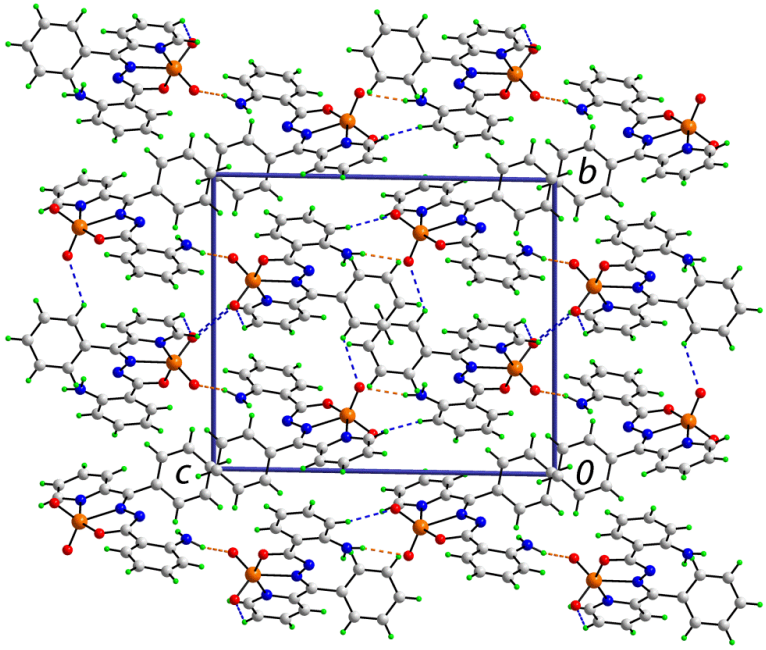

Figure 6.8. Crystal packing in $[VO_2L^2]$ (**2**): (a) a view of the supramolecular chain comprising alternating V1- and V2-containing molecules sustained by N–H…O hydrogen bonding [N4–H1n...O2a^{i} = 2.406(19) Å, N4...O2a^{i} = 3.063(2) Å, with angle at H1n = 132.1(18)° for symmetry operation i: 1-x, 1-y, -z; N4a–H3n...O3^{ii} = 2.259(14) Å, N4a...O3^{ii} = 3.033(2) Å, with angle at H3n = 148.6(19) for symmetry operation ii: -x, 1-y, 1-z], shown as blue dashed lines; and (b) a view of the unit cell contents in projection down the a-axis. The C–H…O [C4a–H4a3...O3a^{iii} = 2.50 Å, C4a...O3a^{iii} = 3.149(2) Å, angle at H4a3 = 126° for symmetry operation iii: 1-x, -y, -z; C5a–H5a...O3a^{i} = 2.55 Å, C5a...O3a^{i} = 3.178(2) Å, angle at H5a = 124°; C10a–H10a...O2^{ii} = 2.47 Å, C10a...O2^{ii} = 3.283(2) Å, angle at H10a = 143°; and C15a–H15a...O3 = 2.57 Å, C15a...O3 = 3.235(2) Å, angle at H15a = 127°] interactions are shown as orange dashed lines.

(a)

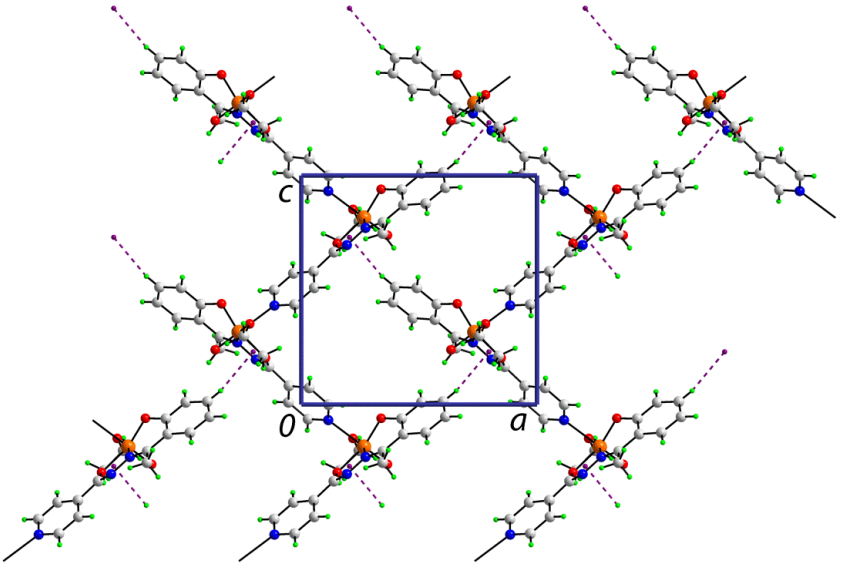

(b)

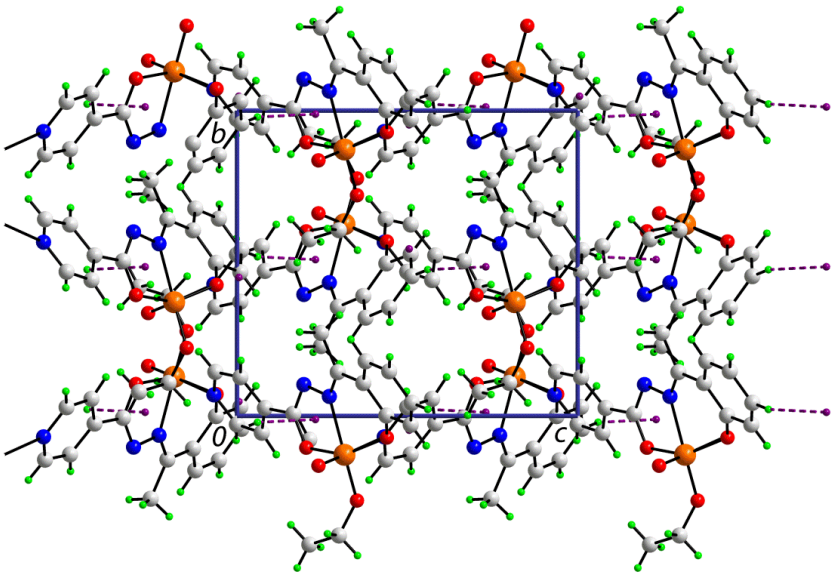

Figure 6.9. Crystal packing in [VOL^3(OEt)] (**3**): (a) a view of the supramolecular layer in the ac-plane whereby the supramolecular chains are linked C–H…π(chelate) ring interactions [C4–H4...π(V,O1,N2,N3,C8)^i = 2.68 Å, C4...π(V,O1,N2,N3,C8)^i = 3.582(4) Å, with angle at H4 = 164° for symmetry operation i: 1-x, 2-y, ½+z] shown as purple dashed lines, and (b) a view of the unit cell contents in projection down the a-axis showing the ...ABA... pattern of supramolecular layers stacked along the b-axis.

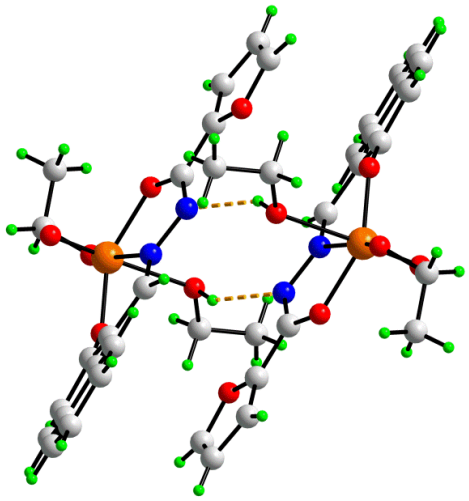

(a)

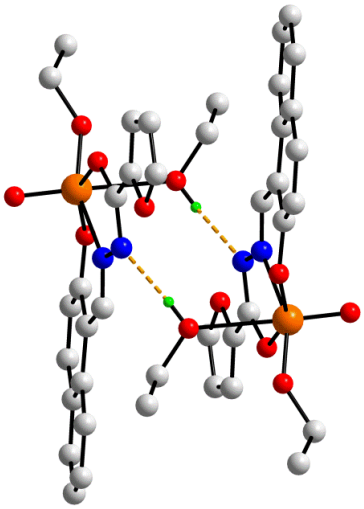

(b)

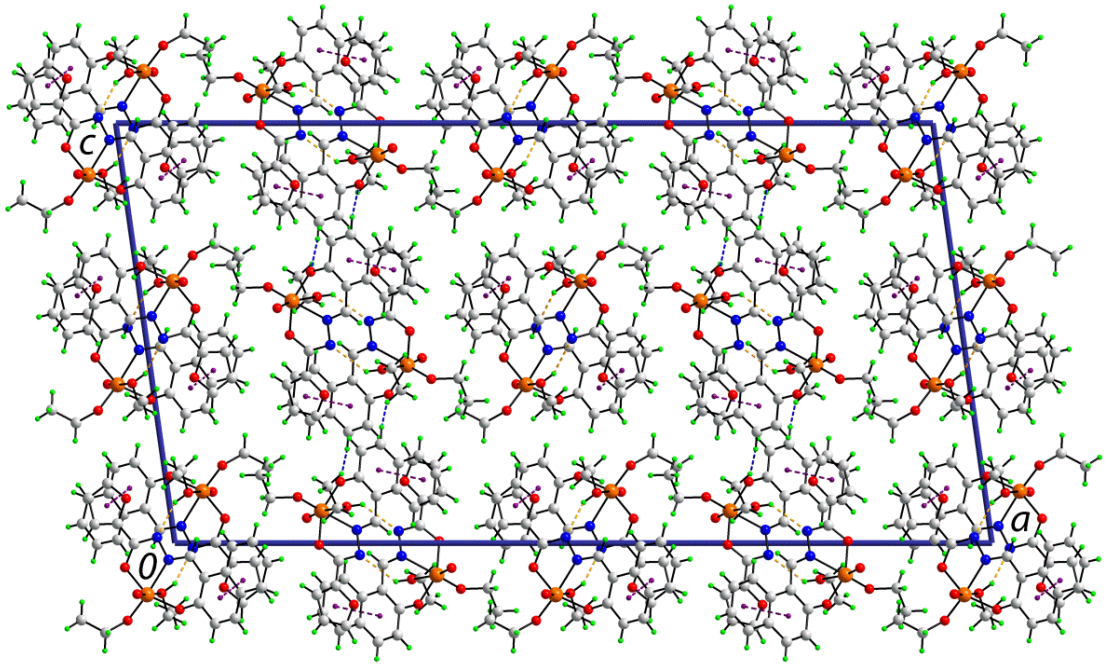

(c)

Figure 6.10. Crystal packing in [VOL^4(OEt)EtOH)] (**4**): (a) a view of the two-molecule aggregate whereby centro symmetrically related V1-containing molecules are linked by ethanol-O–H…N hydrogen bonds, (b) equivalent dimer formed by the V2-containing molecule; second orientation of the disordered ethanol molecule and all non-participating hydrogen atoms removed for clarity [O6–H6o...N1^{i} = 2.12 Å, O6...N1^{i} = 2.873(3) Å, with angle at H6o = 149° for symmetry operation i: -x, 1-y, 1-z; O6a–H6oa...N1a^{ii} = 2.31 Å, O6a...N1a^{ii} = 2.95(2) Å, with angle at H6oa = 136° for symmetry operation ii: ½-x, ½-y, -z; for the second disordered conformation: O6b–H6ob...N1a^{ii} = 2.20 Å, O6b...N1a^{ii} = 2.99(2) Å, with angle at H6ob = 164°] shown as orange dashed lines, and (c) a view of the unit cell contents in projection down the b-axis showing the stacking of alternating layers of V1- and V2-containing molecules along the a-axis. The C–H…O [C8a–H8a...O2a^{iii} = 2.57 Å, C8a...O2a^{iii} = 3.398(4) Å, with angle at H8a = 149° for symmetry operation iii: ½-x, ½+y, ½-z] and π...π [Cg(O3,C13-C16)…Cg(C1,C2,C7-C10)^{i} = 3.702(2) Å, angle of inclination = 13.45(19)°; Cg(O3a,C13a-C16a)…Cg(C1a,C2a,C7a-C10a)^{ii} = 3.641(2) Å, angle of inclination = 8.64(18)°] interactions are shown as blue and purple dashed lines, respectively.

6.3.4. DNA binding studies.

6.3.4.1. Absorption spectroscopic studies. The binding propensity of **1**–**4** to CT-DNA was studied using different spectroscopic techniques. Complexes **1**–**4** show absorption bands in the regions 440–400 and 340–300 nm which are attributed to L–V(dπ) LMCT and intra-ligand transitions, respectively.[60a] UV-Vis titration experiments were carried out to determine the equilibrium binding constant (K_b) of the complexes to CT-DNA (**Table 6.3** and **Figure 6.11**). Upon addition of CT-DNA the UV-Vis absorption bands in the region 340–300 nm showed a hypochromic shift for **1** whereas **2**–**4** exhibited hyperchromism (**Figure 6.11**), indicating interaction between each complex and CT-DNA. The binding affinity of the interaction between CT-DNA and each of **1**–**4** is indicated by the binding constant, K_b, which was calculated using the following equation[36e]:

$$\frac{[\mathrm{DNA}]}{\varepsilon_a - \varepsilon_f} = \frac{[\mathrm{DNA}]}{\varepsilon_b - \varepsilon_f} + \frac{1}{K_b(\varepsilon_b - \varepsilon_f)} \qquad \textbf{Eq. 1}$$

where [DNA] is the concentration of DNA base pairs, ε_a, ε_f, and ε_b correspond to apparent extinction coefficient for the complex i.e. Abs/[complex] in presence of DNA, in absence of DNA and to fully bound DNA, respectively. A plot of [DNA]/(ε_a -ε_f) vs [DNA] gave a slope and intercept equal to 1/(ε_b - ε_f) and 1/K_b(ε_b - ε_f), respectively; K_b is calculated from the ratio of the slope to the intercept. The data reported in **Table 6.3** reveal K_b has values for **1**–**4** from 1.13×10^5 to 5.03×10^3 M^{-1} with the order of DNA binding strength being **2 > 1 > 3 > 4**. These results suggest that **1**–**4** binds CT-DNA through the groove binding mode. The binding affinity of the ligands to CT-DNA were also estimated and gave values lower than their corresponding complexes (**Table 6.4**).

Table 6.3. DNA binding parameters for 1–4.

Complex	Binding constant (K_b)[a] (M^{-1})	ΔT_m[b] (^oC)
1	8.56×10^4	+1.31
2	1.13×10^5	+1.83
3	4.95×10^4	+1.32
4	5.03×10^3	-1.70

[a] DNA binding constants were determined by the UV-Vis spectral method.

[b] Change in the melting temperature of CT-DNA.

Table 6.4. DNA binding parameters for Ligands.

Ligand	Binding constant (K_b) (M^{-1})
HL[1]	7.42×10^3
HL[2]	3.88×10^3
H_2L[3]	2.91×10^4
H_2L[4]	2.48×10^3

[a] The DNA binding constant was determined by the UV-Vis spectral method.

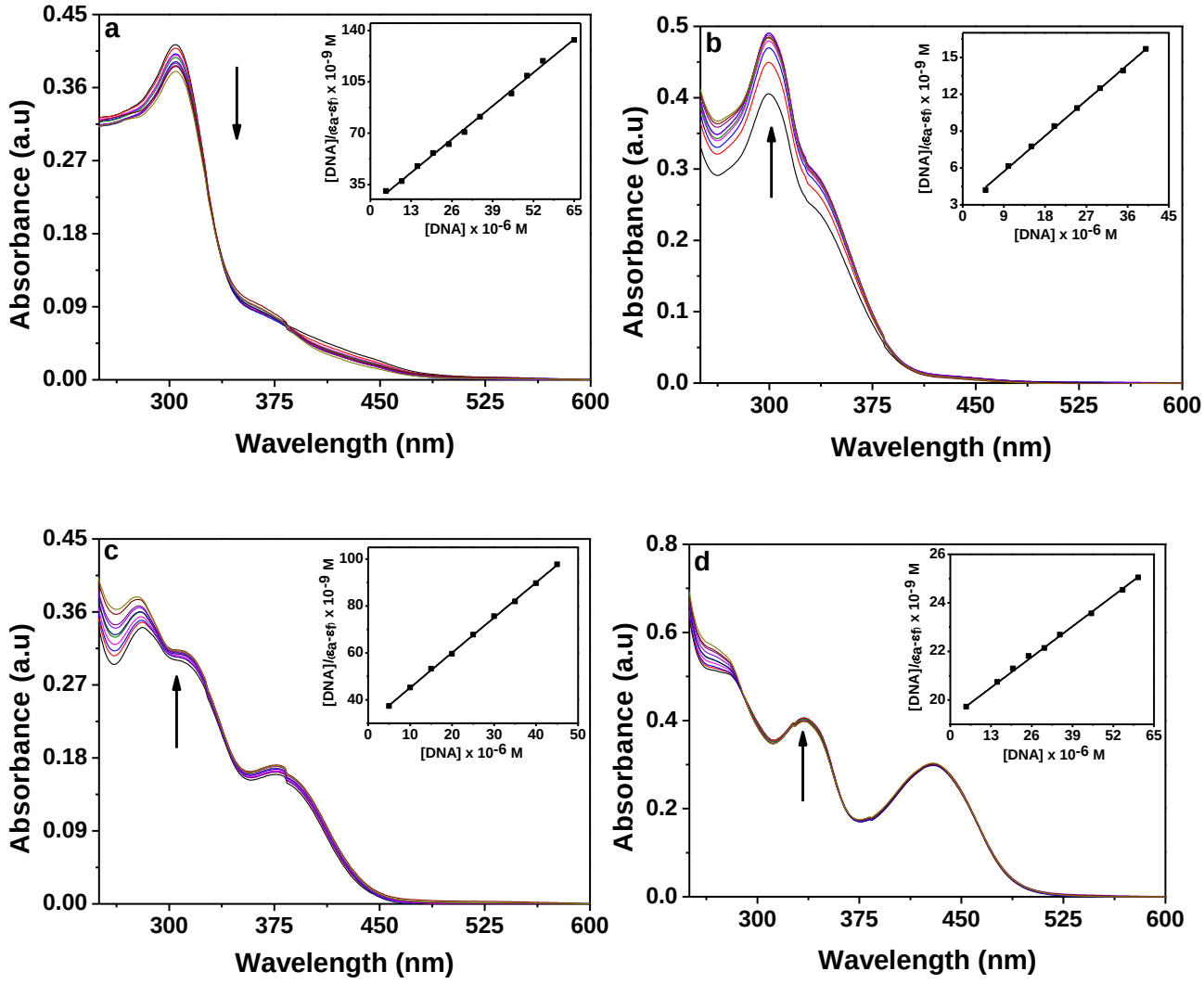

Figure 6.11. Electronic absorption spectra of **1** (a), **2** (b), **3** (c), and **4** (d) (25 μM each) upon the titration of CT-DNA (0 – 70 μM) in 10 mM Tris-HCl buffer (pH 8.0) containing 1% DMF. Arrow shows the changes in absorbance with respect to an increase in the CT-DNA concentration. The inset shows the linear fit of $[DNA]/(\varepsilon_a - \varepsilon_f)$ vs [DNA] and the binding constant (K_b) was calculated using **Eq. 1**.

6.3.4.2. Thermal denaturation studies. To investigate whether the stability of DNA alters upon interaction with the complexes, DNA melting experiments were performed in the absence and presence of **1**–**4.**[57] The midpoint transition temperature or melting temperature (T_m) of CT-DNA in absence of any complex is ~65.7 °C. The T_m increased very slightly (~1.3–1.8 °C) upon interaction with **1**–**3** whereas **4** showed a slight decrease (1.7 °C) in the thermal melting of CT-DNA (**Figure 6.12.** and **Table 6.3**). The low ΔT_m values for **1**–**3** primarily suggest groove binding of the complexes to CT-DNA rather than an intercalative mode of binding to DNA which usually gives a large positive ΔT_m value.[77,78] The slight negative ΔT_m value of -1.70 °C for **4** (**Figure 6.12.** and **Table 6.3**) may be due to the destabilisation of the DNA double helix by this complex.[79]

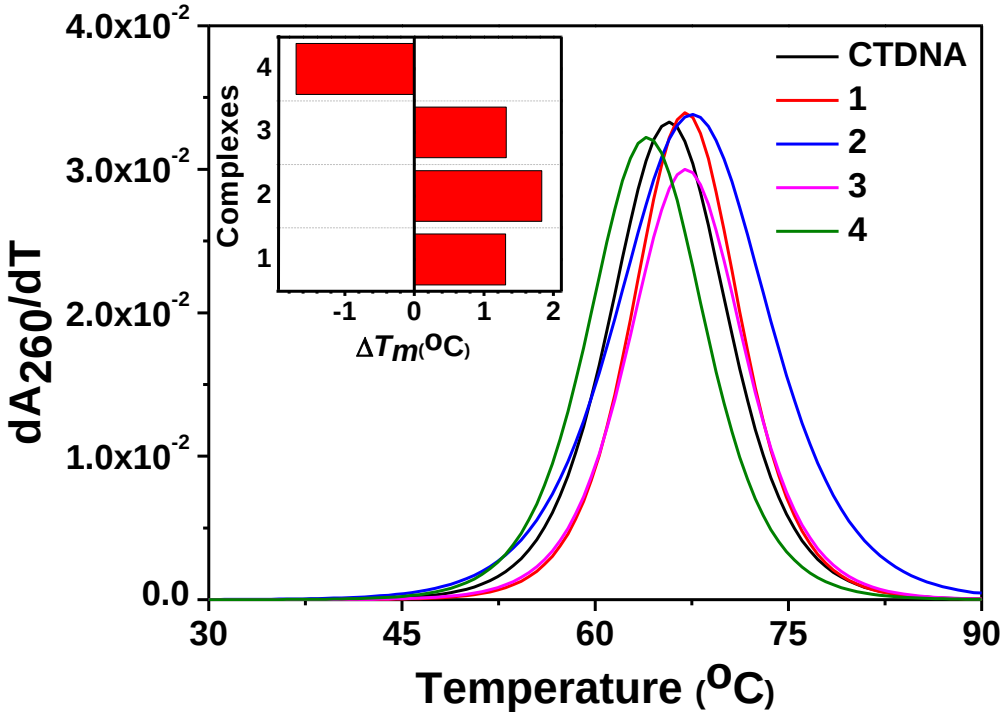

Figure 6.12. Derivative plot of thermal denaturation of CT-DNA (160 μM) in the absence and presence of **1**–**4** (150 μM). The experiment was done in 10 mM Tris-HCl buffer (pH 8.0) containing 1% DMF. Inset shows the ΔT_m (^oC) of the complexes as compared to CT-DNA.

6.3.5. DNA cleavage studies.

6.3.5.1. Chemical-induced DNA cleavage. The DNA cleavage activity of the complexes **1**–**4** (1-500 μM) was studied in the dark in the presence of hydrogen peroxide (500 μM) as the oxidising agent using supercoiled pUC19 DNA (300 ng) in 50 mM Tris-HCl buffer (pH 8.0) containing 1% DMF. The complexes do not show any chemical-induced DNA cleavage activity .

6.3.5.2. Photo-induced DNA cleavage. To investigate whether the DNA binding properties of the complexes were accompanied with photo-nuclease activity, a photo-induced DNA cleavage activity assay was performed. Photo-induced DNA nuclease activity of **1**–**4** was studied using supercoiled (SC) pUC19 DNA in 50 mM Tris-HCl buffer (pH 8.0) containing 1% DMF, upon irradiation of UVA light of 350 nm in the presence and absence of the complexes (**Figure 6.13**). The percentage of net DNA cleavage by the complexes was estimated using the following equation:

$$\text{Net DNA cleavage } \% = \frac{\text{Form IIs} + 2 \times \text{Form IIIs}}{\text{Form Is} + \text{Form IIs} + 2 \times \text{Form IIIs}} - \frac{\text{Form IIc} + 2 \times \text{Form IIIc}}{\text{Form Ic} + \text{Form IIc} + 2 \times \text{Form IIIc}} \qquad \textbf{Eq. 2}$$

The subscripts "s" and "c" refers to the sample and control, respectively.[80] The net DNA cleavage by **1**–**4** was plotted in a concentration dependent manner (**Figure 6.14**). Approximately 10% DNA cleavage was observed in the presence of 10 μM of **1**–**4** (**Figure 6.14**, inset). The cleavage activity was saturated for each of the complexes at a concentration of 100 μM. At this concentration, the photo-nuclease activity of **1**, **2**, **3** and **4** was 50, 33, 65 and 45%, respectively, indicating that **3** has the highest photo-nuclease activity over the series. The photo-induced DNA cleavage experiments were also carried out with phosphate buffer returning similar activity as for the experiments in tris buffer, an observation in accord with previous studies with dioxido vanadium complexes.[47] Control experiments revealed that neither DMF (1%) nor the ligand molecules showed any photo-induced DNA cleavage activity, implying that DMF and the ligands are cleavage inactive under similar conditions.

In order to understand the mechanistic pathways involved in the photo-cleavage reactions, the photo-induced DNA cleavage activity of **1**–**4** was investigated in the presence of various additives. The DNA cleavage reaction involving molecular oxygen can proceed in two

mechanistic pathways: (a) a type-II process involving singlet oxygen species ($^1O_2$), or (b) by a photo-redox pathway involving reactive hydroxyl radicals (OH).[81] The addition of NaN_3 (singlet oxygen quencher) inhibited the DNA cleavage activity of **1**, **3** and **4** by 8, 14 and 10 %, respectively (**Figure 6.15**). By contrast, the other singlet oxygen quencher (L-histidine) slightly inhibited the photo-induced DNA cleavage activity of complexes **1**, **3** and **4**. Surprisingly, it was observed that the DNA cleavage activity of **2** did not alter in the presence of these two additives. The hydroxyl radical scavenger, KI, inhibited the photo-nuclease activity of **1**, **3** and **4** by 10, 15 and 13 %, respectively, whereas the other hydroxyl radical scavenger D-mannitol inhibited the DNA cleavage activity of these three complexes moderately. However it is to mention that no inhibition of DNA cleavage was observed for **2** in the presence of these two additives (**Figure 6.15**). Therefore, it is concluded that **1**, **3** and **4** exhibit photo-induced DNA cleavage activity via both singlet oxygen and hydroxyl radical pathways, while the mechanistic pathways involved in the photo-induced DNA cleavage by **2** cannot be stated with certainty.

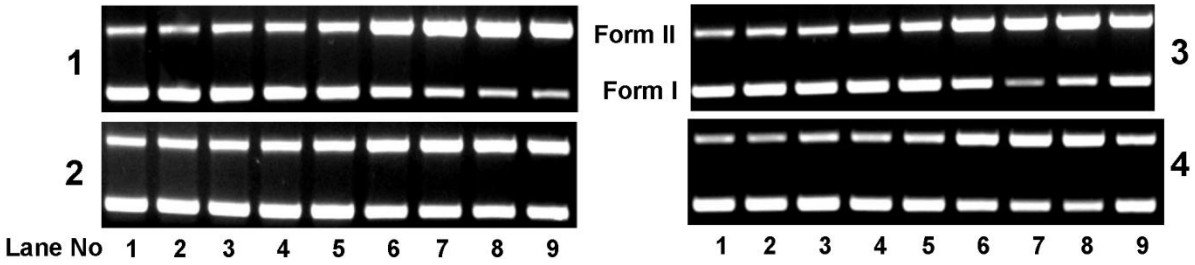

Figure 6.13. Gel diagram showing concentration dependent DNA cleavage by **1**–**4**; 300 ng of SC pUC19 DNA at different concentrations of the complexes [1–500 µM in 50 mM Tris-HCl buffer (pH 8.0) containing 1% DMF] was photo-irradiated with UVA at 350 nm for 3 h. Lanes **1**–**9**: 1, 2.5, 5.0, 7.5, 10, 50, 75, 100 and 500 µM of **1**–**4**.

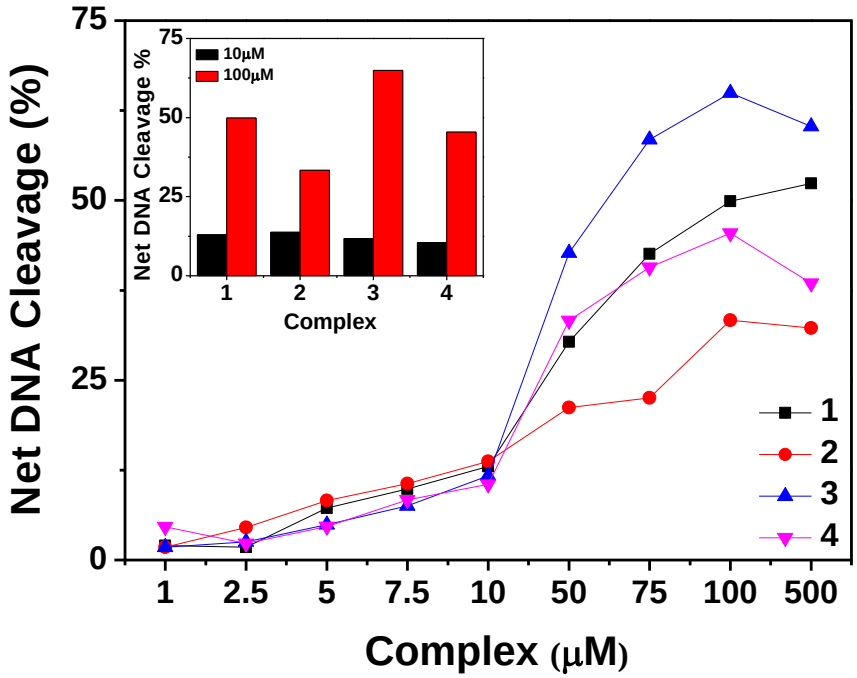

Figure 6.14. Concentration dependent DNA cleavage by **1**–**4**; 300 ng of SC pUC19 DNA at different concentration of the complexes [1–500 µM in 50 mM Tris-HCl buffer (pH 8.0) containing 1% DMF] was photo-irradiated with UVA at 350 nm for 3 h. The net DNA cleavage percent was calculated using Eq. 2. Inset shows a bar diagram representation of the net DNA cleavage of different complexes at 10 and 100 µM.

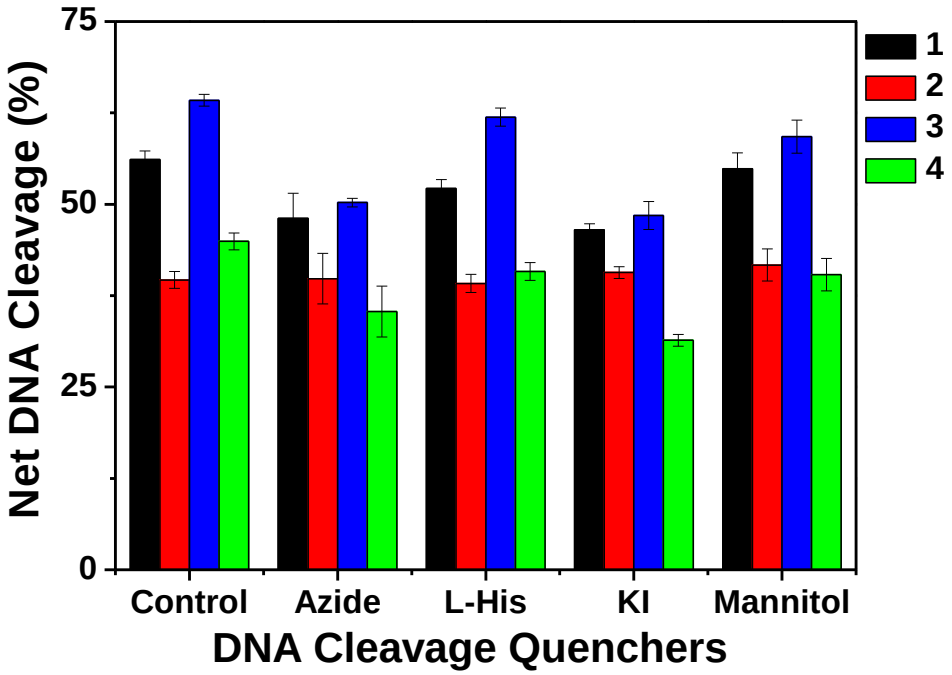

Figure 6.15. DNA cleavage of SC pUC19 DNA by **1**–**4** in presence of various additives in 50 mM Tris-HCl buffer (pH 8.0) containing 1% DMF. SC pUC19 DNA (300 ng) in the presence of various additives was photo-irradiated at 350 nm for 3 h with **1**–**4** (100 μM). The additive concentrations were: sodium azide (0.5 mM), L-histidine (0.5 mM), KI (0.5 mM) and D-mannitol (0.5 mM).

6.3.6. Cytotoxicity studies.

6.3.6.1. MTT assay. The in vitro cytotoxicities of **1**–**4** were evaluated by the MTT assay against the cervical cancer cell line HeLa; the IC_{50} values are presented in **Table 6.5**. The species HL^{1-2}, H_2L^{3-4} and $VO(acac)_2$ gave high IC_{50} values of > 200 μM, whereas **1**–**4** gave values in the range 10–20 μM. Under the same experimental conditions, the commonly used chemotherapeutic drugs cisplatin, gefitinib, gemcitabine, 5-fluorouracil and vinorelbine are comparably effective in HeLa cells with IC_{50} values of 13, 20, 35, 40 and 48 μM, respectively.[82] The significant decrease in the inhibitory ability of the ligand molecules as well as their lower binding affinity to CT-DNA compared to their metal complexes clearly indicates that incorporation of vanadium has a marked effect on cytotoxicity. A possible explanation is that by coordination, the polarity of the ligand and the central metal ion are reduced through charge equilibration which favours permeation of the complexes through the lipid layer of the cell membrane.[83,84] The results of DNA binding/cleavage ability for the ligands have been considered and are consistent with the observation that metal complexes can exhibit greater biological activities than the free ligands.[85]

Within the series **1**–**4**, the cytotoxicities of **1**, **2** and **3** are approximately similar whereas **4** is more potent, **Table 6.5**. Their dose dependencies are illustrated in **Figure 6.16**. The variation in cytotoxicity may be affected by the various functional groups attached to the aroylhydrazone derivative. Very recently, the anti-proliferative activity of some vanadium complexes were reported by Yamaguchi et al.[86] and us[32,47] using U937 cells and HeLa cells, respectively. The present results are in accord with these results.

6.3.6.2. Nuclear Staining Assay. To investigate the apoptotic potential of the test complexes in HeLa cells, DAPI staining was performed. Chromatin condensation during the process of apoptosis (type I programmed cell death) is a characterising marker of nuclear alteration. HeLa cells were treated with 18, 15, 16, and 5μM of **1**–**4**, respectively. The cells were incubated for 24 h before DAPI nuclear staining and were examined under a fluorescent microscope fitted with a DAPI filter. As shown in **Figure 6.17**, control cells (treated with 10% (v/v) DMF) hardly showed any sort of condensation in comparison to the treated cells. All images, taken in gray-scale, demonstrate the brightly condensed chromatin bodies and the nuclear blebbings as marked by

arrows in **Figure 6.17**. Besides showing nuclear change, the treated cells exhibited a shrinking morphology which is another important hallmark of apoptosis.

Table 6.5. Cytotoxic scores in HeLa cancer cells for 1–4.

Complex	IC_{50} (μM)
1	20±4.52
2	18±3.38
3	19.5±3.54
4	9.9±3.18

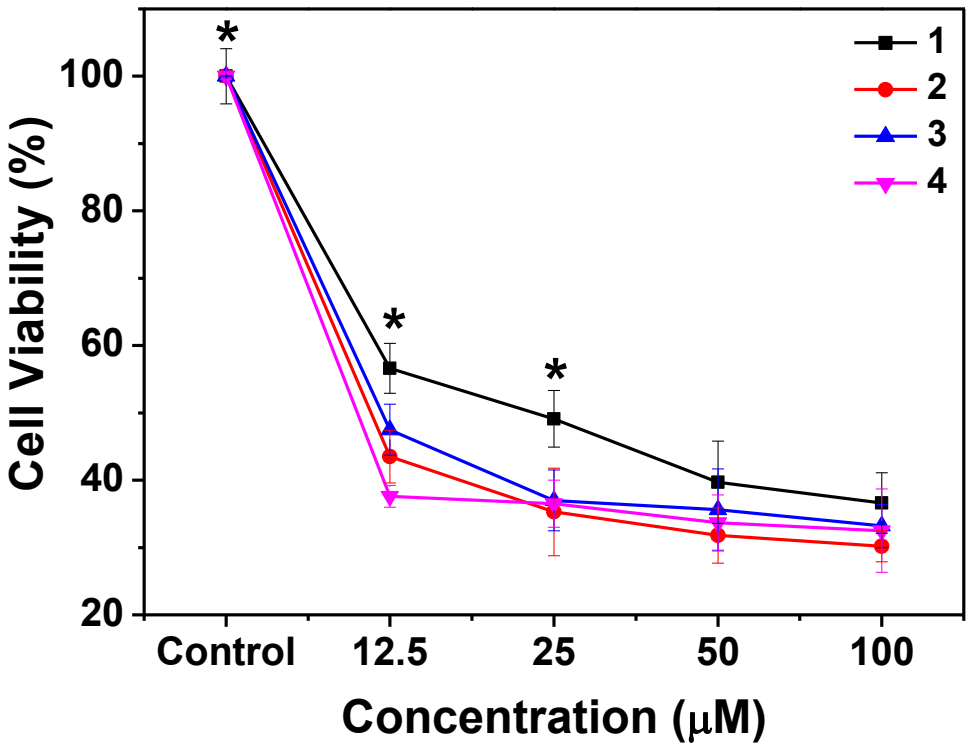

Figure 6.16. Effect of **1**–**4** on cell viability and growth: HeLa cells were treated with different concentrations of the test compound for 72 h and then cell viability was measured by MTT assay. Data are reported as the mean ± S.D. for *n* = 6 and compared against 10% (v/v) DMF treated control by using a Student's *t*-test. (*significant compared to control).

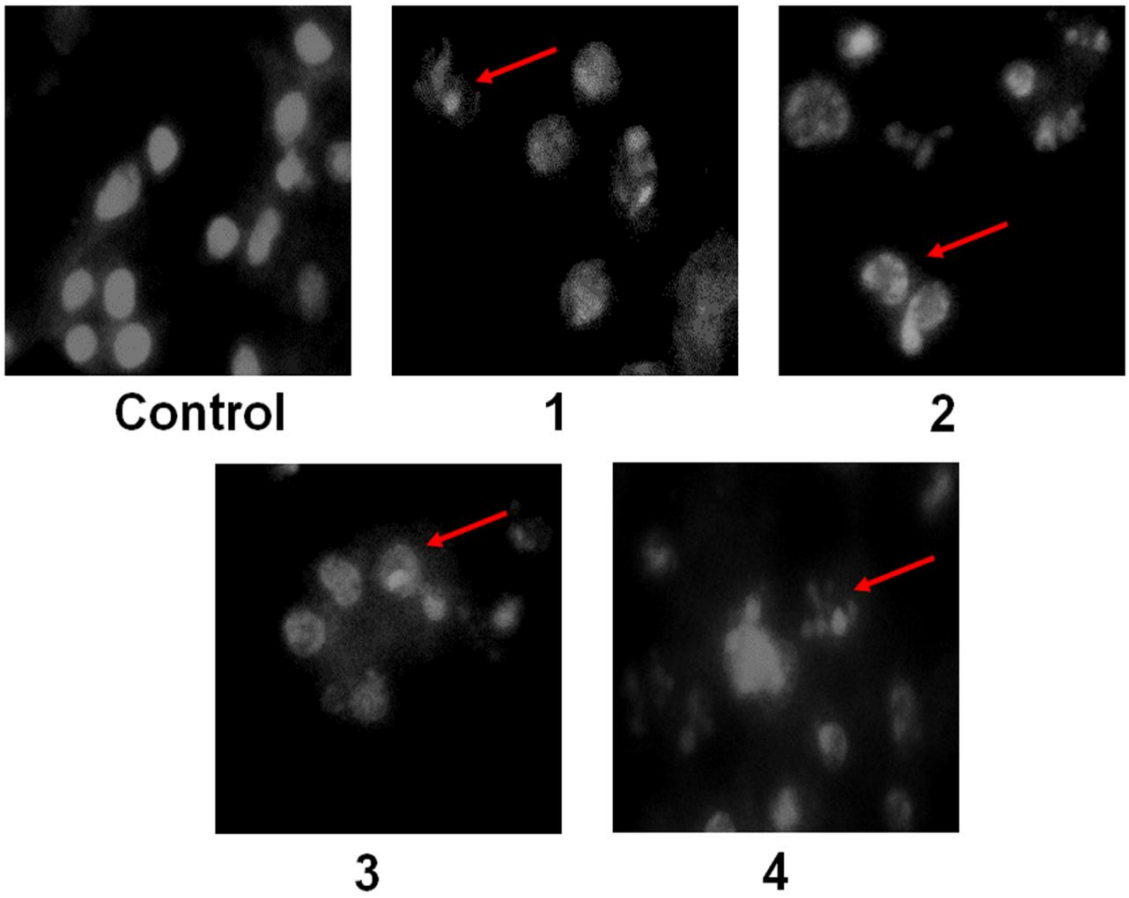

Figure 6.17. Study of apoptosis by morphological changes in nuclei of HeLa cells: HeLa cells, from control and treated groups, were fixed with 3.7% formaldehyde for 15 min, permeabilised with 0.1% Triton X-100 and stained with 1 µg/ml DAPI for 5 min at 37 °C. The cells were then washed with PBS and examined by fluorescence microscopy (Olympus IX 71) (200×). HeLa cells were treated with 18, 15, 16, and 5 µM of complexes **1**–**4**, respectively. Arrows showing the morphological changes in nuclei of HeLa cells observed on application of **1**–**4** in comparison to the control group treated with 10% (v/v) DMF.

6.4. CONCLUSION

The synthesis and characterisation of four neutral oxido vanadium(V) complexes (**1**−**4**) with bioactive hydrazone scaffolds containing furan, thiophene and pyridine residues has been achieved. X-ray crystallography confirm the spectroscopic analyses and show N_2O_3 five-coordinate geometries, distorted toward square pyramidal, for each of **1** and **2**. The dianion in **3** is tetradentate as the pyridyl-N atom also bridges a second V atom leading to a helical coordination polymer and an N_2O_4 octahedral geometry. A NO_5 octahedral geometry is found in mononuclear **4**. Biological studies reveal that the oxido vanadium(V) complexes (**1**–**4**) show considerable DNA binding propensity. DNA binding activities were investigated using UV-Vis absorption titration and thermal denaturation studies, and shows that the complexes interact with CT-DNA by a minor groove binding mode, with binding constants ranging from 10^3–10^5 M^{-1}. All complexes show good photo-induced cleavage of pUC19 supercoiled plasmid DNA with **3** showing the highest photo-induced DNA cleavage activity of ~65%. The results from the mechanistic study suggested that the photolytic DNA cleavage of **1**, **3** and **4** preceded possibly via both singlet oxygen and hydroxyl radical pathways. Additionally, the cytotoxic activities of **1**–**4** were evaluated against human cervical cancer cell lines (HeLa). All are appreciably cytotoxic compared with standard drugs (cisplatin, gefitinib, gemcitabine, 5-fluorouracil and vinorelbine) with IC_{50} values ranging from 10 to 20 μM. This potency correlates with the presence of a bioactive heterocycle attached to the hydrazone moiety. Despite having a lower binding affinity, the higher cytotoxicity of **4** may be due to the destabilising interaction between the complex and the DNA as evidenced from the thermal denaturation data. The results reported herein will inspire further work on oxido vanadium(V) complexes for the development of metal-based agents for anti-cancer applications.

6.5. REFERENCES

(1) Maldonado, C. R.; Salassa, L.; Blanco, N. G.; Rivas, J. C. M. *Coord. Chem. Rev.* **2013**, *257*, 2668.

(2) Almeida, A.; Oliveira, B. L.; Correia, J. D. G.; Soveral, G.; Casini, A. *Coord. Chem. Rev.* **2013**, *257*, 2689.

(3) Easmon, J.; Pürstinger, G.; Heinisch, G.; Roth, T.; Fiebig, H. H.; Holzer, W.; Jäger, W.; Jenny, M.; Hofmann, J. *J. Med. Chem.* **2001**, *44*, 2164.

(4) Mishra, A.; Kaushik, N. K.; Verma, A. K.; Gupta, R. *Eur. J. Med. Chem.* **2008**, *43*, 2189.

(5) Arjmand, F.; Mohani, B.; Ahmad, S. *Eur. J. Med. Chem.* **2005**, *40*, 1103.

(6) Hoonur, R. S.; Patil, B. R.; Badiger, D. S.; Vadavi, R. S.; Gudasi, K. B.; Dandawate, P. R.; Ghaisas, M. M.; Padhye, S. B.; Nethaji, M. *Eur. J. Med. Chem.* **2010**, *45*, 2277.

(7) Bakale, R. P.; Naik, G. N.; Mangannavar, C. V.; Muchchandi, I. S.; Shcherbakov, I. N.; Frampton, C.; Gudasi, K. B. *Eur. J. Med. Chem.* **2014**, *73*, 38.

(8) (a) Hafez, H. N.; El-Gazzar, A. B. A. *Bioorg. Med. Chem. Lett.* **2008**, *18*, 5222. (b) Fujita, M.; Hirayama, T.; Ikeda, N. *Bioorg. Med. Chem.* **2002**, *10*, 3113. (c) Chaviara, A. T.; Kioseoglou, E. E.; Pantazaki, A. A.; Tsipis, A. C.; Karipidis, P. A.; Kyriakidis, D. A.; Bolos, C. A. *J. Inorg. Biochem.* **2008**, *102*, 1749. (d) Zhu, Y.; Zhou, J. *ACS Med. Chem. Lett.* **2012**, *3*, 844.

(9) (a) Laraia, L.; Stokes, J.; Emery, A.; McKenzie, G. J.; Venkitaraman, A. R.; Spring, D. R. *ACS Med. Chem. Lett.* **2014**, *5*, 598. (b) Yu, Z.; Brannigan, J. A.; Moss, D. K.; Brzozowski, A. M.; Wilkinson, A. J.; Holder, A. A.; Tate, E. W.; Leatherbarrow, R. J. *J. Med. Chem.* **2012**, *55*, 8879.

(10) (a) Xie, W.; Xie, S.; Zhou, Y.; Tanga, X.; Liu, J.; Yang, W.; Qiu, M. *Eur. J. Med. Chem.* **2014**, *81*, 22. (b) Kumar, K. S. S.; Hanumappa, A.; Hegde, M.; Narasimhamurthy, K. H.; Raghavan, S. C.; Rangappa, K. S. *Eur. J. Med. Chem.* **2014**, *81*, 341. (c) Bollinger, S.; Hubner, H.; Heinemann, F. W.; Meyer, K.; Gmeiner, P. *J. Med. Chem.* **2010**, *53*, 7167.

(11) Bharti, N.; Maurya, M. R.; Naqvi, F.; Bhattacharya, A.; Bhattacharya, S.; Azam, A. *Eur. J. Med. Chem.* **2000**, *35*, 481.

(12) Manegold, C.; Gatzemeier, U.; von Pawel, J.; Pirker, R.; Malayeri, R.; Blatter, J.; Krejcy, K. *Ann. Oncol.* **2000**, *11*, 435.

(13) Rosenberg, B.; Camp, L. V.; Trosko, J. E.; Mansour, V. H. *Nature* **1969**, *222*, 385.

(14) Jamieson, E. R.; Lippard, S. J. *Chem. Rev.* **1999**, *99*, 2467.

(15) Wu, Z.; Liu, Q.; Liang, X.; Yang, X.; Wang, N.; Wang, X.; Sun, H.; Luand, Y.; Guo, Z. *J. Biol. Inorg. Chem.* **2009**, *14*, 1313.

(16) Jung, Y.; Lippard, S. J. *Chem. Rev.* **2007**, *107*, 1387.

(17) In: Sigel, H.; Sigel, A. (Eds), Vanadium and its Role in Life, Metal Ions in Biological Systems, vol. 31, Marcel Dekker, New York, **1995**.

(18) Crans, D. C.; Smee, J. J.; Gaidamauskas, E.; Yang, L. *Chem. Rev.* **2004**, *104*, 849.

(19) Tracey, A. S.; Willsky, G. R.; Takeuchi, E. S. *Vanadium Chemistry, Biochemistry, Pharmacology and Practical Applications*, CRC Press, Boca Raton, **2007**.

(20) Rehder, D. *Org. Biomol. Chem.* **2008**, *6*, 957.

(21) Butler, A.; Walker, J. V. *Chem. Rev.* **1993**, *93*, 1937.

(22) Cornman, C. R.; Zovinka, E. P.; Meixner, M. H. *Inorg. Chem.* **1995**, *34*, 5099.

(23) Thompson, K. H.; McNeill, J. H.; Orvig, C. *Chem. Rev.* **1999**, *99*, 2561.

(24) Yasui, H.; Adachi, Y.; Katoh, A.; Sakurai, H. *J. Biol. Inorg. Chem.* **2007**, *12*, 843.

(25) Shechter, Y.; Goldwaser, I.; Mironchik, M.; Fridkin, M.; Gefel, D. *Coord. Chem. Rev.* **2003**, *237*, 3.

(26) Bastos, A. M. B.; da Silva, J. G.; Maia, P. I. S.; Deflon, V. M.; Batista, A. A.; Ferreira, A. V. M.; Botion, L. M.; Niquet, E.; Beraldo, H. *Polyhedron* **2008**, *27*, 1787.

(27) Eady, R. R. *Coord. Chem. Rev.* **2003**, *237*, 23.

(28) Sasmal, P. K.; Patra, A. K.; Chakravarty, A. R. *J. Inorg. Biochem.* **2008**, *102*, 1463.

(29) Patra, S.; Chatterjee, S.; Si, T. K.; Mukherjea, K. K. *Dalton Trans.* **2013**, *42*, 13425.

(30) Xie, M.-J; Niu, Y.-F.; Yang, X.-D.; Liu, W.-P.; Li, L.; Gao, L.-H.; Yan, S.-P.; Meng, Z.-H. *Eur. J. Med. Chem.* **2010**, *45*, 6077.

(31) Khan, N. H.; Pandya, N.; Maity, N. C.; Kumar, M.; Patel, R. M.; Kureshy, R. I.; Abdi, S. H. R.; Mishra, S.; Das, S.; Bajaj, H. C. *Eur. J. Med. Chem.* **2011**, *46*, 5074.

(32) Dash, S. P.; Pasayat, S.; Bhakat, S.; Roy, S.; Dinda, R.; Tiekink, E. R. T.; Mukhopadhyay, S.; Bhutia, S. K.; Hardikar, M. R.; Joshi, B. N.; Patil, Y. P.; Nethaji, M. *Inorg. Chem.* **2013**, *52*, 14096.

(33) Terra, L. H. A.; Areias, M. C.; Gaubeur, I.; Suez-Iha, M. E. V. *Spectrosc. Lett.* **1999**, *32*, 257.

(34) (a) Maurya, M. R.; Agarwal, S.; Abid, M.; Azam, A.; Bader, C.; Ebel, M.; Rehder, D. *Dalton Trans.* **2006**, 937. (b) Savini, L.; Chiasserini, L.; Travagli, V.; Pellerano, C.; Novellino, E. *Eur. J. Med. Chem.* **2004**, *39*, 113. (c) Cui, Z.; Yang, X.; Shi, Y.; Uzawa, H.; Cui, J.; Dohi, H.; Nishida, Y. *Bioorg. Med. Chem. Lett.* **2011**, *21*, 7193.

(35) (a) Easmon, J.; Puerstinger, G.; Thies, K. S.; Heinisch, G.; Hofmann, J. *J. Med. Chem.* **2006**, *49*, 6343. (b) Chaston, T. B.; Watts, R. N.; Yuan, J.; Richardson, D. R. *Clin. Cancer Res.* **2004**, *10*, 7365. (c) Darnell, G.; Richardson, D. R. *Blood* **1999**, *94*, 781. (d) Morgan, L. R.; Jursic, B. S.; Hooper, C. L.; Neumann, D. M.; Thangaraj, K.; LeBlanc, B. *Bioorg. Med. Chem. Lett.* **2002**, *12*, 3407. (e) Hassan, G. S.; Kadry, H. H.; Abou-Seri, S. M.; Ali, M. M.; Mahmoud, A. E. *Bioorg. Med. Chem.* **2011**, *19*, 6808.

(36) (a) Chaston, T. B.; Richardson, D. R. *J. Biol. Inorg. Chem.* **2003**, *8*, 427. (b) Wang, Q.; Yang, Z. Y.; Qi, G. F.; Qin, D. D. *Eur. J. Med. Chem.* **2009**, *44*, 2425. (c) Li, Y.; Yang, Z.-Y.; Wang, M.-F. *Eur. J. Med. Chem.* **2009**, *44*, 4585. (d) Ghosh, K.; Kumar, P.; Tyagi, N.; Singh, U. P.; Aggarwal, V.; Baratto, M. C. *Eur. J. Med. Chem.* **2010**, *45*, 3770. (e) Krishnamoorthy, P.; Sathyadevi, P.; Cowley, A. H.; Butorac, R. R.; Dharmaraj, N. *Eur. J. Med. Chem.* **2011**, *46*, 3376.

(37) Raja, D. S.; Bhuvanesh, N. S. P.; Natarajan, K. *J. Biol. Inorg. Chem.* **2012**, *17*, 223.

(38) Liu, Y.-C.; Yang, Z.-Y. *Eur. J. Med. Chem.* **2009**, *44*, 5080.

(39) Liu, Y.-C.; Yang, Z.-Y. *J. Inorg. Biochem.* **2009**, *103*, 1014.

(40) Léonard, F.; Andrémont, A.; Tancréde, C. *J. Appl. Bacteriol.* **1985**, *58*, 545.

(41) Shikova, Y. V.; Likhoded, V. A.; Khasanov, A. G.; Chuykin, S. V.; Khasanov, T. A.; Shaybakov, D. G. *Russ.* **2012**, RU 2438650 C1 20120110.

(42) Tempone, A. G.; Mortara, R. A.; De Andrade Jr, H. F.; Reimão, J. Q. *Int. J. Antimicrob. Agents* **2010**, *36*, 159.

(43) Rubin, L. J.; Peter, R. H. *J. Med.* **1980**, *302*, 69.

(44) Todorovic, S.; Juranic, N.; Macura, S.; Rusnak, F. *J. Am. Chem. Soc.* **1999**, *121*, 10962.

(45) (a) Fan, C. D.; Su, H.; Zhao, J.; Zhao, B. X.; Zhang, S. L.; Miao, J. Y. *Eur. J. Med. Chem.* **2010**, *45*, 1438. (b) Angelusiu, M. V.; Barbuceanu, S. -F.; Draghici, C.; Almajan, G. L. *Eur. J. Med. Chem.* **2010**, *45*, 2055. (c) Kumar, G.; Devi, S.; Johari, R.; Kumar, D. *Eur. J. Med. Chem.* **2012**, *52*, 269. (d) Raja, D. S.; Ramachandran, E.; Bhuvanesh, N. S. P.; Natarajan, K. *Eur. J.*

Med. Chem. **2013**, *64*, 148. (e) Netalkar, P. P.; Netalkar, S. P.; Budagumpi, S.; Revankar, V. K. *Eur. J. Med. Chem.* **2014**, *79*, 47.

(46) (a) Sahani, M. K.; Yadava, U.; Pandey, O. P.; Sengupta, S. K. *Spectrochim. Acta, Part A* **2014**, *125*, 189. (b) Maurya, M. R.; Khan, A. A.; Azam, A.; Ranjan, S.; Mondal, N.; Kumar, A.; Avecilla, F.; Pessoa, J. C. *Dalton Trans.* **2010**, *39*, 1345. (c) Maurya, R. C.; Rajput, S. J. *Mol. Struct.* **2007**, *833*, 133. (d) Maurya, M. R.; Agarwal, S.; Bader, C.; Rehder, D. *Eur. J. Inorg. Chem.* **2005**, 147.

(47) Dash, S. P.; Panda, A. K.; Pasayat, S.; Dinda, R.; Biswas, A.; Tiekink, E. R. T.; Patil, Y. P.; Nethaji, M.; Kaminsky, W.; Mukhopadhyay, S.; Bhutia, S. K. ***Dalton Trans.*** **2014**, *43*, 10139.

(48) Rowe, R.A.; Jones, M. M. *Inorg. Synth.* **1957**, *5*, 113.

(49) APEX2, SAINT and SADABS, BrukerAXS Inc, Madison, Wisconsin, USA, **2007**.

(50) CrysAlis PRO, Agilent Technologies, Yarnton, Oxfordshire, England, **2011**.

(51) Sheldrick, G. M. *Acta Crystallogr*. **2008**, *A64*, 112.

(52) Farrugia, L. J. *J. Appl. Crystallogr.* **2012**, *45*, 849.

(53) Flack, H.D. *Acta Crystallogr.* **1983**, *A39*, 876.

(54) Gans, J.; Shalloway, D. *J. Mol. Graphics Modell.* **2001**, *19*, 557.

(55) Brandenburg, K. *DIAMOND. Crystal Impact GbR*, Bonn, Germany, **2006**.

(56) Spek, A. L. *Acta Crystallogr.* **2009**, *D65*, 148.

(57) Kumar, P.; Gorai, S.; Santra, M. K.; Mondal, B.; Manna, D. *Dalton Trans.* **2012**, *41*, 7573.

(58) Bhutia, S. K.; Mallick, S. K.; Stevens, S. M.; Prokai, L.; Vishwanatha, J. K.; Maiti, T. K.; *Toxicol. Vitro* **2008**, *22*, 344.

(59) Mukhopadhyay, S.; Panda, P. K.; Behera, B.; Das, C. K.; Hassan, M. K.; Das, D. N.; Sinha, N.; Bissoyi, A.; Pramanik, K.; Maiti, T. K; Bhutia. S. K. *Food Chem. Toxicol*. **2014**, *64*, 369.

(60) (a) Dinda, R.; Sengupta, P.; Ghosh, S.; Mak, T. C. W. *Inorg. Chem.* **2002**, *41*, 1684. (b) Dinda, R.; Sengupta, P.; Sutradhar, M.; Mak, T. C. W.; Ghosh, S. *Inorg. Chem.* **2008**, 47, 5634.

(61) Das, S.; Muthukumaragopal, G. P.; Pal, S. N.; Pal, S. *New J. Chem.* **2003**, *27*, 1102.

(62) (a) Dinda, R.; Majhi, P. K.; Sengupta, P.; Pasayat, S.; Ghosh, S. *Polyhedron* **2010**, *29*, 248. (b) Hazra, A.; Gupta, S.; Roy, S.; Mandal, T. N.; Das, K.; Konar, S.; Jana, A.; Ray, S.; Butcher, R.J.; Kar, S. K. *Polyhedron* **2011**, *30*, 187.

(63) Moon, M.; Pyo, M.; Myoung, Y. C.; Ahn, C.; Lah, M. S. *Inorg. Chem.* **2001**, *40*, 554.

(64) Jin, Y.; Lee, H.; Pyo, M.; Lah, M. S. *Dalton Trans.* **2005**, 797.

(65) (a) Maurya, M. R.; Kumar, A.; Ebel, M.; Rehder, D. *Inorg. Chem.* **2006**, *45*, 5924. (b) Maurya, M. R.; Haldar, C.; Kumar, A.; Kuznetsov, M. L.; Avecilla, F.; Pessoa, J. C. *Dalton Trans.* **2013**, *42*, 11941.

(66) Geng, L.-Z.; Xing, J.; Zhou, Y.-Z. *Chin. J. Struct. Chem.* **2012**, *31*, 185.

(67) Addison, A. W.; Rao, T. N.; Reedijk, J.; van Rijn, J.;.Verschoor, G. C. *Dalton Trans.* **1984** 1349.

(68) Deflon, V. M.; de Oliveira, D. M.; de Sousa, G. F.; Batista, A. A.; Dinelli, L. R.; Castellano, E. E. *Z. Anorg. Allg. Chem.* **2002**, *628*, 1140.

(69) Hydrogen bonding interactions in the crystal structure of **2**. Intramolecular N–H...N interactions. First independent molecule: N4–H2n...N3 = 2.02(2) Å, N4...N3 = 2.699(2) Å, with angle at H2n = 133.1(16)°; second independent molecule: N4a–H4n...N3a = 2.01(2) Å, N4a...N3a = 2.677(2) Å, with angle at H4n = 132.6(18)°.

(70) Veerapur, R. S.; Gudasi, K. B.; Sairam, M.; Shenoy, R. V.; Netaji, M.; Raju, K. V. S. N.; Sreedhar, B.; Aminabhavi, T. M. *J. Mater. Sci.* **2007**, *42*, 4406.

(71) Gatto, C. C.; Lang, E. S.; Burrow, R. A.; Abram, U. *J. Braz. Chem. Soc.* **2006**, *17*, 1612.

(72) Allen, F. H. *Acta Crystallogr.* **2002**, *B58*, 380.

(73) Wang, C.-Y.; Hu, J.-J.; Tu, H.-Y.; Zhu, P.-F.; Sheng, S.-J. *Acta Crystallogr.* **2011**, *E67*, m1475.

(74) Milčič, M. K.; Medaković, V. B.; Sredojević, D. N.; Juranić, N. O.; Tomić, Z. D.; Zarić, S. D. *Inorg. Chem.* **2006**, *45*, 4755.

(75) Tiekink, E. R. T.; Haiduc, I. *Prog. Inorg. Chem.* **2005**, *54*, 127.

(76) Tiekink, E. R. T.; Zukerman-Schpector, J.; *Chem. Commun.* **2011**, 47, 6623.

(77) An, Y.; Liu, S.D.; Deng, S.Y.; Ji, L.N.; Mao, Z.W. *J. Inorg. Biochem.* **2006**, *100*, 1586.

(78) Banerjee, S.; Hussain, A.; Prasad, P.; Khan, I.; Banik, B.; Kondaiah, P.; Chakravarty, A. R. *Eur. J. Inorg. Chem.* **2012**, 3899.

(79) Poklar, N.; Pilch, D. S.; Lippard, S. J.; Redding, E. A.; Dunham, S. U.; Breslauer, K. J. Proc Natl Acad Sci U S A **1996**, *93*, 7606.

(80) Dai, W. M.; Lai, K. W.; Wu, A.; Hamaguchi, W.; Lee, M. Y.; Zhou, L.; Ishii, A.; Nishimoto, S. *J. Med. Chem*. **2002**, *45*, 758.

(81) Sasmal, P. K.; Saha, S.; Majumdar, R.; De, S.; Dighe, R. R.; Chakravarty, A. R. Dalton *Trans.* **2010**, *39*, 2147.

(82) Ahmed, M.; Jamil, K. *Biol. Med.* **2011**, *3*, 60.

(83) Ramadan, A. M. *J. Inorg. Biochem.* **1997**, *65*, 183.

(84) Avaji, P. G.; Kumar, C. H. V.; Patil, S. A.; Shivananda, K. N.; Nagaraju, C. *Eur. J. Med. Chem.* **2009**, *44*, 3552.

(85) Rosu, T.; Pahontu, E.; Pasculescu, S.; Georgescu, R.; Stanica, N.; Curaj, A.; Popescu, A.; Leabu, M. *Eur. J. Med. Chem.* **2010**, *45*, 1627.

(86) Yamaguchi, T.; Watanabe, S.; Matsumura, Y.; Tokuoka, Y.; Yokoyama, A. *Bioorg. Med. Chem.* **2012**, *20*, 3058.

Chapter 7

Chemistry of mononuclear nonoxido V^{IV}, oxido V^{V}, and binuclear oxido $V^{V}V^{V}$ complexes with a tridentate (ONO) ligand: Exploration of solution behavior of oxido vanadium(V) complexes

Chapter 7

Chemistry of mononuclear nonoxido V^{IV}, oxido V^{V}, and binuclear oxido $V^{V}V^{V}$ complexes with a tridentate (ONO) ligand: Exploration of solution behavior of oxido vanadium(V) complexes

ABSTRACT

In this chapter, series of mononuclear nonoxido vanadium(IV) [$V^{IV}(L^{1-4})_2$] (**1**–**4**), oxidoethoxido vanadium(V) [$V^{V}O(L^{1-4})OEt$] (**5**–**8**), and binuclear μ-oxido vanadium(V) [$V^{V}{}_2O_3(L^1)_2$] (**9**) complexes, taking potentially tridentate binegative aroylhydrazone ligands are reported [where H_2L^1 = 2-furoyl hydrazone of 2-hydroxy-1-acetonaphthone, H_2L^2 =2-thiophenoylhydrazone hydrazone of 2-hydroxy-1-acetonaphthone, H_2L^3 =1-napthoyl hydrazone of 2-hydroxy-1-acetonaphthone, H_2L^4 =3-hydroxy-2-napthoyl hydrazone of 2-hydroxy-1-acetonaphthone]. All the mononuclear complexes were characterized by elemental analysis as well as by various spectroscopic techniques. The nonoxido vanadium(IV) complexes are quite stable in open air as well as in solution. The solution study of the oxidoethoxido vanadium(V) species (**5**-**8**) were carried out which indicates the existence of two different species in solution. The new species, a μ-oxido divanadium complex, [$V_2O_3(L^1)_2$] (**9**) is generated *in situ* in solution state from corresponding mononuclear complex [$V^{V}O(L^1)OEt$] (**5**), successfully isolated in solid state and fully characterized by several physicochemical techniques. Single crystal X-ray diffraction crystallography of nonoxido vanadium (IV) (**2)** showed the N_2O_4 donor set to define a trigonal prismatic geometry and that of oxido vanadium (V) (**5 & 6)** and μ-oxido divanadium(V) (**9)** reveals that the metal centre is in distorted square pyramidal geometry with O_4N coordination spheres.

7.1. INTRODUCTION

Hydrazones, –NH–N=CRR' (R and R′ = H, alkyl, aryl), are versatile ligands and the study of complexes with these is of unabated interest to inorganic chemists because of their relevance to apparently dissimilar fields, like bioinorganic chemistry,[1] and catalysis.[2] The phenolic-hydrazone ligands with good π-donor atoms are expected to stabilize higher oxidation states with highly covalent M–O(phenolate) bonds. On the other hand, the diversified roles of vanadium among others in biological systems[3,4] are primarily responsible for stimulating a recent increasing interest in vanadium coordination chemistry. However, in contrast to the well known vanadium(IV)/(V) complexes containing VO^{2+} or VO^{3+} units,[5] only very few octahedral nonoxido (V^{IV} and V^{V}) complexes, the so-called 'bare' complexes, have been isolated and structurally characterized.[6] This type of nonoxido V^{IV} centers[7] have been found in amavadin,[8] a compound isolated from the mushroom *Amanita muscaria* and such class of vanadium species are still scarce.[6]

We have been exploring the feasibility of using tridentate aroylhydrazone ligands, which comprise the three donor atoms [ONO] for generating novel transition metal complexes. Thus, we reported several oxido-, nonoxido-, μ-oxido divanadium complexes of general formula, $[V^{V}O(L)OEt]$, $[V^{IV}(L)_2]$ and $[V^{V}{}_2O_3(L)_2]$ with potentially tridentate binegative aroylhydrzone ligands.[9] Here, we extend our studies to a potentially tridentate hydrazone ligand with an aim to scrutinize the effect of the sterically hindered/bulky naphthoyl- derivative and bioactive hetero aromatic thiophenoyl and furoyl-derivative arm on these types of ligands, which are expected to yield homoleptic bis (tridentate) nonoxido vanadium(IV) complexes and mono ligand, oxido alkoxido vanadium(V), whose relevance to solution chemistry has been mentioned quite often in the literature.[10]

This work forms part of a study on the synthesis, characterization, of a series of nonoxido vanadium(IV) and oxido alkoxido vanadium(V) complexes incorporating oxygen and nitrogen donor ligands.[9] Herein we explore the binding of some new dibasic tridentate ligands (**Scheme 7.1**), abbreviated H_2L where we wanted to see, if the change in ligand environment by varying the steric bulk of the aroylhydrazones can control the coordination number of the vanadium in these complexes. Here mononuclear nonoxido vanadium(IV) (**1**-**4**) and oxido vanadium(V) (**5**-**8**)

species have been isolated, structurally characterized, and scanned for solution study. Solution study results (IR and NMR) of oxido vanadium(V) complexes (**5**-**8**) indicate that two species simultaneously exists in solution, the monomeric complexes and as well as their corresponding μ-oxido dimeric species. One of these μ-oxido bridged trioxido binuclear vanadium(V) species (**9**) is now successfully isolated in the solid state, characterized by spectroscopic techniques and the molecular structure is solved by X-ray crystallography.

7.2. EXPERIMENTAL SECTION

7.2.1. General Methods and Materials. $[VO(acac)_2]$ was prepared as described in the literature.[11] Reagent grade solvents were dried and distilled prior to use. Elemental analyses were performed on a Vario ELcube CHNS Elemental analyzer. IR spectra were recorded on a Perkin-Elmer Spectrum RXI spectrophotometer. ^{1}H and ^{13}C NMR spectra were recorded on a Bruker Ultrashield 400 MHz spectrometer using $SiMe_4$ as an internal standard. Electronic spectra were recorded on a Lamda25, PerkinElmer spectrophotometer. Cyclic voltammograms were recorded in DMF solutions, containing 0.1 M TEAP (Tetraethyl ammonium perchlorate) as supporting electrolyte, using a CH1120A potentiostat, with Pt disc/glassy carbon working electrode, Pt wire as counter electrode and Ag, AgCl/saturated KCl as reference electrode. X-band EPR measurements were performed on **JEOL, Model: JES-FA200** ESR Spectrometer.

7.2.2. Synthesis of Ligands ($H_2L^{1–4}$). Schiff base ligands, 2-furoyl hydrazone of 2-hydroxy-1-acetonaphthone (H_2L^1), 2-thiophenoylhydrazone hydrazone of 2-hydroxy-1-acetonaphthone (H_2L^2), 1-napthoyl hydrazone of 2-hydroxy-1-acetonaphthone (H_2L^3), and 3-hydroxy-2-napthoyl hydrazone of 2-hydroxy-1-acetonaphthone (H_2L^4) were prepared by the condensation of 2-hydroxy-1-acetonapthone and the respective acidhydrazide in equimolar ratio in ethanol by a standard procedure.[9d] The resulting white compounds were filtered, washed with ethanol and dried over fused $CaCl_2$. Elemental analysis results, NMR (^{1}H and ^{13}C) and IR data for all of these verified their preparation.

H_2L^1. Yield: 74%. Anal. Calcd. for $C_{17}H_{14}N_2O_3$: C, 69.38; H, 4.79; N, 9.52. Found: C, 69.35; H, 4.78; N, 9.50. IR (KBr pellet, cm^{-1}): 3331 ν(O–H); 3102 ν(N–H); 1652 ν(C=O); 1622 ν(C=N). ^{1}H NMR (400 MHz, DMSO-d_6): δ 10.51 (s, 1H, OH), 9.09 (s, 1H, NH), 7.96–6.51 (m, 9H, Aromatic), 2.33 (s, 3H, CH_3).^{13}C NMR (100 MHz, DMSO-d_6): δ 163.29, 152.34, 146.10, 135.11,

134.67, 134.23, 131.87, 130.17, 129.13, 128.32, 128.18, 127.43, 123.92, 122.85, 118.83, 112.65, 24.19.

H_2L^2. Yield: 71%. Anal. Calcd. for $C_{17}H_{14}N_2O_2S$: C, 65.79; H, 4.55; N, 9.03. Found: C, 65.77; H, 4.56; N, 9.07. IR (KBr pellet, cm^{-1}): 3353 *ν*(O–H); 3108 *ν*(N–H); 1658 *ν*(C=O); 1621 *ν*(C=N). ^{1}H NMR (400 MHz, DMSO-d_6): *δ* 10.31 (s, 1H, OH), 9.56 (s, 1H, NH), 8.08–7.20 (m, 9H, Aromatic), 2.38 (s, 3H, CH_3).^{13}C NMR (100 MHz, DMSO-d_6): *δ* 161.48, 152.83, 149.48, 135.52, 135.18, 134.23, 131.45, 130.42, 129.05, 128.44, 127.85, 127.08, 123.59, 123.00, 119.03, 113.62, 24.03.

H_2L^3. Yield: 69%. Anal. Calcd. for $C_{23}H_{18}N_2O_2$: C, 77.95; H, 5.12; N, 7.90. Found C, 77.91; H, 5.14; N, 7.88. IR (KBr pellet, cm^{-1}): 3448 *ν*(O–H); 3113 *ν*(N–H); 1661 *ν*(C=O); 1611 *ν*(C=N). ^{1}H NMR (400 MHz, DMSO-d_6): *δ* 10.32 (s, 1H, OH), 10.08 (s, 1H, NH), 8.02–7.30 (m, 13H, Aromatic), 2.40 (s, 3H, CH_3). ^{13}C NMR (100 MHz, DMSO-d_6): *δ* 165.05, 154.35, 153.00, 152.73, 133.77, 133.37, 131.17, 130.40, 130.36, 130.17, 128.95, 128.60, 128.32, 127.70,125.86, 125.41, 125.24, 123.53, 123.36, 118.98, 114.47, 24.43.

H_2L^4. Yield: 64%. Anal. Calcd. for $C_{23}H_{18}N_2O_3$: C, 74.58; H, 4.90; N, 7.56. Found: C, 74.57; H, 4.88; N, 7.58. IR (KBr pellet, cm^{-1}): 3648 *ν*(O–H); 3188 *ν*(N–H); 1652 *ν*(C=O); 1622 *ν*(C=N). ^{1}H NMR (400 MHz, DMSO-d_6): *δ* 11.87 (s, 1H, OH), 11.67 (s, 1H, naphthoyl hydrazide–OH), 10.15 (s, 1H, NH), 8.68–7.24 (m, 12H, Aromatic), 2.38 (s, 3H, CH_3). ^{13}C NMR (100 MHz, DMSO-d_6): *δ* 166.82, 154.89, 153.33, 153.01, 136.33, 132.81, 130.22, 129.43, 128.79, 128.20, 127.68, 127.12, 126.24, 124.41, 124.35, 124.17, 123.25, 121.09, 119.91, 118.74, 111.19, 111.04, 24.15.

7.2.3. Synthesis of nonoxido vanadium(IV) complexes $[V^{IV}(L^{1–4})_2]$ (1–4). $[VO(acac)_2]$ (0.5 mmol) was added to a hot solution of appropriate ligand H_2L^{1-4} (1.0 mmol) in CH_3CN (20 mL), the color changed instantly to greenish black. After 3 h of reflux, black crystals were obtained from reaction mixture, which were filtered off, washed thoroughly with ethanol and dried. Some crystals are of diffraction quality and were used directly for X-ray structure determination using single crystal X-ray diffractometer.

$[V^{IV}(L^1)_2]$ (1). Yield: 68%. Anal. Calcd. for $C_{34}H_{24}N_4O_6V$: C, 64.26; H, 3.81; N, 8.82. Found: C, 64.24; H, 3.82; N, 8.79. IR (KBr pellet, cm^{-1}): 1608 ν(C=N); 1243 $\nu(C–O)_{enolic}$; 1043 ν(N–N). UV–Vis ($CHCl_3$) [λ_{max}, nm (ε, M^{-1} cm^{-1})]: 624 (20115), 514 (18381), 369 (79017), 317 (129132), 232 (211098).

$[V^{IV}(L^2)_2]$ (2). Yield: 60%. Anal. Calcd. for $C_{34}H_{24}N_4O_4S_2V$: C, 61.67; H, 3.62; N, 8.39. Found: C, 61.65; H, 3.61; N, 8.43. IR (KBr pellet, cm^{-1}): 1611 ν(C=N); 1242 $\nu(C–O)_{enolic}$; 1044 ν(N–N). UV–Vis ($CHCl_3$) [λ_{max}, nm (ε, M^{-1} cm^{-1})]: 627 (23006), 511 (21387), 371 (78555), 324 (121850), 261 (122081), 229 (130231).

$[V^{IV}(L^3)_2]$ (3). Yield: 61%. Anal. Calcd. for $C_{47}H_{34}Cl_2N_4O_4V$: C, 67.15; H, 4.08; N, 6.66. Found: C, 67.16; H, 4.07; N, 6.67. IR (KBr pellet, cm^{-1}): 1591 ν(C=N); 1244 $\nu(C–O)_{enolic}$; 1045 ν(N–N). UV–Vis ($CHCl_3$) [λ_{max}, nm (ε, M^{-1} cm^{-1})]: 616 (19132), 515 (20289), 374(70635), 329 (104277), 232 (180057).

$[V^{IV}(L^4)_2]$ (4). Yield: 66%. Anal. Calcd. for $C_{46}H_{32}N_4O_6V$: C, 70.14; H, 4.09; N, 7.11. Found: C, 70.15; H, 4.08; N, 7.13. IR (KBr pellet, cm^{-1}): 3362 ν(O–H); 1609 ν(C=N); 1239 $\nu(C–O)_{enolic}$; 1022 ν(N–N). UV–Vis ($CHCl_3$) [λ_{max}, nm (ε, M^{-1} cm^{-1})]: 623 (18092), 514 (15606), 377(76242), 322 (121676), 234 (204913).

7.2.4. Synthesis of oxidoethoxido vanadium(V) complexes $[V^VO(L^{1–4})OEt]$ (5–8). A general synthetic procedure taking $[VO(acac)_2]$ as metal precursor is described below:
$[VO(acac)_2]$ (1.0 mmol) was added to a hot solution of appropriate ligand $H_2L^{1–4}$ (1.0 mmol) in EtOH (20 mL), the color changed instantly to brownish. After 3 h of refluxing, reaction mixture was filtered off, and kept for crystallisation. After 3 to 4 days, crystals of diffraction quality were obtained which were used for X-ray structure determination using single crystal X-ray diffractometer.

7.2.4.1. Solid state characterization of 5-8.

[$V^{V}O(L^{1})OEt$] (5). Yield: 66%. Anal. Calcd. for $C_{19}H_{17}N_2O_5V$: C, 56.45; H, 4.24; N, 6.93. Found: C, 56.46; H, 4.22; N, 6.92. IR (KBr pellet, cm^{-1}): 1604 ν(C=N); 1241 $\nu(C–O)_{enolic}$; 1034 ν(N–N); 994 ν(V=O). UV–Vis ($CHCl_3$) [λ_{max}, nm (ε, M^{-1} cm^{-1})]: 427 (14509), 338 (29884), 247 (48266).

[$V^{V}O(L^{2})OEt$] (6). Yield: 66%. Anal. Calcd. for $C_{19}H_{17}N_2O_4VS$: C, 54.29; H, 4.08; N, 6.66. Found: C, 54.27; H, 4.04; N, 6.67. IR (KBr pellet, cm^{-1}): 1612 ν(C=N); 1238 $\nu(C–O)_{enolic}$; 1037 ν(N–N); 999 ν(V=O). UV–Vis ($CHCl_3$) [λ_{max}, nm (ε, M^{-1} cm^{-1})]: 431 (40405), 335 (83006), 232(122775).

[$V^{V}O(L^{3})OEt$] (7). Yield: 66%. Anal. Calcd. for $C_{25}H_{21}N_2O_4V$: C, 64.66; H, 4.56; N, 6.03. Found: C, 64.63; H, 4.54; N, 6.06. IR (KBr pellet, cm^{-1}): 1593 ν(C=N); 1241 $\nu(C–O)_{enolic}$; 1037 ν(N–N); 998 ν(V=O). UV–Vis ($CHCl_3$) [λ_{max}, nm (ε, M^{-1} cm^{-1})]: 431 (34046), 329 (74508), 231 (158497).

[$V^{V}O(L^{4})OEt$] (8). Yield: 66%. Anal. Calcd. for $C_{25}H_{21}N_2O_5V$: C, 62.51; H, 4.41; N, 5.83. Found: C, 62.48; H, 4.40; N, 5.82. IR (KBr pellet, cm^{-1}): 3156 ν(O–H); 1571 ν(C=N); 1239 $\nu(C–O)_{enolic}$; 1035 ν(N–N); 1001 ν(V=O). UV–Vis ($CHCl_3$) [λ_{max}, nm (ε, M^{-1} cm^{-1})]: 432 (30057), 342 (60635), 313 (69826), 234 (148843).

7.2.4.2. Solution state characterization of 5-8.

[$V^{V}O(L^{1})OEt$] (5). IR (KBr pellet, cm^{-1}): 1009, 966 ν(V=O); 820 ν(V–O–V). ^{1}H NMR (400 MHz, DMSO-d_6): δ 8.20–6.63 (m, 18H, Aromatic), 5.51–5.46 (m, 2H, CH_2 (OEt)), 3.47–3.42 (q, 4H, CH_2 (EtOH)), 2.92 (s, 3H, CH_3), 2.86 (s, 3H, CH_3), 1.49–1.46 (t, 3H, CH_3 (OEt)), 1.08–1.04 (t, 6H, CH_3 (EtOH)). ^{13}C NMR (100 MHz, DMSO-d_6): δ 166.53, 166.03, 163.73, 163.53, 159.72, 159.49, 146.81, 146.47, 146.25, 145.45, 134.53, 133.81, 131.95, 131.74, 129.92, 129.49, 129.33, 128.82, 127.93, 127.55, 126.43, 126.13, 124.83, 124.33, 123.93, 119.42, 118.69, 118.24, 118.11, 116.30, 115.51, 112.62, 80.80, 56.52, 23.89, 19.00, 18.63. ^{51}V NMR (DMSO-d_6): δ –542, –522. ^{1}H NMR (400 MHz, DMSO-d_6 + EtOH): δ 8.09–6.67 (m, 9H, Aromatic), 5.50–5.48 (m, 2H, CH_2 (OEt)), 3.48–3.43 (q, 27H, CH_2 (EtOH)), 2.86 (s, 3H, CH_3), 1.49–1.46 (t, 3H, CH_3 (OEt)), 1.08–1.04 (t, 38H, CH_3 (EtOH)). ^{13}C NMR (100 MHz, DMSO-d_6 + EtOH): δ 166.01, 163.73, 159.48,

146.38, 147.27, 133.74, 131.95, 129.56, 129.28, 127.49, 126.09, 124.27, 119.38, 118.24, 115.43, 112.53, 80.80, 56.52, 23.81, 18.88, 18.55. ^{51}V NMR (DMSO-d_6 + EtOH): δ –522.

[$V^{V}O(L^{2})OEt$] (6). IR (KBr pellet, cm^{-1}): 1005, 965 ν(V=O); 817 ν(V–O–V). ^{1}H NMR (400 MHz, DMSO-d_6) δ 8.20–7.08 (m, 18H, Aromatic), 5.49–5.48 (m, 2H, CH_2 (OEt)), 3.46–3.43 (q, 4H, CH_2 (EtOH)), 2.92 (s, 3H, CH_3), 2.86 (s, 3H, CH_3), 1.50–1.48 (t, 3H, CH_3 (OEt)), 1.08–1.05 (t, 6H, CH_3 (EtOH)). ^{13}C NMR (100 MHz, DMSO-d_6): δ 167.33, 166.50, 166.03, 158.91, 134.83, 133.77, 133.60, 131.97, 131.75, 131.54, 130.95, 129.96, 129.59, 129.50, 129.32, 128.55, 127.95, 127.55, 126.43, 126.15, 124.82, 124.32, 119.38, 118.18, 80.67, 56.53, 23.71, 19.00, 18.59. ^{51}V NMR (DMSO-d_6): δ –537, –519. ^{1}H NMR (400 MHz, DMSO-d_6 + EtOH) δ 8.08–7.17 (m, 9H, Aromatic), 5.49–5.48 (m, 2H, CH_2 (OEt)), 3.48–3.43 (q, 62H, CH_2 (EtOH)), 2.85 (s, 3H, CH_3), 1.51–1.48 (t, 3H, CH_3 (OEt)), 1.08–1.04 (t, 95H, CH_3 (EtOH)). ^{13}C NMR (100 MHz, DMSO-d_6 + EtOH): δ 167.33, 165.97, 158.89, 134.83, 133.59, 131.94, 131.22, 130.76, 129.58, 129.18, 128.28, 127.38, 126.03, 124.16, 119.26, 118.16, 80.68, 56.55, 23.48, 18.65, 18.27. ^{51}V NMR (DMSO-d_6 + EtOH): δ –520.

[$V^{V}O(L^{3})OEt$] (7). IR (KBr pellet, cm^{-1}): 1004, 965 ν(V=O); 818 ν(V–O–V). ^{1}H NMR (400 MHz, DMSO-d_6) δ 9.30–7.25 (m, 26H, Aromatic), 5.52–5.44 (m, 2H, CH_2 (OEt)), 3.47–3.42 (q, 4H, CH_2 (EtOH)), 3.03 (s, 3H, CH_3), 2.95 (s, 3H, CH_3), 1.49–1.45 (t, 3H, CH_3 (OEt)), 1.07–1.04 (t, 6H, CH_3 (EtOH)). ^{13}C NMR (100 MHz, DMSO-d_6): δ 172.46, 171.75, 171.35, 166.78, 166.66, 166.32, 160.65, 160.14, 134.91, 134.01, 132.63, 132.20, 132.06, 131.85, 131.22, 130.97, 130.89, 130.27, 129.95, 129.57, 129.37, 129.21, 129.16, 129.02, 128.96, 128.01, 127.90, 127.61, 127.43, 127.34, 127.30, 126.57, 126.21, 125.59, 125.31, 124.91, 124.36, 119.58, 118.85, 118.60, 118.17, 118.02, 117.87, 80.05, 56.50, 24.12, 19.02, 18.75. ^{51}V NMR (DMSO-d_6): δ –540, –521. ^{1}H NMR (400 MHz, DMSO-d_6 + EtOH): δ 9.16–7.24 (m, 13H, Aromatic), 5.56–5.42 (m, 2H, CH_2 (OEt)), 3.48–3.43 (q, 92H, CH_2 (EtOH)), 2.95 (s, 3H, CH_3), 1.50–1.47 (t, 3H, CH_3 (OEt)), 1.08–1.04 (t, 136H, CH_3 (EtOH)). ^{13}C NMR (100 MHz, DMSO-d_6 + EtOH): δ 172.45, 166.29, 160.15, 134.02, 133.92, 132.05, 131.79, 131.24, 129.59, 129.27, 129.15, 128.85, 127.49, 127.29, 127.21, 126.43, 126.13, 125.45, 124.25, 119.50, 118.16, 80.03, 56.51, 23.97, 18.78, 18.55. ^{51}V NMR (DMSO-d_6 + EtOH): δ –522.

[$V^{V}O(L^{4})OEt$] (8). IR (KBr pellet, cm^{-1}): 1009, 970 ν(V=O); 822 ν(V–O–V). ^{1}H NMR (400 MHz, DMSO-d_6): δ 11.78 (s, 1H, OH), 11.42 (s, 1H, OH), 8.54–7.10 (m, 24H, Aromatic), 5.72–5.67 (m, 2H, CH_2 (OEt)), 3.47–3.42 (q, 4H, CH_2 (EtOH)), 3.01 (s, 3H, CH_3), 2.91 (s, 3H, CH_3), 1.61–1.58 (t, 3H, CH_3 (OEt)), 1.07–1.04 (t, 6H, CH_3 (EtOH)). ^{13}C NMR (100 MHz, DMSO-d_6): δ 170.65, 164.19, 159.74, 155.19, 136.79, 134.39, 131.93, 131.06, 129.97, 129.63, 129.40, 129.34, 129.06, 128.83, 128.32, 128.14, 127.79, 127.36, 127.24, 126.42, 126.17, 125.96, 124.91, 124.54, 124.09, 123.70, 122.91, 119.43, 118.79, 117.86, 117.31, 111.01, 110.74, 82.36, 56.51, 23.56, 19.00, 18.84. ^{51}V NMR (DMSO-d_6): δ –564, –529. ^{1}H NMR (400 MHz, DMSO-d_6 + EtOH): δ 11.77 (s, 1H, OH), 8.53–7.22 (m, 12H, Aromatic), 5.70–5.69 (m, 2H, CH_2 (OEt)), 3.47–3.42 (q, 47H, CH_2 (EtOH)), 2.91 (s, 3H, CH_3), 1.61–1.58 (t, 3H, CH_3 (OEt)), 1.07–1.04 (t, 72H, CH_3 (EtOH)). ^{13}C NMR (100 MHz, DMSO-d_6 + EtOH): δ 170.66, 166.17, 159.69, 155.22, 136.79, 134.32, 131.92, 131.02, 129.63, 129.35, 129.27, 128.74, 127.72, 127.35, 126.37, 126.12, 124.47, 124.02, 119.38, 117.85, 117.30, 110.97, 82.36, 56.51, 23.48, 18.88. ^{51}V NMR (DMSO-d_6 + EtOH): δ –532.

7.2.5. Synthesis of μ-oxido divanadium(V) complexes [$V^{V}_2O_3(L^{1})_2$] (9). Complex **5** was made soluble in CH_2Cl_2 and layered with CH_3CN. The above mixture was kept for recrystallisation. After seven days X-ray quality crystals obtained, which were filtered off, washed thoroughly with CH_3CN and dried. Some crystals are of diffraction quality and were used directly for X-ray structure determination using single crystal X-ray diffractometer.

[$V^{V}_2O_3(L^{1})_2$] (9). Yield: 66%. Anal. Calcd. for $C_{34}H_{24}N_4O_9V_2 \cdot C_{0.5}HCl$: C, 53.29; H, 3.22; N, 7.21. Found: C, 53.31; H, 3.21; N, 7.24. IR (KBr pellet, cm^{-1}): 1608 ν(C=N); 1237 $\nu(C–O)_{enolic}$; 1040 ν(N–N); 999, 963 ν(V=O), 823 ν(V–O–V). UV–Vis ($CHCl_3$) [λ_{max}, nm (ε, M^{-1} cm^{-1})]: 425 (21618), 336 (40982), 246 (61040). ^{1}H NMR (400 MHz, DMSO-d_6) δ 8.20–6.63 (m, 9H, Aromatic), 2.92 (s, 3H, CH_3).^{13}C NMR (100 MHz, DMSO-d_6): δ 166.52, 163.51, 163.17, 159.97, 159.70, 146.82, 146.13, 145.53, 145.41, 134.52, 131.73, 130.18, 129.92, 129.50, 129.13, 128.21, 127.93, 127.04, 126.43, 124.83, 122.87, 118.69, 118.55, 118.11, 117.98, 116.30, 116.13, 112.69, 24.22, 24.10. ^{51}V NMR (DMSO-d_6): δ –544.

7.2.6. X-ray Crystallography. Crystals suitable for X-ray diffraction study were obtained at room temperature by slow evaporation from a CH_2Cl_2 solution. The X-ray diffraction data for (**2**, **5**, **6**, **9**) were collected at 100(2) K on SuperNova diffractometer (Agilent) with a CCD detector and Mo-K_α radiation. A summary of crystal data and refinement details for **2**, **5**, **6** and **9** is provided in **Table 7.1**. The crystal data were processed with CrysAlisPro (data collection, cell refinement and data reduction).[12] The crystal structure was solved using direct methods with *SHELXD* and refined with *SHELXL*.[13] All hydrogen atoms were initially located in electron-density difference maps and were constrained to idealized positions, with C-H = 0.95-0.99 Å and with U_{iso}(H) = 1.5U_{eq}(C) for methyl hydrogen atoms and U_{iso}(H) = 1.2U_{eq}(C) for others. The non-hydrogen atoms were refined anisotropically..*PLATON* software[14] was used to validate the crystallographic data

Table 7.1. Crystal data and refinement details for 2, 5, 6, 9

Complex	2	5	6	9
Empirical formula	$C_{34}H_{24}N_4O_4S_2V$	$C_{19}H_{17}N_2O_5V$	$C_{19}H_{17}N_2O_4SV$	$C_{34}H_{24}N_4O_9V_2{\cdot}C_{0.5}HCl$
Formula weight	667.63	404.29	420.35	776.92
Temperature	100(2) K	100(2) K	100(2) K	100(2) K
Crystal system	monoclinic	Triclinic	monoclinic	Triclinic
Space group	$P2_1/c$	$P\text{-}1$	$P2_1/n$	$P\text{-}1$
Unit cell dimensions	a =13.03105(9) A b= 23.24945 (14) A c = 10.37682 (9) A α = 90° β= 104.2945 (8)° γ = 90°	a = 8.3450(6) A b = 10.1037(7)A c = 10.5931(7)A α = 79.973(3)° β = 81.273(2)° γ = 78.461(2)°	a = 9.75757(9) A b = 15.62094(14) A c = 11.92282(11) A α = 90 ° β = 91.8964(8)° γ = 90 °	a =10.39154 (19)Å b= 12.21149 (18) Å c = 13.8273 (2)Å, α = 99.9444 (13)° β= 108.6135 (16)° γ =103.0069 (14)°
Volume	3046.48 (4) $Å^3$	855.39(10) $Å^3$	1816.31(3) $Å^3$	1562.34 (4) $Å^3$
Z	4	2	4	2
Density (calculated)	1.456 $g{\cdot}cm^{-3}$	1.570 $mg{\cdot}m^{-3}$	1.537 $g{\cdot}cm^{-3}$	1.651$g{\cdot}cm^{-3}$
Absorption coefficient	4.39 mm^{-1}	0.615 mm^{-1}	0.69 mm^{-1}	6.37mm^{-1}
F(000)	1372	416	864	790
Crystal size	0.21 × 0.19 × 0.02 mm^3	0.32 x 0.16 x 0.12 mm^3	0.23× 0.14× 0.07 mm^3	0.21 × 0.19 × 0.02 mm^3
Theta range for data collection	3.5° to 67.2°	2.64 to 28.00 °.	3.0 to 37.0°.	3.5° to 72.9°
Independent reflections	5304	4113	9244	6187
Final R indices [I>2sigma(I)]	R1 = 0.034 wR2=0.095	R1 = 0.0302 wR2 = 0.0790	R1 = 0.031 wR2 = 0.091	R1 = 0.045 wR2 =0.119

7.3. RESULT AND DISSCUSSION

7.3.1. Mononuclear nonoxido vanadium(IV) $[V^{IV}(L^{1-4})_2]$ (1–4) and oxidoethoxido vanadium(V) $[V^{V}O(L^{1-4})OEt]$ (5–8) complexes.

7.3.1.1. Synthesis. Scheme 7.1 represents the various pathways through which the nonoxido vanadium(IV), oxidoethoxido vanadium(V) and μ-oxido divanadium(V) complexes were obtained. Monomeric nonoxido bis(tridentate)-vanadium(IV) complexes $[V(L^{1–4})_2]$ (**1**–**4**) have been synthesized by the reactions of aroylhydrazones ($H_2L^{1–4}$) with $[VO(acac)_2]$ in CH_3CN. The same reaction in ethanol lead to the formation of monomeric oxido vanadium(V) $[VO(L^{1-4})OEt]$ (**5**–**8**). The reactions are clean, affording large quantities of pure crystalline products in good yield (~ 70%). These compounds are highly soluble in CH_2Cl_2, DMF and DMSO and sparingly soluble in MeOH, EtOH and CH_3CN.

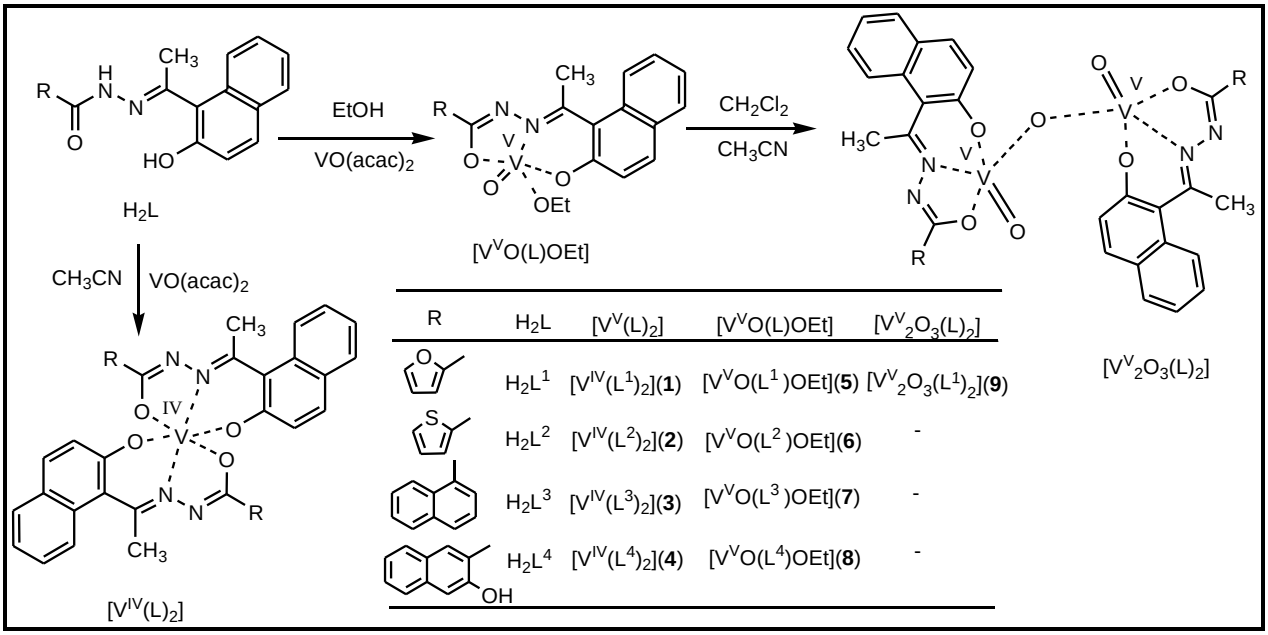

R	H_2L	$[V^V(L)_2]$	$[V^VO(L)OEt]$	$[V^V_2O_3(L)_2]$
	H_2L^1	$[V^{IV}(L^1)_2]$(**1**)	$[V^VO(L^1)OEt]$(**5**)	$[V^V_2O_3(L^1)_2]$(**9**)
	H_2L^2	$[V^{IV}(L^2)_2]$(**2**)	$[V^VO(L^2)OEt]$(**6**)	-
	H_2L^3	$[V^{IV}(L^3)_2]$(**3**)	$[V^VO(L^3)OEt]$(**7**)	-
	H_2L^4	$[V^{IV}(L^4)_2]$(**4**)	$[V^VO(L^4)OEt]$(**8**)	-

Scheme 7.1. Schematic diagram of various pathways through which the mononuclear nonoxido vanadium(IV) $[V^{IV}(L)_2]$, oxido vanadium(V) $[V^VO(L)OEt]$ and binuclear μ-oxido vanadium(V) $[V^V_2O_3(L^1)_2]$ complexes were synthesized.

7.3.1.2. Description of the X-ray structure of complexes (2, **5** and **6)**. The observed elemental (C, H, N) analytical data of all the nonoxido vanadium(IV) and oxidoethoxido vanadium(V) are consistent with their composition. It appears from the formulation of all these above complexes that the hydrazones are serving as tridentate ligands in them. Although the preliminary characterization data (microanalysis and IR) gives idea about the presence of various functionality in the complexes, they could not point to any definite stereochemistry of the complexes, or the coordination mode of H_2L. In order to authenticate the coordination mode of the hydrazones in these complexes, the structure of all the complexes has been determined by X-ray crystallography. The atom numbering scheme for these complexes are given in **Figure 7.1** with the relevant bond distances and angles collected in **Table 7.2**−**7.3**.

Nonoxido vanadium(IV) $[V^{IV}(L^2)_2]$ (2). Molecular structure of **2,** one of the four nonoxido vanadium(IV) complexes has been determined by single crystal X-ray crystallography. The details of the structure of $[V^{IV}(L^2)_2]$ (**2**) is shown in **Figure 7.1a** and selected geometric parameters are collected in **Table 7.2.** The remarkable feature of the structure is the trigonal prismatic co-ordination of the d^l V^{IV} ion. In complexes **2**, the vanadium(IV) centre is coordinated to two ligands forming a N_2O_4 coordination sphere, constituting the rare trigonal prism structure.[6a] The central V atom is coordinated by two dinegative, NO_2 coordinating hydrazone ligands forming five membered CN_2OV and six membered C_3NOV chelate rings. The bite angle for the two five membered ring around the vanadium centre, O(2)−V(1)−N(1) and O(4)−V(1)−N(3) found in the range 74.43(5)−74.37(5)° and similarly for the six membered ring O(1)−V(1)−N(1) and O(3)−V(1)−N(3) it is in the range 82.54(6)−82.33(5)°. The four V−O bonds around the central vanadium atoms are in the range 1.912(1) to 1.900(1) Å, among which, the V−O bond length follows the order V−O(phenolate) < V−O(enolate). The other distances and angles made by the donor atoms are in the expected range as previously reported for compounds containing the $[V^{IV}(ONO)_2]$ moiety.[9d,6x]

Oxidoethoxido vanadium(V) $[V^{V}O(L^{1-2})OEt]$ (5 & 6). In complexes $[VOL^{1-2}(OEt)]$ (**5** and **6**), the vanadium(V) centre is occupied by O_4N coordination sphere, constituting a square pyramidal structure (**Figure 7.1b**,**c)**. The details of the selected geometric parameters are collected in **Table 7.3**. The basal plane is made up by the phenolate oxygen, enolate oxygen, imine nitrogen from the ligand and the oxygen from deprotonated alkoxide. The Schiff base ligand forms a six

membered and a five membered chelate ring at the V(V) accepter centre with O(1)–V(1)–N(1) and O(2)–V(1)–N(1) bite angles in the range of 81.28(3)−80.87(5)° and 75.03(4)−74.96(3)° respectively. The apical position of square pyramid is occupied by the terminal oxido group O(3). The short V(1)−O(3) distance in the range of 1.592(7)−1.587(1)A° indicates the presence of vanadium oxygen double bond (V=O), which is commonly found in five and six coordinated octahedral complexes[15] of vanadium(IV) and vanadium(V). For all the complexes, the four V−O bond lengths are unequal, the V=O bond being the shortest and V−O (enolate) being the longest. The V−O bond length follows the order, V−O(oxido) < V−O(alkoxido) < V−O(phenolate) < V−O(enolate). These data indicate the stronger binding of alkoxido group compared to those of phenolate and enolate oxygen atom.[15]

Table 7.2. Selected bond distances (Å) and angles (^{0}) for 2

Distances			
V(1)-O(1)	1.905(1)	V(1)-N(1)	2.076(2)
V(1)-O(2)	1.909(1)	V(1)-N(3)	2.069(1)
V(1)-O(3)	1.900(1)	N(1)-N(2)	1.400(2)
V(1)-O(4)	1.912(1)	N(3)-N(4)	1.389(2)
Angles			
O(1)-V(1)-N(1)	82.33(5)	O(2)-V(1)-O(3)	86.05(5)
O(1)-V(1)-O(2)	127.04(5)	O(1)-V(1)-O(4)	86.49(5)
O(2)-V(1)-N(1)	74.37(5)	O(3)-V(1)-O(4)	127.51(5)
O(3)-V(1)-N(3)	82.54(6)	O(2)-V(1)-O(4)	137.26(5)
O(4)-V(1)-N(3)	74.43(5)	O(1)-V(1)-O(3)	84.23(5)

Table 7.3. Selected bond distances (Å) and angles (^{0}) for 5 and 6

	5	**6**
Distances		
V(1)-O(1)	1.885(1)	1.8385(7)
V(1)-O(2)	1.926(1)	1.9123(7)
V(1)-O(3)	1.587(1)	1.592(7)
V(1)-O(4)	1.771(1)	1.7826(7)
V(1)-N(1)	2.126(1)	2.0994(8)
N(1)-N(2)	1.392(2)	1.391(1)
Angles		
O(1)-V(1)-N(1)	80.87(5)	81.28(3)
O(1)-V(1)-O(3)	102.78(5)	110.63(3)
O(1)-V(1)-O(2)	143.72(4)	132.38(3)
O(2)-V(1)-O(4)	95.26(5)	90.48(3)
O(2)-V(1)-O(3)	105.67(5)	112.21(3)
O(2)-V(1)-N(1)	75.03(4)	74.96(3)
O(3)-V(1)-O(4)	102.80(5)	104.72(3)
O(3)-V(1)-N(1)	94.28(5)	95.48(3)
O(4)-V(1)-N(1)	162.19(5)	158.53(3)

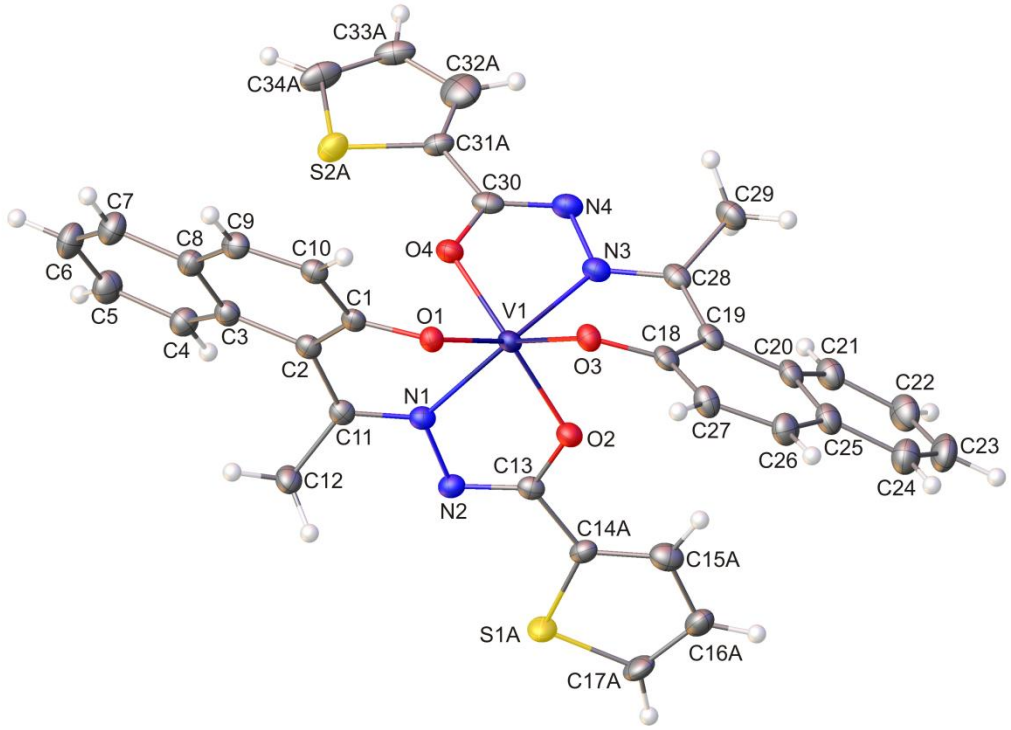
C33A
C32A
C34A
C31A
S2A
C30
N4
C29
C7
C8
C9
C10
O4
N3
C6
C28
C1
C5
O1
V1
C19
C4
C3
C18
C20
C21
C2
O3
C22
N1
C27
C11
O2
C26
C25
C23
C13
C12
N2
C24
C14A
C15A
S1A
C16A
C17A

a)

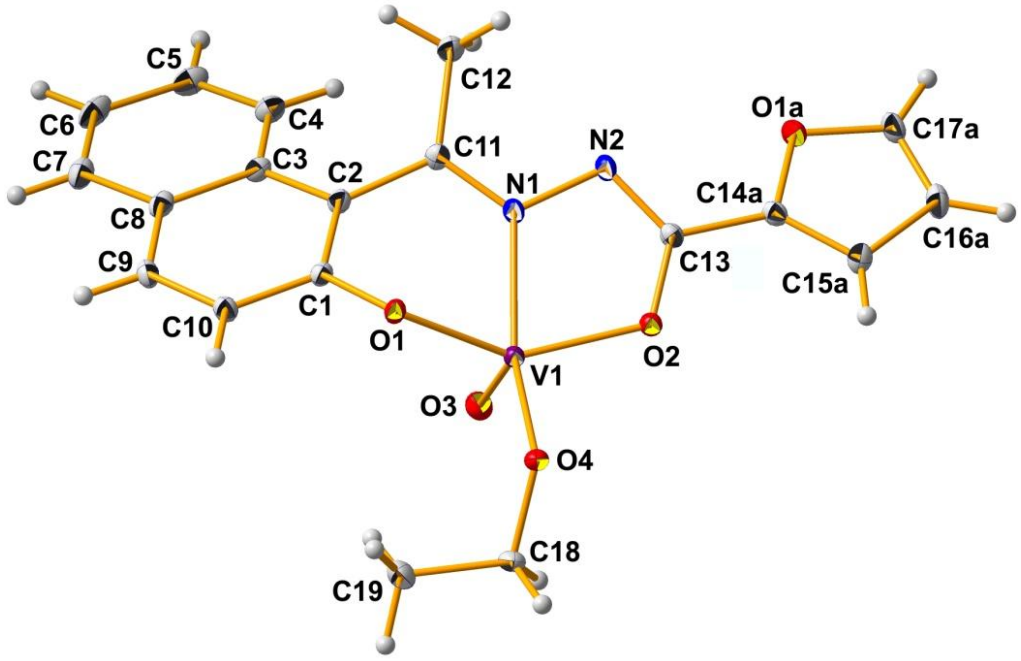
C5
C12
O1a
C17a
C6
C4
C11
N2
C7
C3
C2
N1
C14a
C8
C16a
C9
C13
C15a
C1
C10
O1
O2
V1
O3
O4
C18
C19

b)

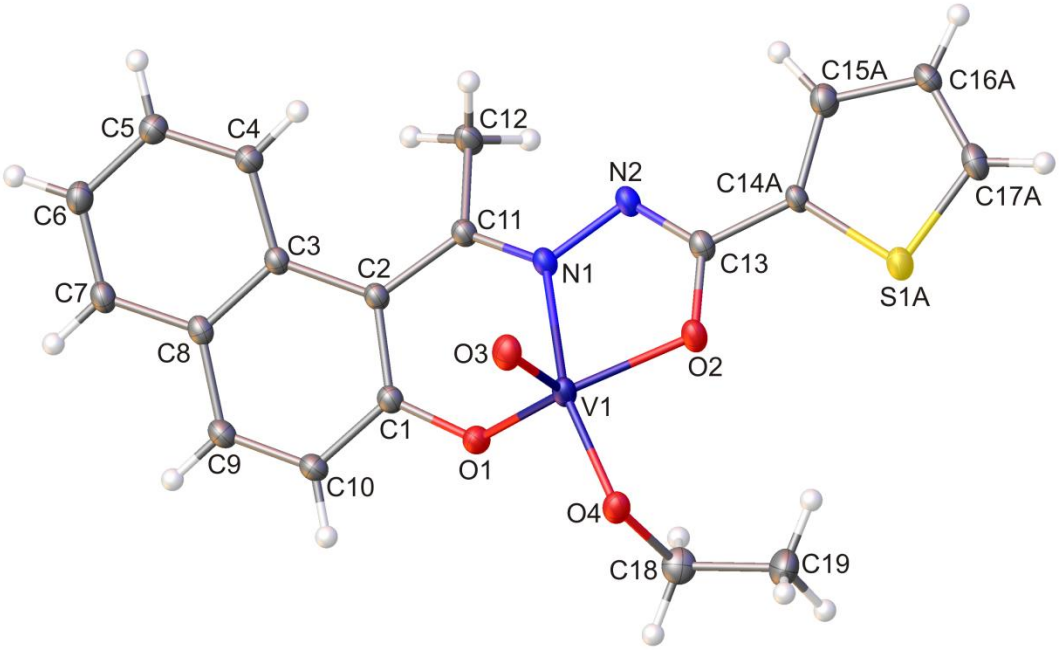

c)

Figure 7.1. ORTEP diagram of (a) $[V(L^2)_2]$ (**2**), (b) $[VO(L^1)OEt]$ (**5**), (c) $[VO(L^2)OEt]$ (**6**)

7.3.1.3. IR Spectroscopy. The IR data of all the ligands, H_2L^{1-4} and their corresponding metal complexes, **1–8** are given in the experimental section. All the ligands possess a band in the region of 3648–3331 cm^{-1} due to the –OH present in the ketone part, which is found to be absent in the corresponding metal complexes due to the coordination. However, the presence of band in the range 3362–3156cm^{-1} in case of complex **4** and **8** is due to the pending –OH group attached to the hydrazide nucleus of ligand (H_2L^4) that does not take part in metallation. Disappearance of bands for –NH and –C=O and appearance of new bands in the range 1244–1238 cm^{-1} indicates the enolization of these two groups forming –N=C–O– type of bond. For **5**–**8**, presence of sharp band in the range 1001–994 cm^{-1} is assigned to V=O stretching of a penta coordinated oxido vanadium(V) complex[9a] whereas absence of *v*(V=O) bands in the range 1035–935 cm^{-1} clearly indicate the nonoxido nature of the complexes (**1**–**4**).[16]

7.3.1.4. UV Spectroscopy. Electronic spectra of complexes, **1–8** were recorded in $CHCl_3$. The spectral data are summarized in experimental section. Complexes, **1−4** possess similar characteristic spectral features. A representative spectrum of **2** is shown in **Figure 7.2**. There are two bands in the 627–511 nm range, among which, the lowest-energy transition band around 627–616 nm is situated in the d−d transition region, but the intensity ($\varepsilon_{max,}$ 23006–18092 $M^{-1}cm^{-1}$) of this band appears too large for a pure d−d transition, for which the intensity is generally very low for vanadium(IV) complexes. The high intensity of these two bands (627–511nm) and analogy with other 'bare' vanadium(IV) complexes[6a,b,c,e,j,h,o,p,x] suggest that these transitions are most reasonably assigned as ligand-to-metal charge transfer in origin. The other bands in the higher energy absorptions (377–229 nm) are likely to be due to ligand centered transitions.[10b] For oxido vanadium(V) complexes (**5**–**8**), the spectral features are similar and the representative spectrum of **8** is shown in **Figure 7.3**. The strong absorptions observed in the wavelength range 432–427 nm are assignable to the ligand-to-metal charge transfer transitions whereas the other bands in the higher energy region (342–231 nm) are likely to be due to ligand centred transitions.[9a,10b]

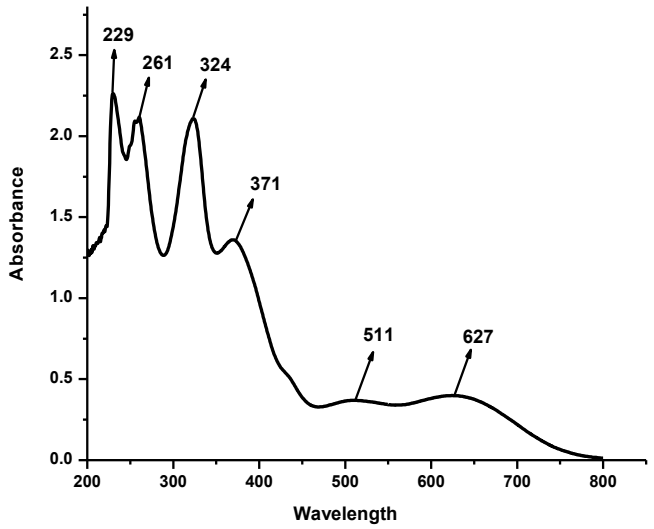

Figure 7.2. UV-Vis spectra of **2** (1.83 x 10^{-5} M) in $CHCl_3$.

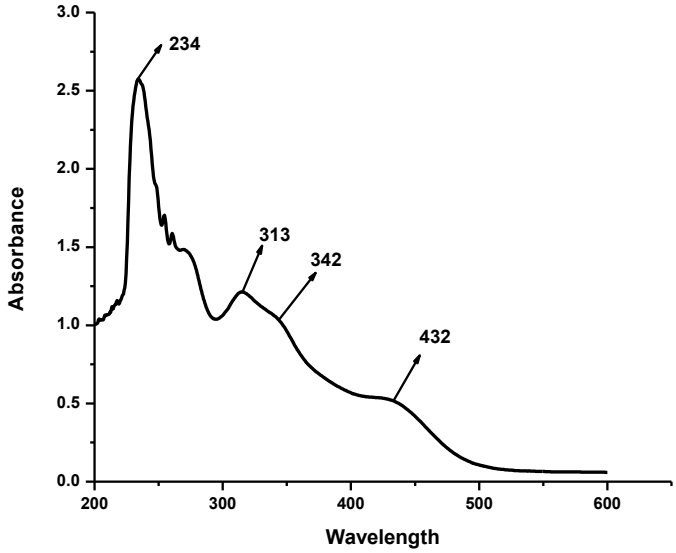

Figure 7.3. UV-Vis spectra of **8** (1.83 x 10^{-5} M) in $CHCl_3$.

7.3.1.5. NMR Spectroscopy. ^{1}H and ^{13}C NMR of the ligands (H_2L^{1-4}) were recorded in DMSO-d_6 and the data are given in the experimental section. The spectra of the free ligands, (H_2L^{1-4}) exhibit a resonance in the range, δ = 11.87–10.31 ppm due to –OH, δ = 10.15–9.09 ppm due to –NH and δ = 2.40–2.33 ppm due to $–CH_3$ protons. In H_2L^4 an extra peak at δ = 11.67 ppm is observed which is due to the –OH group attached to the hydrazide nucleus. All the aromatic protons of the ligands are clearly observed in the expected region, δ = 8.68–6.51 ppm.[10b]

From the ^{13}C NMR spectra, it is observed that, signals for (CO–N) and [N=C(Me)] carbon resonate in the downfield region in the range, δ = 166.82–161.48 ppm and δ = 154.89–152.34 ppm respectively whereas the carbon due to the methyl groups ($–CH_3$) are found in the upfield region (δ = 24.43–24.03 ppm). Furthermore appearance of signals in the range δ = 153.33–111.04 ppm due to aromatic carbon confirm the formation of the ligands.[2a]

Results of NMR spectra for complexes **5**–**8** are summarized in the solution study part

7.3.1.6. Electrochemical properties of nonoxido vanadium(IV) complexes [$V^{IV}(L^{1-4})_2$] (1–4). The electrochemical properties of **1**–**4**, have been examined in CH_2Cl_2 solution (0.1 M TEAP) by cyclic voltammetry using a Pt working electrode, Pt counter electrode, and an Ag/AgCl reference electrode. The voltammogram pattern is similar for **1**–**4**, which includes both oxidation and reduction process corresponding to one electron transfer. The potential data are listed in **Table 7.4** and **Figure 7.4** depicts a representative voltammogram of **2**. In the cathodic region V(IV) is reduced to V(III) showing a quasi-reversible single electron wave (**Figure 7.4a**) at $E_{1/2}$ values within the potential window –0.53 to –0.40 V.[17] In the anodic region, complexes show a quasi-reversible single electron wave (**Figure 7.4b**) at $E_{1/2}$ values within the potential window 1.20 to 1.05 V is assigned to the oxidation of the metal, V(IV)/V(V).[18]

Table 7.4. Cyclic voltammetric results for 1–4 at 298 K

Complex	$E^{c}_{1/2}$ (V)	ΔE^{c}_{P} (mV)	$E^{a}_{1/2}$ (V)	ΔE^{a}_{P} (mV)
$[V^{IV}(L^{1})_2]$ (**1**)	– 0.53	98	1.13	120
$[V^{IV}(L^{2})_2]$ (**2**)	– 0.40	96	1.10	100
$[V^{IV}(L^{3})_2]$ (**3**)	– 0.50	95	1.05	108
$[V^{IV}(L^{4})_2]$ (**4**)	– 0.52	102	1.20	124

In CH_2Cl_2 at a scan rate of 100 mV s^{-1}. $E_{1/2} = (E_{pa} + E_{pc})/2$, where E_{pa} and E_{pc} are anodic and cathodic peak potentials vs. Ag/AgCl, respectively. $\Delta E_P = E_{pa} - E_{pc.}$

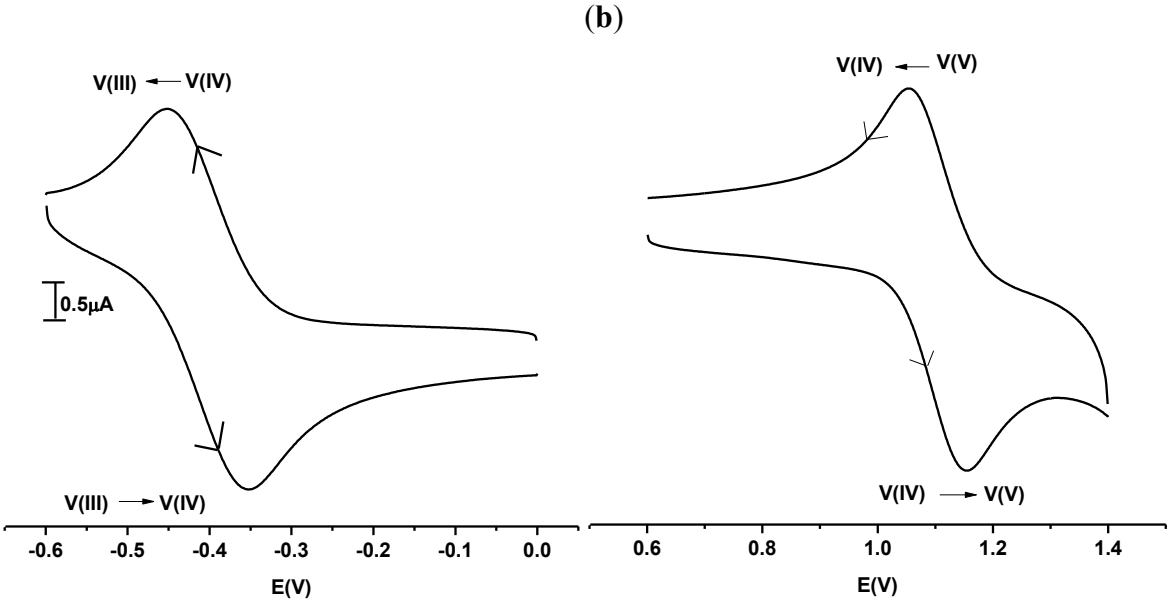

Figure 7.4. Cyclic voltammogram of **2** showing (a) reduction (V(IV) →V(III)) and (b) oxidation (V(IV) →V(V)) of the vanadium(IV) centre.

7.3.1.7. EPR Spectroscopy of nonoxido vanadium(IV) complexes, 1–4. X-band EPR spectra of **1**–**4** were recorded in CH_2Cl_2 solution at 300 K. The data are listed in **Table 7.5**. A representative spectrum for **2** is shown in **Figure 7.5**. which reveals well-resolved axial anisotropy with 8-line hyperfine structure, characteristic of a mononuclear vanadium complex with nuclear spin (^{51}V, I = 7/2).[19] Corresponding spin-Hamiltonian parameters (g, 1.948−1.941; A, 46.47 × 10^{-4} cm^{-1}–45.59 × 10^{-4} cm^{-1}) are typical of trigonal prismatic oxido vanadium(IV) complexes under comparable ON-containing donor environments.[6a] Analysis of the EPR spectra of vanadium(IV) complexes showed that, the anisotropic hyperfine parameters of six-coordinate complexes[19] have significantly lower values compared to the corresponding values obtained with the five-coordinated complexes,[10b,20] as is observed in the present case.

Table 7.5. X-band EPR data for complexes 1–4 at 300 K

Complex	g	A (10^{-4} cm^{-1})
$[V^{IV}(L^1)_2]$, **1**	1.947	46.47
$[V^{IV}(L^2)_2]$, **2**	1.948	45.59
$[V^{IV}(L^3)_2]$, **3**	1.941	45.86
$[V^{IV}(L^4)_2]$, **4**	1.943	46.11

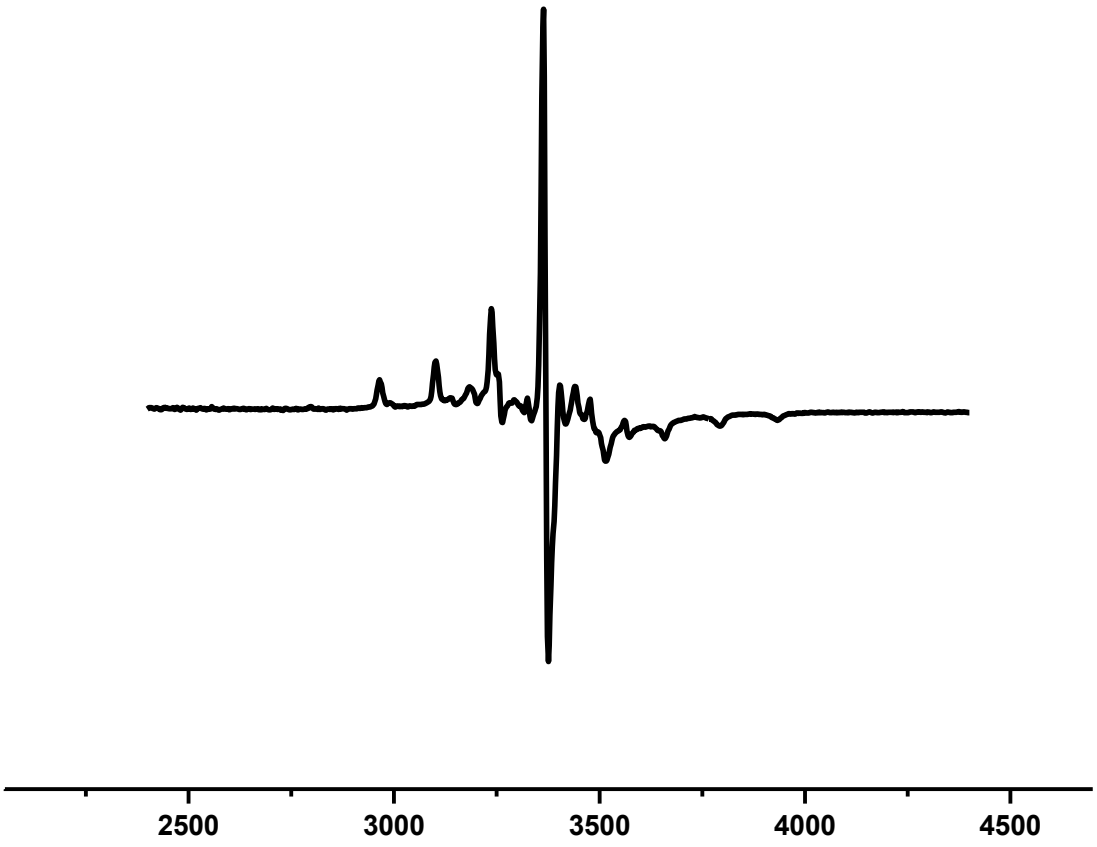

Figure 7.5. X-band EPR spectrum (300 K) in CH_2Cl_2 of complex **2**.

7.3.1.8. Study of solution behavior of oxidoethoxido vanadium(V) complexes (5–8). Study of solution behavior of all the oxidoethoxido vanadium(V) complexes (**5**–**8**) were carried out in DMSO/$CHCl_3$. The IR spectrum of all the complexes (**5−8)** in DMSO/$CHCl_3$ shows two V=O stretch bands in the range 1009–1004 $cm^{-1}$and 970–965 cm^{-1}, which suggests that two different V=O groups exist in solution.[10a] Another new band corresponding to the *ν*(V–O–V) [10b,9a] mode was also observed in the range 822−817 cm^{-1}, which was absent in the spectrum of **5**−**8** in the solid state. The IR spectrum in solution pointed to the retention of their mononuclear nature what was in the solid state and simultaneous formation of the corresponding dimeric complexes as a 2nd species. So, these observations suggest that two species may exist in solution and demand proper explanation.

The ^{1}H NMR spectra of **5**−**8** in DMSO-d_6 (which contained trace water) yielded two close but separate sets of bands in an approximate 1:1 ratio. A representative spectrum of **7** is shown in **Figures 7.6a**. The set of sharp ^{1}H NMR signals correspond to the monomeric form of the species [VO(L^{1-4})OEt] (**5**−**8**) which are isolated in the solid state and structurally characterized. The relatively less sharp signals were assigned to the other species (let the corresponding 2nd species). So, like our previous report (chapter 4) the NMR results suggest that two species exist in DMSO solution. The spectrum of **5**–**8** exhibits two sets of singlets corresponding to the $–CH_3$ group in the range 3.03–2.86 ppm and that of **8** exhibits two sets of OH resonance at 11.78 and 11.42 ppm. The aromatic protons of **5** and **6** (a total of 18), of **7** (a total of 26) and **8** (a total of 24) appear in the range 9.30−6.63 ppm. In addition, all the complexes exhibit separate bands corresponding to bound ethoxido group in the range 5.72–5.44 ($–CH_2$) and 1.61–1.45 ($–CH_3$) ppm[10a,b,21] and the sharp peaks observed in the range 3.47–3.42 ($–CH_2$) and 1.08–1.04 ($–CH_3$) ppm were assigned to free, non-ligated ethanol that is most likely to be formed *in situ* in solution. Though the chemical shifts of the methylene and methyl protons of the ethanol are very close to those of the free ethanol, the alcoholic proton is not detected may be because of less concentration or overlap of the signals.

On addition of few drops of ethanol to the DMSO-d_6 solution of complexes **5**−**8**, the 2nd set of bands disappeared and a clear spectrum resulted (**Figures 7.6b)**. The clear spectrum exhibits only one OH resonance at 11.77 ppm for **8**, one $–CH_3$ proton signal in the range 2.95–2.85 ppm for **5**–**8**, and signals for a total of nine aromatic protons for **5** and **6,** thirteen for **7** and twelve for

8 in the range 9.16−6.67 ppm. In addition, the coordinated ethoxido bands in the range 5.70–5.42 ppm (–CH_2) and 1.61–1.46 (–CH_3) ppm[10a,b,21,22] broadened and the intensity of free ethanol bands in the range 3.48–3.42 ppm due to (–CH_2) and 1.08–1.04 ppm due to (–CH_3) ppm increased.

Like above, the ^{51}V NMR spectrum of complexes **5−8** in DMSO-d_6 display two sets of bands at an approximate ratio of 1:1 in the range –564 to –519 ppm (**Figures 7.7a**) and the 2nd set of band disappeared on addition of small amount of ethanol (**Figures 7.7b**). Similar observations were also obtained from ^{13}C NMR data **(Figure 7.8).**

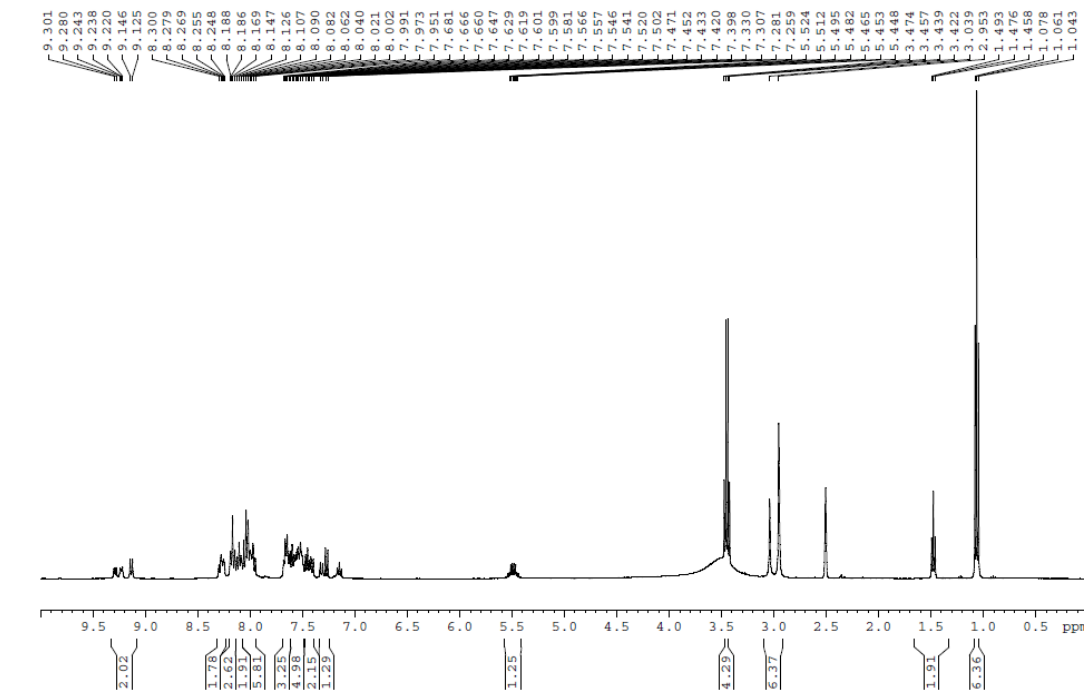

a)

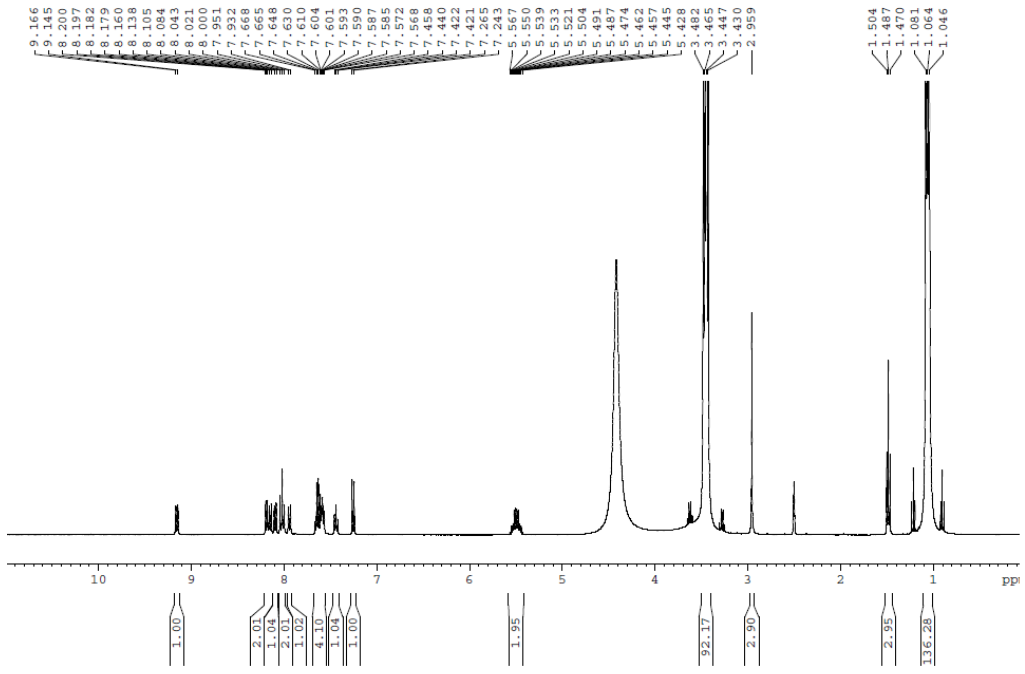

b)

Figure 7.6. [1]H NMR spectrum of complex **7** in DMSO-d_6: a) before addition of ethanol b) after addition of ethanol.

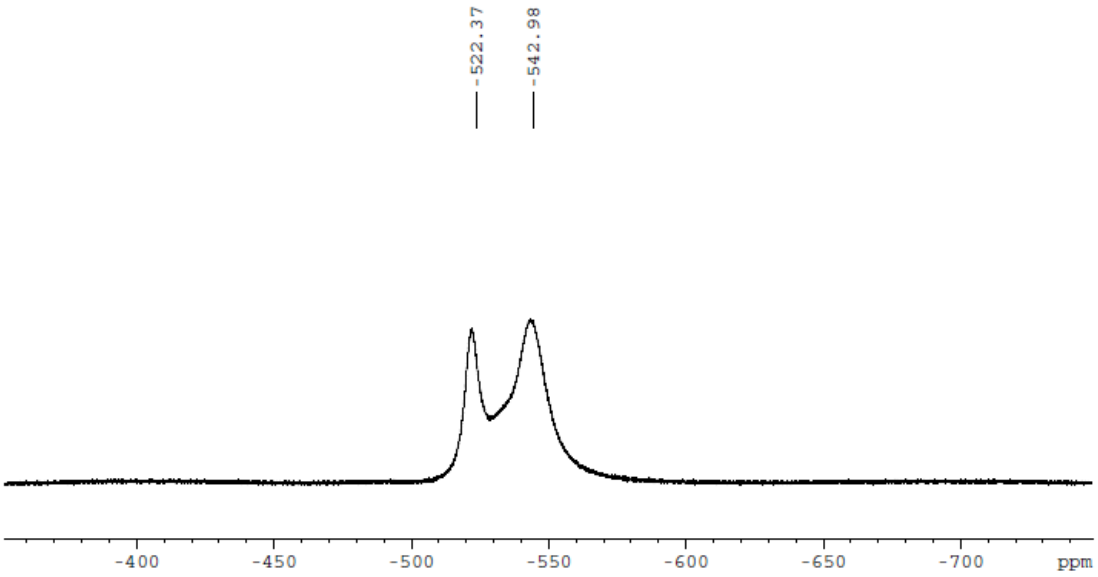

a)

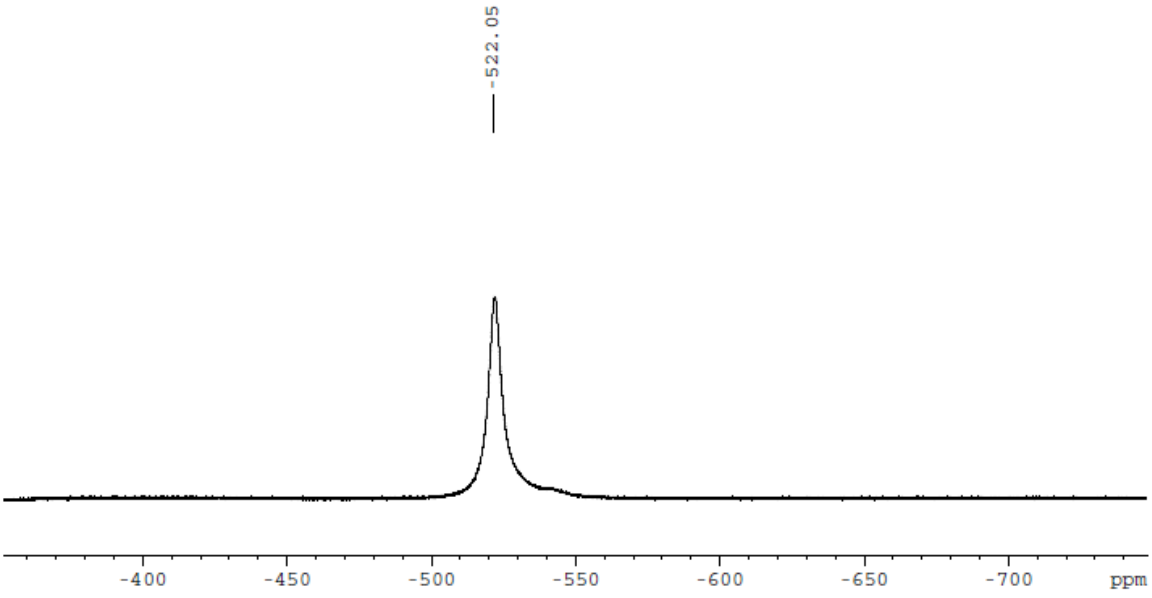

b)

Figure 7.7. Representative ^{51}V NMR spectrum of complex **5** in DMSO-d_6: a) before addition of ethanol b) after addition of ethanol.

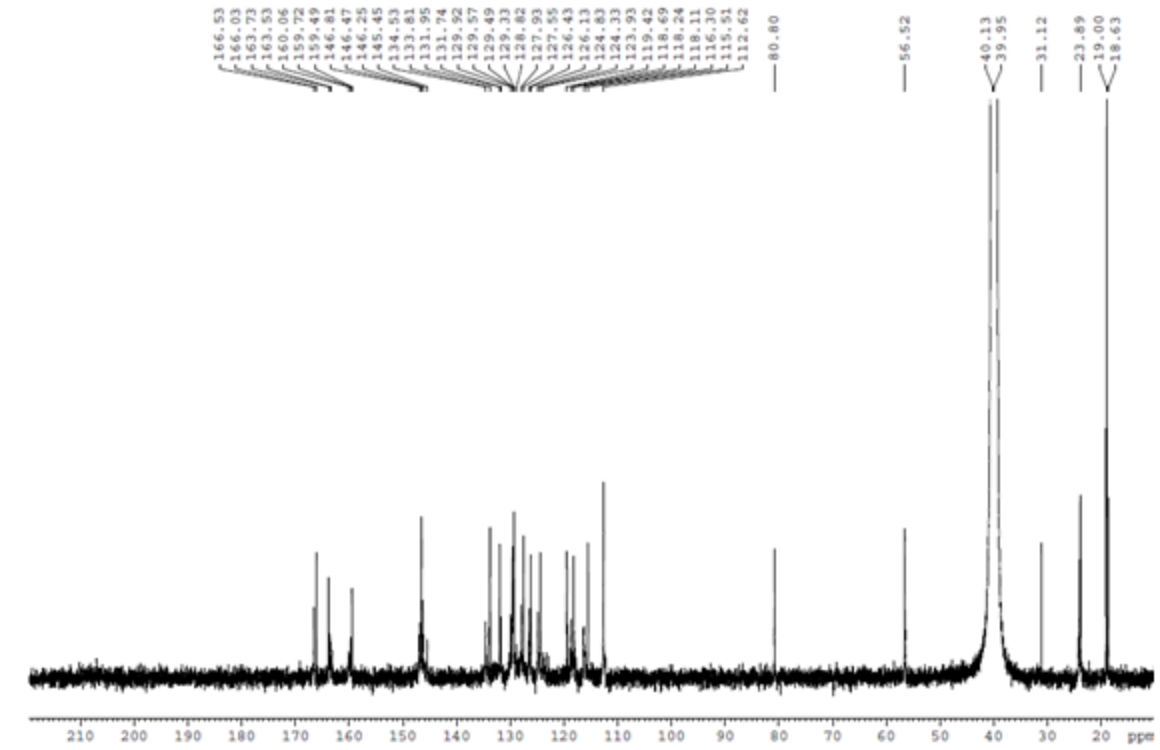

a)

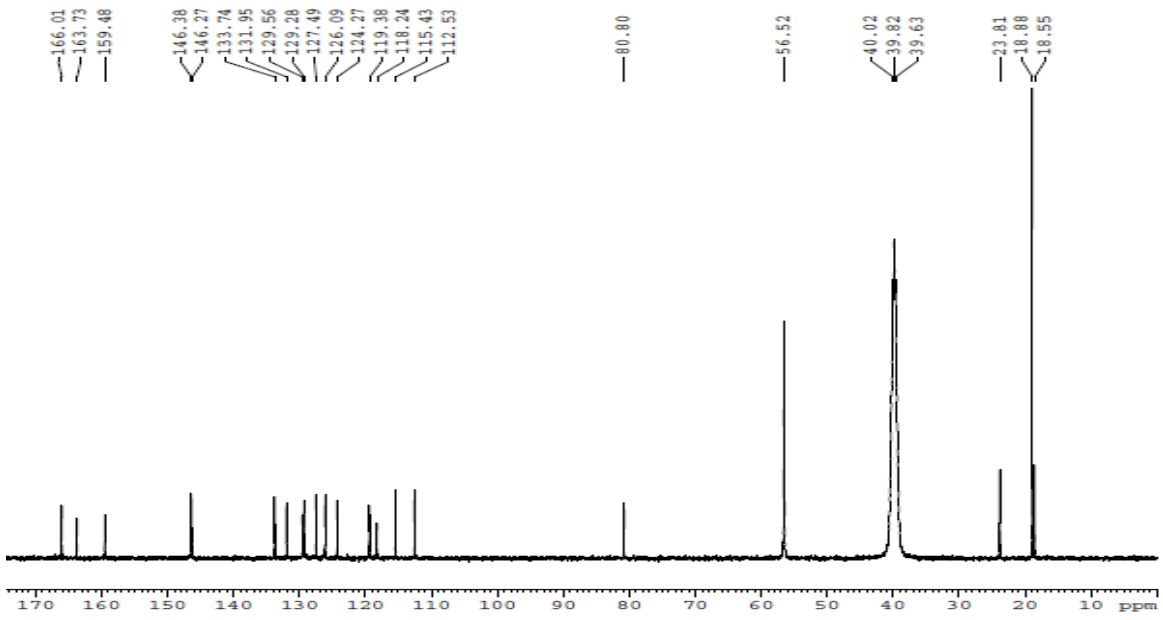

b)

Figure 7.8. Representative ^{13}C NMR spectrum of complex **5** in DMSO-d_6: a) before addition of ethanol b) after addition of ethanol.

So, the NMR results also support the existence of a second species in the solution state and it must be the corresponding dimeric species as it is evidenced form the IR as well as NMR spectroscopy.

On the basis of the explanation described in our previous results (chapter 4) containing similar type complexes, these solution behavior of **5**–**8** can be interpreted as by proposing the following equilibrium (**Chart 7.1**) existing in DMSO/$CHCl_3$ containing a little water, which also explains the simultaneous presence of the two species, **M** (monomer, isolated in the solid state and solved by X-ray crystallography) and **D** (2nd species, generated *in situ* as μ-oxido dimer) in solution.

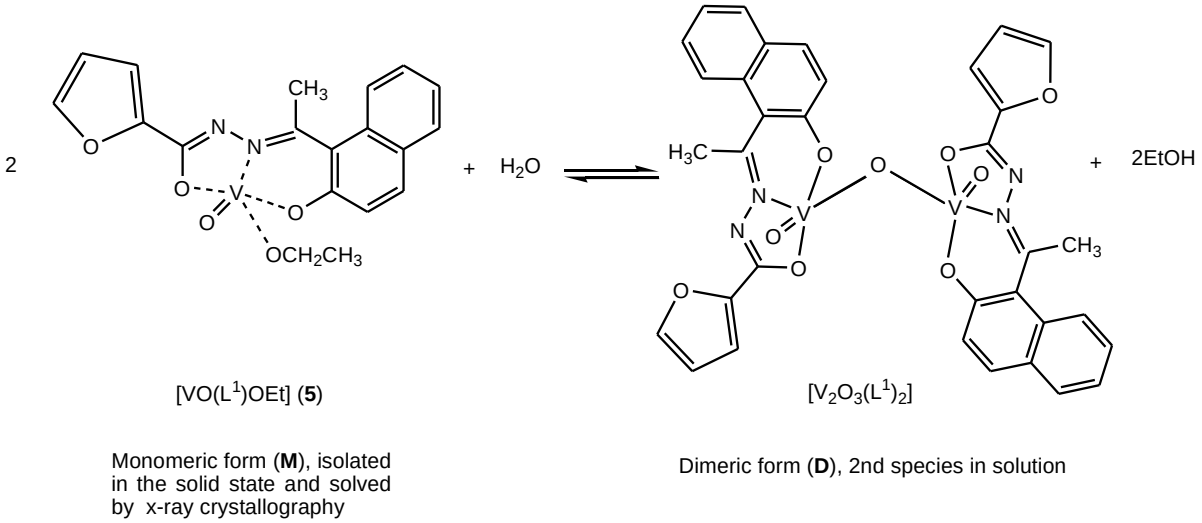

Chart 7.1. Schematic diagram for the inter-conversion of monomeric and dimeric species in solution taking Complex **5**.

The confirmation of the second species as μ-oxido dioxido divanadium(V) was further evidenced by the isolation of this complex in solid state. The details of synthesis and full characterization of this dimeric complex are described in next section.

7.3.1.9. Electrochemical properties of oxido vanadium(V) complexes (5–8). Electrochemical properties of all the mono- and dioxido vanadium(V) complexes have been studied by cyclic voltammetry in dichloromethane solution (0.1 M TEAP). Voltammetric data are given in **Table 7.6**. All the monooxido ethoxido vanadium(V) complexes **(5**–**8**) show one reversible oxidative response on the positive side of Ag/AgCl and two quasi-reversible reductive responses on the negative side. A representative voltammogram is displayed in **Figure 7.9** In positive side the complexes display a well-defined cyclic voltammetric response at platinum electrode due to the VO^{3+}–VO^{2+} couple[16b,23] at the range $E_{1/2}$ = 0.35 − 0.31V (ΔE_P = 166 − 157 mV), eqs 1, whereas in negative side the voltammogram is found to undergo two successive one electron reductions at the range $E_{1/2}$ = − 0.67 V (ΔE_P = 279 mV) to – 0.74 (ΔE_P = 287 mV) and $E_{1/2}$ = − 1.34 V (ΔE_P = 278 mV) to $E_{1/2}$ = − 1.37 V (ΔE_P = 280 mV) which are assigned to $V^{V}V^{V}/V^{IV}V^{V}$ and $V^{IV}V^{V}/V^{IV}V^{IV}$ couples,[9a] eqs 2.

$$[VO(ONO)(OEt)] + e^- \rightleftharpoons [VO(ONO)(OEt)]^- \quad \ldots\ldots\ldots\ldots\ldots\ldots\ldots\ldots(1)$$

$$V^{V}{}_2O_3L_2 + 2e^- \rightleftharpoons V^{IV}V^{IV}O_3L_2{}^{2-} \ldots\ldots\ldots\ldots\ldots\ldots\ldots\ldots\ldots\ldots(2)$$

The above results clearly supports that there were two species present in the solution state, one is the monooxido ethoxido vanadium(V) monomer isolated in the solid state and the other is the corresponding μ-oxido bridged dioxido divanadium(V) species generated *in situ* in the solution.

Table 7.6. Cyclic voltammetric results for 5–9 at 298 K

Complex	$E^a_{1/2}$ (ΔE^a_P) / V(mV)	$E^c_{1/2}$ (ΔE^c_P) / V(mV)
$[V^{V}O(L^1)OEt]$ (**5**)	0.35 (166)	–0.74 (287), –1.37 (280)
$[V^{V}O(L^2)OEt]$ (**6**)	0.31 (157)	–0.69 (289), –1.34 (278)
$[V^{V}O(L^3)OEt]$ (**7**)	0.32 (164)	–0.71 (285), –1.36 (277)
$[V^{V}O(L^4)OEt]$ (**8**)	0.31 (162)	–0.67 (279), –1.36 (245)
$[V^{V}{}_2O_3(L^1)_2]$ (**9**)	0.34 (167)	–0.72 (254), –1.37 (211)

In CH_2Cl_2 at a scan rate of 100 mV s^{-1}. $E_{1/2} = (E_{pa} + E_{pc})/2$, where E_{pa} and E_{pc} are anodic and cathodic peak potentials vs. Ag/AgCl, respectively. $\Delta E_P = E_{pa} - E_{pc}$.

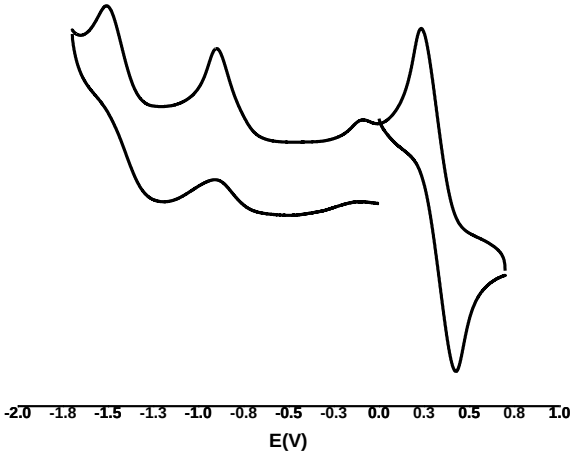

Figure 7.9. Cyclic voltammogram of complex **5** in CH_2Cl_2.

The confirmation of the second species as μ-oxido divanadium(V) was further evidenced by the isolation of this complex in solid state. The details of synthesis and full characterization of this dimeric complex are described in next section.

7.3.2. μ-oxido dioxido divanadium(V) complex, $[V^{V}_{2}O_3(L^1)_2]$ (9).

7.3.2.1. Synthesis. The μ-oxido dioxido divanadium(V) complex $[V_2O_3(L^1)_2]$ (**9**) was obtained (**Scheme 7.1**) by the areial oxidation of $[VO(L^1)OEt]$ (**5)** in DCM and CH_3CN mixture. The reactions are clean, affording large quantities of pure crystalline products in good yield (~ 70%). The compound **9** is highly soluble in CH_2Cl_2, DMF and DMSO and sparingly soluble in MeOH, EtOH and CH_3CN.

7.3.2.2. Spectroscopy. The spectral (IR, UV-Vis and NMR) data of **9** are summarized in the experimental section. In the IR spectrum (**Figure 7.10)**, a pair of sharp band were observed at 999 and 963 cm^{-1} because of terminal V=O stretching along with a moderately strong band due to V–O–V asymmetric bridge vibration is located at 823 cm^{-1}.[22]

For divanadium(V) complex (**9**), the UV-Vis spectral feature is similar like mononuclear oxido vanadium(V) complexes (**5**-**8**). The strong absorptions observed at 425 nm are assignable to the ligand-to-metal charge transfer transitions whereas the other bands in the higher energy region (336 – 246 nm) are likely to be due to ligand centred transitions.[9a,10b]

The NMR spectrum of **9** shows a multiplet in the range 8.20–6.63 ppm for nine aromatic protons and a singlet at 2.92 ppm due to $–CH_3$ group attached in the ligand fragment. Comparision of the ^{1}H NMR spectrum of complex **5** and **9** in DMSO-d_6 indicates the presence of **9** in the solution state of **5**. When a drop of ethanol was added all peaks corresponding to complex **9** get disappered and a clear spectrum was observed which corresponds to the mononuclear oxido vanadium(V) complex, $[V^{V}O(L^1)OEt]$ (**5**) and that is the compound isolated in the solid state.

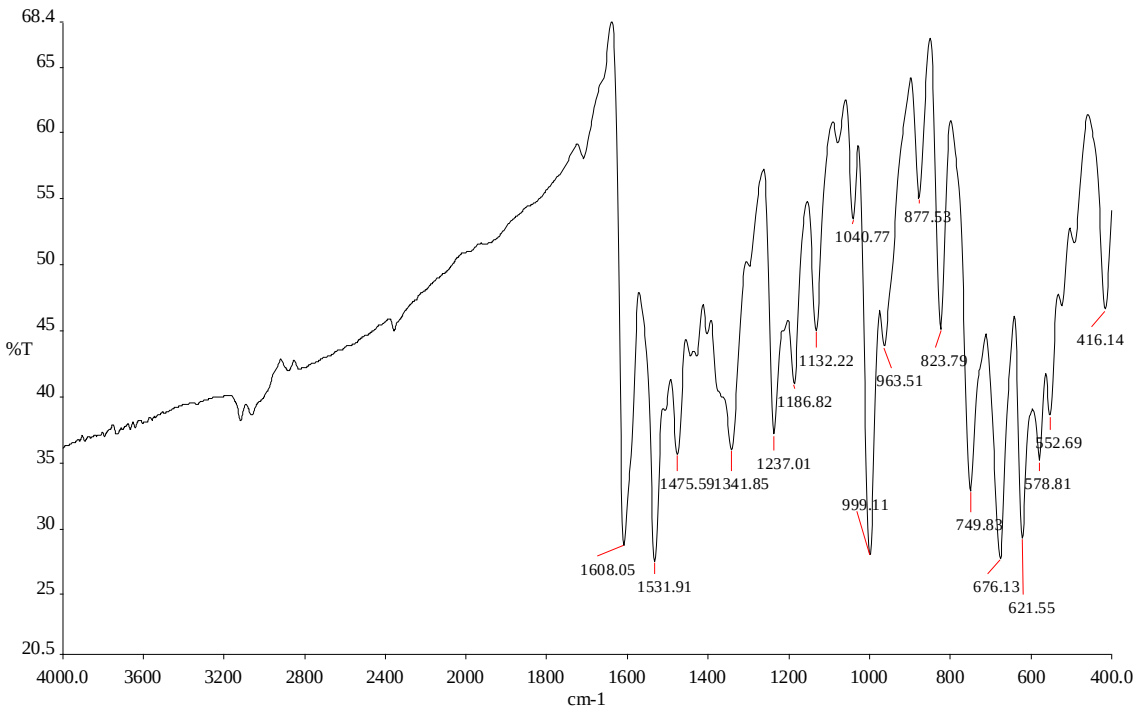

Figure 7.10. IR spectrum of $[V^{V}_{2}O_{3}(L^{1})_{2}]$ (**9**).

7.3.2.3. Electrochemical property of μ-oxido dioxido divanadium(V) complex, $[V^{V}_{2}O_{3}(L^{1})_{2}]$ (9). The electrochemical property of **9** has been examined in CH_2Cl_2 solution (0.1 M TEAP) by cyclic voltammetry (CV) using a Pt working electrode, Pt counter electrode, and an Ag/AgCl reference electrode. The voltammogram pattern of **9** is almost similar and the result matches well with the voltammogram of corresponding monomeric oxido vanadium(V) complex, **5**, discussed earlier. Thus, the CV result also suggests that the dimeric complex may converts to the corresponding monomeric species in solution state. The cyclic voltammogram of **9** is shown in **Figure 7.11** and data are given in **Table 7.6**.

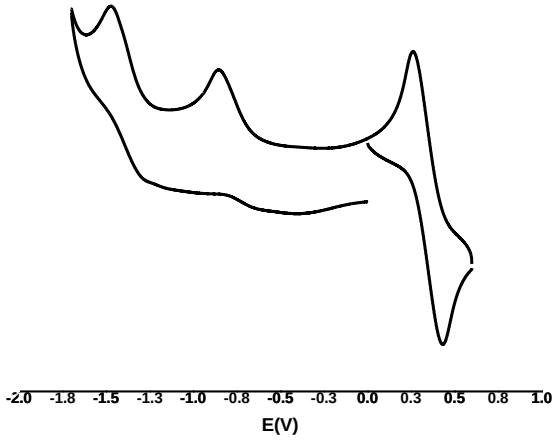

Figure 7.11. Cyclic voltammogram of complex **9** in CH_2Cl_2.

7.3.2.4. Description of X-ray structure of μ-oxido dioxido divanadium(V) [$V^{V}_{2}O_3(L^1)_2$] (9).

The divanadium(V) complex (**9**) afforded good crystals as the solvate $V_2O_3L_2{\cdot}CH_2Cl_2$. The lattice consist of CH_2Cl_2 molecules which are not bonded to the metal atom in any way. A view of the binuclear complex is shown in **Figure 7.12**, and selected bond parameters are listed in **Table 7.7**. The geometry of the metal atom is similar to that in [$VOL^{1\text{-}2}$(OEt)] (**5** & **6**), but here the pyramidal base is constituted of ONO of L^{2-} and the bridging oxygen atom O(4). Both the metal atoms have distorted square pyramidal geometry[9a,24] of coordination type VO_4N. The two coordination pyramids are metrically distinct. The basal positions are occupied by the donor atoms O(1)/O(5), N(1)/N(3), O(2)/O(6) and O4, contributed by the tridentate ligand $(L)^{2-}$, together with the bridging oxygen atom. The apical positions are taken up by the terminal oxygen atom O3 and O7. The terminal V−O distances 1.586(2) Å [V(1)−O(3)] and 1.585(1) Å [V(2)−O(7)] are typical of a vanadium-oxygen double bond. [9a,24] In **9**, the *trans* angles in the basal plane O(1)−V(1)−O(2) 147.41(7)° and N(1)−V(1)−O(4) 149.08(7) (corresponding angles in V(1) center) and O(5)−V(2)−O(6) 146.55(7)° and N(3)−V(2)−O(4) 149.44(7)° (corresponding angles in V(2) center) are much short of linearity, giving indications of distortions in the meridian plane. The angles at the vanadium centers subtended by the terminal and bridging oxido-atoms, that is, O(3)−V(1)−O(4) [106.52(7)°] and O(7)−V(2)−O(4) [105.97(7)°] are in the ranges, as expected for a nearly ideal square pyramidal geometry around V(1) and V(2), respectively. The bridge angles V(1)−O(4)−V(2) for **9** have value of 109.81(8)°, in-between those expected for asymmetric divanadium(V) compounds with square pyramidal vanadium centers. [9a,24,25] The other distances and angles made by the donor atoms in the equatorial plane at V(1) and V(2) (**Table 7.7**) are in the expected range as previously reported for compounds containing the [$V_2O_3(ONO)_2$] moiety. [9a,24]

Table 7.7. Selected bond distances (Å) and angles (^{0}) for 9

Distances			
V(1)-O(1)	1.833(2)	V(2)-O(5)	1.811(2)
V(1)-O(2)	1.971(1)	V(2)-O(6)	1.961(2)
V(1)-O(3)	1.586(2)	V(2)-O(7)	1.585(1)
V(1)-O(4)	1.798(2)	V(2)-O(4)	1.824(2)
V(1)-N(1)	2.082(2)	V(2)-N(3)	2.090(2)
N(1)-N(2)	1.397(2)	N(3)-N(4)	1.399(3)
Angles			
O(1)-V(1)-O(3)	102.11(7)	O(5)-V(2)-O(7)	104.21(7)
O(1)-V(1)-O(4)	106.45(7)	O(5)-V(2)-O(4)	105.97(7)
O(1)-V(1)-N(1)	82.88(7)	O(5)-V(2)-N(3)	82.97(7)
O(2)-V(1)-N(1)	74.53(7)	O(6)-V(2)-N(3)	75.14(7)
O(2)-V(1)-O(4)	83.38(7)	O(6)-V(2)-O(4)	82.67(7)
O(3)-V(1)-O(4)	106.52(7)	O(7)-V(2)-O(4)	105.97(7)
O(1)-V(1)-O(2)	147.41(7)	O(5)-V(2)-O(6)	146.55(7)
O(4)-V(1)-N(1)	149.08(7)	O(4)-V(2)-N(3)	149.44(7)
V(1)-O(4)-V(2)	109.81 (8)		

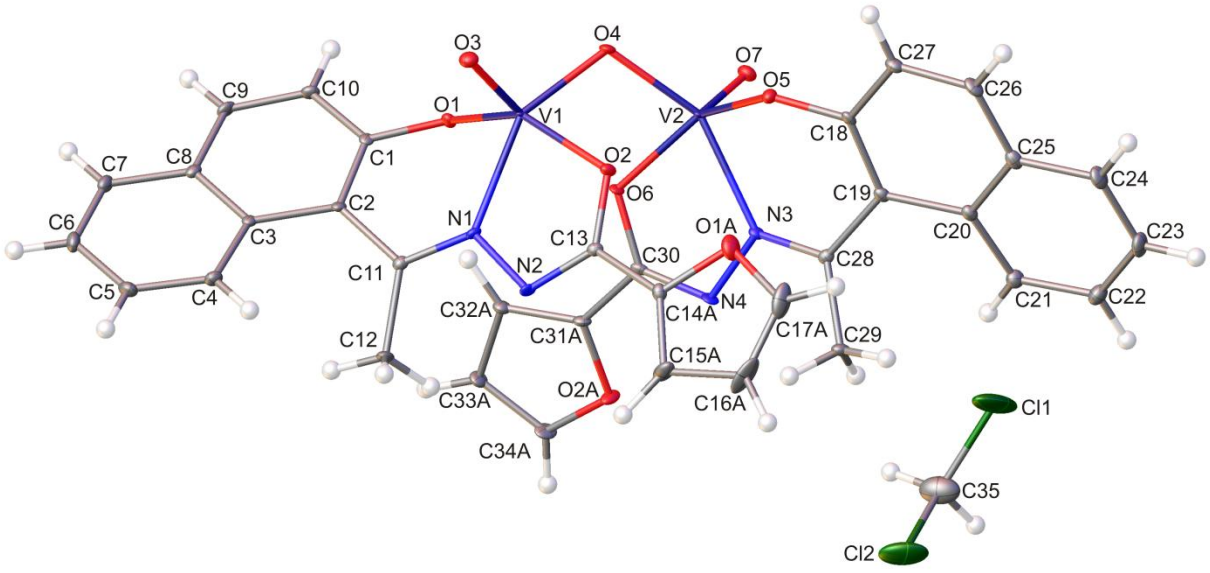

Figure 7.12. ORTEP diagram of $[V_2O_3(L^1)_2]$ (**9**).

From the successful isolation of divanadium(V) complex, **9** in the solid state and the solution study results (UV-Vis, NMR and CV) of mononuclear as well as dinuclear oxidovanadium(V) complexes, it is concluded that, both the mononuclear oxido vanadium(V) complexes (**5**−**8)** and binuclear divanadium(V) complexes exist in the solution. On addition of few drops of ethanol these dimeric species, reconverted into the mononuclear state. The binuclear species exhibits all the characteristic signals of a μ-oxido bridged dioxido vanadium(V) species, which matches well with the similar results reported earlier.[10b]

7.4. CONCLUSION

The following are the salient observations and findings of this work:

a) Four aroylhydrazone ligands, possessing a rigid bulky 2-hydroxy-1-acetonaphthone core and a selection of sterically hindered/bulky naphthoyl- derivative have been synthesized and utilized in the synthesis of the corresponding variable valance mononuclear nonoxido vanadium $[V^{IV}(L)_2]$, oxidoalkoxido vanadium $[V^{V}O(L)OEt]$, and dimeric μ-oxido divanadium $[V^{V}{}_2O_3(L)_2]$ complexes.

b) The monomeric, hexacoordinated and bis(tridentate)-vanadium(IV) $[V^{IV}(L)_2]$ complexes isolated, do not contain any oxido-group and are structurally characterized with tridentate aroylhydrazonates containing ONO- donor atoms. X-ray crystallography of **2** showed the N_2O_4 donor set to define a trigonal prismatic geometry in each case. EPR data provide reference values for typical V(IV) sites. Cyclic voltammogram result suggests that the electrochemical oxidations and reductions are not ligand-centered but metal-centered generating V^{V} and V^{III} species respectively. All the nonoxido vanadium(IV) complexes (**1**–**4)** are highly stable both in the solid state and in solution.

c) The new oxido vanadium(V) complexes $[V^{V}O(L^{1\text{-}4})OEt]$ (**5**–**8**) reported were successfully synthesized and characterized through various spectroscopic techniques. X-ray diffraction study of **5** and **6**, reveals that the metal centre is in distorted square pyramidal geometry O_4N coordination spheres where the O,N,O donor ligand and the ethoxido group constitute a satisfactory O_3N basal plane.

d) The solution behavior of **5**–**8** was also examined. Where there is an indication of generation of a new dimeric μ-oxido species (**9**) in solution.

e) One of the dimeric species $[V_2O_3(L^{1})_2]$ (**9**), is successfully isolated in the solid state and characterized through various spectroscopic techniques and finally structurally characterized by single crystal X-ray technique.

7.5. REFERENCES.

(1) (a) Rehder, D. *Bioinorganic Vanadium Chemistry*; Wiley: Chichester, UK, **2008**. (b) Kustin, K.; Pesssoa, J. C.; Crans, D. C.; Eds. *Vanadium: The Versatile Metal*; ACS Symposium Series 974; American Chemical Society: Washington, DC, **2007**. (c) Tracey, A. S.; Willsky, G. R.; Takeuchi, E. S. *Vanadium Chemistry, Biochemistry, Pharmacology and Practical Applications*; CRC Press: Boca Raton, FL, **2007**. (d) Crans, D. C.; Smee, J. J.; Gaidamauskas, E.; Yang, L. *Chem. Rev.* **2004**, *104*, 849. (e) Fraústo da Silva, J. J. R.; Williams, R. J. P. *The Biological Chemistry of the Element*; Oxford University Press: Oxford, UK, **2001**. (f) Mueller, A.; Peters, F.; Pope, M. T.; Gatteschi, D. *Chem. Rev.* **1998**, *98*, 849.

(2) (a)Adao, P.; Pessoa, J. C.; Henriques, R. T.; Kuznetsov, M. L.; Avecilla, F.; Maurya, M. R.; Kumar, U.; Correia, I. *Inorg. Chem.* **2009**, *48*, 3542. (b) Maurya, M. R.; Kumar, N., *J. Mol. Catal. A: Chem.* **2014**, *383-384*, 172.

(3) a) Henze, M. *Hoppe-Seyler's Z. Physiol. Chem.* **1911**, *72*, 494. b) Robson, R. L.; Eady, R. R.; Richardson, T. H.; Miller, R. W.; Hawkins, M.; Postgate, J. R. *Nature (London)* **1986**, *322*, 388. c) Vilter, H. *Phytochemistry* **1984**, *23*, 1387. d) de Boer, E.; van Kooyk, Y.; Tromp, M. G. M.; Plat, H.; Wever, R. *Biochim. Biophys. Acta* **1986**, *869*, 48. e) Butler, A,; Walker, J. V. *Chem Rev.* **1993**, *93*, 1937. e) Antipov, A. A.; Sorokin, D. Y.; L'Vov, N. P.; Kuenen, J. G. *Biochem. J.* **2003**, *369*, 185. f) Coulombe, R. A.; Briskin, D. P.; Keller, R. J.; Thornley, W. R.; Sharma, R. P. *Arch. Biochem. Biophys.* **1987**, *255*, 267.

(4) (a) Wei, Y.; Zhang, C.; Zhao, P.; Yang, X.; Wang, K. *J. Inorg. Biochem*. **2011**, *105*, 1081. (b) Rehder, D.; Pessoa, J. C.; Geraldes, C. F. G. C.; Kabanos, T.; Kiss, T.; Meier, B.; Micera, G.; Pettersson, L.; Rangel, M.; Salifoglou, A.; Turel, I.; Wang, D. *J. Biol. Inorg. Chem.* **2002**, *7*, 384. (c) Saltiel, A. R.; Khan, C. R.; *Nature* **2001**, *414*, 799. (d) Noblía, P.; Baran, E. J.; Otero, L.; Gambino, D**.** *Eur. J. Inorg. Chem.* **2004**, 322. (e) Nilsson, J.; Shteinman A. A.; Rehder, D.; Nordlander, E. *J. Inorg. Biochem.* **2011**, *105*, 1795. (f) Willsky, G. R.; Chi, L.-H.; Hu, Z.; Crans, D. C. *Coord. Chem. Rev.* **2011**, *255*, 2258. (g) Rehder, D. *Inorg. Chem. Commun*. **2003**, *6*, 604. (h) Pillai, S. I.; Subramanian, S. P.; Kandaswamy, M. *Eur. J. Med. Chem.* **2013**, *63*, 109. i) Ramanadham, S.; Mongold, J. J.; Brownsey, R. W.; Cros, G. H.; McNeill, J. H. *Am. J. Physiol*. **1989**, *257*, H904. j) McNeill, J. H.; Yuen, V. G.; Hoveyda, H. R.; Orvig, C. *J. Med. Chem.* **1992**, *35*, 489.

(5) (*a*) Wilkinson, G., ed.; Gillard, R. D.; McCleverty, J. A. *Comprehensive Coordination Chemistry;* Pergamon Press, Oxford, England, **1987**, *3*, 453. (b) Cotton, F. A.; Wilkinson G. *Advanced Inorganic Chemistry*, 5th edn, John Wiley & Sons, New York, **1988**, 665.
(6) (a) Diamantis, A. A.; Snow, M. R.; Vanzo, J. A.; *Chem. Commun.* **1976**, 264. (b) Comba, P.; Engelhardt, L. M.; Harrowfield, J. M.; Lawrance, G. A.; Martin, L. L.; Sargeson, A. M.; White, A. H., *Chem. Commun.* **1985**, 174. (c) Cooper, S. R.; Koh, Y. B.; Raymond, K. N. *J. Am. Chem. Soc.* **1982**, *104*, 5092. (d) Diamantis, A. A.; Manikas, M.; Salam, M.; Snow, M. R.; Tiekink, E. R. T. *Aust. J. Chem.* **1988**, *41*, 453. (e) Auerbach, U.; Della Vedova, B. P. C.; Wieghardt, K.; Nuber, B.; Weiss J. *Chem. Commun.* **1990**, 1004. (f) Kang, B.; Wenig, L.; Liu, H.; Wu, D.; Huang, L.; Lu, C.; Cai, J.; Chen, X.; Lu, J. *Inorg. Chem.* **1990**, *29*, 4873. (g) Kabanos, T. A.; White, A. J. P.; Williams, D. J.; Woolins, J. D. *Chem. Commun.* **1992**, 17. (h) Kabanos, T. A.; Slawin, A. M. Z.; Williams, D. J.; Woolins, J. D. *Dalton Trans.* **1992**, 1423. (i) Bruni, S.; Caneschi, A.; Cariatia, F.; Delfs, C.; Dei, A.; Gatteschi, D. *J. Am. Chem. Soc.* **1994**, *116*, 1388. (j) Neves, A.; Ceccato, A. S.; Vencato, I.; Mascarenhas, Y. P.; Erasmus- Buhr, C. *Chem. Commun.* **1992**, 652. (k) Vergopoulos, V.; Jantzen, S.; Rodewald, D.; Rehder, D. *Chem. Commun.* **1995**, 377. (l) Ludwig, E.; Hefele, H.; Uhlemann, E.; Weller, F.; Kläui, W.; *Z. Anorg. Allg. Chem.* **1995**, *621*, 23. (m) Hefele, H.; Ludwig, E.; Uhlemann, E.; Weller, F. *Z. Anorg. Allg. Chem.* **1995**, *621*, 1973. (n) Klich, P. R.; Daniher, A. T.; Challen, P. R.; McConville, D. B.; Youngs, W. J. *Inorg. Chem.* **1996**, *35*, 347. (o) Paine, T. K.; Weyhermüller, T.; Slep, L. D.; Neese, F.; Bill, E.; Bothe, E.; Wieghardt, K.; Chaudhuri, P. *Inorg. Chem.* **2004**, *43*, 7324. (p) Sutradhar, M.; Mukherjee, G.; Drew, M. G. B.; Ghosh S. *Inorg. Chem.* **2007**, *46*, 5069. (q) Farahbakhsh, M.; Schmidt, H.; Rehder, D. *Chem. Commun.* **1998**, 2009. (r) Kajiwara, T.; Wagner, R.; Bill, E.; Weyhermüller, T.; Chaudhuri, P. *Dalton Trans.* **2011**, *40*, 12719. (s) Sanna, D.; Várnagy, K.; Lihi, N.; Micera, G.; Garribba, E. *Inorg. Chem.* **2013**, *52*, 8202. (t) Stiefel, E. I.; Dori, Z.; Gray, H. B. *J. Am. Chem. Soc.* **1967**, *89*, 3353. (u) Raymond, K. N.; Isied, S. S.; Brown, L. D.; Fronczek, F. R.; Nibert, J. H. *J. Am. Chem. Soc.* **1976**, *98*, 1767. (v) Karpishin, T. B.; Stack, T. D. P.; Raymond, K. N. *J. Am. Chem. Soc.* **1993**, *115*, 182. (w) Kondo, M.; Minakoshi, S.; Iwata, K.; Shimizu, T.; Matsuzaka, H.; Kamigata, N.; Kitagawa, S. *Chem. Lett.* **1996**, *25*, 489. (x) Paine, T. K.; Weyhermueller, T.; Bill, E.; Bothe, E.; Chaudhuri, P. *Eur. J. Inorg. Chem.* **2003**, 4299. (y) Morgenstern, B.; Steinhauser, S.; Hegetschweiler, K.; Garribba, E.; Micera, G.;

Sanna, D.; Nagy, L. *Inorg. Chem.* **2004**, *43*, 3116. (z) Morgenstern, B.; Kutzky, B.; Neis, C.; Stucky, S.; Hegetschweiler, K.; Garribba, E.; Micera, G. *Inorg. Chem.* **2007**, *46*, 3903.

(7) Berry, R. E.; Armstrong, E. M.; Beddoes, R. L.; Collison, D.; Ertok, S. N.; Helliwell, M.; Garner, C. D. *Angew. Chem., Int. Ed.* **1999**, *38*, 795.

(8) (a) Bayer, E.; Kneifel, H. *Z. Naturforsch., B: Chem. Sci.* **1972**, *27*, 207. (b) Kneifel, H.; Bayer, E. *J. Am. Chem. Soc.* **1986**, *108*, 3075.

(9) (a) Dinda, R.; Sengupta, P.; Ghosh, S.; Mak, T. C. W. *Inorg. Chem.* **2002**, *41*, 1684. (b) Dinda, R.; Majhi, P. K.; Sengupta, P.; Pasayat, S.; Ghosh, S.; *Polyhedron* **2010**, *29*, 248. (c) Dash, S. P.; Pasayat, S.; Bhakat, S.; Dash, H. R.; Das, S.; Butcher, R. J.; Dinda, R. *Polyhedron*, **2012**, *31*, 524. (d) Dash, S. P.; Pasayat, S.; Bhakat, S.; Roy, S.; Dinda, R.; Tiekink, E. R. T.; Mukhopadhyay, S.; Bhutia, S. K.; Hardikar, M. R.; Joshi, B. N.; Patil, Y. P.; Nethaji, M. *Inorg. Chem*. **2013**, *52*, 14096. (e) Dash, S. P.; Panda, A. K.; Pasayat, S.; Dinda, R.; Biswas, A.; Tiekink, E. R. T.; Patil, Y. P.; Nethaji, M.; Kaminsky, W.; Mukhopadhyay, S.; Bhutia, S. K. *Dalton Trans.* **2014**, *43*, 10139.

(10) (a) Moon, M.; Pyo, M.; Myoung, Y. C.; Ahn, C.; Lah, M. S. *Inorg. Chem.* **2001**, *40*, 554. (b) Dinda, R.; Sengupta, P.; Sutradhar, M.; Mak, T. C. W.; Ghosh, S. *Inorg. Chem.*, **2008**, *47*, 5634. (c) Asgedom, G.; Sreedhara, A.; Kivikoski, J.; Valkonen, J.; Kolehmainnen, E.; Rao, C. P. *Inorg. Chem.* **1996**, *35*, 5674.(d) Keramidas, A. D.; Miller, S. M.; Anderson, O. P.; Crans, D. C. *J. Am. Chem. Soc.* **1997**, *119*, 8901. (e) Hamstra, B. J.; Houseman, A. L. P.; Colpas, G. J.; Kampf, J. W.; LoBrutto, R.; Frasch, W. D,. Pecoraro, V. L. *Inorg. Chem.* **1997**, *36*, 4866.

(11) Rowe, R. A.; Jones, M. M. *Inorg, Synth.* **1957**, *5*, 113.

(12) *CrysAlisPro*, Agilent Technologies, Yarnton, UK, **2011**.

(13) G. M. Sheldrick, *Acta Crystallogr.* **2008,**A*64*, 112.

(14) A. L. Spek, *Acta Crystallogr.***2009**, D*65*, 148.

(15) (a) Glas, H.; HerdTweck, E.; Artus, G. R. J.; Thil, W. R. *Inorg. Chem.* **1998**, *37*, 3644. (b) Soon, Y.; Melchior, M.; Summers, D. A.; Thompson, R. C.; Retting, S. J.; Orvig, C. *Inorg. Chem.* **1998**, *37*, 3119.

(16) (a) Selbin, J. *Chem. Re*v. **1965**, *65*, 153. (b) Selbin, J. *Coord. Chem. Re*v. **1966**, *1*, 293.

(17) Mandal, D.; Chaudhury, M. *Struct. Chem.* **2007**, *18*, 187.

(18) Chatterjee, P. B.; Bhattacharya, S.; Audhya, A.; Ki-Young C.; Endo A.; Chaudhury M.; *Inorg. Chem.* **2008**, *47*, 4891.

(19) Parihar, S.; Pathan, S.; Jadeja, R. N.; Patel, A.; Gupta, V. K. *Inorg. Chem.* **2012**, *51*, 1152.
(20) Samanta, S.; Ghosh, D.; Mukhopadhyay, S.; Endo, A.; Weakley, T. J. R.; Chaudhury, M. *Inorg. Chem.* **2003**, *42*, 1508.
(21) Jin, Y.; Lee, H.; Pyo, M.; Lah, M. S. *Dalton Trans.* **2005**, 797.
(22) Dutta, S. K.; Kumar, S. B.; Bhattacharyya, S.; Tiekink, E. R. T.; Chaudhury, M. *Inorg. Chem*. **1997**, *36*, 4954.
(23) Chakravarty, J.; Dutta, S.; Chandra, S. K.; Basu, P.; Chakravorty, A. *Inorg. Chem.* **1993**, *32*, 4249.
(24) a) Dutta, S.; Basu, P.; Chakravorty, A. *Inorg. Chem*. **1993**, *32*, 5343. b) Mondal, S.; Ghosh, P.; Chakravorty, A. *Inorg. Chem.* **1997**, *36*, 59.
(25) (a) Gruning, C.; Schmidt, H.; Rehder, D. *Inorg. Chem. Commun.* **1999**, *2*, 57. b) Schmidt, H.; Bashirpoor, M.; Rehder, D. *J. Chem. Soc., Dalton Trans*. **1996**, 3865.

A Brief Resume of the Work Embodied in this Dissertation and Concluding Remark

A Brief Resume of the Work Embodied in this Dissertation and Concluding Remark

The aim of this dissertation was to explore in depth certain aspects of the chemistry of a series of mono- and binuclear nonoxido vanadium(IV) and oxido vanadium(V) complexes of some selected multidentate ONO- and ONN- donor ligands. Major emphasis was given to the structural and spectroscopic characterization of the synthesized complexes as well as their study of chemical, electrochemical, pharmacological and catalytic activity. Works described in **chapter 2-7** reveal the results of the attempts taken to fulfill all the objectives. The following chapter-wise summary of the work presented in this dissertation reveals the extent to which the above-mentioned objectives are fulfilled.

Chapter 2 deals with the synthesis, X-ray structure and characterization of three highly stable, hexacoordinated nonoxido vanadium(IV), $V^{IV}(L)_2$, complexes with tridentate aroylhydrazonates containing ONO- donor ligands. All the complexes are stable in open air in the solid state as well as in solution, a phenomenon rarely observed in nonoxido vanadium(IV) complexes. The complexes have good solubility in organic solvents, permitting electrochemical and various spectroscopic investigations. The existence of nonoxido vanadium(IV) complexes was confirmed by elemental analysis, ESI mass spectroscopy, cyclic voltammetry, EPR and magnetic susceptibility measurements. X-ray crystallography showed the N_2O_4 donor set to define a trigonal prismatic geometry in each case. All the complexes show *in vitro* insulin mimetic activity against insulin responsive L6 myoblast cells. In addition, the *in vitro* antiproliferative activity of all the complexes against HeLa cell line was assayed, where the complexes found to show good cytotoxic activity.

In ***Chapter 3*** the chemistry of some new oxido vanadium(V) complexes $[VOL^{1\text{-}3}(OEt)(EtOH)]$ (**1**-**3**) have been reported which were obtained from the reaction of the Schiff bases ($H_2L^{1\text{-}3}$) (Where H_2L^1= salicylhydrazone of diacetyl monoxime; H_2L^2= 4-methoxy salicylhydrazone of diacetyl monoxime and H_2L^3 = 4-hydroxy salicylhydrazone of diacetyl monoxime) with $VO(acac)_2$ in 1:1 molar ratio. Three 4-R- aroylhydrazoneoximes have been used as ligands in the present study, differing in the inductive effect of the substituent R (R = H, OCH_3 and OH), in

order to observe their influence, if any, on the redox potentials and biological activity of the complexes. All the synthesized ligands and the metal complexes were successfully characterized by elemental analysis, IR, UV-Vis and NMR spectroscopy. X-ray diffraction study of $[VOL^1(OEt)(EtOH)]$, **1** reveals that the metal centre is in distorted octahedral O_5N coordination spheres where the ONO- donor ligand and the ethoxo group constitute a satisfactory O_3N basal plane. Cyclic voltammetry of the complexes show a quasi-reversible cyclic voltammetric response in the potential range of 0.29−0.36 V involving single electron V(V)−V(IV) reduction. The complexes have also been screened for their antibacterial activity against *Escherichia coli, Bacillus, Proteus and Klebsiella*. Minimum inhibitory concentration of these complexes and antibacterial activity indicates the compound **1** as the potential lead molecule for drug designing.

Chapter 4 describes the report of four oxidoethoxido vanadium(V) $[V^VO(L^{1\text{-}4})OEt]$ (**1**–**4**) and one dinuclear oxidoalkoxido mixed-ligand vanadium(V) $[\{VO(L^2)OEt\}_2(Q)]\{Q$ = 4,4'-bipyridine$\}$(**5**), complexes, taking potentially tridentate binegative aroylhydrazone ligands [where H_2L^1 = anthranylhydrazone of 2-hydroxy-1-napthaldehyde, H_2L^2 = salicylhydrazone of 2-hydroxy-1-napthaldehyde, H_2L^3 = benzoylhydrazone of 2-hydroxy-1-acetonaphthone, H_2L^4 = anthranylhydrazone of 2-hydroxy-1-acetonaphthone]. All the complexes were characterized by various physicochemical techniques. Single crystal X-ray crystallography of **1**–**4** reveals that the metal centre is in distorted square pyramidal geometry with O_4N coordination spheres, where as **5** exhibits a distorted octahedral geometry around the metal center. The solution behavior of the oxidoethoxido vanadium(V) species was studied, which indicates the existence of two species (1:1 ratio) in solution. Catalytic potential of these complexes was tested for the oxidative bromination of styrene, salicylaldehyde and oxidation of methyl phenyl sulphide. All the complexes (**1**–**5)** showed good DNA binding and photo-nuclease propensity. Among these, **3** and **4** show high binding affinity towards CT-DNA than others.

In ***chapter 5*** eight alkali metal ion-mediated dioxido vanadium(V), $[\{V^VO_2L^{1-6}\}A(H_2O)_n]_\infty$(**1-8**), complexes for A = Li^+, Na^+, K^+ and Cs^+, containing tridentate ONO- donor aroylhydrazonate ligands are described. All the synthesised ligands and the metal complexes were successfully characterised by elemental analysis, IR, UV-Vis and NMR spectroscopy. X-ray crystallographic investigation of **3**, **5**−**7** shows the presence of distorted NO_4 coordination geometry. The

dioxidovanadium(V) complexes were found to exhibit DNA binding activity due to their interaction with CT-DNA by the groove binding mode, with binding constants ranging from 10^3 -10^4 M^{-1}. Complexes **1**−**8** were also tested for DNA nuclease activity against pUC19 plasmid DNA which showed that **6** and **7** had the best DNA binding and photonuclease activity; these results support their good protein binding and cleavage activity with binding constants ranging from 10^4 -10^5 M^{-1}. Finally, the *in vitro* antiproliferative activity of all complexes was assayed against the HeLa cell line. Some of the complexes **(2**, **5**, **6** and **7**) show considerable activity compared to commonly use chemotherapeutic drugs.

In this ***chapter*** (***6***), four neutral oxido vanadium(V) complexes $[VO_2L^1]$(**1**), $[VO_2L^2]$(**2**), $[VOL^3(OEt)]$(**3**), $[VOL^4(OEt)EtOH]$(**4**) [where HL^1= 2-thiophenoylhydrazone of 2-acetylpyridine, HL^2= 2-amino benzoylhydrazone of 2-benzoyl pyridine, H_2L^3= isonicotinoylhydrazone of 2-hydroxy acetophenone, H_2L^4= 2-furoylhydrazone of 2-hydroxy-1-napthaldehyde] with a bioactive hydrazone scaffold containing furan, thiophene and pyridine-residues have been synthesized. All complexes were thoroughly characterized by various spectroscopic (IR, UV-Vis, NMR and ESI-MS) and single crystal X-ray diffraction techniques. Biological studies reveal that, **1**–**4** show good DNA binding propensity and interact with CT-DNA by a minor groove binding mode, with binding constants ranging from 10^3−10^5 M^{-1}. All complexes show good photo-induced cleavage of pUC19 supercoiled plasmid DNA with **3** showing the highest photo-induced DNA cleavage activity of ~ 65%. Additionally, **1**–**4** show satisfactory cytotoxic activity against the human cervical cancer cell line (HeLa) following the order **4** > **2** > **3** > **1** with IC_{50} values ranging from 10 to 20 μM.

The essence of the work presented in ***chapter 7*** is the detailed account of a series of nonoxido vanadium(IV) $[V^{IV}(L^{1\text{-}4})_2]$ (**1**–**4**), oxidoethoxido vanadium(V) $[V^{V}O(L^{1\text{-}4})OEt]$ (**5**–**8**), and μ-oxido divanadium(V) $[V^{V}{}_2O_3(L^1)_2]$ (**9**) complexes, taking potentially tridentate dibasic aroylhydrazone ligands [where H_2L^1 = 2-furoyl hydrazone of 2-hydroxy-1-acetonaphthone, H_2L^2 =2-thiophenoylhydrazone hydrazone of 2-hydroxy-1-acetonaphthone, H_2L^3 =1-napthoyl hydrazone of 2-hydroxy-1-acetonaphthone, H_2L^4 =3-hydroxy-2-napthoyl hydrazone of 2-hydroxy-1-acetonaphthone]. All the complexes were characterized by elemental analysis as well as various spectroscopic techniques. Most of the complexes (**2**, **3**, **5**, **6** and **8**) were also

characterized by single crystal X-ray crystallography. The nonoxido vanadium(IV) complexes are quite stable in open air as well as in solution. The solution chemistry of the oxidoethoxido vanadium(V) complexes were reported. This indicates the existence of two different species in solution. The new species, a μ-oxido divanadium(V) complex, $[V_2O_3(L^1)_2]$ (**9**), is successfully isolated in solid state and fully characterized by several physicochemical techniques & single crystal X-ray crystallography.

The author is very much aware of the fact that some portions of the work described in the present dissertation left scope for future work especially the pharmacological and catalytic studies. All the reported complexes can be used for the study of several other catalytic and bio activities. This dissertation also left scope for further qualitative improvement by the utilization of some relevant instrumental data, which could have been really helpful in arriving at completely unambiguous conclusions. As those instrumental facilities were not available to us, we were rather helpless. However, the above discussion on the entire work presented in **chapter 2-7** reveals that the aims and objectives of the present dissertation are mostly fulfilled.

List of Publications [Published in cited Journals (SCI)]

1. 'Oxidovanadium(V) complexes of aroylhydrazones containing bioactive heterocycles: Synthesis, characterization and study of DNA binding, photoinduced DNA cleavage and cytotoxic activities', **Subhashree P. Dash**, A. K. Panda, S. Pasayat, R. Dinda, A. Biswas, S. Mukhopadhyay, S. K. Bhutia, Edward R. T. Tiekink, W. Kaminsky, Ekk Sinn, **Eur. J. Med. Chem. (Communicated).**

2. 'Syntheses and structural investigation of some alkali metal ion-mediated $LV^{V}O_2^-$ (L^{2-} = Tridentate ONO ligands) species: DNA binding, photo-induced DNA cleavage and cytotoxic activities', **Subhashree P. Dash**, A. K. Panda, S. Pasayat, R. Dinda, A. Biswas, E. R. T. Tiekink, Y. P. Patil, M. Nethaji, W. Kaminsky, S. Mukhopadhyay and S. K. Bhutia, **Dalton Trans. 43 (2014) 10139.**

3. 'Highly Stable Hexacoordinated Nonoxidovanadium(IV) Complexes of Sterically Constrained Ligands: Syntheses, Structure and Study of Antiproliferative and Insulin Mimetic Activity', **Subhashree P. Dash**, S. Pasayat, S. Bhakat, S. Roy, R. Dinda, E. R. T. Tiekink, Su. Mukhopadhyay, S. K. Bhutia, M. R. Hardikar, B. N. Joshi, Y. P. Patil and M. Nethaji, **Inorganic Chemistry 52 (2013) 14096.**

4. 'Oxovanadium(V) complexes incorporating tridentate aroylhydrazoneoximes: Synthesis, characterizations and antibacterial activity', **Subhashree P. Dash**, S. Pasayat, Saswati, H. R Dash, S. Das; Ray J Butcher, R. Dinda, **Polyhedron, 31 (2012) 524.**

5. 'Synthesis, Structure, Characterization and Study of Antiproliferative Activity of Dimeric and Tetrameric Oxidomolybdenum(VI) Complexes of *N*,*N*'-Disalicyloylhydrazine', Sagarika Pasayat, **Subhashree P. Dash**, S. Majumder, R. Dinda, E. Sinn, H. Stoeckli-Evans, S. Mukhopadhyay, S. K. Bhutia and P. Mitra, **Polyhedron 80 (2014) 198.**

6. 'Synthesis, structural studies and catalytic activity of dioxidomolybdenum(VI) complexes with aroylhydrazones of naphthol-derivative', S. Pasayat, **Subhashree P. Dash**, S. Roy, R. Dinda , S. Dhaka, M. R. Maurya, W. Kaminsky, Y. P. Patil, M. Nethaji, **Polyhedron 67 (2014) 1.**

7. 'Mixed-ligand aroylhydrazone complexes of molybdenum: Synthesis, structure and biological activity, S. Pasayat', **Subhashree P. Dash**, Saswati, P. Kumar Majhi, Y. P. Patil, M. Nethaji, H. R. Dash, S. Das, Rupam Dinda, **Polyhedron, 38 (2012) 198.**

Bio-data

Subhashree Priyadarsini Dash

Research Scholar

Department of Chemistry

National Institute of Technology, Rourkela

Rourkela-769008, Odisha, India

Research experience

a. Doctoral Research (January 2010 – Continuing)

Supervisor: Dr. Rupam Dinda, Department of Chemistry, National Institute of Technology Rourkela, India,

Research area: Bio-Inorganic Chemistry

b. Project Assistant (August 2009 – December 2009)

Supervisor: Dr. Rupam Dinda, Department of Chemistry, National Institute of Technology Rourkela, India,

Research area: Synthetic Inorganic Chemistry

c. Project Fellow (**January 2009 – August 2009**)

Supervisor: Dr. A. Sree, Department of Natural products, IMMT, Bhubaneswar.

Research area: Potential drugs from ocean.

d. M. Phil in Chemistry (December 2007 – December 2008)

Supervisor: Dr. A.K. Behera, School of Chemistry, Sambalpur University, Odisha, India.

Research area: Synthesis of condensed heterocycles containing pharmacologically active moiety.

Analytical Techniques

Spectroscopy : Acquisition and analysis of ^{1}H, ^{13}C, ^{51}V NMR, ESI-Mass spectra. Recording and interpretation of GC-MS, FT-IR, UV-Vis spectra, Magnetic Susceptibility and Cyclic voltammetry. Interpretation of X-ray crystal structure

X-Ray Crystallography Software: MERCURY & ORTEP

Education Profile

1999 Secondary (**10th**), BSE Odisha Board, St. Mary's Girls High School, Sundargarh, Odisha, India.

2001 Higher Secondary **(+2 Science)**, CHSE Odisha Board, Government College, Sundargarh, Odisha, India.

2004 Graduation (**B.Sc. Hons. in Chemistry)**, Government College, Sundargarh, Sambalpur University, Odisha, India.

2006 Post graduation (**M.Sc. in Chemistry)**, School of Chemistry, Sambalpur University Odisha, India.

2008 Master of Philosophy (**M. Phil. in Chemistry)**, School of Chemistry, Sambalpur University Odisha, India.

Honors and Fellowship

- Fellowship, DST Women Scientist, Scheme WOS-A

Personal Profile

- Date of Birth 22nd June 1984
- Nationality Indian
- Permanent Address At-New Amlipali, P.O.- Rangadhipa
  Dist- Sundargarh, Odisha - 770002